frontiers | Research Topics

Neuroinflammation, neurodegeneration and metabolic disease: From molecular mechanisms to therapeutic innovation

Edited by
Fawaz Alzaid, Mohammed Al-Onaizi and Ayman ElAli

Published in
Frontiers in Neurology
Frontiers in Immunology

ISSN 1664-8714
ISBN 978-2-8325-5409-8
DOI 10.3389/978-2-8325-5409-8

About Frontiers

Frontiers is more than just an open access publisher of scholarly articles: it is a pioneering approach to the world of academia, radically improving the way scholarly research is managed. The grand vision of Frontiers is a world where all people have an equal opportunity to seek, share and generate knowledge. Frontiers provides immediate and permanent online open access to all its publications, but this alone is not enough to realize our grand goals.

Frontiers journal series

The Frontiers journal series is a multi-tier and interdisciplinary set of open-access, online journals, promising a paradigm shift from the current review, selection and dissemination processes in academic publishing. All Frontiers journals are driven by researchers for researchers; therefore, they constitute a service to the scholarly community. At the same time, the *Frontiers journal series* operates on a revolutionary invention, the tiered publishing system, initially addressing specific communities of scholars, and gradually climbing up to broader public understanding, thus serving the interests of the lay society, too.

Dedication to quality

Each Frontiers article is a landmark of the highest quality, thanks to genuinely collaborative interactions between authors and review editors, who include some of the world's best academicians. Research must be certified by peers before entering a stream of knowledge that may eventually reach the public - and shape society; therefore, Frontiers only applies the most rigorous and unbiased reviews. Frontiers revolutionizes research publishing by freely delivering the most outstanding research, evaluated with no bias from both the academic and social point of view. By applying the most advanced information technologies, Frontiers is catapulting scholarly publishing into a new generation.

What are Frontiers Research Topics?

Frontiers Research Topics are very popular trademarks of the *Frontiers journals series*: they are collections of at least ten articles, all centered on a particular subject. With their unique mix of varied contributions from Original Research to Review Articles, Frontiers Research Topics unify the most influential researchers, the latest key findings and historical advances in a hot research area.

Find out more on how to host your own Frontiers Research Topic or contribute to one as an author by contacting the Frontiers editorial office: frontiersin.org/about/contact

Neuroinflammation, neurodegeneration and metabolic disease: From molecular mechanisms to therapeutic innovation

Topic editors
Fawaz Alzaid — Sorbonne Universités, France
Mohammed Al-Onaizi — Kuwait University, Kuwait
Ayman ElAli — Laval University, Canada

Citation
Alzaid, F., Al-Onaizi, M., ElAli, A., eds. (2024). *Neuroinflammation, neurodegeneration and metabolic disease: From molecular mechanisms to therapeutic innovation*. Lausanne: Frontiers Media SA. doi: 10.3389/978-2-8325-5409-8

Table of contents

04 Editorial: Neuroinflammation, neurodegeneration and metabolic disease: from molecular mechanisms to therapeutic innovation
Mohammed Al-Onaizi, Ayman ElAli and Fawaz Alzaid

07 Assessing impulse control behaviors in early Parkinson's disease: a longitudinal study
Xiaobo Zhu, Jing Gan, Na Wu, Ying Wan, Lu Song, Zhenguo Liu and Yu Zhang

29 Mapping knowledge of the stem cell in traumatic brain injury: a bibliometric and visualized analysis
Tingzhen Deng, Ruiwen Ding, Yatao Wang, Yueyang Chen, Hongtao Sun and Maohua Zheng

44 Recent insights from non-mammalian models of brain injuries: an emerging literature
Nicole J. Katchur and Daniel A. Notterman

55 Regulatory SVA retrotransposons and classical HLA genotyped-transcripts associated with Parkinson's disease
Jerzy K. Kulski, Shingo Suzuki, Takashi Shiina, Abigail L. Pfaff and Sulev Kõks

77 Fructose overconsumption-induced reprogramming of microglia metabolism and function
Kenneth K. Y. Ting

83 Case report: Transition from anti-CD20 therapy to inebilizumab for 14 cases of neuromyelitis optica spectrum disorder
Benjamin Osborne, Gabriela Romanow, J. Michael Hemphill, Myassar Zarif, Tracy DeAngelis, Tyler Kaplan, Unsong Oh, Johnathan Pinkhasov, Kristina Patterson and Michael Levy

93 Interactions between circulating inflammatory factors and autism spectrum disorder: a bidirectional Mendelian randomization study in European population
Junzi Long, Hui Dang, Wenlong Su, Md. Moneruzzaman and Hao Zhang

102 A helping HAND: therapeutic potential of MAGL inhibition against HIV-1-associated neuroinflammation
Alexis F. League, Barkha J. Yadav-Samudrala, Ramya Kolagani, Calista A. Cline, Ian R. Jacobs, Jonathan Manke, Micah J. Niphakis, Benjamin F. Cravatt, Aron H. Lichtman, Bogna M. Ignatowska-Jankowska and Sylvia Fitting

120 Elucidating sleep disorders: a comprehensive bioinformatics analysis of functional gene sets and hub genes
Junhan Lin, Changyuan Liu and Ende Hu

135 Usefulness of bioelectrical impedance analysis in multiple sclerosis patients—the interrelationship to the body mass index
Edyta Matusik

frontiers | Frontiers in Neurology

TYPE Editorial
PUBLISHED 28 August 2024
DOI 10.3389/fneur.2024.1478550

OPEN ACCESS

EDITED AND REVIEWED BY
Hans-Peter Hartung,
Heinrich Heine University, Germany

*CORRESPONDENCE
Fawaz Alzaid
✉ fawaz.alzaid@dasmaninstitute.org

RECEIVED 10 August 2024
ACCEPTED 16 August 2024
PUBLISHED 28 August 2024

CITATION
Al-Onaizi M, ElAli A and Alzaid F (2024) Editorial: Neuroinflammation, neurodegeneration and metabolic disease: from molecular mechanisms to therapeutic innovation. *Front. Neurol.* 15:1478550. doi: 10.3389/fneur.2024.1478550

Editorial: Neuroinflammation, neurodegeneration and metabolic disease: from molecular mechanisms to therapeutic innovation

Mohammed Al-Onaizi[1,2], Ayman ElAli[3,4] and Fawaz Alzaid[2,5]*

[1]Department of Anatomy, Faculty of Medicine, Kuwait University, Kuwait City, Kuwait, [2]Dasman Diabetes Institute, Kuwait City, Kuwait, [3]Neuroscience Axis, Research Center of CHU de Québec, Université Laval, Québec City, QC, Canada, [4]Department of Psychiatry and Neuroscience, Faculty of Medicine, Université Laval, Québec City, QC, Canada, [5]INSERM UMR-S1151, CNRS UMR-S8253, Université Paris Cité, Institut Necker Enfants Malades, Paris, France

KEYWORDS

neuroinflammation, neurodegeneration, metabolic disease, microglia, parkinson's disease

Editorial on the Research Topic
Neuroinflammation, neurodegeneration and metabolic disease: from molecular mechanisms to therapeutic innovation

The nervous system dynamically communicates and interacts with each tissue and organ system to regulate various critical physiological processes. The cellular components of these systems require a tightly functional and adaptable metabolism to meet their physiological needs. Inflammation, and more specifically neuroinflammation, is common in the development and progression of neurological and metabolic diseases.

This Research Topic features recent studies that span the domains of neuroinflammation, neurodegeneration, and metabolic disease. We navigate through research at multiple levels, from longitudinal cohorts to clinical trials, bibliometric analyses, basic science, and reviews, to further our understanding of the intersection of neurological and metabolic diseases through the topic's focus areas. As we highlight novel genetic markers, predictive indicators, and the influence of diet on neuronal integrity, we have set a theme for current and future priority research areas in neurology. We aimed to highlight the breadth of manifestations of neuroinflammation in neurodegenerative and metabolic diseases. The summary schematic in Figure 1 illustrates the focus of the contributed articles.

Zhu et al. carried out a study based on data from the Parkinson's Progression Markers Initiative (PPMI) (1), to assess impulse control behavior (ICB) in early Parkinson's disease (PD). They reported that ICBs increase during the early stages of PD and that anxiety, rapid eye movement sleep behavior disorder, and p-tau levels in cerebrospinal fluid are predictors of the incident development of ICBs in early PD (Zhu et al.).

Further in the context of PD, another PPMI-based study by Kulski et al. investigated genetic and transcriptomic features in 1,521 individuals to assess the genotypes of eight classical HLA class I and II genes and the DRB3/4/5 haplotypes. They identified significant differences in HLA alleles and SVA (SINE-VNTR-Alu) retrotransposon insertions

between PD patients and healthy controls, highlighting the influence of these genetic elements on PD progression and the immune response.

Moving to traumatic brain injury (TBI), Deng et al. conducted a bibliometric analysis of the role of stem cells in TBI recovery. Analyzing literature from the past 24 years, including 459 articles from 45 countries, the authors suggested that "immunomodulation" and "cellular therapy" are among the research hotspots in TBI, and that "exosomes," "neuroinflammation," and "microglia" are essential future research directions (Deng et al.).

Katchur and Notterman provided a topical review of non-mammalian models for studying the long-term effects of TBI and repetitive TBIs. These include sea lamprey, zebrafish and others, which are advantageous for their genetic tractability, reduced cost, and ethical considerations. These models are useful for mechanistic investigations of neurodegeneration associated with TBI, offering viable alternatives (Katchur and Notterman).

In autoimmune conditions, Osborne et al. carried out a retrospective study of patients with neuromyelitis optica spectrum disorder (NMOSD) who transitioned from rituximab to inebilizumab. Remarkably, 71.4% of patients experienced relapses during rituximab therapy, whereas no relapses were observed with inebilizumab for an average of 19.3 months. This suggests the effectiveness and safety of inebilizumab for NMOSD patients (Osborne et al.).

Matusik's work on multiple sclerosis (MS) assessed body mass index (BMI) and bioelectrical impedance analysis (BIA) in 176 MS patients. The BIA found a higher prevalence of overfatness compared to overweight by BMI, and BMI underestimated fat mass, especially in those with moderate disability. BIA correlated better with abdominal obesity and disability status. BIA has been shown to be superior for assessing nutritional status in MS patients (Matusik).

Moving further into the realm of immunity, Long et al. investigated circulating inflammatory factors in autism spectrum disorders (ASD). Two-sample bidirectional Mendelian

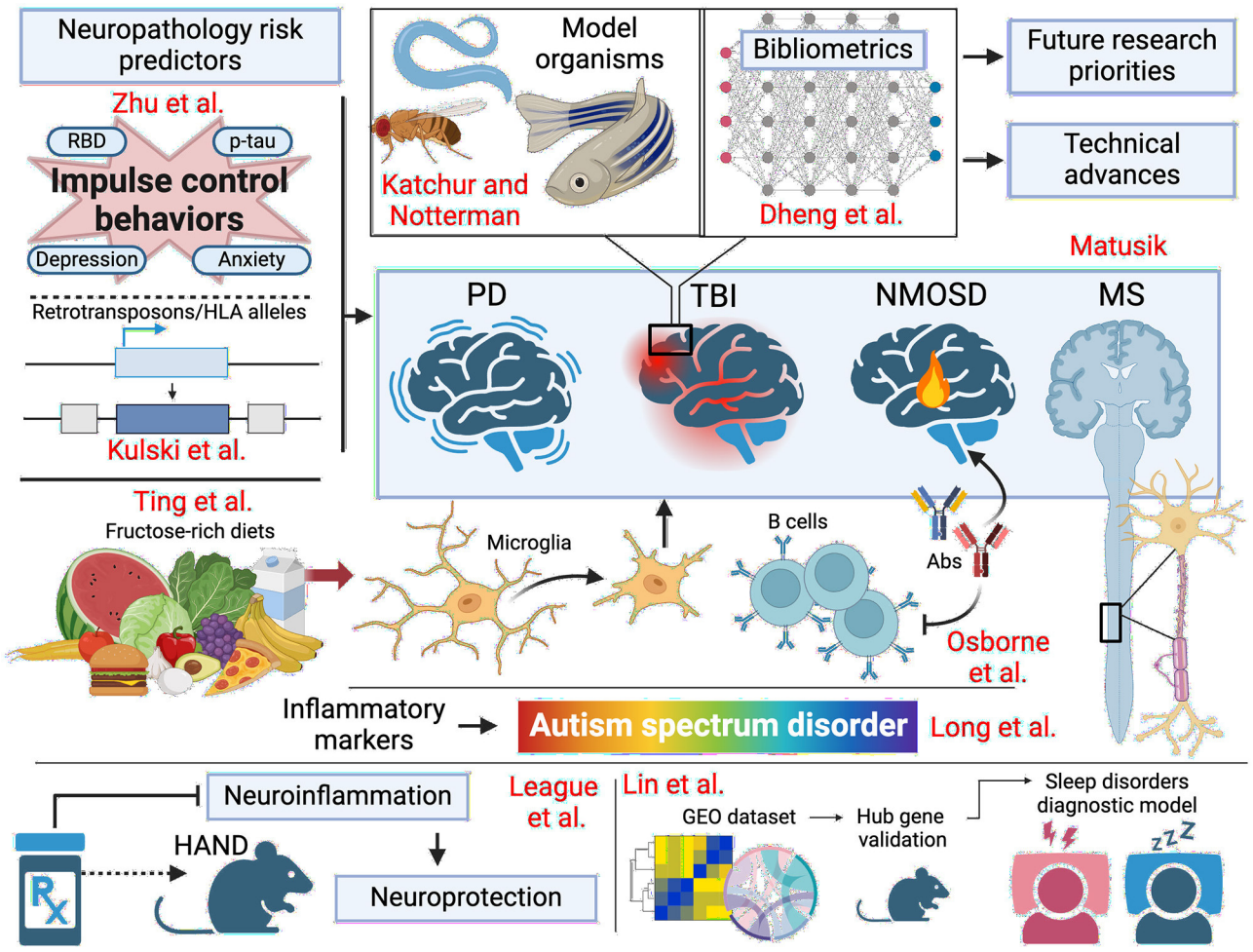

FIGURE 1
Schematic summary of the subjects covered by the articles contributing to this Frontiers in Neurology Research Topic "*Neuroinflammation, neurodegeneration and metabolic disease: from molecular mechanisms to therapeutic innovation.*" PD, Parkinson's disease; TBI, traumatic brain injury; NMOSD, neuromyelitis optica spectrum disorder; MS, multiple sclerosis; HAND, HIV-associated neurocognitive disorders; GEO, gene expression omnibus. Created with Biorender.com.

randomization (MR) revealed that certain inflammatory factors (e.g., natural killer cell receptor 2B4) are positively associated with ASD, while others, like interleukin-7, are inversely associated. The authors suggested that inflammatory factors may indicate immunologic dysfunction in ASD.

In a mechanistic study of HIV-associated neurocognitive disorders (HAND), League et al. explored the potential of the monoacylglycerol lipase (MAGL) inhibitor MJN110 to mitigate Tat-induced neuroinflammation. In female Tat transgenic mice, MJN110 protected against neuroinflammatory hallmarks (e.g., dendritic injury) without altering behavior. The findings also show the neuroprotection by MJN110 is achieved without cannabimimetic behavioral effects (League et al.).

Next, Lin et al. investigated the mechanisms of sleep disorder (SD) by analyzing public datasets with advanced bioinformatics tools (e.g., LASSO, PPI networks). Differentially expressed genes were enriched in immune activity, stress response, and neural regulation, with elevated T cell levels found in SD patients. Hub genes were identified (e.g., IPO9, RAP2A), and then validated, and a diagnostic model using these genes demonstrated high accuracy.

Finally, and at the heart of this Research Topic, Ting provided a mini-review of a relevant area of nutrition and neurological health. Studies suggest that fructose may alter microglial function in the brain through metabolic reprogramming. This may influence activation and inflammation, increasing the risk of neurological dysfunction. Ting's review summarized the current findings and suggested directions for future research.

In conclusion, the collection of articles presented in this Research Topic not only underscores the multifaceted nature of neuroinflammation at the crossroads of neurological and metabolic diseases, but also provides insights into its understanding. From genetic landscapes to the metabolic triggers of neuroinflammatory responses, the insights offered represent a leap toward precision medicine. The therapeutic potential unlocked by the transition from rituximab to inebilizumab in treating NOMSD further exemplifies the advancements possible when innovative research converges with clinical application. By continuing along the path of converging biological domains and regrouping research at multiple levels, from clinical trials to bibliometrics, we hope to expand the range of promising areas for future research.

Author contributions

MA-O: Writing – original draft, Writing – review & editing. AE: Writing – original draft, Writing – review & editing. FA: Writing – original draft, Writing – review & editing.

Funding

The author(s) declare financial support was received for the research, authorship, and/or publication of this article. MA-O was supported by Kuwait University Research Sector Grant No. RM01/19. AE was supported by grants from the Canadian Institutes of Health Research (CIHR) (#169062; #186148), from the Heart and Stroke Foundation of Canada (G-23-0035047) and holds a Tier 2 Canada Research Chair in molecular and cellular neurovascular interactions. FA was supported by the French National Research Agency (*Agence Nationale de la Recherche*; ANR) ANR-PRCI grant ANR-23-CE14-0088-02; and by the Kuwait Foundation for the Advancement of Sciences (KFAS; Grant Nos. RA AM-2022-009, RA AM-2023-007, and RA AM-2023-020).

Conflict of interest

The authors declare that the research was conducted in the absence of any commercial or financial relationships that could be construed as a potential conflict of interest.

Publisher's note

References

1. *The Parkinson progression marker initiative (PPMI) - pubmed* (2011). Available at: https://pubmed.ncbi.nlm.nih.gov/21930184/ (accessed June 4, 2024).

frontiers | Frontiers in Neurology

TYPE Original Research
PUBLISHED 25 October 2023
DOI 10.3389/fneur.2023.1275170

OPEN ACCESS

EDITED BY
Ayman ElAli,
Laval University, Canada

REVIEWED BY
Jorge Hernandez-Vara,
Hospital Universitari Vall D¨Hebron, Spain
Luca Weis,
University of Padua, Italy

*CORRESPONDENCE
Yu Zhang
✉ zhangyu06@xinhuamed.com.cn
Zhenguo Liu
✉ liuzhenguo@xinhuamed.com.cn

†These authors have contributed equally to this work

RECEIVED 09 August 2023
ACCEPTED 12 October 2023
PUBLISHED 25 October 2023

CITATION
Zhu X, Gan J, Wu N, Wan Y, Song L, Liu Z and Zhang Y (2023) Assessing impulse control behaviors in early Parkinson's disease: a longitudinal study.
Front. Neurol. 14:1275170.
doi: 10.3389/fneur.2023.1275170

Assessing impulse control behaviors in early Parkinson's disease: a longitudinal study

Xiaobo Zhu, Jing Gan, Na Wu, Ying Wan, Lu Song, Zhenguo Liu*† and Yu Zhang*†

Department of Neurology, Xinhua Hospital Affiliated to Shanghai Jiao Tong University School of Medicine, Shanghai, China

Objective: Impulse control behaviors (ICBs) frequently coexist with Parkinson's disease (PD). However, the predictors of ICBs in PD remain unclear, and there is limited data on the biological correlates of ICBs in PD. In this study, we examined clinical, imaging, and biological variables to identify factors associated with longitudinal changes in ICBs in early-stage PD.

Methods: The data for this study were obtained from the Parkinson's Progression Markers Initiative, an international prospective cohort study that evaluates markers of disease progression in PD. We examined clinical, imaging, and biological variables to determine their associations with ICBs over a period of up to 5 years. Cox regression models were employed to investigate the predictors of ICBs in early-stage, untreated PD.

Results: The study enrolled 401 individuals with PD and 185 healthy controls (HC). At baseline, 83 PD subjects (20.7%) and 36 HC (19.5%) exhibited ICBs. Over the course of 5years, the prevalence of ICBs increased in PD (from 20.7% to 27.3%, p <0.001), while it decreased in HC (from 19.5% to 15.2%, p <0.001). Longitudinally, the presence of ICBs in PD was associated with depression, anxiety, autonomic dysfunction, and excessive daytime sleepiness (EDS). However, there was no significant association observed with cognitive dysfunction or motor severity. Treatment with dopamine agonists was linked to ICBs at years 3 and 4. Conversely, there was no association found between ICBs and presynaptic dopaminergic dysfunction. Additionally, biofluid markers in baseline and the first year did not show a significant association with ICBs. A predictive index for ICBs was generated, incorporating three baseline characteristics: anxiety, rapid eye movement sleep behavior disorder (RBD), and p-tau levels in cerebrospinal fluid (CSF).

Conclusion: During the early stages of PD, there is a notable increase in ICBs over time. These ICBs are associated with depression, anxiety, autonomic dysfunction, EDS, and the use of dopaminergic medications, particularly dopamine agonists. Anxiety, RBD, and p-tau levels in CSF are identified as predictors for the incident development of ICBs in early PD. Further longitudinal analyses will provide a more comprehensive understanding of the associations between ICBs and imaging findings, as well as biomarkers. These analyses will help to better characterize the relationships and implications of these factors in the context of ICBs in early PD.

KEYWORDS

Parkinson's disease, impulse control behaviours, longitudinal assessment, dopamine transporter imaging, biomarkers

1. Introduction

While Parkinson's disease (PD) is primarily defined by its motor manifestations, it is important to note that non-motor symptoms (NMS) are also prevalent and can significantly impact an individual's quality of life. These non-motor symptoms include impulse control behaviors (ICBs), which can be particularly detrimental (1). ICBs are characterized as repetitive, excessive, and compulsive abnormal behaviors that are driven by a strong desire and prove challenging to self-control (2, 3). Impulse Control Disorders (ICDs) represent the more severe manifestations of ICBs and encompass four specific types: pathological gambling (PG), hypersexuality (HS), compulsive buying (CB), and binge eating (BE). Furthermore, ICBs encompass additional related behaviors such as excessive hobbyism, punding, walkabout, and dopamine dysregulation syndrome (DDS) (3–5). Furthermore, as research progresses, the clinical spectrum of ICBs is expected to expand further. Recent studies have reported that newly relevant behaviors, such as over-donation and over-indulgence in mobile devices, may be included within the scope of ICBs (6–8).

Several studies have reported a wide variation in the prevalence of PD-ICBs, ranging from 3.5% to 59.0%. However, it is important to note that the majority of these studies were conducted on patients with intermediate to advanced stages of the disease who were already undergoing drug treatment (9–15). The mechanisms underlying PD-ICBs are currently unknown, and multiple factors have been implicated. These factors include being male, unmarried, younger age at the onset of PD, longer disease duration, certain medications (such as dopaminergic agonists, levodopa, amantadine, and rasagiline), personal or family history of smoking, drug or alcohol abuse, cultural factors (specifically residing in the United States), depression, anxiety, cognitive impairment, rapid eye movement sleep behavior disorder (RBD), restless legs syndrome (RLS), and genetic factors (3, 5, 15–19).

While numerous cross-sectional studies have investigated ICBs in PD, there is a limited number of studies that have examined their longitudinal incidence and prevalence. Furthermore, only a few studies have followed ICBs longitudinally for more than 5 years. The ICARUS study aimed to address this gap by examining longitudinal changes in the occurrence of ICBs over a 2-year period. The findings from this study indicated that the presence of ICBs remained relatively stable between the initial visit and the 2-year follow-up visit (20). However, several studies have reported a higher incidence of ICBs in early PD populations, and this incidence tends to increase over time (11, 14, 21). In a longitudinal study, the prevalence of ICDs was found to increase from 19.7% at baseline to 32.8% after a period of 5 years (21). Additionally, a study reported that ICBs were observed in 21 (19.8%) patients with PD and this prevalence increased to 29.2% at year 5 (11). In another study, ICBs were found in 38 (30.6%) patients with PD, and this prevalence significantly increased to 46.8% after a 4-year period (14). The variations in these findings can be attributed to the differences in the studied populations and the assessment methods employed. However, it is worth noting that previous studies have seldom reported the impact of biomarkers, such as cerebrospinal fluid (CSF) markers, on the prevalence of ICBs in newly diagnosed and untreated individuals with PD. Considering the potential association between PD-ICBs and biomarkers, investigating this aspect could hold substantial significance (2, 5, 20).

Given the existing knowledge gaps, our objective was to conduct a systematic investigation to provide a more comprehensive understanding of the prevalence, clinical spectrum, longitudinal evolution over a 5-year period, and biological correlates of ICBs in PD. To accomplish this, we utilized the Parkinson's Progression Markers Initiative (PPMI) cohort. Additionally, we sought to assess the baseline biological factors that could potentially predict the development of ICBs in PD. By addressing these research objectives, we aimed to contribute valuable insights into the understanding and characterization of ICBs in PD, ultimately enhancing our knowledge of this important aspect of the disease.

2. Methods

2.1. Study design and participants

All the data utilized in this study were obtained from the PPMI database, which has been previously published and is accessible on the PPMI website[1] (22). The PPMI study received approval from the institutional review board at each study center, and all participants provided signed written informed consent. The data utilized in this paper were derived from the baseline and 5-year follow-up dataset, which was downloaded on August 29, 2021.

During the screening process, individuals with PD were required to meet the following criteria: (1) exhibit at least two of the following: resting tremor, bradykinesia, and rigidity, or have an asymmetric resting tremor or asymmetric bradykinesia; (2) have received an idiopathic PD diagnosis within the past 2 years and remain untreated; (3) be aged 30 years or older; (4) undergo a screening dopamine transporter SPECT scan that demonstrates a dopamine transporter deficit. Regarding the healthy controls (HC), the following criteria were applied: (1) match PD participants in terms of age, gender, and education; (2) exhibit no significant neurological dysfunction; (3) demonstrate no cognitive impairment, as assessed by a Montreal Cognitive Assessment (MoCA) score of greater than 26; (4) have no family history of PD.

2.2. Study outcomes

To evaluate PD-ICBs, we employed the validated short version of the Questionnaire for Impulsive-Compulsive Disorders in Parkinson's Disease (QUIP-S), a widely recognized and extensively validated tool recommended for screening ICBs in individuals with PD. The QUIP-S has been proven effective over time and is considered a reliable assessment instrument for this purpose (23). The scale comprises eight items that pertain to ICDs such as PG, HS, CB, and BE, as well as other behaviors including excessive hobbyism, punding, walkabout, and DDS. Consistent with previous studies, the presence of symptoms related to ICBs was defined as a score of $\geq$1 on any of the eight items. If a patient exhibits a combination of multiple symptoms simultaneously, it is considered as having multiple ICBs (24).

Furthermore, demographic and clinical data were collected for all subjects. Motor symptoms and disease severity were assessed using the Movement Disorders Society Unified Parkinson's Disease Rating

1 http://www.ppmi-info.org

Scale (MDS-UPDRS) (25) and Hoehn and Yahr stage (H&Y) (26) respectively. These measures provide a comprehensive evaluation of motor symptoms and the overall severity of the disease in Parkinson's patients. The MDS-UPDRS was used to calculate both the tremor score and the Postural Instability Gait Disorder (PIGD) score simultaneously. Additionally, the ratio of these scores was utilized to classify patients as having tremor-dominant (TD) or non-tremor-dominant (non-TD) subtypes (27). Additional assessments of NMS included the use of the Modified Schwab and England Activities of Daily Living Scale (S&E) (28), MoCA (29), the 15-item Geriatric Depression Scale (GDS) (30), the State–Trait Anxiety Inventory (STAI) state and trait subscores (31), the Epworth Sleepiness Scale (ESS) (32), the REM Sleep Behaviour Disorder Screening Questionnaire (RBDSQ) (33), the Scales for Outcomes in Parkinson's Disease-Autonomic (SCOPA-AUT) (34). In this study, participants were considered to have a positive screening for RBD if they scored ≥5 on the RBDSQ (35). Dopaminergic therapy usage was quantified using the levodopa equivalent daily dose (LEDD), calculated according to a previously described method. The LEDD provides a standardized measure for comparing the dosage of different dopaminergic medications by converting them to an equivalent dose of levodopa (36).

We also conducted 123-I Ioflupane dopamine transporter (DaTscan) imaging to assess the dopamine transporter in all subjects. The analysis of the DaTscan images was performed according to the relevant manuals available at http://ppmi-info.org/ (22). Biological sample tests included measurements of serum urate, neurofilament light chain (NfL), and CSF analysis of A-beta 1–42, total tau (T-tau), tau phosphorylated at threonine 181 (P-tau181), and alpha-synuclein. Detailed information regarding sample collection, processing, and analysis can be found in the previously published reports related to this study (37).

2.3. Statistical analysis

All statistical analyses were conducted using SPSS 26. The t-test or chi-square test was used to compare baseline demographics and clinical characteristics between PD subjects and controls, as well as to compare demographics, clinical characteristics, DaTscan measures, and medication use at each time point between patients with PD with and without ICBs. Mann–Whitney U tests were employed to compare biologics between patients with PD with and without ICBs. T-test for normally distributed data, Mann–Whitney U tests for non-normally distributed data, and chi-square for categorical variables.

Logistic mixed models were employed to examine changes in ICB-related characteristics over time in patients with PD and HC separately. These models were also used to assess differences in ICBs between the two groups over time. In the latter models, an interaction term between visit and groups was initially tested to evaluate potential differential effects over time. If the interaction test did not reach statistical significance at the 0.10 level, the interaction term was removed from the model, and the overall group differences were reported.

In addition, Cox regression models were utilized to explore the univariate and multivariable relationships between baseline demographic, clinical, biological, imaging, and sedative use predictors and the prevalence of ICBs in PD, as well as their predictive value for changes over a 5-year period. To account for covariance, a specific scheme was adopted. For the DaTscan variables, if either the contralateral or ipsilateral side of the putamen or caudate measure exhibited statistical significance in univariate analysis, the contralateral side of the measure was prioritized for inclusion in the multivariate model. Likewise, for CSF biomarkers and the CSF ratios, only the biomarker was included in the multivariate model if both the specific biomarker and its associated ratio were found to be significant. CSF ratios were considered in the multivariate model only if there were instances where neither of the two biomarkers reached significance, but the CSF ratio showed significant associations. Lastly, plot Nomogram based on Cox result for better representation.

3. Results

3.1. Impulse control behaviours over time in PD and HC

Figure 1 presents an overview of the sample selection process. Initially, data was obtained from 423 PD subjects and 196 HC. However, after thorough assessment, it was determined that only 401 PD subjects and 185 HC possessed all the required data. Consequently, for PD participants, data was accessible for 401 individuals at baseline, 362 individuals at year 1, 362 individuals at year 2, 360 individuals at year 3, 340 individuals at year 4, and 311 individuals at year 5. As for HC, data was available for 185 participants at baseline, 182 participants at year 1, 170 participants at year 2, 164 participants at year 3, 159 participants at year 4, and 151 participants at year 5.

Table 1 provides an overview of the baseline demographics of the cohort. It indicates that there were no significant differences observed between PD and HC groups in terms of demographics, including gender, age, and education.

Figure 2 and Table 2 illustrate the longitudinal changes in the occurrence of ICBs among PD and HC participants. The results show a significant increase in the proportion of PD participants classified as having ICBs over time ($p < 0.001$). In contrast, HC participants demonstrated a significant decrease in the proportion classified as having ICBs ($p = 0.005$). Furthermore, there was a significant difference in the rates of change in ICBs over time between the PD and HC groups (group × visit interaction, $p = 0.001$).

Furthermore, the proportion of PD participants with ICDs ($p < 0.001$), any other behavior ($p < 0.001$), or DDS ($p < 0.001$) also showed a significant increase over time. On the other hand, HC participants with ICDs ($p < 0.001$) or any other behavior ($p = 0.014$) demonstrated a significant longitudinal decrease in the proportion (Table 2). However, there were too few HC participants with DDS to perform a longitudinal analysis on this group. Additionally, the rates of change in ICDs or any other behavior over time differed significantly between the PD and HC groups.

Regarding specific symptoms, the proportion of PD participants with PG ($p < 0.001$), HS ($p < 0.001$), CB ($p < 0.001$), BE ($p < 0.001$), or excessive hobbyism ($p < 0.001$) also significantly increased over time. Conversely, HC participants with HS ($p = 0.003$), CB ($p = 0.012$), BE ($p < 0.001$), or excessive hobbyism ($p = 0.038$) demonstrated a significant longitudinal decrease in the proportion (Table 2). Additionally, the rates of change in PG, HS, CB, BE, excessive

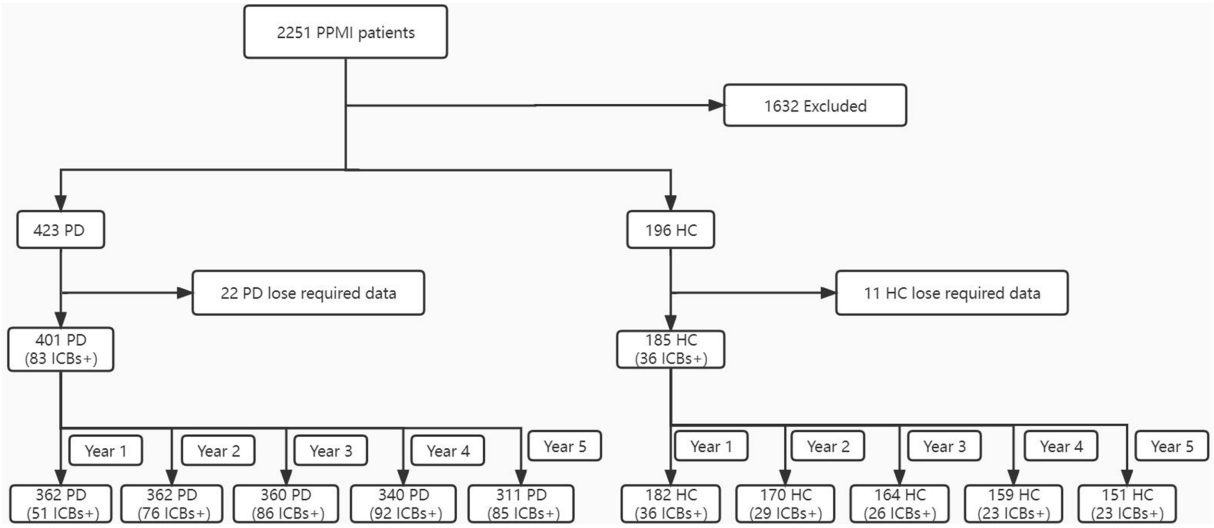

FIGURE 1
Flowchart of the participant selection. ICBs, impulse control behaviours; PD, Parkinson disease; HC, healthy controls; PPMI, Parkinson's Progression Markers Initiative.

hobbyism, or punding over time differed significantly between the PD and HC groups.

Regarding clinical subtypes, the proportion of PD participants with one ICB ($p = 0.033$) or multiple ICBs ($p < 0.001$) significantly increased over time. Conversely, HC participants with one ICB ($p = 0.019$) or multiple ICBs ($p = 0.024$) demonstrated a significant longitudinal decrease in the proportion (Table 2). Additionally, the rates of change in the percentage of one ICB or multiple ICBs over time differed significantly between the PD and HC groups.

3.2. Longitudinal assessment of impulse control behaviours in PD

The demographic characteristics and PD characteristics of participants with PD who had ICBs at baseline ($n = 83$) and those without ICBs ($n = 318$) are presented in Table 1. There were no significant differences in terms of demographics between the PD participants with and without ICBs.

The motor and non-motor characteristics of participants with PD with and without ICBs over the 5-year follow-up period are presented in Table 3. At each time point, subjects with ICBs had higher scores on part I of the MDS-UPDRS, which assesses neuropsychiatric and non-motor symptoms. They were also more likely to have worse scores on part II, which evaluates patient-completed experiences of daily living. However, there were no significant differences in part III of the MDS-UPDRS, which measures motor symptoms, or in the Hoehn and Yahr stage between the two groups.

At year 1 only, subjects with ICBs had worse scores on part IV of the MDS-UPDRS, which assesses motor complications. They also had higher tremor scores and were more likely to be affected on the left side. There were no significant differences in clinical subtype or PIGD scores between the two groups.

Regarding the association of ICBs with other NMS, there were no significant differences in activities of daily living, cognition, or RBD between the groups at any time point. However, similar to the baseline findings in this cohort, ICBs were associated with depression, autonomic dysfunction, and anxiety at each time point (Table 3). Although there was no statistical difference in the ESS at baseline, subjects with ICBs had worse ESS scores over the next 5 years (Table 3).

Regarding dopaminergic therapy, subjects with ICBs had higher total LEDD at year 3 only, but there were no significant differences in the LEDD subtotal for dopamine agonists or non-dopamine agonists between the groups at any time point (Table 4). Regarding the use of specific drug types, subjects with ICBs had a higher frequency of Dopamine agonist use at year 3 and 4, as well as a higher frequency of MAO-B inhibitor use at year 3. However, there were no significant differences in the use of Levodopa, entacapone, amantadine, or anticholinergic drugs between the groups at any time point (Table 4).

Regarding presynaptic dopaminergic dysfunction as measured by DaT scan in relation to clinical symptoms, there were no significant differences in terms of contralateral caudate, ipsilateral caudate, contralateral putamen, or ipsilateral putamen at baseline, year 1, 2, and 4 (Table 5). However, data for year 3 and 5 were not yet available at the time of data access.

Regarding biological data, there were also no significant differences between groups in CSF biomarkers, serum urate, or neurofilament light (NfL) at baseline and year 1 (Table 6). However, data for year 2–5 were not yet available at the time of data access.

3.3. Cox regression analysis of individual risk factors of ICBs in PD subjects from baseline to year 5

To determine the baseline demographic, clinical, biological, imaging, and pharmacological variables that predict the incident development of ICBs over time, we evaluated the 318 participants with

10.3389/fneur.2023.1275170

TABLE 1 Baseline demographics and PD characteristic.

Variable	PD subjects			HCs subjects	*p* Value	*p* Value
	n = 423	PD ICBs+ *n* = 87	PD ICBs– *n* = 335	*n* = 196	(PDvs HC)	(ICBs + *vs* –)
QUIP-S					0.616	N/A
Positive (≥1)	87 (20.62%)	N/A	N/A	37 (18.88%)		
Negative (<1)	335 (79.38%)	N/A	N/A	159 (81.12%)		
Missing	1	N/A	N/A	0		
Gender					0.771	0.779
Male	277 (65.48%)	56 (64.37%)	221 (65.97%)	126 (64.29%)		
Female	146 (34.52%)	31 (35.63%)	114 (34.03%)	70 (35.71%)		
Missing	0	0	0	0		
Age (years)					0.319	0.284
Mean (SD)	61.69 (9.72)	60.66 (10.33)	61.91 (9.52)	60.81 (11.23)		
(Min, Max)	(34.00, 85.00)	(36.00, 83.00)	(34.00, 85.00)	(31.00, 84.00)		
Missing	0	0	0	0		
Age at PD onset (years)					N/A	0.225
Mean (SD)	59.70 (9.98)	58.51 (10.94)	59.96 (9.68)	N/A		
(Min, Max)	(25.00, 83.00)	(25.00, 81.00)	(30.00, 83.00)	N/A		
Missing	0	0	0	N/A		
Disease duration (month)					N/A	0.602
Mean (SD)	6.57 (6.49)	6.85 (7.01)	6.44 (6.31)	N/A		
(Min, Max)	(0.00, 36.00)	(1.00, 36.00)	(0.00, 35.00)	N/A		
Missing	0	0	0	N/A		
Education (years)					0.057	0.480
Mean (SD)	15.56 (2.97)	15.36 (2.79)	15.61 (3.02)	16.04 (2.89)		
(Min, Max)	(5.00, 26.00)	(5.00, 20.00)	(5.00, 26.00)	(8.00, 24.00)		
Missing	0	0	0	0		
Family history of PD					<0.001	0.522
Family members w/PD	103 (24.41%)	19 (21.84%)	84 (25.15%)	10 (5.10%)		
No family members w/PD	319 (75.59%)	68 (78.16%)	250 (74.85%)	186 (94.90%)		
Missing	1	0	1	0		
MDS-UDPRS part I					<0.001	<0.001
Mean (SD)	5.57 (4.07)	7.38 (4.09)	5.10 (3.93)	2.95 (2.96)		
(Min, Max)	(0.00, 24.00)	(1.00, 18.00)	(0.00, 24.00)	(0.00, 17.00)		
Missing	1	0	0	1		
MDS-UDPRS part II					<0.001	0.043
Mean (SD)	5.90 (4.19)	6.71 (4.23)	5.69 (4.16)	0.46 (1.02)		
(Min, Max)	(0.00, 22.00)	(1.00, 18.00)	(0.00, 22.00)	(0.00, 6.00)		
Missing	1	0	0	1		
MDS-UDPRS part III					<0.001	0.105
Mean (SD)	20.89 (8.85)	19.51 (7.65)	21.24 (9.12)	1.21 (2.20)		
(Min, Max)	(4.00, 51.00)	(6.00, 41.00)	(4.00, 51.00)	(0.00, 13.00)		
Missing	0	0	0	2		
H&Y					<0.001	0.620
Stage 0	0 (0.00%)	0 (0.00%)	0 (0.00%)	193 (98.97%)		

(Continued)

TABLE 1 (Continued)

Variable	PD subjects			HCs subjects	*p* Value	*p* Value
	n = 423	PD ICBs+ *n* = 87	PD ICBs– *n* = 335	*n* = 196	(PDvs HC)	(ICBs + *vs* –)
Stage 1	185 (43.74%)	42 (48.28%)	143 (42.69%)	2 (1.03%)		
Stage 2	236 (55.79%)	45 (51.72%)	190 (56.72%)	0 (0.00%)		
Stage 3–5	2 (0.47%)	0 (0.00%)	2 (0.60%)	0 (0.00%)		
Missing	0	0	0	1		
PD clinical subtype					N/A	0.484
TD	299 (70.85%)	59 (67.82%)	240 (71.64%)	N/A		
Non-TD	123 (29.85%)	28 (32.18%)	95 (28.36%)	N/A		
Missing	1	0	0	N/A		
Tremor score					<0.001	0.915
Mean (SD)	0.49 (0.32)	0.49 (0.29)	0.49 (0.32)	0.03 (0.08)		
(Min, Max)	(0.00, 1.82)	(0.00, 1.64)	(0.00, 1.82)	(0.00, 0.64)		
Missing	1	0	0	2		
PIGD score					<0.001	0.921
Mean (SD)	0.23 (0.22)	0.22 (0.21)	0.23 (0.23)	0.02 (0.09)		
(Min, Max)	(0.00, 1.40)	(0.00, 1.00)	(0.00, 1.40)	(0.00, 0.08)		
Missing	1	0	0	1		
Side most affected					N/A	0.252
Left	179 (42.32%)	32 (36.78%)	146 (43.58%)	N/A		
Non-Left	244 (57.68%)	55 (63.22%)	189 (56.42%)	N/A		
Missing	0	0	0	N/A		
MoCA					<0.001	0.341
Mean (SD)	27.14 (2.32)	26.89 (2.33)	27.16 (2.31)	28.23 (1.11)		
(Min, Max)	(17.00, 30.00)	(20.00, 30.00)	(17.00, 30.00)	(26.00, 30.00)		
Missing	0	0	0	0		

PD, Parkinson disease; HC, healthy controls; MDS-UPDRS, Movement Disorders Society-Unified Parkinson's Disease Rating Scale; H&Y, Hoehn and Yahr; PIGD, Postural instability Gait Disorder; TD, tremor dominant; S&E, Modified Schwab and England Activities of Daily Living Scale; MoCA, Montreal Cognitive Assessment.

PD in this cohort who did not have ICBs at baseline. Among them, 116 participants (36.5%) subsequently developed ICBs. Results based on in-sample concordance and cross-validated prediction accuracy revealed that the best model included three variables: STAI-state subscore, RBD, and p-tau (Table 7; Supplementary Table S1). Additionally, estimated survival probabilities from the multivariate Cox regression models were obtained and are presented in Figures 3, 4.

4. Discussion

This international, multicenter study represents the largest reported longitudinal investigation of the incidence of ICBs and its associated clinical, imaging, and biological characteristics in patients with *de novo*, untreated PD at baseline. Furthermore, to our knowledge, this is the only study that has examined the association between biologics and ICBs in patients with PD. At baseline, there were no differences in the prevalence of ICBs between untreated patients with PD and HC. However, over time, the occurrence of ICBs increased among patients with PD while decreasing among HC. These findings are consistent with previous longitudinal studies that have examined ICBs in PD (11, 14, 21). In the PD cohort, there were notable differences in symptoms, particularly in non-motor symptoms, between patients with and without ICBs. This finding indicates that, in early untreated PD, the development of ICBs is influenced by factors beyond the presence of PD-related pathology alone. These factors may encompass various biological variables that affect neurochemical, neural network, and psychological systems as the disease advances, as well as clinical variables that impact disease progression, particularly the use of dopaminergic medications (2). In this study, we provide a thorough and systematic examination of the longitudinal changes in clinical and biological factors associated with PD-ICBs over a 5-year period. Additionally, we analyze the baseline clinical and biological predictors of ICB development in PD. The results obtained yield several intriguing insights into the pathophysiology of ICBs in PD.

Given that there are dynamic changes in ICBs in PD patients over the course of the observation, this is similar to other nonmotor symptoms of PD, which may disappear or recur. Supplementary Table S2 shows the data on the fluctuation of ICBs that

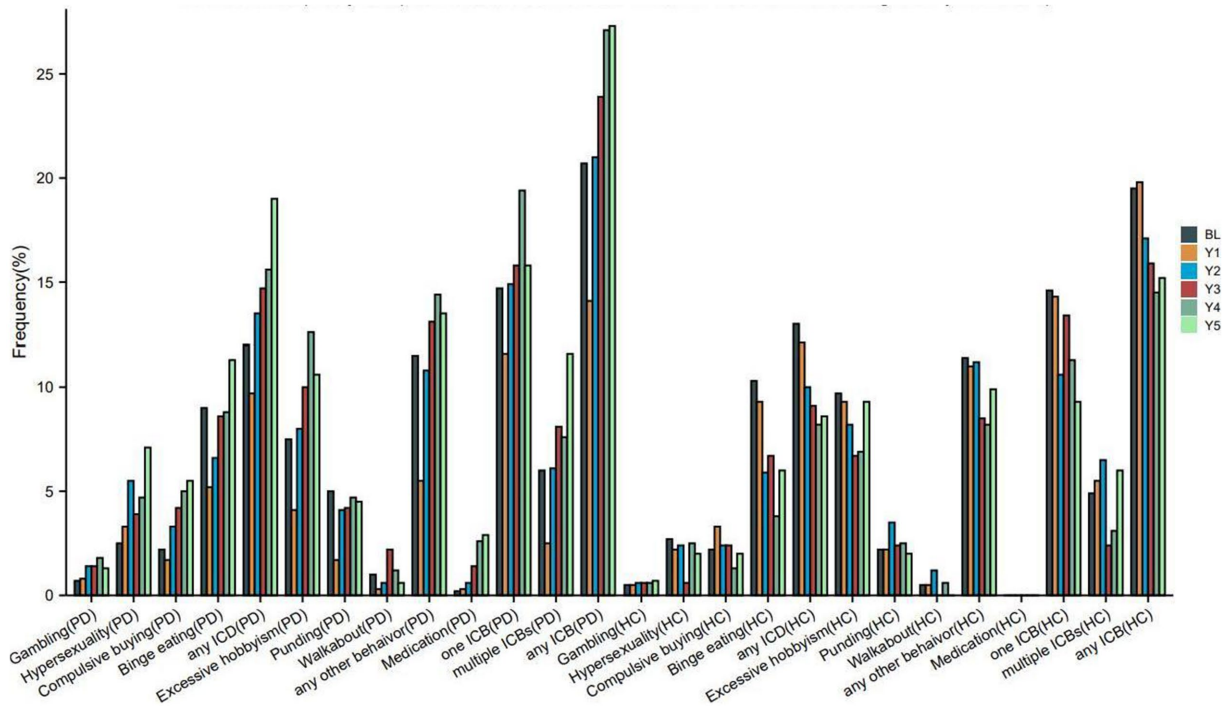

FIGURE 2
Frequency of impulse control behaviours in PD and HC at baseline and during the 5-years follow up. PD, Parkinson disease; HC, healthy controls; ICBs, Impulse control behaviours; ICD, impulse control disorders; BL, baseline; Y1, year 1; Y2, year 2; Y3, year 3; Y4, year 4; Y5, year 5. Each instance of ICB consists of a single ICB as well as cases where it coexists with other ICBs. For example, as long as that patient has gambling that patient is in the Gambling group, whether or not that patient combines other ICBs.

we observed. We could find that the percentage of persistent ICBs+ ranged from 52.9% to 84.7% from the first to the fifth year, accounting for more than half of the cases. We recognize that therapeutic interventions and changes in a patient's clinical course can affect their ICBs status over time.

In our cohort, demographic factors such as age, sex, education, and family history of PD, as well as disease characteristics including age of PD onset, disease duration, and severity of motor disability, were not found to be significant predictors of ICBs at baseline. This is in contrast to a previous cross-sectional study that identified male gender and younger age at onset of PD as risk factors for ICBs. The discrepancy in findings could be attributed to differences in study design, sample size, or other factors that may influence the development of ICBs in PD. Given this, we revisited the role of gender in our analysis after categorizing the dataset according to the classification of early-onset Parkinson's disease (EOPD). That is, we performed a subgroup analysis of the dataset, taking into account the EOPD± classification. Interestingly, we observed no significant gender differences from baseline to year 5 in the EOPD+ subgroup, whether patients had ICBs or not. In contrast, within the EOPD− subgroup, it was only in the fifth year that the proportion of men in the ICBs+ group surpassed that in the ICBs− group (Supplementary Table S3). This suggests that the impact of gender on the occurrence of ICBs in non-EOPD patients may become more pronounced in the later stages of the disease, although further validation is required. Further research is needed to better understand the complex interplay of these factors in relation to ICBs in PD (15).

We speculate that the lack of significant association between ICBs and motor impairment measured in Part III of the MDS-UPDRS or other disease characteristics (such as H&Y stage, motor complications, clinical subtype, tremor score, PIGD score, and side most affected) may be due to the early stage of PD in our cohort and the possibility of interactions arising during disease progression or drug interventions. These factors were also not reported as significant predictors of ICBs in previous studies. However, we observed significant associations between ICBs and the neuro-psychiatric and non-motor symptoms assessed in Part I and the patient-reported experiences of daily living assessed in Part II of the MDS-UPDRS. This is not surprising, as previous studies have identified numerous non-motor symptoms as risk factors for ICBs in PD. These findings suggest that non-motor symptoms captured in Part I and Part II of the MDS-UPDRS may play a more prominent role in the development of ICBs in early-stage PD patients (3, 15, 16, 38). Considering that patients with EOPD may be more prone to the development of dyskinesia (39), we made the necessary distinction between two further distinct categories: EOPD+ (age at PD onset ≤50) and EOPD− (age at PD onset >50) (Supplementary Table S4). Our analysis revealed a higher percentage of EOPD+ individuals in the first year among patients with ICB+, whereas no significant difference was observed in the subsequent 4 years. This observation may also explain why the MDS-UPDRS Part IV scores were higher in the first year for patients with ICBs+ and then declined in the subsequent 4 years.

Our findings, in line with previous research, support the association between ICBs and anxiety in PD (38). This result is

TABLE 2 Impulse control behaviours over time in PD and HC.

Variable	Patients with PD							HC							*p* Values	
	BL *n* = 401	Year 1 *n* = 362	Year 2 *n* = 362	Year 3 *n* = 360	Year 4 *n* = 340	Year 5 *n* = 311	*p* Value (change over time)	BL *n* = 185	Year 1 *n* = 182	Year 2 *n* = 170	Year 3 *n* = 164	Year 4 *n* = 159	Year 5 *n* = 151	*p* Value (change over time)	Group × visit interaction	PD *vs* HC
ICBs							<0.001							0.005	<0.001	N/A[a]
Positive	83 (20.7%)	51 (14.1%)	76 (21.0%)	86 (23.9%)	92 (27.1%)	85 (27.3%)		36 (19.5%)	36 (19.8%)	29 (17.1%)	26 (15.9%)	23 (14.5%)	23 (15.2%)			
Negative	318 (79.3%)	311 (85.9%)	286 (79.0%)	274 (76.1%)	248 (72.9%)	226 (72.7%)		149 (80.5%)	146 (80.2%)	141 (82.9%)	138 (84.1%)	136 (85.5%)	128 (84.8%)			
ICDs							<0.001							<0.001	<0.001	N/A[a]
Positive	48 (12.0%)	35 (9.7%)	49 (13.5%)	53 (14.7%)	53 (15.6%)	59 (19.0%)		24 (13.0%)	22 (12.1%)	17 (10.0%)	15 (9.1%)	13 (8.2%)	13 (8.6%)			
Negative	353 (88.0%)	327 (90.3%)	313 (86.5%)	307 (85.3%)	287 (84.4%)	252 (81.0%)		161 (87.0%)	160 (87.9%)	153 (90.0%)	149 (90.9%)	146 (91.8%)	138 (91.4%)			
Other behaivors							<0.001							0.014	<0.001	N/A[a]
Positive	46 (11.5%)	20 (5.5%)	39 (10.8%)	47 (13.1%)	49 (14.4%)	42 (13.5%)		21 (11.4%)	20 (11.0%)	19 (11.2%)	14 (8.5%)	13 (8.2%)	15 (9.9%)			
Negative	355 (88.5%)	342 (94.5%)	323 (89.2%)	313 (86.9%)	291 (85.6%)	269 (86.5%)		164 (88.6%)	162 (89.0%)	151 (88.8%)	150 (91.5%)	146 (91.8%)	136 (90.1%)			
DDS							<0.001							NA[b]	NA[b]	NA[b]
Positive	1 (0.2%)	1 (0.3%)	2 (0.6%)	5 (1.4%)	9 (2.6%)	9 (2.9%)		0 (0.0%)	0 (0.0%)	0 (0.0%)	0 (0.0%)	0 (0.0%)	0 (0.0%)			
Negative	400 (99.8%)	361 (99.7%)	360 (99.4%)	355 (98.6%)	331 (97.4%)	302 (97.1%)		185 (100.0%)	182 (100.0%)	170 (100.0%)	164 (100.0%)	159 (100.0%)	151 (100.0%)			
Pathological gambling							<0.001							0.861	<0.001	N/A[a]
Positive	3 (0.7%)	3 (0.8%)	5 (1.4%)	5 (1.4%)	6 (1.8%)	4 (1.3%)		1 (0.5%)	1 (0.5%)	1 (0.6%)	1 (0.6%)	1 (0.6%)	1 (0.7%)			
Negative	398 (99.3%)	359 (99.2%)	357 (98.6%)	355 (98.6%)	334 (98.2%)	307 (98.7%)		184 (99.5%)	181 (99.5%)	169 (99.4%)	163 (99.4%)	158 (99.4%)	150 (99.3%)			
Hypersexuality							<0.001							0.003	<0.001	N/A[a]
Positive	10 (2.5%)	12 (3.3%)	20 (5.5%)	14 (3.9%)	16 (4.7%)	22 (7.1%)		5 (2.7%)	4 (2.2%)	4 (2.4%)	1 (0.6%)	4 (2.5%)	3 (2.0%)			
Negative	391 (97.5%)	350 (96.7%)	342 (94.5%)	346 (96.1%)	324 (95.3%)	289 (92.9%)		180 (97.3%)	178 (97.8%)	166 (97.6%)	163 (99.4%)	155 (97.5%)	148 (98.0%)			
Compulsive buying							<0.001							0.012	<0.001	N/A[a]

(Continued)

10.3389/fneur.2023.1275170

TABLE 2 (Continued)

Variable	Patients with PD							HC							*p* Values	
	BL *n* = 401	Year 1 *n* = 362	Year 2 *n* = 362	Year 3 *n* = 360	Year 4 *n* = 340	Year 5 *n* = 311	*p* Value (change over time)	BL *n* = 185	Year 1 *n* = 182	Year 2 *n* = 170	Year 3 *n* = 164	Year 4 *n* = 159	Year 5 *n* = 151	*p* Value (change over time)	Group × visit interaction	PD *vs* HC
Positive	9 (2.2%)	6 (1.7%)	12 (3.3%)	15 (4.2%)	17 (5.0%)	17 (5.5%)		4 (2.2%)	6 (3.3%)	4 (2.4%)	4 (2.4%)	2 (1.3%)	3 (2.0%)			
Negative	392 (97.8%)	356 (98.3%)	350 (96.7%)	345 (95.8%)	323 (95.0%)	294 (94.5%)		181 (97.8%)	176 (96.7%)	166 (97.6%)	160 (97.6%)	157 (98.7%)	148 (98.0%)			
Binge eating							<0.001							<0.001	<0.001	N/A[a]
Positive	36 (9.0%)	19 (5.2%)	24 (6.6%)	31 (8.6%)	30 (8.8%)	35 (11.3%)		19 (10.3%)	17 (9.3%)	10 (5.9%)	11 (6.7%)	6 (3.8%)	9 (6.0%)			
Negative	365 (91.0%)	343 (94.8%)	338 (93.4%)	329 (91.4%)	310 (91.2%)	276 (88.7%)		166 (89.7%)	165 (90.7%)	160 (94.1%)	153 (93.3%)	153 (96.2%)	142 (94.0%)			
Excessive hobbyism							<0.001							0.038	<0.001	N/A[a]
Positive	30 (7.5%)	15 (4.1%)	29 (8.0%)	36 (10.0%)	43 (12.6%)	33 (10.6%)		18 (9.7%)	17 (9.3%)	14 (8.2%)	11 (6.7%)	11 (6.9%)	14 (9.3%)			
Negative	371 (92.5%)	347 (95.9%)	333 (92.0%)	324 (90.0%)	297 (87.4%)	278 (89.4%)		167 (90.3%)	165 (90.7%)	156 (91.8%)	153 (93.3%)	148 (93.1%)	137 (90.7%)			
Punding							0.069							0.073	0.030	N/A[a]
Positive	20 (5.0%)	6 (1.7%)	15 (4.1%)	15 (4.2%)	16 (4.7%)	14 (4.5%)		4(2.2%)	4(2.2%)	6(3.5%)	4(2.4%)	4(2.5%)	3(2.0%)			
Negative	381 (95.0%)	356 (98.3%)	347 (95.9%)	345 (95.8%)	324 (95.3%)	297 (95.5%)		181(97.8%)	178(97.8%)	164(96.5%)	160(97.6%)	155(97.5%)	148(98.0%)			
Walkabout							0.595							1.000	0.400	0.212
Positive	4 (1.0%)	1 (0.3%)	2 (0.6%)	8 (2.2%)	4 (1.2%)	2 (0.6%)		1 (0.5%)	1 (0.5%)	2 (1.2%)	0 (0.0%)	1 (0.6%)	0 (0.0%)			
Negative	397 (99.0%)	361 (99.7%)	360 (99.4%)	352 (97.8%)	336 (98.8%)	309 (99.4%)		184 (99.5%)	181 (99.5%)	168 (98.8%)	164 (100.0%)	158 (99.4%)	151 (100.0%)			
Clinical subtypes																
One ICB	59 (14.7%)	42 (11.6%)	54 (14.9%)	57 (15.8%)	66 (19.4%)	49 (15.8%)	0.033	27 (14.6%)	26 (14.3%)	18 (10.6%)	22 (13.4%)	18 (11.3%)	14 (9.3%)	0.019	0.003	N/A[a]
Multiple ICBs	24 (6.0%)	9 (2.5%)	22 (6.1%)	29 (8.1%)	26 (7.6%)	36 (11.6%)	<0.001	9 (4.9%)	10 (5.5%)	11 (6.5%)	4 (2.4%)	5 (3.1%)	9 (6.0%)	0.024	<0.001	N/A[a]
Negative	318 (79.3%)	311 (85.9%)	286 (79.0%)	274 (76.1%)	248 (72.9%)	226 (72.7%)		149 (80.5%)	146 (80.2%)	141 (82.9%)	138 (84.1%)	136 (85.5%)	128 (84.8%)			

PD, Parkinson disease; HC, healthy controls; ICBs, Impulse control behaviours; ICD, impulse control disorders; DDS, dopamine dysregulation syndrome.

[a]PD versus HC comparison is not applicable if test of interaction was significant.

[b]There were not enough positive results in the HC group to run analysis.

10.3389/fneur.2023.1275170

TABLE 3 PD motor and non-motor characteristics over time by ICBs status.

Variable	Baseline			Year 1			Year 2			Year 3			Year 4			Year 5		
	PD ICBs+ *n* = 83	PD ICBs− *n* = 318	*p* Value	PD ICBs+ *n* = 51	PD ICBs− *n* = 311	*p* Value	PD ICBs+ *n* = 76	PD ICBs− *n* = 286	*p* Value	PD ICBs+ *n* = 86	PD ICBs− *n* = 274	*p* Value	PD ICBs+ *n* = 92	PD ICBs− *n* = 248	*p* Value	PD ICBs+ *n* = 85	PD ICBs− *n* = 226	*p* Value
MDS-UDPRS part I			<0.001			0.014			0.006			0.001			0.004			0.001
Mean (SD)	7.16 (3.93)	5.03 (3.94)		8.29 (5.33)	6.56 (4.54)		9.07 (4.69)	7.29 (5.09)		10.35 (6.96)	7.68 (4.72)		10.50 (6.29)	8.49 (5.49)		11.34 (6.59)	8.47 (5.62)	
(Min, Max)	(1.00, 18.00)	(0.00, 24.00)		(0.00, 29.00)	(0.00, 27.00)		(0.00, 26.00)	(0.00, 25.00)		(0.00, 36.00)	(0.00, 25.00)		(0.00, 29.00)	(0.00, 30.00)		(1.00, 34.00)	(0.00, 31.00)	
Missing	0	0		0	0		0	0		0	0		0	0		0	0	
MDS-UDPRS part II			0.032			0.021			0.104			0.011			0.020			0.004
Mean (SD)	6.70 (4.27)	5.60 (4.12)		8.86 (5.81)	7.14 (4.74)		8.91 (5.58)	7.79 (5.20)		10.24 (5.86)	8.47 (5.55)		11.15 (7.40)	9.29 (6.14)		11.76 (6.38)	9.36 (6.54)	
(Min, Max)	(1.00, 18.00)	(0.00, 22.00)		(0.00, 30.00)	(0.00, 25.00)		(0.00, 23.00)	(0.00, 27.00)		(0.00, 29.00)	(0.00, 29.00)		(1.00, 37.00)	(0.00, 35.00)		(1.00, 31.00)	(0.00, 40.00)	
Missing	0	0		0	1		1	1		0	0		1	0		0	0	
MDS-UDPRS part III			0.197			0.444			0.792			0.841			0.709			0.820
Mean (SD)	19.70 (7.73)	21.11 (9.10)		25.53 (12.13)	24.12 (9.97)		27.41 (13.28)	26.96 (10.84)		28.74 (11.46)	28.43 (12.37)		31.11 (12.58)	30.51 (12.38)		30.10 (12.49)	30.49 (13.77)	
(Min, Max)	(6.00, 41.00)	(4.00, 51.00)		(4.00, 56.00)	(2.00, 60.00)		(6.00, 68.00)	(3.00, 59.00)		(4.00, 57.00)	(4.00, 80.00)		(6.00, 63.00)	(6.00, 80.00)		(7.00, 66.00)	(3.00, 90.00)	
Missing	0	0		2	24		6	29		5	29		8	27		1	16	
MDS-UDPRS part IV			NA			0.029			0.423			0.516			0.577			0.282
Mean (SD)	NA	NA		0.94 (1.69)	0.25 (0.97)		0.52 (1.34)	0.72 (1.85)		0.87 (1.77)	1.04 (2.00)		1.42 (2.54)	1.61 (2.66)		1.83 (3.02)	2.24 (2.93)	
(Min, Max)				(0.00, 5.00)	(0.00, 7.00)		(0.00, 6.00)	(0.00, 11.00)		(0.00, 6.00)	(0.00, 11.00)		(0.00, 13.00)	(0.00, 12.00)		(0.00, 16.00)	(0.00, 17.00)	
Missing				18	127		14	42		9	19		7	10		2	12	
H&Y			0.762			0.874			0.169			0.660			0.888			0.969
Stage 0	0 (0.00%)	0 (0.00%)		0 (0.00%)	1 (0.35%)		1 (1.43%)	0 (0.00%)		0 (0.00%)	1 (0.41%)		0 (0.00%)	1 (0.45%)		0 (0.00%)	0 (0.00%)	

(Continued)

10.3389/fneur.2023.1275170

TABLE 3 (Continued)

Variable	Baseline			Year 1			Year 2			Year 3			Year 4			Year 5		
	PD ICBs+ *n* = 83	PD ICBs– *n* = 318	*p* Value	PD ICBs+ *n* = 51	PD ICBs– *n* = 311	*p* Value	PD ICBs+ *n* = 76	PD ICBs– *n* = 286	*p* Value	PD ICBs+ *n* = 86	PD ICBs– *n* = 274	*p* Value	PD ICBs+ *n* = 92	PD ICBs– *n* = 248	*p* Value	PD ICBs+ *n* = 85	PD ICBs– *n* = 226	*p* Value
Stage 1	39 (46.99%)	138 (43.40%)		14 (28.57%)	83 (28.72%)		13 (18.57%)	65 (25.19%)		13 (16.05%)	48 (19.59%)		13 (15.29%)	32 (14.48%)		9 (10.72%)	22 (10.38%)	
Stage 2	44 (53.01%)	178 (55.97%)		34 (69.39%)	193 (66.78%)		51 (72.86%)	181 (70.16%)		64 (79.01%)	177 (72.24%)		64 (75.29%)	163 (73.76%)		68 (80.95%)	174 (82.07%)	
Stage 3–5	0 (0.00%)	2 (0.63%)		1 (2.04%)	12 (4.15%)		5 (7.14%)	12 (4.65%)		4 (4.94%)	19 (7.76%)		8(9.41%)	25 (11.31%)		7 (8.33%)	16 (7.55%)	
Missing	0	0		2	22		6	28		5	29		7	27		1	14	
PD clinical subtype			0.523			0.328			0.062			0.132			0.334			0.207
TD	56 (67.47%)	226 (71.07%)		35 (71.43%)	185 (64.24%)		39 (55.71%)	174 (67.70%)		42 (55.56%)	159 (64.90%)		54 (63.53%)	127 (57.47%)		42 (50.00%)	122 (58.10%)	
non-TD	27 (32.53%)	92 (28.93%)		14 (28.57%)	103 (35.76%)		31 (44.29%)	83 (32.30%)		36 (45.44%)	86 (35.10%)		31 (36.47%)	94 (42.53%)		42 (50.00%)	88 (41.90%)	
Missing	0	0		2	23		6	29		5	29		7	27		1	16	
Tremor score			0.981			0.043			0.611			0.418			0.540			0.449
Mean (SD)	0.49 (0.29)	0.49 (0.32)		0.65 (0.43)	0.53 (0.37)		0.56 (0.46)	0.59 (0.42)		0.57 (0.42)	0.62 (0.45)		0.68 (0.48)	0.65 (0.47)		0.59 (0.45)	0.63 (0.46)	
(Min, Max)	(0.00, 1.64)	(0.00, 1.82)		(0.00, 2.00)	(0.00, 1.55)		(0.00, 2.18)	(0.00, 2.45)		(0.00, 1.82)	(0.00, 2.27)		(0.00, 1.73)	(0.00, 2.09)		(0.00, 1.82)	(0.00, 2.09)	
Missing	0	0		2	20		6	28		5	29		7	27		1	14	
PIGD score			0.985			0.781			0.220			0.551			0.726			0.357
Mean (SD)	0.23 (0.22)	0.23 (0.23)		0.32 (0.25)	0.31 (0.31)		0.40 (0.46)	0.34 (0.36)		0.43 (0.36)	0.40 (0.45)		0.47 (0.41)	0.49 (0.52)		0.51 (0.49)	0.52 (0.56)	
(Min, Max)	(0.00, 1.00)	(0.00, 1.40)		(0.00, 1.00)	(0.00, 1.80)		(0.00, 3.00)	(0.00, 2.60)		(0.00, 2.40)	(0.00, 3.00)		(0.00, 1.80)	(0.00, 3.40)		(0.00, 4.00)	(0.00, 3.60)	
Missing	0	0		2	23		6	29		5	29		7	27		1	14	
Side most affected			0.488			0.021			0.148			0.308			0.179			0.243
Left	32 (38.55%)	136 (42.77%)		14 (27.45%)	139 (44.69%)		27 (35.53%)	128 (44.76%)		32 (37.21%)	119 (43.43%)		33 (35.87%)	109 (43.95%)		31 (36.47%)	99 (43.81%)	

(Continued)

10.3389/fneur.2023.1275170

TABLE 3 (Continued)

Variable	Baseline			Year 1			Year 2			Year 3			Year 4			Year 5		
	PD ICBs+ *n* = 83	PD ICBs− *n* = 318	*p* Value	PD ICBs+ *n* = 51	PD ICBs− *n* = 311	*p* Value	PD ICBs+ *n* = 76	PD ICBs− *n* = 286	*p* Value	PD ICBs+ *n* = 86	PD ICBs− *n* = 274	*p* Value	PD ICBs+ *n* = 92	PD ICBs− *n* = 248	*p* Value	PD ICBs+ *n* = 85	PD ICBs− *n* = 226	*p* Value
non-Left	51 (61.45%)	182 (57.23%)		37 (72.55%)	172 (55.31%)		49 (64.47%)	158 (55.24%)		54 (62.79%)	155 (56.57%)		59 (64.13%)	139 (56.05%)		54 (63.53%)	127 (56.19%)	
Missing	0	0		0	0		0	0		0	0		0	0		0	0	
S&E			0.557			0.700			0.150			0.821			0.480			0.141
Mean (SD)	93.55 (5.50)	93.13 (5.96)		91.00 (5.35)	90.61 (6.81)		87.53 (6.70)	89.04 (8.35)		87.53 (8.08)	87.76 (8.02)		86.41 (9.03)	85.57 (10.03)		83.35 (11.94)	85.51 (11.29)	
(Min, Max)	(70.00, 100.00)	(75.00, 100.00)		(80.00, 100.00)	(70.00, 100.00)		(70.00,100.00)	(60.00, 100.00)		(50.00, 100.00)	(60.00, 100.00)		(50.00, 100.00)	(30.00, 100.00)		(20.00, 100.00)	(20.00, 100.00)	
Missing	0	0		1	0		1	0		1	0		0	2		0	0	
MoCA			0.341			0.804			0.785			0.981			0.980			0.337
Mean (SD)	26.89 (2.33)	27.16 (2.31)		26.47 (2.66)	26.31 (2.84)		26.13 (3.05)	26.24 (3.19)		26.36 (3.20)	26.36 (3.07)		26.45 (3.78)	26.46 (3.39)		26.89 (2.79)	26.47 (3.69)	
(Min, Max)	(20.00, 30.00)	(17.00, 30.00)		(20.00, 30.00)	(15.00, 30.00)		(16.00, 30.00)	(9.00, 30.00)		(15.00, 30.00)	(13.00, 30.00)		(11.00, 30.00)	(11.00, 30.00)		(17.00, 30.00)	(2.00, 30.00)	
Missing	0	0		0	1		0	2		1	1		1	3		1	1	
GDS			<0.001			0.010			0.004			0.001			0.003			<0.001
Mean (SD)	3.23 (2.53)	2.08 (2.40)		3.55 (3.20)	2.42 (2.85)		3.53 (2.98)	2.44 (2.84)		3.49 (2.97)	2.36 (2.75)		3.47 (3.25)	2.32 (2.61)		3.74 (3.02)	2.39 (2.52)	
(Min, Max)	(0.00, 11.00)	(0.00, 14.00)		(0.00, 15.00)	(0.00, 14.00)		(0.00, 14.00)	(0.00, 15.00)		(0.00, 13.00)	(0.00, 14.00)		(0.00, 15.00)	(0.00, 15.00)		(0.00, 11.00)	(0.00, 13.00)	
Missing	0	0		0	1		0	2		0	0		0	0		0	0	
STAI—state subscore			0.005			0.429			0.005			0.016			0.002			<0.001
Mean (SD)	35.77 (10.25)	32.20 (10.17)		33.48 (9.07)	32.28 (10.06)		35.54 (9.61)	31.87 (10.16)		34.38 (10.05)	31.41 (9.83)		34.90 (10.49)	31.21 (9.49)		35.88 (10.49)	30.55 (9.26)	
(Min, Max)	(20.00, 64.00)	(20.00, 76.00)		(20.00, 53.00)	(20.00, 69.00)		(20.00, 60.00)	(20.00, 76.00)		(20.00, 68.00)	(20.00, 71.00)		(20.00, 63.00)	(20.00, 73.00)		(20.00, 70.00)	(20.00, 75.00)	
Missing	0	2		1	0		0	2		0	3		0	1		0	1	
STAI—trait subscore			<0.001			0.004			<0.001			0.001			<0.001			<0.001

(Continued)

10.3389/fneur.2023.1275170

TABLE 3 (Continued)

Variable	Baseline			Year 1			Year 2			Year 3			Year 4			Year 5		
	PD ICBs+ *n* = 83	PD ICBs– *n* = 318	*p* Value	PD ICBs+ *n* = 51	PD ICBs– *n* = 311	*p* Value	PD ICBs+ *n* = 76	PD ICBs– *n* = 286	*p* Value	PD ICBs+ *n* = 86	PD ICBs– *n* = 274	*p* Value	PD ICBs+ *n* = 92	PD ICBs– *n* = 248	*p* Value	PD ICBs+ *n* = 85	PD ICBs– *n* = 226	*p* Value
Mean (SD)	36.96 (8.91)	31.18 (9.27)		36.34 (9.81)	32.18 (9.44)		36.29 (9.35)	31.69 (9.44)		35.88 (9.31)	31.82 (9.81)		36.89 (10.49)	31.21 (9.28)		37.82 (11.30)	30.78 (8.99)	
(Min, Max)	(23.00, 55.00)	(20.00, 63.00)		(21.00, 58.00)	(20.00, 73.00)		(21.00, 66.00)	(20.00, 66.00)		(22.00, 59.00)	(20.00, 64.00)		(20.00, 62.00)	(20.00, 69.00)		(20.00, 68.00)	(20.00, 75.00)	
Missing	0	1		1	1		1	5		0	3		0	4		0	1	
RBD			0.104			0.091			0.340			0.798			0.458			0.207
Positive (≥5)	36 (44.44%)	110 (34.70%)		11 (21.57%)	104 (33.44%)		32 (42.11%)	103 (36.14%)		36 (41.86%)	119 (43.43%)		44 (47.82%)	107 (43.32%)		34 (40.00%)	108 (48.00%)	
Negative (<5)	45 (55.56%)	207 (65.30%)		40 (78.43%)	207 (66.56%)		44 (57.89%)	182 (63.86%)		50 (58.14%)	155 (56.57%)		48 (52.18%)	140 (56.68%)		51 (60.00%)	117 (52.00%)	
Missing	2	1		0	0		0	0		0	0		0	1		0	1	
ESS			0.057			0.039			0.007			<0.001			0.002			<0.001
Mean (SD)	6.32 (3.31)	5.52 (3.37)		7.27 (4.69)	6.03 (3.87)		7.87 (4.23)	6.42 (4.12)		9.06 (5.12)	6.80 (4.16)		8.75 (5.11)	6.96 (4.41)		9.58 (5.08)	7.06 (4.40)	
(Min, Max)	(1.00, 15.00)	(0.00, 20.00)		(0.00, 21.00)	(0.00, 18.00)		(0.00, 22.00)	(0.00, 23.00)		(2.00, 24.00)	(0.00, 19.00)		(0.00, 24.00)	(0.00, 22.00)		(1.00, 24.00)	(0.00, 24.00)	
Missing	1	0		0	0		0	1		0	3		0	0		0	0	
SCOPA-AUT			<0.001			0.026			<0.001			<0.001			0.003			<0.001
Mean (SD)	12.51 (7.10)	8.53 (5.43)		12.86 (7.95)	10.65 (6.20)		13.96 (7.48)	10.83 (6.13)		15.40 (7.36)	11.50 (6.73)		15.07 (8.65)	12.01 (6.89)		16.92 (9.91)	12.31 (6.86)	
(Min, Max)	(2.00, 39.00)	(0.00, 32.00)		(0.00, 45.00)	(0.00, 39.00)		(3.00, 42.00)	(0.00, 37.00)		(2.00, 30.00)	(0.00, 34.00)		(2.00, 42.00)	(0.00, 39.00)		(1.00, 45.00)	(0.00, 41.00)	
Missing	0	6		1	4		0	3		1	2		0	0		0	0	

PD, Parkinson disease; ICBs, Impulse control behaviours; MDS-UPDRS, Movement Disorders Society-Unified Parkinson's Disease Rating Scale; H&Y, Hoehn and Yahr; PIGD, Postural instability Gait Disorder; TD, tremor dominant; S&E, Modified Schwab and England Activities of Daily Living Scale; MoCA, Montreal Cognitive Assessment; GDS, Geriatric Depression Scale; STAI, State–Trait Anxiety Inventory; ESS, Epworth Sleepiness Scale; RBD, rapid eye movement sleep behaviour disorder; SCOPA-AUT, Scales for Outcomes in Parkinson's Disease-Autonomic; NA, not applicable.

10.3389/fneur.2023.1275170

TABLE 4 Medication use over time by ICBs status.

Variable	Treated at Year 1			Treated at Year 2			Treated at Year 3			Treated at Year 4			Treated at Year 5		
	PD ICBs+ *n* = 51	PD ICBs− *n* = 311	*p* Value	PD ICBs+ *n* = 76	PD ICBs− *n* = 286	*p* Value	PD ICBs+ *n* = 86	PD ICBs− *n* = 274	*p* Value	PD ICBs+ *n* = 92	PD ICBs− *n* = 248	*p* Value	PD ICBs+ *n* = 85	PD ICBs− *n* = 226	*p* Value
Total LEDD			0.480			0.803			0.040			0.899			0.067
Mean (SD)	177.39 (185.24)	203.48 (252.30)		357.42 (265.83)	347.15 (330.90)		563.22 (629.12)	439.30 (433.89)		539.56 (293.67)	532.94 (467.45)		792.68 (1139.88)	622.97 (487.83)	
(Min, Max)	(0.00, 750.00)	(0.00, 1740.00)		(0.00, 1140.00)	(0.00, 2314.20)		(0.00, 5300.00)	(0.00, 5000.00)		(0.00, 1670.00)	(0.00, 5360.00)		(0.00, 10300.00)	(0.00, 5460.00)	
Missing	0	0		0	0		0	0		0	0		0	0	
LEDD subtotal—dopamine agonists			0.348			0.578			0.133			0.726			0.644
Mean (SD)	56.81 (107.55)	41.92 (80.94)		66.43 (86.95)	76.64 (153.40)		129.69 (269.70)	87.83 (209.24)		95.27 (114.06)	104.90 (253.33)		104.52 (176.04)	93.53 (187.17)	
(Min, Max)	(0.00, 450.00)	(0.00, 391.80)		(0.00, 320.00)	(0.00, 1638.00)		(0.00, 2058.00)	(0.00, 2880.00)		(0.00, 450.00)	(0.00, 2880.00)		(0.00, 1460.40)	(0.00, 1396.50)	
Missing	0	0		0	0		0	0		0	0		0	0	
LEDD subtotal—non-dopamine agonists			0.104			0.603			0.152			0.738			0.086
Mean (SD)	120.59 (148.38)	161.56 (244.33)		290.99 (255.30)	270.51 (316.87)		433.53 (600.81)	351.47 (410.54)		444.29 (296.16)	428.05 (427.70)		688.16 (1142.50)	529.44 (481.01)	
(Min, Max)	(0.00, 600.00)	(0.00, 1740.00)		(0.00, 1140.00)	(0.00, 2314.20)		(0.00, 5300.00)	(0.00, 5000.00)		(0.00, 1670.00)	(0.00, 5360.00)		(0.00, 10300.00)	(0.00, 5300.00)	
Missing	0	0		0	0		0	0		0	0		0	0	
classes of PD medications															
Levodopa	14 (27.45%)	82 (26.37%)	0.871	40 (52.63%)	128 (44.76%)	0.221	55 (63.95%)	169 (61.68%)	0.704	71 (77.17%)	170 (68.55%)	0.120	74 (87.06%)	1764 (77.88%)	0.069
Entacapone	0 (0.00%)	0 (0.00%)	NA[a]	0 (0.00%)	3 (1.05%)	NA[a]	3 (3.49%)	5 (1.828%)	0.403	2 (2.17%)	11 (4.44%)	0.526	5 (5.88%)	10 (4.42%)	0.564
MAO-B inhibitors	12 (23.53%)	96 (30.87%)	0.288	37 (48.68%)	108 (37.76%)	0.084	45 (52.33%)	107 (39.05%)	0.030	41 (44.57%)	102 (41.13%)	0.569	40 (47.06%)	92 (40.70%)	0.313
Dopamine agonists	16 (31.37%)	84 (27.01%)	0.518	34 (44.73%)	104 (36.36%)	0.182	45 (52.33%)	107 (39.05%)	0.030	51 (55.43%)	98 (39.52%)	0.009	42 (49.41%)	88 (38.94%)	0.095
Amantadine	6 (11.76%)	21 (6.75%)	0.245	9 (11.84%)	34(11.89%)	0.991	18 (20.93%)	35 (12.77%)	0.063	12 (13.04%)	41 (16.53%)	0.431	13 (15.29%)	39 (17.26%)	0.679
Anticholinergics	1 (1.96%)	4 (1.27%)	0.534	0 (0.00%)	6(2.10%)	0.350	3 (3.49%)	8 (2.92%)	0.728	1 (1.09%)	7 (2.82%)	0.688	3 (3.53%)	7 (3.10%)	1.000

PD, Parkinson disease; ICBs, Impulse control behaviours; LEDD, levodopa equivalent daily dose; MAO-B, Monoamine oxidase-B.

[a]There were not enough positive results to run analysis.

10.3389/fneur.2023.1275170

TABLE 5 Presynaptic dopaminergic dysfunction over time as measured by DaTscan.

Variable	Baseline			Year 1			Year 2			Year 3			Year 4		
	PD ICBs+ *n* = 83	PD ICBs− *n* = 318	*p* Value	PD ICBs+ *n* = 51	PD ICBs− *n* = 311	*p* Value	PD ICBs+ *n* = 76	PD ICBs− *n* = 286	*p* Value	PD ICBs+ *n* = 86	PD ICBs− *n* = 274	*p* Value	PD ICBs+ *n* = 92	PD ICBs− *n* = 248	*p* Value
Contralateral caudate			0.685			0.986			0.741			NA			0.223
Mean (SD)	1.83 (0.63)	1.81 (0.51)		1.64 (0.49)	1.64 (0.50)		1.51 (0.56)	1.53 (0.51)		NA	NA		1.29 (0.43)	1.37 (0.52)	
(Min, Max)	(0.57, 3.70)	(0.35, 3.57)		(0.63, 3.01)	(0.26, 3.58)		(0.06, 3.02)	(0.48, 3.52)					(0.20, 2.61)	(0.13, 3.09)	
Missing	5	12		4	18		10	18					12	38	
Ipsilateral caudate			0.183			0.227			0.666			NA			0.679
Mean (SD)	2.21 (0.66)	2.11 (0.56)		2.02 (0.62)	1.92 (0.54)		1.84 (0.64)	1.80 (0.56)		NA	NA		1.59 (0.55)	1.62 (0.55)	
(Min, Max)	(0.68, 3.75)	(0.42, 3.98)		(0.60, 3.25)	(0.31, 3.81)		(0.27, 3.48)	(0.25, 3.72)					(0.40, 3.24)	(0.33, 3.75)	
Missing	5	12		4	18		10	18					12	38	
Contralateral putamen			0.112			0.610			0.803			NA			0.172
Mean (SD)	0.72 (0.27)	0.67 (0.25)		0.59 (0.17)	0.61 (0.24)		0.56 (0.22)	0.56 (0.21)		NA	NA		0.47 (0.19)	0.51 (0.21)	
(Min, Max)	(0.27, 2.16)	(0.12, 1.74)		(0.03, 1.01)	(0.07, 1.93)		(0.07, 1.36)	(0.03, 1.52)					(0.07, 0.99)	(0.05, 1.61)	
Missing	5	12		4	18		10	18					12	38	
Ipsilateral putamen			0.767			0.579			0.849			NA			0.874
Mean (SD)	0.94 (0.39)	0.95 (0.37)		0.82 (0.36)	0.79 (0.32)		0.72 (0.34)	0.73 (0.30)		NA	NA		0.61 (0.25)	0.61 (0.25)	
(Min, Max)	(0.25, 2.18)	(0.22, 2.60)		(0.24, 2.21)	(0.03, 2.70)		(0.01, 2.12)	(0.07, 1.91)					(0.16, 1.73)	(0.01, 1.60)	
Missing	5	12		4	18		10	18					12	38	

DaTscan data of year 3 and year 5 are not yet available. PD, Parkinson disease; ICBs, Impulse control behaviours; DaT scan, dopamine transporter deficit on 123I ioflupane imaging.

10.3389/fneur.2023.1275170

10.3389/fneur.2023.1275170

TABLE 6 Biologics at baseline and year 1 in participants with PD by ICBs status.

Variable	Baseline			Year 1		
	PD ICBs+ *n* = 83	PD ICBs− *n* = 318	*p* Value	PD ICBs+ *n* = 51	PD ICBs− *n* = 311	*p* Value
A-beta (pg/mL)			0.787			0.708
Mean (SD)	369.24 (105.61)	372.10 (100.29)		370.53 (106.44)	377.51 (104.11)	
(Min, Max)	(155.60, 669.20)	(129.20, 796.50)		(184.40, 578.90)	(144.10, 732.50)	
Missing	3	8		26	172	
T-tau (pg/mL)			0.435			0.823
Mean (SD)	42.86 (17.60)	44.67 (17.99)		41.98 (12.80)	42.97 (18.42)	
(Min, Max)	(15.60, 99.30)	(14.40, 121.00)		(25.40, 70.10)	(16.60, 128.80)	
Missing	3	12		26	173	
p-tau (pg/mL)			0.764			0.446
Mean (SD)	16.07 (10.62)	15.56 (9.99)		17.36 (11.76)	18.66 (11.88)	
(Min, Max)	(4.70, 67.00)	(5.70, 94.10)		(6.60, 47.50)	(5.40, 61.80)	
Missing	3	10		26	173	
Alpha-synuclein (pg/mL)			0.999			0.509
Mean (SD)	1826.88 (765.21)	1857.83 (802.35)		1741.05 (621.56)	1889.30 (827.64)	
(Min, Max)	(363.12, 4709.78)	(332.93, 6694.55)		(797.87, 3438.47)	(352.36, 5157.08)	
Missing	3	8		26	172	
T-tau/A-beta			0.316			0.402
Mean (SD)	0.12 (0.06)	0.13 (0.06)		0.12 (0.06)	0.12 (0.07)	
(Min, Max)	(0.06, 0.49)	(0.04, 0.52)		(0.08, 0.36)	(0.06, 0.51)	
Missing	3	12		26	173	
p-tau/A-beta			0.781			0.619
Mean (SD)	0.05 (0.03)	0.04 (0.04)		0.05 (0.05)	0.05 (0.04)	
(Min, Max)	(0.02, 0.26)	(0.01, 0.51)		(0.02, 0.26)	(0.01, 0.28)	
Missing	3	10		26	173	
p-tau/T-tau			0.301			0.570
Mean (SD)	0.39 (0.21)	0.37 (0.23)		0.41 (0.22)	0.48 (0.36)	
(Min, Max)	(0.12, 1.04)	(0.14, 2.14)		(0.18, 1.00)	(0.07, 2.48)	
Missing	3	14		26	174	
Urate (umol/L)			0.915			0.879
Mean (SD)	317.60 (82.60)	317.93 (77.64)		312.34 (93.41)	312.13 (74.12)	
(Min, Max)	(167.00, 523.00)	(167.00, 541.00)		(172.00, 529.00)	(161.00, 500.00)	
Missing	1	4		4	24	
NfL (pg/mL)			0.107			0.537
Mean (SD)	11.84 (5.80)	13.17 (7.33)		12.84 (5.88)	14.60 (11.18)	
(Min, Max)	(2.76, 28.00)	(1.80, 76.60)		(3.67, 34.80)	(2.18, 131.00)	
Missing	10	18		8	40	

Cerebrospinal fluid biomarkers data of year 2–5 are not yet available. PD, Parkinson disease; ICBs, Impulse control behaviours; A-beta, A-beta 1–42; T-tau, total tau; P-tau181, tau phosphorylated at threonine 181; NfL, neurofilament light chain.

supported by a large number of neuroimaging studies with altered striatum and amygdala-orbital frontal cortex (OFC) circuits in patients with ICDs and anxiety (40–42). This association may suggest a biological basis, potentially involving noradrenergic and serotonergic structures that regulate mood. These neurochemical systems could play a role in the onset of ICBs. Additionally, it is possible that neuropsychological mechanisms are also involved in this association. Further investigation is needed to elucidate the specific pathways and mechanisms underlying the relationship between ICBs, anxiety, and the neurobiological and neuropsychological factors in PD (2). The diagnostic process of PD can indeed induce anxiety in patients, leading to possible excessive

TABLE 7 Cox regression analysis of individual risk factors of ICBs in PD subjects from baseline to year 5.

Variable	Univariate analysis		Multivariable analysis	
	HR (95% CI)	*p*-Value	HR(95% CI)	*p*-Value
Gender (male)	1.369 (0.914–2.048)	0.127	NS	NS
Age (years)	0.983 (0.965–1.001)	0.071	Not included	Not included
Age at PD onset (years)	0.983 (0.965–1.001)	0.067	NS	NS
Disease duration (month)	0.949 (0.915–0.984)	0.004	Not included	Not included
Education (years)	0.950 (0.892–1.011)	0.109	NS	NS
Family members with PD	1.306 (0.876–1.947)	0.190	NS	NS
MDS-UDPRS Part I	1.050 (1.006–1.095)	0.026	Not included	Not included
MDS-UDPRS Part II	1.015 (0.972–1.060)	0.506	–	–
MDS-UDPRS Part III	1.003 (0.983–1.023)	0.773	–	–
H&Y (stage > 1)	1.010 (0.702–1.455)	0.955	–	–
TD/non-TD classification	0.837 (0.565–1.241)	0.376	–	–
Tremor score	0.826 (0.460–1.486)	0.524	–	–
PIGD score	1.475 (0.648–3.359)	0.355	–	–
Side most affected (Left)	0.783 (0.537–1.140)	0.201	–	–
S&E	0.973 (0.944–1.002)	0.064	NS	NS
MoCA	1.005 (0.928–1.089)	0.903	–	–
GDS	1.064 (0.993–1.139)	0.077	NS	NS
STAI—state subscore	1.030 (1.013–1.047)	<0.001	1.027 (1.010–1.044)	0.002
STAI—trait subscore	1.030 (1.013–1.048)	0.001	NS	NS
RBD	1.641 (1.137–2.368)	0.008	1.555 (1.053–2.297)	0.027
ESS	1.045 (0.993–1.100)	0.089	NS	NS
SCOPA-AUT	1.018 (0.985–1.051)	0.290	–	–
Contralateral caudate	1.119 (0.784–1.598)	0.536	–	–
Ipsilateral caudate	1.185 (0.851–1.652)	0.315	–	–
Contralateral putamen	1.096 (0.522–2.303)	0.808	–	–
Ipsilateral putamen	1.298 (0.800–2.106)	0.291	–	–
A-beta (pg/mL)	0.999 (0.997–1.001)	0.262	–	–
T-tau (pg/mL)	1.000 (0.989–1.011)	0.959	–	–
p-tau (pg/mL)	1.016 (0.998–1.034)	0.076	1.021 (1.003–1.039)	0.021
Alpha-synuclein (pg/mL)	1.000 (1.000–1.000)	0.379	–	–
T-tau/A-beta	1.943 (0.093–40.751)	0.669	–	–
p-tau/A-beta	102.613 (2.548–4132.103)	0.014	Not included	Not included
p-tau/T-tau	1.690 (0.815–3.503)	0.158	Not included	Not included
Urate (umol/L)	1.001 (0.999–1.004)	0.301	–	–
NfL (pg/mL)	1.002 (0.976–1.028)	0.894	–	–
LEDD at DRT initiation (perΔ10 pts)	0.989 (0.974–1.005)	0.180	NS	NS
DRT delay from PD onset evaluations (month)	0.980 (0.965–0.996)	0.013	NS	NS

PD, Parkinson disease; ICBs, Impulse control behaviours; MDS-UPDRS, Movement Disorders Society-Unified Parkinson's Disease Rating Scale; H&Y, Hoehn and Yahr; PIGD, Postural instability Gait Disorder; TD, tremor dominant; S&E, Modified Schwab and England Activities of Daily Living Scale; MoCA, Montreal Cognitive Assessment; GDS, Geriatric Depression Scale; STAI, State–Trait Anxiety Inventory; ESS, Epworth Sleepiness Scale; RBD, rapid eye movement sleep behaviour disorder; SCOPA-AUT, Scales for Outcomes in Parkinson's Disease-Autonomic; QUIP, Questionnaire for Impulsive-Compulsive Disorders in Parkinson's Disease; UPSIT, University of Pennsylvania Smell Identification Test; A-beta, A-beta 1–42; T-tau, total tau; P-tau181, tau phosphorylated at threonine 181; NfL, neurofilament light chain; LEDD, levodopa equivalent daily dose; DRT, dopamine replacement therapy; NS, not significant; ICBs, Impulse control behaviours; RBD, rapid eye movement sleep behaviour disorder. Age was not included in the multivariable model because Age at PD onset was already being considered. And p-tau/t-tau and p-tau/A-beta were not included in the multivariable model because p-tau was already being considered. Similarly, Total initial LEDD was not included in the multivariable model because Initial LEDD subtotal—non-dopamine agonists was already being considered.

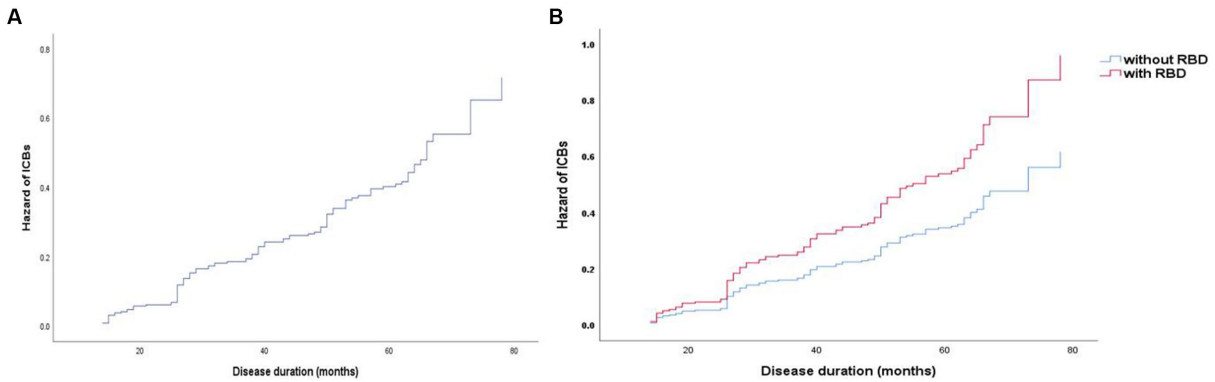

FIGURE 3
Survival curves of PD-ICBs. **(A)** Survival curves of PD-ICBs. **(B)** Survival curves of PD-ICBs with or without RBD. PD, Parkinson disease; ICBs, Impulse control behaviours; RBD, rapid eye movement sleep behaviour disorder.

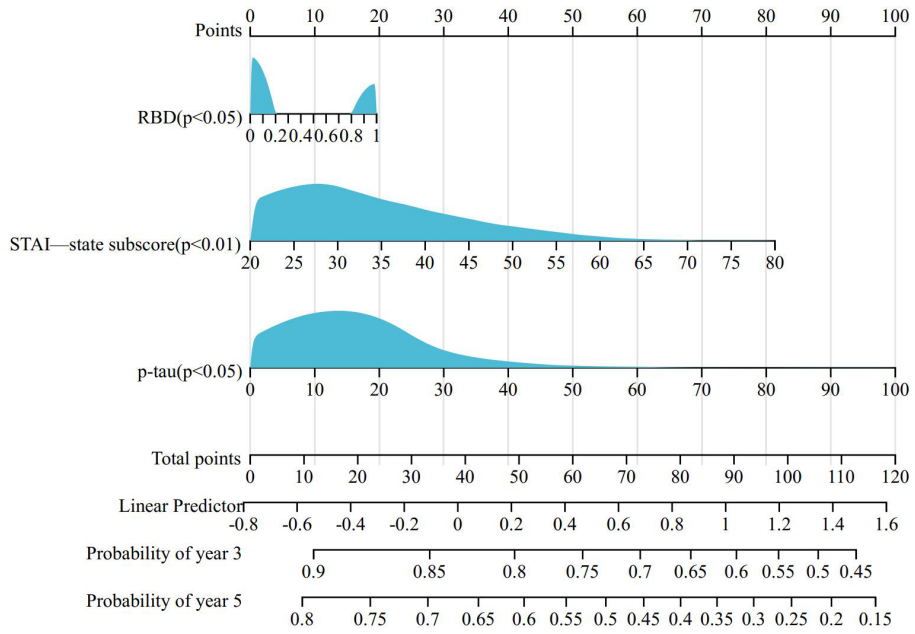

FIGURE 4
Nomogram for predicting prognosis of PD-ICBs. PD, Parkinson disease; ICBs, Impulse control behaviours; RBD, rapid eye movement sleep behaviour disorder.

psychological distress. These psychological stresses may further increase patients' susceptibility to developing ICBs. This association between anxiety and ICBs has been supported by previous research (38). However, in contrast to anxiety, our study did not find baseline depression levels to be a significant risk factor for the development of ICBs in early PD patients. It is important to note that the relationship between depression and ICBs may vary at different stages of the disease. While our study did not find a significant association between baseline depression and ICBs, there was a strong significant relationship between the two at the 5-year follow-up. This finding is inconsistent with a longitudinal study that reported an increased risk of ICBs later in the disease for individuals diagnosed with depression shortly after PD diagnosis (16). Indeed, the inconsistent result regarding the association between depression and the risk of developing ICBs in PD could be attributed to several factors. One possible explanation is the variation in the definition and assessment of depression used in different studies. Differences in the diagnostic criteria, assessment tools, and time points of assessment may contribute to the inconsistent findings. Additionally, the population characteristics and disease stage of the included participants could also play a role in the disparate results. In our study, we focused on early PD patients, whereas the longitudinal study that showed an association between depression and increased ICBs risk later in the disease may have included individuals with more advanced PD. It is possible that the impact of depression on ICBs risk varies

throughout the course of the disease, with depression representing a greater risk factor in advanced stages of PD. Furthermore, it is noteworthy that neuroimaging studies have also provided evidence for a relationship. Namely, the dorsolateral prefrontal cortex (DLPFC) is altered in patients with ICDs, and this region is important as a key neural locus for depression (40, 41, 43). While these factors may partially explain the conflicting results, it is clear that further investigation is needed to fully understand the relationship between depression and ICBs in PD. Considering the potential significance of depression as a risk factor, it is important to incorporate the assessment of depression when screening for risk factors associated with the development of ICBs in patients with PD. By doing so, we can gain a more comprehensive understanding of the factors contributing to the occurrence of ICBs and potentially identify individuals at higher risk who may benefit from early interventions or tailored management strategies.

The relationship between EDS and ICBs in early PD is intriguing and has not been systematically explored. A study found associations between poor sleep efficiency, restless legs symptoms, and increased daytime sleepiness with impulsivity in PD (44). The study suggested that daytime sleepiness may disrupt the prefrontal cortex, which is responsible for inhibitory control of impulsive behavior, or that it may amplify the reactivity of brain reward networks (45). In our study, EDS was not found to be a significant risk factor for the development of ICBs. However, there was a significant difference between EDS and ICBs at the 5-year follow-up. Our results suggest that EDS may not facilitate the occurrence of ICBs but rather that ICBs lead to the emergence of EDS, which needs further validation in subsequent studies. Furthermore, PD patients with ICBs had higher rates of mood disturbance, which could potentially impact sleep quality directly (46). However, the result regarding RBD was different. In our study, RBD was not clearly associated with the development of ICBs in early PD, whereas multivariable analysis suggested RBD as a risk factor for ICBs development. RBD emerged as the strongest predictor of incident ICBs, with a hazard ratio (HR) of 1.555 (95% confidence interval: 1.053–2.297). Another study based on the PPMI found a significant association between RBD and ICBs in cross-sectional analyses, as well as an increased risk for ICBs symptoms in RBD patients in longitudinal univariate analysis. However, after adjustment for covariates, only a trend toward an increased risk was observed (47). Therefore, patients with PD who have RBD should be alerted to the potential development of ICBs.

The association between ICBs and autonomic dysfunction has not been systematically explored in early PD. Similar to EDS, our study did not identify autonomic dysfunction as an independent risk factor for the development of ICBs, although a significant difference was observed between autonomic dysfunction and ICBs at the 5-year follow-up. We speculate that autonomic damage may contribute further to the development of ICBs in patients. Interestingly, a study found that autonomic dysfunction is associated with reduced amygdala grey matter volume (48), which is considered part of the anatomical substrate of ICBs (49). This could suggest a common underlying mechanism between ICBs and autonomic dysfunction. However, this finding is inconsistent with the data from Ricciardi et al. (50) which indicated that autonomic dysfunction was a predictor of ICBs. The disparity in results may be attributed to differences in the study population and methodology. While there appears to be some association between autonomic dysfunction and ICBs, further investigations are necessary to confirm the intrinsic relationship between the two factors.

Many previous studies have indicated that drugs, particularly dopaminergic agonists, play a significant role in the development of ICBs in PD. However, limited research has focused on ICBs in early PD patients without medication use. A previous study proposed that PD itself may not increase the risk of developing ICBs, suggesting that the higher prevalence of ICBs in the PD population is driven by PD medications or other treatments such as deep brain stimulation. They suggested that certain clinical and demographic variables, such as younger age and family or personal history of similar behaviors, might simply moderate the risk of ICB development (51). However, we remain skeptical about this conclusion and question whether there are biological factors associated with PD itself that directly or indirectly influence the occurrence of ICBs. To address these hypotheses and explore potentially relevant factors, we conducted a systematic analysis of the demographic, clinical, dopamine transporter (DaT) scan imaging, and biological characteristics of the PD cohort. In the third and fourth years of follow-up, we observed a higher usage of dopamine agonists in patients with ICBs. Although the difference decreased in the fifth year compared to the previous year, this may be attributed to result bias caused by patient dropout during follow-up and delayed initiation of medication in early-stage patients. Therefore, the conclusion regarding the association between dopamine agonist use and ICBs does not contradict previous studies. As our baseline study population was not yet on medication and patients were not consistently taking medications, we included evaluations of LEDD at dopamine replacement therapy (DRT) initiation and the delay of DRT initiation from PD onset for correction. These factors did not contribute to the occurrence of ICBs in early PD patients in our study.

The novelty of our current study lies in the analysis of the association between biomarkers and ICBs in early PD patients. Unfortunately, we did not find a significant link between presynaptic dopaminergic dysfunction, as measured by DaTscan, and the occurrence of ICBs. However, a previous study based on pilot data from the PPMI suggested that the availability of dopamine receptors in the right striatum consistently decreased in PD patients with ICBs (52). The discrepancy in findings may be attributed to differences in study design, evaluation criteria, and the selection of laterality. The precise biological relationship between presynaptic dopaminergic dysfunction and ICBs remains unclear.

Impulsivity and reward-based decision-making are mediated by a complex neural network involving interconnected mesocortical and mesolimbic circuits. One hypothesis is that a combination of pre-existing biological and genetic risk factors contributes to the relative preservation of dopamine receptor functions. An alternative hypothesis is that the relative preservation of dopamine receptors may lead to impaired inhibition of impulsivity, potentially contributing to the development of ICBs in PD patients. However, in our study conducted in early PD patients, we did not find evidence supporting these hypotheses. Further exploration of these relationships in advanced-stage PD patients is warranted.

Although no significant association was found between ICBs and CSF biomarkers, such as NfL or urate, at baseline and year 1, our multifactorial analysis suggested that levels of p-tau in CSF may serve as an independent risk factor for the development of ICBs. This

finding is novel and has not been proposed before. However, it's important to note that the CSF data in our study were limited to the first year, and further confirmation of this association in patients with longer disease duration is necessary. Given the role of p-tau as a biomarker of neurodegeneration, it will be of great interest to investigate in future analyses whether CSF p-tau values increase at higher rates in individuals with ICBs. This could provide insights into the potential relationship between ICBs and the progression of neurodegenerative processes. Further studies with longer-term follow-up and more comprehensive CSF biomarker assessments are warranted to explore this potential link.

5. Limitations

Despite the comprehensive exploration of factors associated with ICBs in early PD, there are several limitations to acknowledge in our study. Firstly, the assessment of ICBs relied on a short version of the QUIP, which primarily screened for the presence of ICBs but did not provide a detailed evaluation of the severity of symptoms. This limited our ability to capture the full spectrum of ICB-related symptoms and their impact on patients. Additionally, we acknowledge that there are pending longitudinal data analyses for CSF and imaging data beyond the initial years of follow-up. The analysis of CSF data from years 2 to 5 and imaging data from years 3 and 5 on this cohort is still underway. These data could provide valuable insights into the long-term associations between these factors and the development of ICBs in early PD. These limitations highlight the need for further studies that employ more comprehensive and detailed assessment methods for ICBs and include longer-term follow-up to better understand the complexity of ICBs in PD.

6. Conclusion

In conclusion, our study, which included the largest longitudinal case–control cohort of *de novo* unmedicated PD patients, provides valuable insights into the clinical and biological factors associated with ICBs in PD. We observed that the prevalence of ICBs increases over time in PD patients, while it decreases over time in the healthy control group. Our findings support previous research indicating that ICBs are associated with comorbid conditions such as depression and anxiety, as well as autonomic dysfunction, EDS, and the use of dopaminergic medications, particularly dopamine agonists. Moreover, our study identified several predictors of the incident development of ICBs in early PD. These predictors include anxiety, RBD, and elevated levels of p-tau in CSF. These findings suggest that these factors may play a role in the pathogenesis of ICBs in PD and could potentially be used as indicators for the development of preventive strategies or targeted interventions. Overall, our study contributes to the understanding of ICBs in PD and highlights the importance of considering both clinical and biological factors in assessing the risk and progression of ICBs in early PD patients. Further research is needed to validate these findings and to explore potential mechanisms underlying the observed associations.

Data availability statement

The datasets presented in this study can be found in online repositories. The names of the repository/repositories and accession number(s) can be found in the article/Supplementary material.

Ethics statement

The studies involving humans were approved by Ethics Committee of Xinhua Hospital Affiliated to Shanghai Jiao Tong University School of Medicine. The studies were conducted in accordance with the local legislation and institutional requirements. The participants provided their written informed consent to participate in this study.

Author contributions

XZ: Conceptualization, Data curation, Formal analysis, Visualization, Writing – original draft. JG: Supervision, Validation, Writing – review & editing. NW: Supervision, Validation, Resources, Writing – review & editing. YW: Supervision, Validation, Resources, Writing – review & editing. LS: Supervision, Validation, Resources, Writing – review & editing. ZL: Conceptualization, Funding acquisition, Resources, Supervision, Writing – review & editing. YZ: Conceptualization, Funding acquisition, Methodology, Resources, Visualization, Writing – review & editing.

Funding

The author(s) declare financial support was received for the research, authorship, and/or publication of this article. This study was supported by the Project of Shanghai Science and Technology Commission (22015831100), Shanghai Pujiang Program (2020PJD032), Projects of National Science Foundation of China (81974173), Shanghai Municipal Commission of Health (2019SY024), Projects of the Shanghai Committee of Science and Technology (19401932100), Pilot project of clinical cooperation between Chinese and Western medicine in Shanghai (ZXYXZ-201907), Special project of integrated traditional Chinese and Western medicine in Shanghai General Hospital (ZHYY-ZXYJHZX-202021).

Acknowledgments

The data used for this study were provided by the Parkinson's Progression Markers Initiative (PPMI). PPMI (a public private partnership) is funded by the Michael J. Fox Foundation for Parkinson's Research and funding partners, including AbbVie, Avid Radiopharmaceuticals, Biogen, Bristol-Myers Squibb, Covance, GE Healthcare, Genentech, GlaxoSmithKline, Lilly, Lundbeck, Merck, Meso Scale Discovery, Pfizer, Piramal, Roche, Servicer, UCB and Golub Capital. Data used in the preparation of this article were obtained from the PPMI database (www.Ppmi-info.Org/data).

Conflict of interest

The authors declare that the research was conducted in the absence of any commercial or financial relationships that could be construed as a potential conflict of interest.

Publisher's note

All claims expressed in this article are solely those of the authors and do not necessarily represent those of their affiliated organizations, or those of the publisher, the editors and the reviewers. Any product that may be evaluated in this article, or claim that may be made by its manufacturer, is not guaranteed or endorsed by the publisher.

Supplementary material

The Supplementary material for this article can be found online at: https://www.frontiersin.org/articles/10.3389/fneur.2023.1275170/full#supplementary-material

References

1. Tolosa E, Wenning G, Poewe W. The diagnosis of Parkinson's disease. *Lancet Neurol*. (2006) 5:75–86. doi: 10.1016/S1474-4422(05)70285-4

2. Kelly MJ, Baig F, Hu MT, Okai D. Spectrum of impulse control behaviours in Parkinson's disease: pathophysiology and management. *J Neurol Neurosurg Psychiatry*. (2020) 91:703–11. doi: 10.1136/jnnp-2019-322453

3. Cao L, Xu T, Zhao G, Lv D, Lu J, Zhao G. Risk factors of impulsive-compulsive behaviors in PD patients: a meta-analysis. *J Neurol*. (2022) 269:1298–315. doi: 10.1007/s00415-021-10724-1

4. Weintraub D, Claassen DO. Impulse control and related disorders in Parkinson's disease. *Int Rev Neurobiol*. (2017) 133:679–717. doi: 10.1016/bs.irn.2017.04.006

5. Gatto EM, Aldinio V. Impulse control disorders in Parkinson's disease. A brief and comprehensive review. *Front Neurol*. (2019) 10:351. doi: 10.3389/fneur.2019.00351

6. Kovács M, Makkos A, Pintér D, Juhász A, Darnai G, Karádi K, et al. Screening for problematic internet use may help identify impulse control disorders in Parkinson's disease. *Behav Neurol*. (2019) 2019:1–08. doi: 10.1155/2019/4925015

7. Galifianakis NB, Byrd EA, Ostrem JL, Tanner CM, Racine CA. Problematic mobile gaming in Parkinson's disease: an impulse control disorder for the smartphone. *Mov Disord Clin Pract*. (2017) 4:277–8. doi: 10.1002/mdc3.12378

8. El OH, Abdulhakeem Z, El MB, Bellakhdar S, Rafai MA. Excessive charity: a new aspect of impulse control disorders in Parkinson's disease? *Int Psychogeriatr*. (2020) 32:665–6. doi: 10.1017/S1041610220000253

9. Lee JY, Kim JM, Kim JW, Cho J, Lee WY, Kim HJ, et al. Association between the dose of dopaminergic medication and the behavioral disturbances in Parkinson disease. *Parkinsonism Relat Disord*. (2010) 16:202–7. doi: 10.1016/j.parkreldis.2009.12.002

10. Zurowski M, O'Brien JD. Developments in impulse control behaviours of Parkinson's disease. *Curr Opin Neurol*. (2015) 28:387–92. doi: 10.1097/WCO.0000000000000209

11. Marković V, Stanković I, Petrović I, Stojković T, Dragašević-Mišković N, Radovanović S, et al. Dynamics of impulsive–compulsive behaviors in early Parkinson's disease: a prospective study. *J Neurol*. (2020) 267:1127–36. doi: 10.1007/s00415-019-09692-4

12. Parra-Diaz P, Chico-Garcia JL, Beltran-Corbellini A, Rodriguez-Jorge F, Fernandez-Escandon CL, Alonso-Canovas A, et al. Does the country make a difference in impulse control disorders? A systematic review. *Mov Disord Clin Pract*. (2021) 8:25–32. doi: 10.1002/mdc3.13128

13. Vargas AP, Cardoso F. Impulse control and related disorders in Parkinson's disease. *Arq Neuropsiquiatr*. (2018) 76:399–410. doi: 10.1590/0004-282X20180052

14. Erga AH, Alves G, Tysnes OB, Pedersen KF. Evolution of impulsive–compulsive behaviors and cognition in Parkinson's disease. *J Neurol*. (2020) 267:259–66. doi: 10.1007/s00415-019-09584-7

15. Weintraub D, Koester J, Potenza MN, Siderowf AD, Stacy M, Voon V, et al. Impulse control disorders in Parkinson disease: a cross-sectional study of 3090 patients. *Arch Neurol*. (2010) 67:589–95. doi: 10.1001/archneurol.2010.65

16. Marín Lahoz J, Sampedro F, Martinez Horta S, Pagonabarraga J, Kulisevsky J. Depression as a risk factor for impulse control disorders in Parkinson disease. *Ann Neurol*. (2019) 86:762–9. doi: 10.1002/ana.25581

17. Cao R, Chen X, Xing F, Xie C, Hu P, Wang K. Cross-sectional and longitudinal associations between probable rapid eye movement sleep behavior disorder and impulse control disorders in Parkinson's disease. *Eur J Neurol*. (2020) 27:757–63. doi: 10.1111/ene.14177

18. Barone P, Antonini A, Stanzione P, Annoni K, Asgharnejad M, Bonuccelli U. Risk factors for impulse control disorders and related behaviors in Parkinson's disease: secondary analyses of the ICARUS study. *J Drug Assess*. (2019) 8:159–66. doi: 10.1080/21556660.2019.1675670

19. Marques A, Figorilli M, Pereira B, Derost P, Debilly B, Beudin P, et al. Impulse control disorders in Parkinson's disease patients with RLS: a cross sectional-study. *Sleep Med*. (2018) 48:148–54. doi: 10.1016/j.sleep.2018.02.004

20. Antonini A, Barone P, Bonuccelli U, Annoni K, Asgharnejad M, Stanzione P. ICARUS study: prevalence and clinical features of impulse control disorders in Parkinson's disease. *J Neurol Neurosurg Psychiatry*. (2017) 88:317–24. doi: 10.1136/jnnp-2016-315277

21. Corvol J, Artaud F, Cormier-Dequaire F, Rascol O, Durif F, Derkinderen P, et al. Longitudinal analysis of impulse control disorders in Parkinson disease. *Neurology*. (2018) 91:e189–201. doi: 10.1212/WNL.0000000000005816

22. Marek K, Jennings D, Lasch S, Siderowf A, Tanner C, Simuni T, et al. The Parkinson progression marker initiative (PPMI). *Prog Neurobiol*. (2011) 95:629–35. doi: 10.1016/j.pneurobio.2011.09.005

23. Weintraub D, Mamikonyan E, Papay K, Shea JA, Xie SX, Siderowf A. Questionnaire for impulsive-compulsive disorders in Parkinson's disease-rating scale. *Mov Disord*. (2012) 27:242–7. doi: 10.1002/mds.24023

24. Zhang Y, He AQ, Li L, Chen W, Liu ZG. Clinical characteristics of impulse control and related disorders in Chinese Parkinson's disease patients. *BMC Neurol*. (2017) 17:98. doi: 10.1186/s12883-017-0874-6

25. Goetz CG, Tilley BC, Shaftman SR, Stebbins GT, Fahn S, Martinez-Martin P, et al. Movement Disorder Society-sponsored revision of the Unified Parkinson's Disease Rating Scale (MDS-UPDRS): scale presentation and clinimetric testing results. *Mov Disord*. (2008) 23:2129–70. doi: 10.1002/mds.22340

26. Hoehn MM, Yahr MD. Parkinsonism: onset, progression and mortality. *Neurology*. (1967) 17:427–42. doi: 10.1212/wnl.17.5.427

27. Stebbins GT, Goetz CG, Burn DJ, Jankovic J, Khoo TK, Tilley BC. How to identify tremor dominant and postural instability/gait difficulty groups with the movement disorder society unified Parkinson's disease rating scale: comparison with the unified Parkinson's disease rating scale. *Mov Disord*. (2013) 28:668–70. doi: 10.1002/mds.25383

28. Leentjens AF, Moonen AJ, Dujardin K, Marsh L, Martinez-Martin P, Richard IH, et al. Modeling depression in Parkinson disease: disease-specific and nonspecific risk factors. *Neurology*. (2013) 81:1036–43. doi: 10.1212/WNL.0b013e3182a4a503

29. Nasreddine ZS, Phillips NA, Bedirian V, Charbonneau S, Whitehead V, Collin I, et al. The Montreal Cognitive Assessment, MoCA: a brief screening tool for mild cognitive impairment. *J Am Geriatr Soc*. (2005) 53:695–9. doi: 10.1111/j.1532-5415.2005.53221.x

30. Weintraub D, Oehlberg KA, Katz IR, Stern MB. Test characteristics of the 15-item geriatric depression scale and Hamilton depression rating scale in Parkinson disease. *Am J Geriatr Psychiatry*. (2006) 14:169–75. doi: 10.1097/01.JGP.0000192488.66049.4b

31. Kendall PC, Finch AJ, Auerbach SM, Hooke JF, Mikulka PJ. The state-trait anxiety inventory: a systematic evaluation. *J Consult Clin Psychol*. (1976) 44:406–12. doi: 10.1037//0022-006x.44.3.406

32. Johns MW. A new method for measuring daytime sleepiness: the Epworth sleepiness scale. *Sleep (New York, NY)*. (1991) 14:540–5. doi: 10.1093/sleep/14.6.540

33. Stiasny-Kolster K, Mayer G, Schäfer S, Möller JC, Heinzel-Gutenbrunner M, Oertel WH. The REM sleep behavior disorder screening questionnaire-a new diagnostic instrument. *Mov Disord*. (2007) 22:2386–93. doi: 10.1002/mds.21740

34. Rodriguez-Blazquez C, Forjaz MJ, Frades-Payo B, De Pedro-Cuesta J, Martinez-Martin P. Independent validation of the scales for outcomes in Parkinson's disease-autonomic (SCOPA-AUT). *Eur J Neurol*. (2010) 17:194–201. doi: 10.1111/j.1468-1331.2009.02788.x

35. Bolitho SJ, Naismith SL, Terpening Z, Grunstein RR, Melehan K, Yee BJ, et al. Investigating rapid eye movement sleep without atonia in Parkinson's disease using the rapid eye movement sleep behavior disorder screening questionnaire. *Mov Disord*. (2014) 29:736–42. doi: 10.1002/mds.25832

36. Tomlinson CL, Stowe R, Patel S, Rick C, Gray R, Clarke CE. Systematic review of levodopa dose equivalency reporting in Parkinson's disease. *Mov Disord*. (2010) 25:2649–53. doi: 10.1002/mds.23429

37. Kang J. Association of cerebrospinal fluid β-amyloid 1-42, T-tau, P-tau 181, and α-synuclein levels with clinical features of drug-naive patients with early Parkinson disease. *JAMA Neurol*. (2013) 70:1277–87. doi: 10.1001/jamaneurol.2013.3861

38. Waskowiak P, Koppelmans V, Ruitenberg MFL. Trait anxiety as a risk factor for impulse control disorders in de novo Parkinson's disease. *J Parkinsons Dis*. (2022) 12:689–97. doi: 10.3233/JPD-212959

39. Sassone J, Valtorta F, Ciammola A. Early Dyskinesias in Parkinson's disease patients with parkin mutation: a primary corticostriatal synaptopathy? *Front Neurosci*. (2019) 13:273. doi: 10.3389/fnins.2019.00273

40. Biundo R, Weis L, Facchini S, Formento-Dojot P, Vallelunga A, Pilleri M, et al. Patterns of cortical thickness associated with impulse control disorders in Parkinson's disease. *Mov Disord*. (2015) 30:688–95. doi: 10.1002/mds.26154

41. Roussakis AA, Lao-Kaim NP, Piccini P. Brain imaging and impulse control disorders in Parkinson's disease. *Curr Neurol Neurosci Rep*. (2019) 19:67. doi: 10.1007/s11910-019-0980-5

42. Carey G, Gormezoglu M, de Jong J, Hofman P, Backes WH, Dujardin K, et al. Neuroimaging of anxiety in Parkinson's disease: a systematic review. *Mov Disord*. (2021) 36:327–39. doi: 10.1002/mds.28404

43. Pan Z, Park C, Brietzke E, Zuckerman H, Rong C, Mansur RB, et al. Cognitive impairment in major depressive disorder. *CNS Spectr*. (2019) 24:22–9. doi: 10.1017/S1092852918001207

44. Scullin MK, Sollinger AB, Land J, Wood-Siverio C, Zanders L, Lee R, et al. Sleep and impulsivity in Parkinson's disease. *Parkinsonism Relat Disord*. (2013) 19:991–4. doi: 10.1016/j.parkreldis.2013.06.018

45. Gujar N, Yoo SS, Hu P, Walker MP. Sleep deprivation amplifies reactivity of brain reward networks, biasing the appraisal of positive emotional experiences. *J Neurosci*. (2011) 31:4466–74. doi: 10.1523/JNEUROSCI.3220-10.2011

46. O'Sullivan SS, Loane CM, Lawrence AD, Evans AH, Piccini P, Lees AJ. Sleep disturbance and impulsive-compulsive behaviours in Parkinson's disease. *J Neurol Neurosurg Psychiatry*. (2011) 82:620–2. doi: 10.1136/jnnp.2009.186874

47. Fantini ML, Fedler J, Pereira B, Weintraub D, Marques AR, Durif F. Is rapid eye movement sleep behavior disorder a risk factor for impulse control disorder in Parkinson disease? *Ann Neurol*. (2020) 88:759–70. doi: 10.1002/ana.25798

48. Udow SJ, Robertson AD, Mac Intosh BJ, Espay AJ, Rowe JB, Lang AE, et al. 'Under pressure': is there a link between orthostatic hypotension and cognitive impairment in α-synucleinopathies? *J Neurol Neurosurg Psychiatry*. (2016) 87:1311–21. doi: 10.1136/jnnp-2016-314123

49. Weintraub D. Dopamine and impulse control disorders in Parkinson's disease. *Ann Neurol*. (2008) 64:S93–S100. doi: 10.1002/ana.21454

50. Ricciardi L, Lambert C, De Micco R, Morgante F, Edwards M. Can we predict development of impulsive–compulsive behaviours in Parkinson's disease? *J Neurol Neurosurg Psychiatry*. (2018) 89:476–81. doi: 10.1136/jnnp-2017-317007

51. Weintraub D, Papay K, Siderowf A. Screening for impulse control symptoms in patients with de novo Parkinson disease: a case-control study. *Neurology*. (2013) 80:176–80. doi: 10.1212/WNL.0b013e31827b915c

52. Smith KM, Xie SX, Weintraub D. Incident impulse control disorder symptoms and dopamine transporter imaging in Parkinson disease. *J Neurol Neurosurg Psychiatry*. (2016) 87:864–70. doi: 10.1136/jnnp-2015-311827

frontiers | Frontiers in Neurology

TYPE Original Research
PUBLISHED 08 March 2024
DOI 10.3389/fneur.2024.1301277

OPEN ACCESS

EDITED BY
Ayman ElAli,
Laval University, Canada

REVIEWED BY
Rong Hu,
Army Medical University, China
Daniel Manrique-Castano,
Laval University, Canada

*CORRESPONDENCE
Maohua Zheng
✉ 2002maohua@163.com
Hongtao Sun
✉ Chenmo333@163.com

RECEIVED 24 September 2023
ACCEPTED 27 February 2024
PUBLISHED 08 March 2024

CITATION
Deng T, Ding R, Wang Y, Chen Y, Sun H and Zheng M (2024) Mapping knowledge of the stem cell in traumatic brain injury: a bibliometric and visualized analysis. *Front. Neurol.* 15:1301277. doi: 10.3389/fneur.2024.1301277

Mapping knowledge of the stem cell in traumatic brain injury: a bibliometric and visualized analysis

Tingzhen Deng[1,2], Ruiwen Ding[1,2], Yatao Wang[1,2], Yueyang Chen[1,2], Hongtao Sun[1,3]* and Maohua Zheng[1,2]*

[1]The First School of Clinical Medicine, Lanzhou University, Lanzhou, China, [2]Department of Neurosurgery, The First Hospital of Lanzhou University, Lanzhou, China, [3]Tianjin Key Laboratory of Neurotrauma Repair, Institute of Neurotrauma Repair, Characteristic Medical Center of Chinese People's Armed Police Force, Tianjin, China

Background: Traumatic brain injury (TBI) is a brain function injury caused by external mechanical injury. Primary and secondary injuries cause neurological deficits that mature brain tissue cannot repair itself. Stem cells can self-renewal and differentiate, the research of stem cells in the pathogenesis and treatment of TBI has made significant progress in recent years. However, numerous articles must be summarized to analyze hot spots and predict trends. This study aims to provide a panorama of knowledge and research hotspots through bibliometrics.

Method: We searched in the Web of Science Core Collection (WoSCC) database to identify articles pertaining to TBI and stem cells published between 2000 and 2022. Visualization knowledge maps, including co-authorship, co-citation, and co-occurrence analysis were generated by VOSviewer, CiteSpace, and the R package "bibliometrix."

Results: We retrieved a total of 459 articles from 45 countries. The United States and China contributed the majority of publications. The number of publications related to TBI and stem cells is increasing yearly. Tianjin Medical University was the most prolific institution, and Professor Charles S. Cox, Jr. from the University of Texas Health Science Center at Houston was the most influential author. The *Journal of Neurotrauma* has published the most research articles on TBI and stem cells. Based on the burst references, "immunomodulation," "TBI," and "cellular therapy" have been regarded as research hotspots in the field. The keywords co-occurrence analysis revealed that "exosomes," "neuroinflammation," and "microglia" were essential research directions in the future.

Conclusion: Research on TBI and stem cells has shown a rapid growth trend in recent years. Existing studies mainly focus on the activation mechanism of endogenous neural stem cells and how to make exogenous stem cell therapy more effective. The combination with bioengineering technology is the trend in this field. Topics related to exosomes and immune regulation may be the future focus of TBI and stem cell research.

KEYWORDS

traumatic brain injury, TBI, stem cell, bibliometric analysis, VOSviewer, CiteSpace

1 Introduction

Traumatic brain injury (TBI) is an intracranial injury caused by external mechanical damage, it is a significant health and socioeconomic problem around the world, with 50–60 million people suffering from TBI annually, and costing the global economy around $400 billion each year (1). The pathogenesis is a complex and dynamic process, with primary and secondary injuries that lead to impermanent or permanent neurological deficits (2, 3). The primary deficit is directly related to the external impact of the brain, and the secondary injury consists of a chemical, molecular, and inflammatory cascade responsible for further cerebral damage (4). Unlike other organs, mature brain tissue cannot self-repair after damage (5, 6). About half of the TBI patients could not return to their previous work after 1 year, and ~28% never returned to work in any form (7). Numerous monitoring, drug treatments, and operations of TBI exist to reduce neurological damage, unfortunately, there is no effective clinical treatment to improve neural repair and functional recovery of patients (8–11).

Stem cells possess the capacity for differentiation and self-renewal, enabling them to differentiate into specialized cell types necessary for tissue repair (12). Stem cell therapy exerts beneficial effects on neurodegeneration and functional recovery through diverse mechanisms, including the secretion of chemokines and growth factors, the promotion of neurogenesis and angiogenesis, and the regulation of neuroinflammation (13–15). In recent decades, researchers have extensively investigated exogenous stem/progenitor cells for promoting recovery from TBI, spinal cord injury (SCI), Alzheimer's disease, and stroke (14, 16–20). A growing body of evidence supports the use of different types of stem cells to treat TBI, both mesenchymal stem cells (MSCs), neural stem cells (adult or embryonic), and multipotent adult progenitor cells (MAPCs) have all shown efficacy in preclinical models of TBI (21). Furthermore, scholars observed the activation and proliferation of endogenous neural stem cells after TBI (22, 23). Despite unresolved issues in recent years, it is evident that new research offers promising prospects for treating TBI (24).

Given the severity of TBI and the unique characteristics of stem cells, an increasing number of scholars have directed their attention toward exploring TBI and stem cells (25), resulting in a substantial body of literature on this subject. However, while meta-analyses and reviews can provide credible, evidence-based medical findings, these studies often lack comprehensive coverage as they focus on specific aspects. Moreover, they may have integrity and quantitative analysis limitations, which hinder a holistic understanding for researchers in this field (26). In order to overcome these limitations and gain insights into the research landscape, future trends, and dynamic evolution within this domain, we aim to employ bibliometric methodologies in our present study to investigate the current status and frontiers of stem cell applications in traumatic brain injury. Bibliometrics is a quantitative approach for synthesizing multidimensional information within a specific field, utilizing visualization and network technologies to facilitate researchers in rapidly comprehending the research landscape, predicting future research trends, and exploring the dynamic evolution within that particular domain (27, 28). With the development of information technologies, researchers have extensively applied bibliometric tools such as CiteSpace (29), VoSviewer (30), and R package "bibliometrix" (31) in neurology-related fields, including stroke (32), spinal trauma (33), neuro-oncology (34), and seizures (35).

2 Methods

2.1 Data source

The Web of Science Core Collection (WoSCC, Clarivate Analytics, Philadelphia, PA, USA) has been extensively employed in bibliometric studies due to its highly comprehensive and authoritative database platform for accessing global academic information. It provides basic information such as title, country/region, institution, author, and author keywords and includes references. Therefore, it is considered the optimal database for bibliometric research. Journal information, including impact factor (IF) and quartile in category (Q1-Q4), was obtained from the 2022 Journal Citation Reports (Clarivate Analytics, Philadelphia, PA, USA).

2.2 Search strategy and data extraction

Two authors (TD and RD) conducted a comprehensive online search to avoid bias due to potential daily updates in the running database. Based on the title (TI) and author keyword (AK), we identified potentially relevant publications using the following search formula: #1: TI = (traumatic brain injury*) OR AK = (traumatic brain injury*); #2: TI = (stem cell* OR progenitor cell*) OR AK = (stem cell* OR progenitor cell*); Final dataset: [#1 AND #2]. Only English-language literature classified as "articles" or "reviews" from January 1st, 2000, to December 31st, 2022, was included. A total of 478 articles were initially acquired as potential candidates. Subsequently, to check the relevance of the literature, two independent researchers (YW and YC) manually examined the paper titles, abstracts, and full text to exclude any irrelevant content related to the study topic (including disease type, research purposes, animal models, interventions, cell types, outcome indexes). Any divergent viewpoints were resolved through discussions with a third investigator (TD or RD). Eighteen invalid records were excluded, including irrelevant literature, meeting abstracts, and advance access. We obtained 459 valid documents (Supplementary Data 1), exported in TXT format as 'full record and cited references' for further analysis (Figure 1).

2.3 Validation

The search query was validated using three criteria. The first criterion was the top 100 cited documents, which were reviewed by checking the titles and abstracts and consulting two external colleagues in the field of health sciences in case of doubt. The reviewers had to judge the presence of false-positive results. The absence of false-positive results was used as an indicator of validity. The second validity criterion was the relevancy of the top 20 journals to TBI and stem cells. In the final search query, the top 20 active journals were in neurology, molecular, and biology. The third criterion was to investigate two of the most active authors obtained by the search strategy. In the present study, Cox Charles S. Jr. and Zhang Jianning were among the top active authors, with 21 and 15 publications, respectively. To confirm that the research strategy was comprehensive and retrieved all possible data, the research activity of the two researchers was investigated and counted using author search methodology in WoSCC. The result of this approach showed that the two researchers have

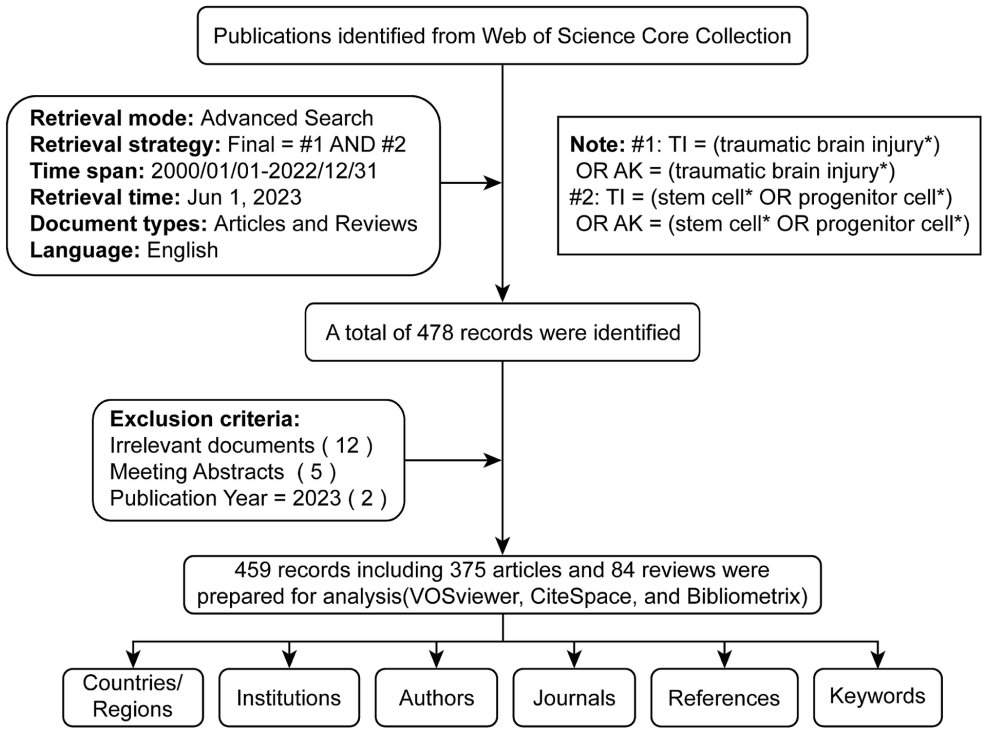

FIGURE 1
Publications screening flowchart.

research output similar to that produced by the search strategy, which indicates the high validity of the search strategy (36).

2.4 Statistical analysis

We conducted statistical analysis and curve fitting procedures using Microsoft Office Excel 2021 (Microsoft, Redmond, Washington, USA) software. Excel was also used to calculate the annual number of publications and citations. Various functions, including exponential, linear, logarithmic, and polynomial, were employed for curve-fitting purposes. We chose the best-fit model based on correlation coefficient value (R^2). Applying a specific formula determined the growth rate of publications over time: Growth rate = [(number of publications in the last year ÷ number of publications in the first year)$^{1/(\text{last year}-\text{first year})}-1]\times100\%$.

2.5 Bibliometric analysis and visualization

VOSviewer (version 1.6.19) is a bibliometric software published by Professor van Eck and Waltman that was used to explore collaboration networks (30, 37). Different nodes indicated different items, such as authors, countries, institutions, journals, and keywords, with the node size reflecting the corresponding number of publications, citations, or occurrences. The links between nodes represented the co-authorship, co-citation, or co-occurrence associations between nodes. The color of the nodes and lines indicated different clusters or corresponding average appearing year (AAY). Line thickness between nodes reflects the level of collaboration or co-citation among them (38).

CiteSpace (version 6.1.R4) was published by Professor Chen Chaomei for bibliometric analysis and visualization (29). In our study, we used Citespace to perform a cooperation analysis of institutions, analyze the co-citation relationship of authors, conduct a dual-map overlay of scientific journals, perform a co-citation analysis of references, identify the top 20 references and 15 keywords with the most robust citation bursts. In the network maps, the nodes represent various items such as institutions, authors, and references. The node size and color rings indicate the number of these items and different years, respectively. The lines between the nodes reflect the co-citation relationships of items. CiteSpace parameters included were as follows: time span (2001–2020), years per slice (1), selection criteria (g-index: $k = 25$), and pruning (minimum spanning tree, pruning sliced networkshttps://www.bibliometrix.org).

For thematic evolution analysis and construction of a global distribution network, the R package "bibliometrix" (version 3.2.1)[1] was employed (31).

3 Results

3.1 Publication volume and trends

From 2001 to 2022, 459 TBI and stem cell articles were published, including 375 articles (81.7%) and 84 reviews (18.3%). Figure 2 shows the gradual growth trend of annual publications, from 4 papers in

1 https://www.bibliometrix.org

2000 to 51 in 2022. The average growth rate of the number of publications is 12.9%, the index function $Y = 1.2469*X^2 - 7.3008*X + 18.961$ (Y is the annual cumulative publications, X is the year minus 2000, $R^2 = 0.9987$) is derived to evaluate further the changing trend of the cumulative number of publications. According to the fitting curve, the number of papers published in 2030 is expected to be close to 100, and the cumulative number of publications will exceed 1,000.

3.2 Country/region and institutional analysis

Forty-five countries/regions contributed to the literature. Figure 3A shows a world map depicting countries' collaboration and contribution. According to the color gradient and the top 10 countries/regions in Table 1 (Part A), researchers from North America, Eastern Asia, and Europe published most articles. Specifically, The United States has the largest number of publications ($n = 172$, 37.5%), followed by China ($n = 158$, 34.4%). Subsequently, a co-authorship network among countries/regions over time is visualized using VOSviewer (Figure 3B), we also observed close cooperation between many countries/regions, especially between China and the United States, Canada, Japan, England, and Taiwan. Different colors marked nodes representing countries/regions based on the average appearing year (AAY). According to the color gradient in the lower right corner, The United States was given the bluish color, indicating that most researchers in the country were relatively early players. In contrast, China and many countries labeled in green are relatively new participants in TBI and stem cell research.

Regarding the analysis of organizations, 637 institutions contributed to this area. Table 1 (Part B) lists the top 10 institutions with the most publications, they are located in the United States ($n = 6$), China ($n = 3$), and Sweden ($n = 1$), these institutions collectively published 125 articles, accounting for 27.2% of all articles. Specifically, Tianjin Medical University emerged as the most prolific institution (22, 4.8%), followed by the University of South Florida (17, 3.70%), University of Miami (13, 2.8%), University of Texas Houston (13, 2.8%), and Henry Ford Hospital (11, 2.4%). We analyzed institutional cooperation networks based on co-authorship using VOSviewer (Figure 4A), 49 institutions with more than five publications were identified. According to the color gradient in the lower right corner, institutions such as Sichuan University, Mashhad University of Medical Sciences, University of Michigan, etc., were given a yellow color with the later AAY values. Conversely, the University of Texas Houston, the University of Pennsylvania, and Kinki University were given a bluish color with the prior AAY values. However, co-citation analysis revealed that despite the high publication volume of the institutions mentioned above, their collaboration with other institutions was relatively limited. CiteSpace analyzed institutional cooperation based on citation relationships (Figure 4B). Harvard University has the highest centrality with a betweenness centrality (BC) value of 0.32, followed closely by Veterans Health Administration (BC = 0.30), indicating their significant influence in this field (institutions

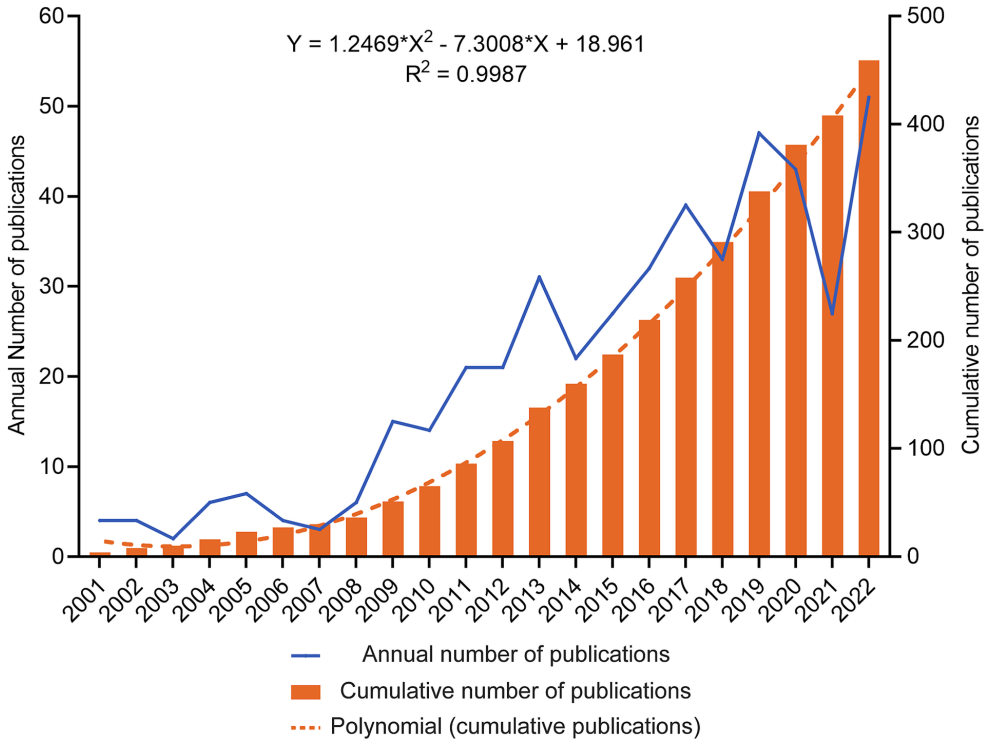

FIGURE 2
Trends in the annual publication of TBI and stem cells were analyzed. The blue line depicts the developmental trend of the yearly publication count, while the orange columns represent the cumulative number of publications. An orange dashed line depicts a fitting curve for the cumulative number of publications.

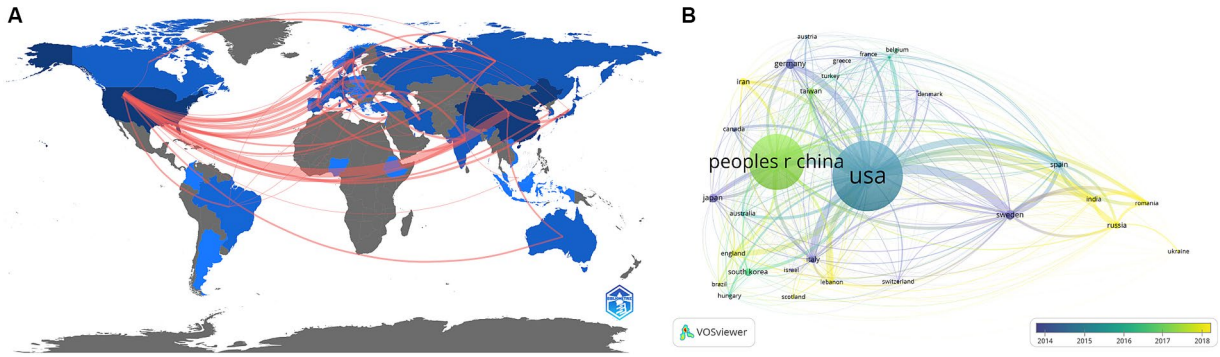

FIGURE 3
(A) A geographical distribution map illustrating the global research contributions in the field. The intensity of the blue color indicates the number of publications published in each country, while gray represents countries with no publications. **(B)** A co-authorship network among countries/regions over time is visualized using VOSviewer. Each node represents a country/region, and the connecting lines between nodes indicate their collaborative relationships. The thickness of the line reflects the strength of cooperation. At the same time, each node's color corresponds to its position on the timeline and indicates when it engaged in cooperative activities with other nodes.

TABLE 1 The top 10 countries and institutions with the most publications in the field on TBI and stem cells.

Rank	Part A			Part B	
	Country/Region	Count	Percent	Institutions	Count
1	United States	172	37.5%	Tianjin Med Univ (China)	22
2	China	158	34.4%	Univ S Florida (United States)	17
3	Japan	13	2.8%	Univ Miami (United States)	13
4	Korea	13	2.8%	Univ Texas Houston (United States)	13
5	Germany	12	2.6%	henry ford hosp (United States)	11
6	Sweden	12	2.6%	Zhengzhou Univ (China)	10
7	Russia	11	2.4%	Uppsala Univ (Sweden)	10
8	Iran	8	1.7%	Virginia Commonwealth Univ (United States)	10
9	Canada	5	1.1%	Sichuan Univ (China)	10
10	Italy	5	1.1%	Univ Calif San Francisco (United States)	10

with a purple outer circle represent having a larger BC). The top 10 institutions based on betweenness centrality are listed in Supplementary Table 1.

3.3 Most prolific and cited journals

One hundred eighty-seven journals published articles related to stem cells and TBI. We summarized the journal information of the top 15 most prolific and cited (Table 2). The *Journal of Neurotrauma* published the most papers ($n = 36$, 7.8%), followed by *Neural Regeneration Research* ($n = 24$, 5.2%), *Cell Transplantation* ($n = 15$, 3.3%), and *Brain Research* ($n = 13$, 2.8%). Among the top 15 journals, *Acta Biomaterialia* (IF = 10.633) is the journal with the highest impact factor, followed by the *Journal of Neuroinflammation* (IF = 9.587) and *Stem Cell Research & Therapy* (IF = 8.079). From Table 2, more than half of the journals belong to Q1. Six publishers were from the USA, three from the UK, and the others from Switzerland, the Netherlands, and India. Subsequently, we screened 46 journals with more than three publications and created the journal coupling map using VOSviewer. The *Journal of Neurotrauma* (IF = 4.869) has active coupling relationships with *Neural Regeneration Research* (IF = 6.058), *Journal of Neurosurgery* (IF = 5.526), and *Stem Cells* (IF = 5.845), etc. (Figure 5A), according to the nodes that represent journals marked by different colors, we can also find the AAY of each periodical.

As for the analysis of cited journals, two-thirds of the journals belong to Q1, five journals have been cited more than 500 times, and the *Journal of Neurotrauma* ($n = 1,665$) was the most cited, followed by the *Journal of Neuroinflammation* ($n = 630$), *Neurosurgery* ($n = 601$), and *Journal of Neuroscience Research* ($n = 600$). Furthermore, the journal with the highest impact factor is *Biomaterials* (IF = 15.304), followed by the *Journal of Neuroinflammation* (IF = 9.587) and *Stem Cell Research & Therapy* (IF = 8.079). The network visualization map of the journal citation analysis was created by filtering journals with less than 50 citations (Figure 5B). *Journal of Neurotrauma* has close citation relationships with *Experimental Neurology*, *Cell transplantation*, *Neurol regeneration research, and Neurosurgery*.

In the WoSCC database, each article was categorized with one or more subject categories. The dual-map overlay of journals represented the disciplinary distribution of journals related to stem cell and TBI research. As depicted in Figure 5C, the citing trajectories were

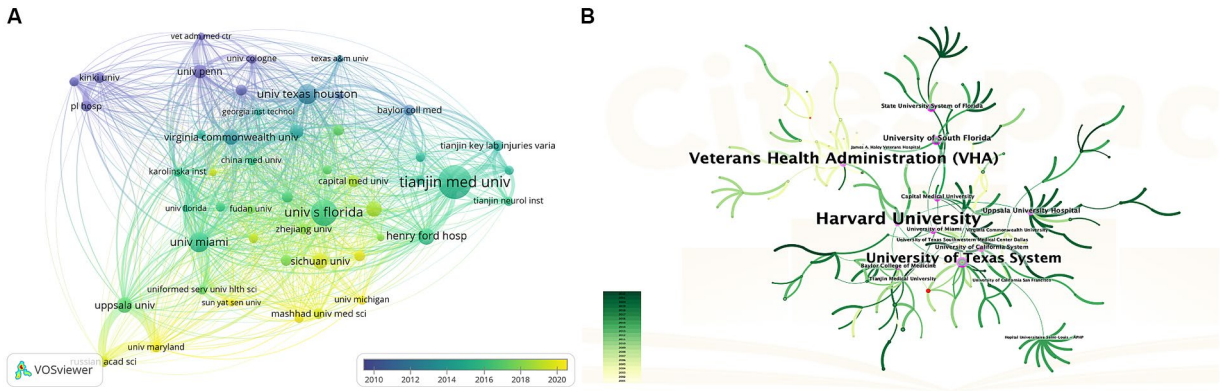

FIGURE 4
(A) The overlay visualization map of Institution co-authorship analysis conducted by VOSviewer. **(B)** Network visualization map of institutional collaborations generated by CiteSpace. A node represents an institution, each line represents the strength of the cooperation relationship between two institutions, Generally, nodes with a BC value of more than 0.1 occupy pivotal positions connecting many nodes and are identified as hubs of nodes displayed in purple rings.

TABLE 2 The top 15 most prolific journals and cited journals.

Rank	Journal	Articles (percent)	IF	JCR	Country	Cited Journal	Citation	IF	JCR
1	Journal of Neurotrauma	36 (7.84)	4.869	Q2	United States	Journal of Neurotrauma	1,665	4.869	Q2
2	Neural Regeneration Research	24 (5.23)	6.058	Q2	China	Journal of Neuroinflammation	630	9.587	Q1
3	Cell Transplantation	15 (3.27)	4.139	Q3	United States	Neurosurgery	601	5.315	Q1
4	Brain Research	13 (2.83)	3.61	Q4	Netherlands	Journal of Neuroscience Research	600	4.433	Q2
5	Experimental Neurology	11 (2.40)	5.62	Q1	United States	Experimental Neurology	515	5.62	Q1
6	Stem Cells	11 (2.40)	5.845	Q1	United States	Journal of Neurosurgery	496	5.526	Q1
7	Stem Cell Research & Therapy	9 (1.96)	8.079	Q1	England	Brain Research	437	3.61	Q4
8	International Journal of Molecular Sciences	8 (1.74)	6.208	Q3	Switzerland	Stem Cells	427	5.845	Q1
9	Journal of Neuroinflammation	7 (1.53)	9.587	Q1	England	Cell Transplantation	385	4.139	Q1
10	Restorative Neurology and Neuroscience	7 (1.53)	2.976	Q2	Netherlands	Neural Regeneration Research	368	4.433	Q3
11	Frontiers in Cellular Neuroscience	6 (1.31)	6.147	Q1	Switzerland	Frontiers in Cellular Neuroscience	324	6.147	Q1
12	Frontiers in Neurology	6 (1.31)	4.086	Q2	Switzerland	Stem Cell Research & Therapy	316	8.079	Q1
13	Molecular Neurobiology	6 (1.31)	5.682	Q2	United States	Journal of Neuroscience	260	6.709	Q1
14	Neurosurgery	6 (1.31)	5.315	Q1	United States	Neurochemistry International	238	4.297	Q2
15	Acta Biomaterialia	5 (1.09)	10.633	Q1	England	Biomaterials	219	15.304	Q1

constructed within the dual-map overlay module, where the left side represents clusters of citing journals and the right side represents clusters of cited journals. The yellow and pink lines indicate that literature published in molecular/biology/immunology and neurology/sports/ophthalmology journals often cite literature published in molecular/biology/genetics journals.

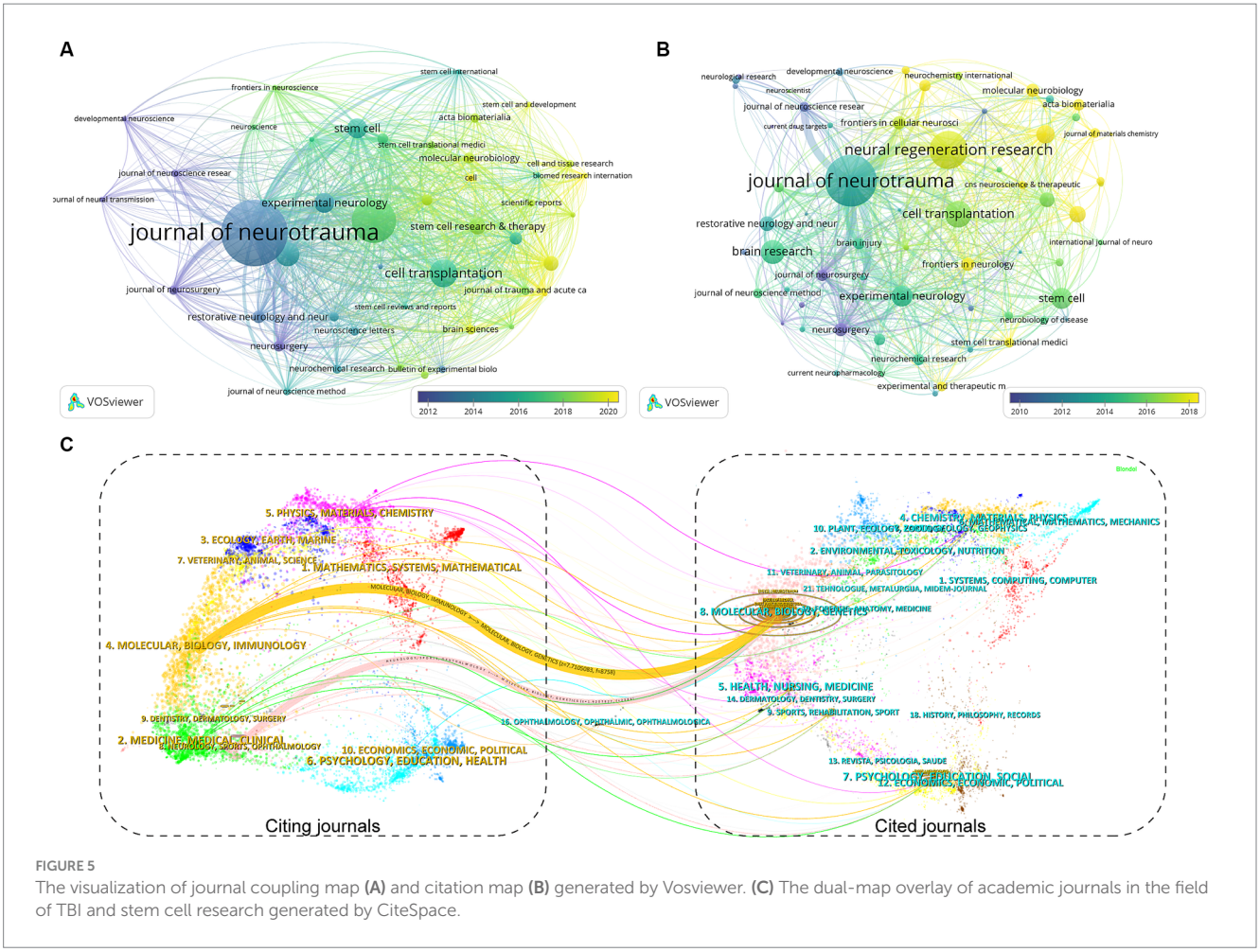

FIGURE 5
The visualization of journal coupling map **(A)** and citation map **(B)** generated by Vosviewer. **(C)** The dual-map overlay of academic journals in the field of TBI and stem cell research generated by CiteSpace.

3.4 Analysis of the influential authors

More than 2,500 authors participated in research on stem cells and TBI. Charles S. Cox, Jr. from The University of Texas Health Science Center at Houston was the author with the most published literature ($n = 21$), followed by Zhang Jianning ($n = 15$), and Zhang Sai ($n = 8$), Zhang Jianning and Zhang Sai came from the same university (Tianjin Medical University) (Table 3).

In Figure 6A, we generated an overlay visualization map of author co-authorship analysis by VOSviewer software. Several researcher clusters have been produced, and each cluster is radiated by a core author such as Cox Charles s. jr., Zhang Jianning, and Zhang Sai. There are only a few connections between different clusters, which indicates that cooperation and communication have not been well developed in this area. In addition, we can also know the AAY of each author based on the color in the lower right corner, we can find that clusters centered around Zhang Sai seem to be relatively young researchers in this field.

The co-citation relationship refers to two authors/works of literature appearing together in the reference list of a third document, the author co-citation analysis is often used to reveal the key authors in a co-citation network of a particular field. Generally, frequently cited authors are thought to have a more significant influence than those less cited. Authors who are co-cited are likely to focus on similar research areas. As shown in Table 3 five authors were co-cited more than 100 times. Asim Mahmood is the most co-cited author ($n = 297$), followed by Sharma Hari Shanker ($n = 151$) and Xiong Ye ($n = 139$). As we can see in Figure 6B, highly co-cited authors occupied key locations connecting many nodes, the hubs of nodes marked with purple rings.

3.5 Cited references and co-cited references

Although there remains some controversy on the value of citation rates (39, 40), the number of citations remains a crucial indicator of scholarly impact (41), as highly cited papers typically reflect a high degree of academic attention and represent the research hotspots in a field. Table 4 lists the top 10 most cited papers, over half were cited at least 200 times. These studies were published from 2001 to 2017, and the majority of articles were published in neurosurgery journals such as the *Journal of Neuroscience Research*, *Journal of Neuroinflammation*, *Journal of Neurotrauma*, and *Neurosurgery*. Nine of them are original articles, and one is a systematic review. Specifically, the most cited paper in this area is the article "Enhanced Neurogenesis in the Rodent Hippocampus Following Traumatic Brain Injury" published by P.K. Dash (42), cited 344 times. The second and third most cited papers were published by Run Zhang et al. (43) and Steven G. Kernie et al. (44), which were animal model studies about the

TABLE 3 The top 10 authors and co-cited authors involved in research on TBI and stem cell.

Rank	Highly published authors	Count	Highly cited authors	Citations	Co-cited authors	Citations
1	Cox Charles S. Jr.	21	Cox Charles S. Jr.	1,190	Asim Mahmood	297
2	Zhang Jianning	15	Mcintosh Tk	674	Sharma Hari Shanker	151
3	Zhang Sai	8	Jimenez Fernando	655	Xiong, Ye	139
4	Jimenez Fernando	8	Harting Matthew T.	575	Lu, Dunyue	115
5	Xue Hasen	8	dash pramod k.	569	Harting Matthew T.	100
6	Mcintosh Tk	8	Xue Hasen	490	Sun, Dong	99
7	Walker Peter a.	7	Walker Peter a.	448	Walker, Peter a.	98
8	Harting Matthew t.	7	shah shinil k.	439	borlongan cesar v.	79
9	borlongan cesar v.	7	pati shibani	407	Riess, Peter	75
10	shah shinil k.	7	Zhang Jianning	274	Cox Charles s. jr.	75

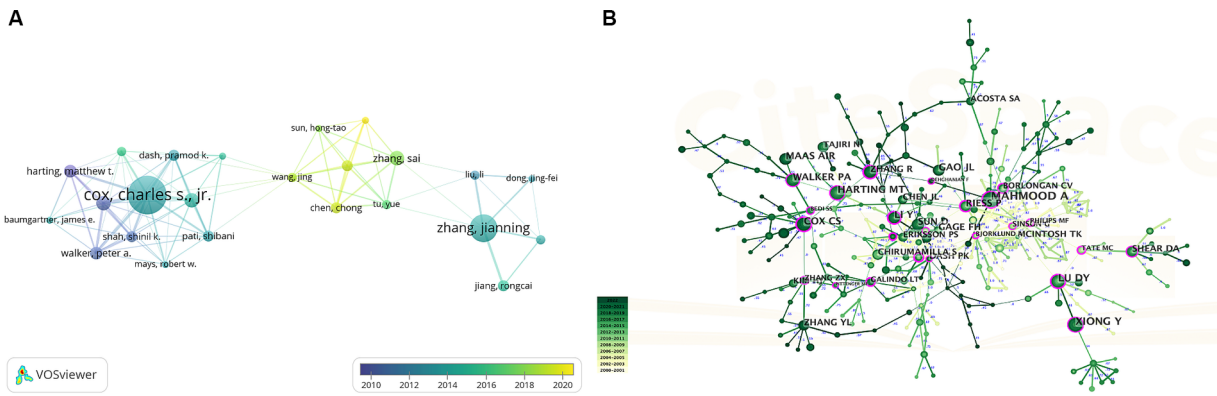

FIGURE 6
(A) Overlay visualization map of author co-authorship analysis generated by VOSviewer. **(B)** Visualization map of author co-citation analysis by using CiteSpace software.

immunomodulatory effect of MSC transplantation and proliferation of neuron and astrocytic after TBI. In summary, the predominant topics covered by these 10 publications include the pharmacologic studies of stem cell or cell-derived exosomes after TBI (43, 45–49), molecular mechanism research underlying TBI-associated neurogenesis (42, 44, 50), and review regarding stem cell therapy for the immune response after TBI (51).

In addition, co-citation analysis of reference is a practical approach for evaluating research hotspots and tracking advancements in the field. The literature network of co-citation was divided into 9 clusters using CiteSpace (Figure 7A), with each cluster focusing on similar research topics. To assess the significance of the cluster structure, we evaluated two parameters: modularity value (*Q*-value) and mean silhouette value (*S*-value). Our findings indicate that the *Q*-value (0.7127) exceeds 0.3, suggesting a reasonable network, while the *S*-value (0.9042) exceeds 0.7, indicating high homogeneity within clusters (52). The largest cluster identified was labeled as "#0 neurogenic niche," followed by "#1immunomodulation," "#2 TBI," and "#3 cellular therapy."

Additionally, we employed a timeline view of co-cited references to conduct a visual analysis by integrating clustering and time-slicing techniques (Figure 7B). The arrangement of cluster labels is based on their appearance order after clustering, providing insights into topic distribution, trends, and correlation over time. Each horizontal line represents a collection of clustered references to which they belong. The closest clusters on the timeline were "#0 neurogenic niche," "#1 immunomodulation," "#6 endothelial progenitor cells," and "#8 collagen."

Moreover, CiteSpace can identify burst detection for highly cited references, a widely employed method for discerning actively researched hotspots or topics over time. Figure 7C shows the top 20 references with significant citation bursts highlighted in red, corresponding to specific time intervals denoted by blue lines. Notably, "Das M, 2019, REV NEUROSCIENCE, V30, P839, DOI 10.1515/revenue-2019-0002" (2019-2022, strength = 7.39), "Taylor CA, 2017, MMWR SURVEILL SUMM, V66, P1, DOI 10.15585/mmwr. ss6609a1" (2019-2022, strength = 6.07), and "Ni HQ, 2019, FRONT NEUROSCI-SWITZ, V13, P0, DOI 10.3389/fnins.2019.00014" (2019-2022, strength = 5.11) represent recently published highly influential literature.

3.6 Analysis of keywords

Besides references, keywords can also represent a specific topic's core themes and primary content (53). After aggregating keywords

TABLE 4 Top 10 cited references of publications in TBI and stem cells.

Rank	Title	Journal	First author	Publication year	Citations
1	Enhanced neurogenesis in the rodent hippocampus following traumatic brain injury	Journal of Neuroscience Research	P.K. Dash	2001	344
2	Anti-inflammatory and immunomodulatory mechanisms of mesenchymal stem cell transplantation in experimental traumatic brain injury	Journal of Neuroinflammation	Run Zhang	2013	263
3	Brain Remodeling Due to Neuronal and Astrocytic Proliferation After Controlled Cortical Injury in Mice	Journal of Neuroscience Research	Steven G. Kernie	2001	248
4	Traumatic Brain Injury Induced Cell Proliferation in the Adult Mammalian Central Nervous System	Journal of Neurotrauma	S. Chirumamilla	2002	238
5	Systemic administration of cell-free exosomes generated by human bone marrow derived mesenchymal stem cells cultured under 2D and 3D conditions improves functional recovery in rats after traumatic brain injury	Neurochemistry Internationa	Yanlu Zhang	2017	220
6	Treatment of Traumatic Brain Injury in Female Rats with Intravenous Administration of Bone Marrow Stromal Cells	Neurosurgery	Asim Mahmood	2001	203
7	Intravenous mesenchymal stem cell therapy for traumatic brain injury	Journal of Neurosurgery	Matthew T. Harting	2009	199
8	Hypoxic preconditioning enhances the therapeutic potential of the secretome from cultured human mesenchymal stem cells in experimental traumatic brain injury	Clinical Science	Ching-Ping Chang	2013	194
9	Transplanted Neural Stem Cells Survive, Differentiate, and Improve Neurological Motor Function after Experimental Traumatic Brain Injury	Neurosurgery	Peter Riess	2002	190
10	New perspectives on central and peripheral immune responses to acute traumatic brain injury	Journal of Neuroinflammation	Mahasweta Das	2012	170

with the same connotation, we analyzed the keywords that appeared more than five times in all literature using VOSviewer (Figure 8A). A total of 70 keywords were identified, and the top five most frequently occurring keywords were traumatic brain injury (349 times), stem cell (86 times), neural stem cell (84 times), mesenchymal stem cell (52 times), and transplantation (43 times).

Meanwhile, we employed CiteSpace's burst detection algorithm to identify keyword bursts. Figure 8B presents the top 15 keywords with the most vigorous bursts. The most prominent keyword was "central nervous system" (strength 8.72), followed by "progenitor cell" (strength 7.17). After 2019, "extracellular vesicles," "inflammation," "activation," and "repair" were keywords with citation bursts.

4 Discussion

4.1 General information

For this study, we conducted a comprehensive search of articles on TBI and stem cells in the Web of Science databases from 2000 to 2022. Our analysis included 459 English papers affiliated with 637 institutions across 45 countries/regions. While there was some variation in publication numbers over the years, an overall upward trend was observed, reaching its peak in 2022, with 51 publications accounting for approximately 11.11% of the total corpus. These findings indicate a growing research interest in investigating the relationship between TBI and stem cells (54).

China and the United States have emerged as significant contributors to these publications, collectively accounting for over 70% of the total publications. The distribution of institutions mirrors this pattern, with six out of the top 10 institutions based in the United States and three in China. Despite the significant contributions made by researchers from Asian countries to paper publications, collaborative networks have yet to be established among research institutions in these regions (Figure 4). It is imperative to remove academic barriers and enhance cooperation and communication between diverse research institutions or groups.

The *Journal of Neurotrauma* ($n = 36$, 7.8%) ranked first in total publications, focusing on the traumatic injury of the central and peripheral nervous system and encompassing fundamental biology and clinical trials. It was followed by *Neural Regeneration Research* ($n = 24$, 5.2%) and *Cell Transplantation* ($n = 15$, 3.3%), indicating their interest in TBI and stem cell research articles. These findings will assist future scholars in selecting appropriate journals for submitting their contributions. Notably, the top 10 journals published only 141 papers, accounting for merely 30.72% of all papers, this suggests further potential for the impact of papers. Furthermore, most of these influential journals are located in

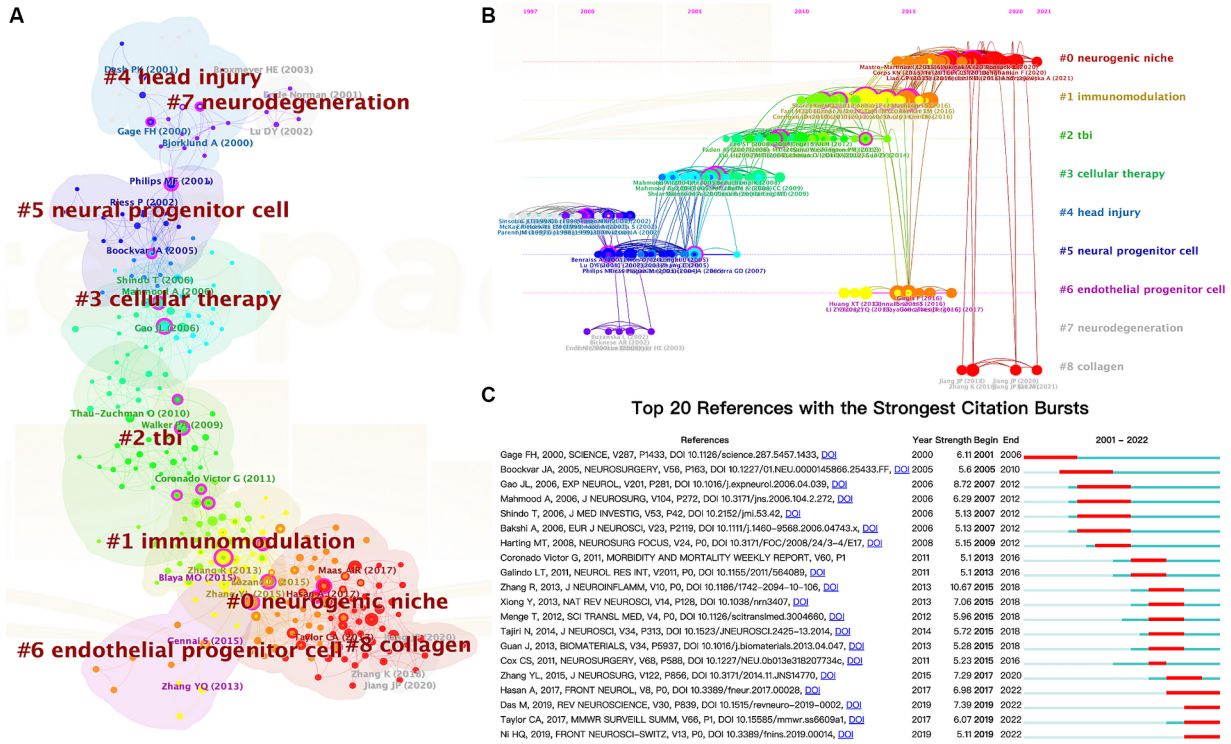

FIGURE 7
The cluster view map **(A)** and timeline view map **(B)** of reference co-citation analysis were generated by CiteSpace. **(C)** Top 20 references with the most robust citation bursts.

Western Europe and North America; China is represented by only one journal, with no representation from Japan or Korea. This situation highlights the need for Asian countries to enhance the development of international journals and augment their academic influence further, particularly in China, where the number of individuals affected by TBI surpasses that of most nations, resulting in a substantial burden on society and families (55). It is commendable that the Chinese government has invested considerable resources in the construction of international journals, with multiple incentive measures in recent years (56).

Charles S. Cox Jr. has published 21 papers and been cited 1,190 times, establishing himself as one of the most prolific scholars with noteworthy achievements. Through a comprehensive analysis of publication frequency, citation impact, and co-citation patterns, we identified that Charles S. Cox Jr., Walker Peter A., and Harting Matthew T. were the scholars who appeared in all three indicators simultaneously, suggesting that they are accomplished authors in this field. Notably, three researchers are all from the University of Texas Health Science Center Houston, this team is known for its essential contribution to the research field (57), particularly concerning cell therapy safety for individuals affected by TBI or SCI (58). They would make excellent potential collaborators for researchers.

Furthermore, it is worth highlighting the lack of close cooperation among scholars in this domain. Out of 78 researchers who have published more than four papers, only approximately 30% could establish co-authorship networks (Figure 6A), indicating that collaboration was primarily confined to specific teams. Scholars from various institutions should strive for technological innovation and breakthroughs within research activities by strengthening cooperation, including personnel exchange and study, research progress communication, and sharing platforms and data.

4.2 Development of stem cell research in TBI

The study of TBI and stem cells continuously evolves, with discoveries and insights emerging regularly. We have created a knowledge map of the research in this field through citation and co-citation analysis. In general, research can be categorized into two main areas. The first area focuses on the endogenous stem cells activated by TBI. This research aims to investigate the mechanisms underlying their activation and enhance their efficiency in differentiating into mature neurons. The second area involves using exogenous stem cells for treating TBI, which stems from the overall advancements in cell therapy. Investigating diverse cell types, identifying specific components that facilitate recovery, and employing novel techniques to enhance cell retention and prognosis constitute the primary focus of studies. Ongoing studies continue to shed new light on the potential of both endogenous and exogenous stem cells in improving outcomes for TBI patients.

4.2.1 Endogenous stem cells

In 2001, P.K. Ash demonstrated that TBI induces a significant upregulation in neurogenesis within the dentate gyrus region, with peak production observed between days 3 and 7 post-injury, returning to baseline levels by day 14 (42), as a result of this groundbreaking study, Ash has received the highest number of citations in the field. In

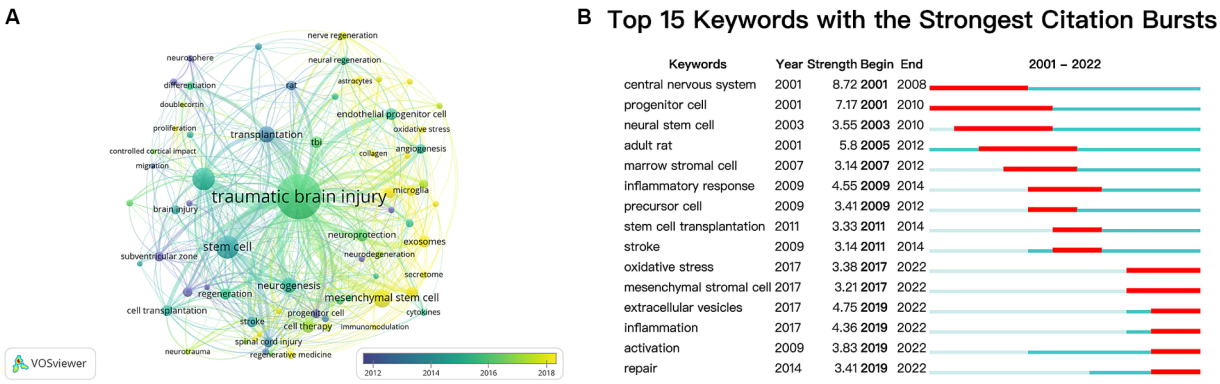

FIGURE 8
(A) Overlay visualization map of keywords analysis based on the VOSviewer. The node size is proportional to the sum of occurrence times. The color of each node implies the average appearing year according to the color gradient in the lower right corner. Bluish represents the keywords that appeared relatively earlier, and yellow reflects the recent occurrence. **(B)** Top 15 keywords with the strongest citation bursts.

parallel, Steven G. Kernie discovered that neural proliferation plays a crucial role in remodeling after TBI and proposed a mechanism for explaining how functional recovery can be sustained over an extended period following such injuries (44). One year later, Chirumamilla, S. observed a significant rise in the overall number of proliferating cells within both the subventricular zone (SVZ) and hippocampus just 48 h after TBI; however, differentiation had not yet commenced among these proliferating cells within SVZ. Additionally, notable growth was explicitly seen in immature astrocytes and activated microglia but not neurons within the hippocampus region (50). These three articles are cornerstones in the research field of endogenous nerve regeneration after TBI, based on these articles' findings, scholars aim to promote outcomes of TBI. Given the inherent limitations of innate recovery capacity, it is necessary to enhance this endogenous process through exogenous means, diverse categories of growth factors and pharmaceutical agents can potentially augment neurogenesis (59). Brain-derived neurotrophic factor (BDNF), bFGF, and EGF can enhance TBI-induced cell proliferation in the hippocampus and the SVZ (60–62). Neurotrophic factors have been widely investigated for their role in promoting NSC survival, proliferation, and differentiation, these findings suggest that neurotrophic factors hold promise as potential therapeutic agents for enhancing endogenous NSC regeneration after TBI.

Additionally, neuroinflammation plays a crucial role in the pathophysiology of TBI, and emerging evidence suggests its modulation of endogenous repair mechanisms (63). Suppression of inflammation through progranulin administration protects hippocampal neurogenesis (64), while hyperbaric oxygen therapy may enhance outcomes of TBI in rats by inhibiting inflammation and gliosis (65). The extracellular matrix (ECM) also regulates the behavior of NSC, where chondroitin sulfate proteoglycans (CSPGs) facilitate endogenous NSC repair following injury through ECM manipulation (66). Furthermore, electrical stimulation promoted anti-inflammatory phenotypes of microglia and increased the population of NSCs, thereby regulating neuroinflammation and enhancing neuroregeneration (67). These findings present a novel opportunity to facilitate endogenous NSC regeneration. Future research should prioritize elucidating the underlying mechanisms governing endogenous NSC behavior and identifying innovative targets for therapeutic intervention.

4.2.2 Exogenous stem cells

While endogenous NSC regeneration holds promise, transplantation strategies involving exogenous NSCs have also been explored. Exogenous stem cells exert their therapeutic effects through various mechanisms. Transplanted stem cells not only can directly differentiate into neuronal and glial cell types, thereby replacing damaged cells within the injured brain (49), but also secrete trophic factors, such as growth factors and cytokines, which promote endogenous repair mechanisms, enhance neuroplasticity, and reduce inflammation (68).

In 2001, Asim Mahmood and colleagues experimented with using marrow stromal cells to treat TBI, they injected cells through the tail vein of rats, resulting in a significant reduction in motor and neurological deficits; the transplanted cells exhibited a preference for implanting themselves into the damaged brain tissue and expressed markers indicative of neurons (NeuN) and astrocytes (GFAP) (46). One year later, Peter Riess and colleagues utilized stereotactic injection to transplant murine neural stem cells (NSCs) into mice with CCI-induced brain injuries; the study demonstrated that the transplanted NSCs were capable of surviving within the injured brain, differentiating into either neurons or glial cells, and subsequent a reduction in motor dysfunction caused by TBI. These pioneering studies signify the inception of exogenous stem cell therapy for TBI. Inspired researchers were dedicated to further stem cell research as a potential therapeutic strategy for various diseases (69, 70). In numerous preclinical studies and early clinical trials, intravenous infusion is a cell delivery method (71). However, Charles S. Cox Jr. and colleagues observed that the majority of MSCs localized primarily in the lungs within 48 h after infusion, only 0.0005% reached the cerebral parenchyma and remained there over time (47), MSCs were largely undetectable in brain tissue after 2 weeks, they described this phenomenon as the "pulmonary first-pass effect," which may impede therapeutic efficacy significantly. Further optimization of strategies for stem cell transplantation is imperative to ensure successful clinical translation. Considerations encompass the timing and delivery routes of transplantation, optimal cell dosage, and immunological compatibility.

Scholars have conducted additional studies to gain deeper insights into the beneficial effects of cell therapy for traumatic brain injury (TBI). In 2012, Mahasweta Das et al. published a review focusing on various effector cells, cytokines, and signaling pathways

involved in the pathophysiology of TBI (51); they also discussed the immunoreaction observed after stem cell transplantation. One year later, Run Zhang and Yi Liu discovered that MSCs can regulate inflammation-related immune cells and cytokines during brain inflammatory responses caused by TBI (43). During this period, researchers have discovered a paracrine mechanism mediated by stem cell releasing factor that plays a crucial role in repairing brain injuries following stem cell mobilization (72). Ching-Ping Chang and colleagues found that MSCs secrete bioactive factors such as HGF and VEGF, which stimulate neurogenesis and improve the prognosis in rat models of TBI (48). However, MSC therapy has a few drawbacks, including tumor formation, which can be avoided using MSC-derived exosomes (73). Yanlu Zhang demonstrated the efficacy of MSC-generated exosomes in enhancing functional recovery by stimulating angiogenesis and neurogenesis (74). Exosomes derived from bone marrow mesenchymal stem cells also potentially mitigate early inflammatory response after TBI (75). Combining exosome therapy with hydrogels for traumatic brain injury repair by promoting angiogenesis and neurogenesis (76), this combination therapy approach holds promise for optimizing exosome delivery and creating a conducive microenvironment for tissue repair in TBI.

Collectively, these highly cited and co-cited articles provide valuable insights into the current understanding of neuroregeneration, the exploration and advancement of cell therapy, and the therapeutic potential of stem cell-derived exosomes. Investigating the pathophysiological changes occurring in stem cells following TBI can enhance our comprehension of factors influencing nerve regeneration. Compared to conventional drugs or surgery, both stem cells and their derived exosomes offer significant advantages for treatment. Therefore, studying strategies involving stem cells for TBI treatment holds immense practical value in promoting nerve regeneration.

4.3 Research hotspots and keywords

To investigate and elucidate the hotspots of TBI and stem cell research further, we did a citation clustering analysis using CiteSpace. As depicted in Figures 7A,B, initial studies focused on understanding the pathophysiology, mechanism underlying neuroregeneration, and experimental stem cell therapy after TBI, including labels "#4 head injury," "#7 neurodegeneration," "#5 neural progenitor cell," and "#3 cellular therapy." However, current research is centered around exploring immunomodulatory aspects, microenvironments associated with stem cells, and enhancing therapeutic efficacy through combination with biomaterials, such as "#1 immunomodulation," "#0 neurogenic niche," and "#8 collagen." Additionally, VOSviewer was employed to generate a visualization map (Figure 8A), which effectively integrates frequently occurring keywords with their corresponding average appearing year (AAY). The AAY for keywords such as "exosomes," "neuroinflammation," and "microglia" indicates that these topics have recently gained attention and hold the potential to become prominent areas of research. Furthermore, utilizing CiteSpace's burst keyword analysis (Figure 8B), we identified emerging hotspots in the field, revealing an upsurge in citations related to "extracellular vesicles" and "inflammation" during the period from 2019 to 2022. As we all know, exosomes are a specific type of extracellular vesicle (77), while microglia play a crucial role in neuroinflammation (78, 79). Therefore, both methods highlight "exosomes" and "neuroinflammation" as candidates with significant potential to emerge as research hotspots.

In recent decades, significant progress has been made in the research of TBI and the potential application of stem cells in the therapeutic intervention (80). Stem cell-based therapy has emerged as a promising approach for addressing injuries and disorders associated with the central nervous system. Investigations into the utilization of stem/progenitor cells for the treatment of brain injury (47, 73), spinal cord injury (81, 82), and stroke (83, 84) have yielded positive outcomes in facilitating rehabilitation.

Researchers have been investigating the impact of neurodegeneration after traumatic brain injury (TBI), which can result in enduring cognitive impairments (85) and chronic neurological deficits, including Alzheimer's and Parkinson's disease (86). Stem cell therapy is currently receiving attention due to its potential to delay or halt the progression of neurodegenerative disorders following TBI (87). Moreover, stem cells may contribute to immunomodulation by mitigating inflammation (4) and promoting neural repair in response to the inflammatory cascade triggered after TBI (88, 89). The stem cell niche, also known as the microenvironment surrounding stem cells, plays a crucial role in regulating cell fate within specific anatomical locations where stem cells reside (90). The term 'niche' denotes the stem-cell microenvironment *in vivo* or *in vitro*. By modulating the neurogenic niche, stem cells can promote neurogenesis and enhance the brain's regenerative capacity following injury (91). Researchers have explored the potential of collagen-based scaffolds to create a conducive environment for the survival and integration of stem cells within damaged brain tissues (92, 93). This approach holds promise for augmenting the efficacy of TBI treatment using stem cell therapy (94). In summary, the research on TBI and stem cells is rapidly advancing, demonstrating significant progress in applying neural stem cells, immunomodulation techniques, regulating the neurogenic niche, and collagen-based scaffolds. These emerging areas hold immense potential for improving the prognosis of patients with brain injuries and neurodegenerative disorders.

Bibliometric research serves as a method for elucidating the structure and dynamics of scientific knowledge, facilitating the visualization of intricate relationships among knowledge clusters (95). Consequently, comprehending these intricate knowledge connections enables researchers to gain valuable insights into domain-specific trends in knowledge. Our studies suggest that immune regulation and inflammatory responses after TBI and exploring strategies to enhance exosome or biomaterial combinations could significantly contribute to future studies in this field.

4.4 Limitations

This study provides an overview of current research, analyzes hot areas of concern, and predicts future trends. However, certain limitations should be acknowledged. Firstly, the literature searches were limited to the WoSCC database, excluding non-English language publications and other databases, which may introduce selection bias. However, as mentioned in previous bibliometric studies, WoSCC is widely used as a reliable database due to its extensive data coverage. Additionally, slight output variations may occur when software applies different parameter settings since no standardized setting is available. Lastly, due to their low citation counts, recent studies published in

high-quality journals might not have been included or fully considered during citation and co-citation analyses.

5 Conclusion

This study represents the first comprehensive bibliometric analysis of literature on TBI and stem cells from 2000 to 2022. The involvement of stem cells in TBI has gradually gained attention among researchers, as evidenced by an increasing number of annual publications and citations. The United States and China have become leading contributors in this field, however, cooperation and exchanges between countries and institutions still need strengthening. Notably, *The Journal of Neurotrauma* has significant influence within this domain, along with Tianjin Medical University and Charles S. Cox Jr., influential organizations and authors, respectively. According to the burst references, "neurogenic niche" and "immunomodulation" have been identified as research hotspots within this field; further investigation is warranted to explore the potential of "exosomes" and "neuroinflammation." The research on TBI and stem cells has entered a new stage. Based on the neurogenesis mechanism of endogenous NSC and the treatment of exogenous stem cells, the development of therapeutic strategies for nerve function recovery is expected. Particularly, addressing the urgent issue of combining bioengineering technology with advancements in immune regulation after TBI will pave the way for future directions in post-TBI stem cell therapy.

Data availability statement

The original contributions presented in the study are included in the article/Supplementary material, further inquiries can be directed to the corresponding authors.

Author contributions

TD: Conceptualization, Data curation, Formal analysis, Methodology, Software, Visualization, Writing – original draft. RD: Data curation, Formal analysis, Software, Writing – review & editing. YW: Software, Validation, Writing – review & editing. YC: Validation, Visualization, Writing – review & editing. HS: Conceptualization, Methodology, Writing – review & editing. MZ: Conceptualization, Methodology, Project administration, Supervision, Writing – review & editing.

Funding

The author(s) declare that financial support was received for the research, authorship, and/or publication of this article. This work was supported by the Medical Innovation and Development Project of Lanzhou University (lzuyxcx-2022-132), the National Natural Science Foundation of China (32070791), the Natural Science Foundation of Gansu Province of China (21JR7RA356), and the Science and Technology Program of Lanzhou (2022-ZD-93). The funders did not participate in the design or conduct of the study.

Conflict of interest

The authors declare that the research was conducted in the absence of any commercial or financial relationships that could be construed as a potential conflict of interest.

Publisher's note

Supplementary material

The Supplementary material for this article can be found online at: https://www.frontiersin.org/articles/10.3389/fneur.2024.1301277/full#supplementary-material

SUPPLEMENTARY TABLE S1
The top 10 institutions and betweenness centrality.

SUPPLEMENTARY DATA S1
Raw file with bibliographic information for all 459 articles.

References

1. Maas AIR, Menon DK, Manley GT, Abrams M, Akerlund C, Andelic N, et al. Traumatic brain injury: progress and challenges in prevention, clinical care, and research. *Lancet Neurol.* (2022) 21:1004–60. doi: 10.1016/S1474-4422(22)00309-X

2. Dixon KJ. Pathophysiology of traumatic brain Injury. *Phys Med Rehabil Clin N Am.* (2017) 28:215–25. doi: 10.1016/j.pmr.2016.12.001

3. Graham NS, Sharp DJ. Understanding neurodegeneration after traumatic brain injury: from mechanisms to clinical trials in dementia. *J Neurol Neurosurg Psychiatry.* (2019) 90:1221–33. doi: 10.1136/jnnp-2017-317557

4. Jassam YN, Izzy S, Whalen M, McGavern DB, El Khoury J. Neuroimmunology of traumatic brain Injury: time for a paradigm shift. *Neuron.* (2017) 95:1246–65. doi: 10.1016/j.neuron.2017.07.010

5. Ma DK, Bonaguidi MA, Ming GL, Song H. Adult neural stem cells in the mammalian central nervous system. *Cell Res.* (2009) 19:672–82. doi: 10.1038/cr.2009.56

6. Gage FH, Temple S. Neural stem cells: generating and regenerating the brain. *Neuron.* (2013) 80:588–601. doi: 10.1016/j.neuron.2013.10.037

7. GBD 2016 Traumatic Brain Injury and Spinal Cord Injury Collaborators. Global, regional, and national burden of traumatic brain injury and spinal cord injury, 1990-2016: a systematic analysis for the global burden of disease study 2016. *Lancet Neurol.* (2019) 18:56–87. doi: 10.1016/S1474-4422(18)30415-0

8. Chesnut RM, Temkin N, Carney N, Dikmen S, Rondina C, Videtta W, et al. A trial of intracranial-pressure monitoring in traumatic brain injury. *N Engl J Med.* (2012) 367:2471–81. doi: 10.1056/NEJMoa1207363

9. Andrews PJ, Sinclair HL, Rodriguez A, Harris BA, Battison CG, Rhodes JK, et al. Hypothermia for intracranial hypertension after traumatic brain injury. *N Engl J Med.* (2015) 373:2403–12. doi: 10.1056/NEJMoa1507581

10. Hutchinson PJ, Kolias AG, Timofeev IS, Corteen EA, Czosnyka M, Timothy J, et al. Trial of decompressive craniectomy for traumatic intracranial hypertension. *N Engl J Med.* (2016) 375:1119–30. doi: 10.1056/NEJMoa1605215

11. Zhou Y, Shao A, Xu W, Wu H, Deng Y. Advance of stem cell treatment for traumatic brain Injury. *Front Cell Neurosci.* (2019) 13:301. doi: 10.3389/fncel.2019.00301

12. Lane SW, Williams DA, Watt FM. Modulating the stem cell niche for tissue regeneration. *Nat Biotechnol.* (2014) 32:795–803. doi: 10.1038/nbt.2978

13. Liu SJ, Zou Y, Belegu V, Lv LY, Lin N, Wang TY, et al. Co-grafting of neural stem cells with olfactory en sheathing cells promotes neuronal restoration in traumatic brain

injury with an anti-inflammatory mechanism. *J Neuroinflammation*. (2014) 11:66. doi: 10.1186/1742-2094-11-66

14. Duan H, Li X, Wang C, Hao P, Song W, Li M, et al. Functional hyaluronate collagen scaffolds induce NSCs differentiation into functional neurons in repairing the traumatic brain injury. *Acta Biomater*. (2016) 45:182–95. doi: 10.1016/j.actbio.2016.08.043

15. Hu W, Liu J, Jiang J, Yang F. Effect of bone marrow mesenchymal stem cells on angiogenesis in rats after brain injury. *Zhong Nan Da Xue Xue Bao Yi Xue Ban*. (2016) 41:489–95. doi: 10.11817/j.issn.1672-7347.2016.05.007

16. Haus DL, Lopez-Velazquez L, Gold EM, Cunningham KM, Perez H, Anderson AJ, et al. Transplantation of human neural stem cells restores cognition in an immunodeficient rodent model of traumatic brain injury. *Exp Neurol*. (2016) 281:1–16. doi: 10.1016/j.expneurol.2016.04.008

17. Lindvall O, Kokaia Z. Stem cells in human neurodegenerative disorders — time for clinical translation? *J Clin Invest*. (2010) 120:29–40. doi: 10.1172/JCI40543

18. Luan Z, Qu S, Du K, Liu W, Yang Y, Wang Z, et al. Neural stem/progenitor cell transplantation for cortical visual impairment in neonatal brain injured patients. *Cell Transplant*. (2013) 22:101–12. doi: 10.3727/096368913X672163

19. Marei HE, Hasan A, Rizzi R, Althani A, Afifi N, Cenciarelli C, et al. Potential of stem cell-based therapy for ischemic stroke. *Front Neurol*. (2018) 9:34. doi: 10.3389/fneur.2018.00034

20. Gao C, Li Y, Liu X, Huang J, Zhang Z. 3D bioprinted conductive spinal cord biomimetic scaffolds for promoting neuronal differentiation of neural stem cells and repairing of spinal cord injury. *Chem Eng J*. (2023) 451:138788. doi: 10.1016/j.cej.2022.138788

21. Cox CS Jr. Cellular therapy for traumatic neurological injury. *Pediatr Res*. (2018) 83:325–32. doi: 10.1038/pr.2017.253

22. Ngwenya LB, Danzer SC. Impact of traumatic brain Injury on neurogenesis. *Front Neurosci*. (2018) 12:1014. doi: 10.3389/fnins.2018.01014

23. Ibrahim S, Hu W, Wang X, Gao X, He C, Chen J. Traumatic brain injury causes aberrant migration of adult-born neurons in the Hippocampus. *Sci Rep*. (2016) 6:21793. doi: 10.1038/srep21793

24. Bonilla C, Zurita M. Cell-based therapies for traumatic brain injury: therapeutic treatments and clinical trials. *Biomedicines*. (2021) 9:669. doi: 10.3390/biomedicines9060669

25. Zakrzewski W, Dobrzynski M, Szymonowicz M, Rybak Z. Stem cells: past, present, and future. *Stem Cell Res Ther*. (2019) 10:68. doi: 10.1186/s13287-019-1165-5

26. Shang Z, Wanyan P, Wang M, Zhang B, Cui X, Wang X. Bibliometric analysis of stem cells for spinal cord injury: current status and emerging frontiers. *Front Pharmacol*. (2023) 14:1235324. doi: 10.3389/fphar.2023.1235324

27. Cooper ID. Bibliometrics basics. *J Med Libr Assoc*. (2015) 103:217–8. doi: 10.3163/1536-5050.103.4.013

28. Ninkov A, Frank JR, Maggio LA. Bibliometrics: methods for studying academic publishing. *Perspect Med Educ*. (2022) 11:173–6. doi: 10.1007/s40037-021-00695-4

29. Chen CM. CiteSpace II: Detecting and visualizing emerging trends and transient patterns in scientific literature. *J Am Soc Inf Sci Technol*. (2006) 57:359–77. doi: 10.1002/asi.20317

30. van Eck NJ, Waltman L. Software survey: VOSviewer, a computer program for bibliometric mapping. *Scientometrics*. (2010) 84:523–38. doi: 10.1007/s11192-009-0146-3

31. Aria M, Cuccurullo C. Bibliometrix: an R-tool for comprehensive science mapping analysis. *J Informet*. (2017) 11:959–75. doi: 10.1016/j.joi.2017.08.007

32. Chen Y, Long T, Xu Q, Zhang C. Bibliometric analysis of ferroptosis in stroke from 2013 to 2021. *Front Pharmacol*. (2021) 12:817364. doi: 10.3389/fphar.2021.817364

33. Cutler HS, Guzman JZ, Connolly J, Al Maaieh M, Skovrlj B, Cho SK. Outcome instruments in spinal trauma surgery: a bibliometric analysis. *Global Spine J*. (2016) 6:804–11. doi: 10.1055/s-0036-1579745

34. Rechberger JS, Thiele F, Daniels DJ. Status quo and trends of intra-arterial therapy for brain tumors: a bibliometric and clinical trials analysis. *Pharmaceutics*. (2021) 13:1885. doi: 10.3390/pharmaceutics13111885

35. Popkirov S, Jungilligens J, Schlegel U, Wellmer J. Research on dissociative seizures: a bibliometric analysis and visualization of the scientific landscape. *Epilepsy Behav*. (2018) 83:162–7. doi: 10.1016/j.yebeh.2018.03.041

36. Sweileh WM. Substandard and falsified medical products: bibliometric analysis and mapping of scientific research. *Glob Health*. (2021) 17:114. doi: 10.1186/s12992-021-00766-5

37. Pan X, Yan E, Cui M, Hua W. Examining the usage, citation, and diffusion patterns of bibliometric mapping software: a comparative study of three tools. *J Informet*. (2018) 12:481–93. doi: 10.1016/j.joi.2018.03.005

38. Cheng K, Guo Q, Yang W, Wang Y, Sun Z, Wu H. Mapping knowledge landscapes and emerging trends of the links between bone metabolism and diabetes mellitus: a bibliometric analysis from 2000 to 2021. *Front Public Health*. (2022) 10:918483. doi: 10.3389/fpubh.2022.918483

39. Fuster V. Impact factor: a curious and capricious metric. *J Am Coll Cardiol*. (2017) 70:1530–1. doi: 10.1016/j.jacc.2017.08.002

40. Nieminen P, Carpenter J, Rucker G, Schumacher M. The relationship between quality of research and citation frequency. *BMC Med Res Methodol*. (2006) 6:42. doi: 10.1186/1471-2288-6-42

41. Chatterjee P, Werner RM. Gender disparity in citations in high-impact journal articles. *JAMA Netw Open*. (2021) 4:e2114509. doi: 10.1001/jamanetworkopen.2021.14509

42. Dash PK, Mach SA, Moore AN. Enhanced neurogenesis in the rodent hippocampus following traumatic brain injury. *J Neurosci Res*. (2001) 63:313–9. doi: 10.1002/1097-4547(20010215)63:4<313::AID-JNR1025>3.0.CO;2-4

43. Zhang R, Liu Y, Yan K, Chen L, Chen XR, Li P, et al. Anti-inflammatory and immunomodulatory mechanisms of mesenchymal stem cell transplantation in experimental traumatic brain injury. *J Neuroinflammation*. (2013) 10:106. doi: 10.1186/1742-2094-10-106

44. Kernie SG, Erwin TM, Parada LF. Brain remodeling due to neuronal and astrocytic proliferation after controlled cortical injury in mice. *J Neurosci Res*. (2001) 66:317–26. doi: 10.1002/jnr.10013

45. Zhang Y, Chopp M, Zhang ZG, Katakowski M, Xin H, Qu C, et al. Systemic administration of cell-free exosomes generated by human bone marrow derived mesenchymal stem cells cultured under 2D and 3D conditions improves functional recovery in rats after traumatic brain injury. *Neurochem Int*. (2017) 111:69–81. doi: 10.1016/j.neuint.2016.08.003

46. Mahmood A, Lu D, Wang L, Li Y, Lu M, Chopp M. Treatment of traumatic brain injury in female rats with intravenous administration of bone marrow stromal cells. *Neurosurgery*. (2001) 49:1196–1203; discussion 203-4. doi: 10.1097/00006123-200111000-00031

47. Harting MT, Jimenez F, Xue H, Fischer UM, Baumgartner J, Dash PK, et al. Intravenous mesenchymal stem cell therapy for traumatic brain injury. *J Neurosurg*. (2009) 110:1189–97. doi: 10.3171/2008.9.JNS08158

48. Chang CP, Chio CC, Cheong CU, Chao CM, Cheng BC, Lin MT. Hypoxic preconditioning enhances the therapeutic potential of the secretome from cultured human mesenchymal stem cells in experimental traumatic brain injury. *Clin Sci*. (2013) 124:165–76. doi: 10.1042/CS20120226

49. Riess P, Zhang C, Saatman KE, Laurer HL, Longhi LG, Raghupathi R, et al. Transplanted neural stem cells survive, differentiate, and improve neurological motor function after experimental traumatic brain injury. *Neurosurgery*. (2002) 51:1043–1052; discussion 1052-4. doi: 10.1227/00006123-200210000-00035

50. Chirumamilla S, Sun D, Bullock MR, Colello RJ. Traumatic brain injury induced cell proliferation in the adult mammalian central nervous system. *J Neurotrauma*. (2002) 19:693–703. doi: 10.1089/08977150260139084

51. Das M, Mohapatra S, Mohapatra SS. New perspectives on central and peripheral immune responses to acute traumatic brain injury. *J Neuroinflammation*. (2012) 9:236. doi: 10.1186/1742-2094-9-236

52. Li KL, Chen YM, Wang XQ, Hu HY. Bibliometric analysis of studies on neuropathic pain associated with depression or anxiety published from 2000 to 2020. *Front Hum Neurosci*. (2021) 15:729587. doi: 10.3389/fnhum.2021.729587

53. Wu H, Cheng K, Guo Q, Yang W, Tong L, Wang Y, et al. Mapping knowledge structure and themes trends of osteoporosis in rheumatoid arthritis: a bibliometric analysis. *Front Med*. (2021) 8:787228. doi: 10.3389/fmed.2021.787228

54. Bjorklund GR, Anderson TR, Stabenfeldt SE. Recent advances in stem cell therapies to address neuroinflammation, stem cell survival, and the need for rehabilitative therapies to treat traumatic brain injuries. *Int J Mol Sci*. (2021) 22:1978. doi: 10.3390/ijms22041978

55. Jiang JY, Gao GY, Feng JF, Mao Q, Chen LG, Yang XF, et al. Traumatic brain injury in China. *Lancet Neurol*. (2019) 18:286–95. doi: 10.1016/S1474-4422(18)30469-1

56. Cyranoski D. China splashes millions on hundreds of home-grown journals. *Nature*. (2019) 576:346–7. doi: 10.1038/d41586-019-03770-3

57. Harting MT, Baumgartner JE, Worth LL, Ewing-Cobbs L, Gee AP, Day MC, et al. Cell therapies for traumatic brain injury. *Neurosurg Focus*. (2008) 24:E18. doi: 10.3171/FOC/2008/24/3-4/E17

58. El Sayed R, Shankar KM, Mankame AR, Cox CS Jr. Innovations in cell therapy in pediatric diseases: a narrative review. *Transl Pediatr*. (2023) 12:1239–57. doi: 10.21037/tp-23-92

59. Sun D. The potential of endogenous neurogenesis for brain repair and regeneration following traumatic brain injury. *Neural Regen Res*. (2014) 9:688–92. doi: 10.4103/1673-5374.131567

60. Kang EM, Jia YB, Wang JY, Wang GY, Chen HJ, Chen XY, et al. Downregulation of microRNA-124-3p promotes subventricular zone neural stem cell activation by enhancing the function of BDNF downstream pathways after traumatic brain injury in adult rats. *CNS Neurosci Ther*. (2022) 28:1081–92. doi: 10.1111/cns.13845

61. Sun D, Bullock MR, McGinn MJ, Zhou Z, Altememi N, Hagood S, et al. Basic fibroblast growth factor-enhanced neurogenesis contributes to cognitive recovery in rats following traumatic brain injury. *Exp Neurol*. (2009) 216:56–65. doi: 10.1016/j.expneurol.2008.11.011

62. Sun D, Bullock MR, Altememi N, Zhou Z, Hagood S, Rolfe A, et al. The effect of epidermal growth factor in the injured brain after trauma in rats. *J Neurotrauma*. (2010) 27:923–38. doi: 10.1089/neu.2009.1209

63. Taupin P. Adult neurogenesis, neuroinflammation and therapeutic potential of adult neural stem cells. *Int J Med Sci*. (2008) 5:127–32. doi: 10.7150/ijms.5.127

64. Ma YB, Matsuwaki T, Yamanouchi K, Nishihara M. Progranulin protects hippocampal neurogenesis via suppression of Neuroinflammatory responses under acute immune stress. *Mol Neurobiol*. (2017) 54:3717–28. doi: 10.1007/s12035-016-9939-6

65. Lin KC, Niu KC, Tsai KJ, Kuo JR, Wang LC, Chio CC, et al. Attenuating inflammation but stimulating both angiogenesis and neurogenesis using hyperbaric oxygen in rats with traumatic brain injury. *J Trauma Acute Care Surg*. (2012) 72:650–9. doi: 10.1097/TA.0b013e31823c575f

66. Sun X, Liu H, Tan Z, Hou Y, Pang M, Chen S, et al. Remodeling microenvironment for endogenous repair through precise modulation of chondroitin sulfate proteoglycans following spinal cord Injury. *Small*. (2023) 19:e2205012. doi: 10.1002/smll.202205012

67. Park E, Lyon JG, Alvarado-Velez M, Betancur MI, Mokarram N, Shin JH, et al. Enriching neural stem cell and anti-inflammatory glial phenotypes with electrical stimulation after traumatic brain injury in male rats. *J Neurosci Res*. (2021) 99:1864–84. doi: 10.1002/jnr.24834

68. Bang OY, Kim JE. Stem cell-derived extracellular vesicle therapy for acute brain insults and neurodegenerative diseases. *BMB Rep*. (2022) 55:20–9. doi: 10.5483/BMBRep.2022.55.1.162

69. Koç ON, Gerson SL, Cooper BW, Dyhouse SM, Haynesworth SE, Caplan AI, et al. Rapid hematopoietic recovery after coinfusion of autologous-blood stem cells and culture-expanded marrow mesenchymal stem cells in advanced breast cancer patients receiving high-dose chemotherapy. *J Clin Oncol*. (2000) 18:307–16. doi: 10.1200/JCO.2000.18.2.307

70. Lorenzini S, Andreone P. Stem cell therapy for human liver cirrhosis: a cautious analysis of the results. *Stem Cells*. (2007) 25:2383–4. doi: 10.1634/stemcells.2007-0056

71. Körbling M, Freireich EJ. Twenty-five years of peripheral blood stem cell transplantation. *Blood*. (2011) 117:6411–6. doi: 10.1182/blood-2010-12-322214

72. Kim HJ, Lee JH, Kim SH. Therapeutic effects of human mesenchymal stem cells on traumatic brain injury in rats: secretion of neurotrophic factors and inhibition of apoptosis. *J Neurotrauma*. (2010) 27:131–8. doi: 10.1089/neu.2008.0818

73. Das M, Mayilsamy K, Mohapatra SS, Mohapatra S. Mesenchymal stem cell therapy for the treatment of traumatic brain injury: progress and prospects. *Rev Neurosci*. (2019) 30:839–55. doi: 10.1515/revneuro-2019-0002

74. Zhang Y, Chopp M, Meng Y, Katakowski M, Xin H, Mahmood A, et al. Effect of exosomes derived from multipluripotent mesenchymal stromal cells on functional recovery and neurovascular plasticity in rats after traumatic brain injury. *J Neurosurg*. (2015) 122:856–67. doi: 10.3171/2014.11.JNS14770

75. Ni H, Yang S, Siaw-Debrah F, Hu J, Wu K, He Z, et al. Exosomes derived from bone mesenchymal stem cells ameliorate early inflammatory responses following traumatic brain injury. *Front Neurosci*. (2019) 13:14. doi: 10.3389/fnins.2019.00014

76. Liu X, Wu C, Zhang Y, Chen S, Ding J, Chen Z, et al. Hyaluronan-based hydrogel integrating exosomes for traumatic brain injury repair by promoting angiogenesis and neurogenesis. *Carbohydr Polym*. (2023) 306:120578. doi: 10.1016/j.carbpol.2023.120578

77. Raposo G, Stoorvogel W. Extracellular vesicles: exosomes, microvesicles, and friends. *J Cell Biol*. (2013) 200:373–83. doi: 10.1083/jcb.201211138

78. Ransohoff RM. How neuroinflammation contributes to neurodegeneration. *Science*. (2016) 353:777–83. doi: 10.1126/science.aag2590

79. Tang Y, Le W. Differential roles of M1 and M2 microglia in neurodegenerative diseases. *Mol Neurobiol*. (2016) 53:1181–94. doi: 10.1007/s12035-014-9070-5

80. Schepici G, Silvestro S, Bramanti P, Mazzon E. Traumatic brain injury and stem cells: an overview of clinical trials, the current treatments and future therapeutic approaches. *Medicina*. (2020) 56:137. doi: 10.3390/medicina56030137

81. Cofano F, Boido M, Monticelli M, Zenga F, Ducati A, Vercelli A, et al. Mesenchymal stem cells for spinal cord Injury: current options, limitations, and future of cell therapy. *Int J Mol Sci*. (2019) 20:2698. doi: 10.3390/ijms20112698

82. Yamazaki K, Kawabori M, Seki T, Houkin K. Clinical trials of stem cell treatment for spinal cord Injury. *Int J Mol Sci*. (2020) 21:3994. doi: 10.3390/ijms21113994

83. Koh SH, Kim KS, Choi MR, Jung KH, Park KS, Chai YG, et al. Implantation of human umbilical cord-derived mesenchymal stem cells as a neuroprotective therapy for ischemic stroke in rats. *Brain Res*. (2008) 1229:233–48. doi: 10.1016/j.brainres.2008.06.087

84. Savitz SI, Chopp M, Deans R, Carmichael T, Phinney D, Wechsler L. Stem cell therapy as an emerging paradigm for stroke (STEPS) II. *Stroke*. (2011) 42:825–9. doi: 10.1161/STROKEAHA.110.601914

85. Cruz-Haces M, Tang J, Acosta G, Fernandez J, Shi R. Pathological correlations between traumatic brain injury and chronic neurodegenerative diseases. *Transl Neurodegener*. (2017) 6:20. doi: 10.1186/s40035-017-0088-2

86. Johnson VE, Stewart JE, Begbie FD, Trojanowski JQ, Smith DH, Stewart W. Inflammation and white matter degeneration persist for years after a single traumatic brain injury. *Brain*. (2013) 136:28–42. doi: 10.1093/brain/aws322

87. De Gioia R, Biella F, Citterio G, Rizzo F, Abati E, Nizzardo M, et al. Neural stem cell transplantation for neurodegenerative diseases. *Int J Mol Sci*. (2020) 21:3103. doi: 10.3390/ijms21093103

88. Russo MV. Inflammatory neuroprotection following traumatic brain injury. *Science*. (2016) 353:783–5. doi: 10.1126/science.aaf6260

89. Borlongan MC, Rosi S. Stem cell therapy for sequestration of traumatic brain injury-induced inflammation. *Int J Mol Sci*. (2022) 23:10286. doi: 10.3390/ijms231810286

90. Chang EH, Adorjan I, Mundim MV, Sun B, Dizon ML, Szele FG. Traumatic brain Injury activation of the adult subventricular zone neurogenic niche. *Front Neurosci*. (2016) 10:332. doi: 10.3389/fnins.2016.00332

91. Taupin P. Adult neural stem cells, neurogenic niches, and cellular therapy. *Stem Cell Rev*. (2006) 2:213–9. doi: 10.1007/s12015-006-0049-0

92. Madl CM, Heilshorn SC, Blau HM. Bioengineering strategies to accelerate stem cell therapeutics. *Nature*. (2018) 557:335–42. doi: 10.1038/s41586-018-0089-z

93. Zhang J, Wang RJ, Chen M, Liu XY, Ma K, Xu HY, et al. Collagen/heparan sulfate porous scaffolds loaded with neural stem cells improve neurological function in a rat model of traumatic brain injury. *Neural Regen Res*. (2021) 16:1068–77. doi: 10.4103/1673-5374.300458

94. Yuan J, Botchway BOA, Zhang Y, Wang X, Liu X. Combined bioscaffold with stem cells and exosomes can improve traumatic brain injury. *Stem Cell Rev Rep*. (2020) 16:323–34. doi: 10.1007/s12015-019-09927-x

95. Shen J, Shen H, Ke L, Chen J, Dang X, Liu B, et al. Knowledge mapping of immunotherapy for hepatocellular carcinoma: a bibliometric study. *Front Immunol*. (2022) 13:815575. doi: 10.3389/fimmu.2022.815575

frontiers | Frontiers in Neurology

TYPE Review
PUBLISHED 19 March 2024
DOI 10.3389/fneur.2024.1378620

OPEN ACCESS

EDITED BY
Fawaz Alzaid,
Sorbonne Universités, France

REVIEWED BY
Jacek Szczygielski,
University of Rzeszow, Poland
Jonathan D. Cherry,
Boston University, United States

*CORRESPONDENCE
Nicole J. Katchur
✉ nkatchur@princeton.edu

RECEIVED 29 January 2024
ACCEPTED 26 February 2024
PUBLISHED 19 March 2024

CITATION
Katchur NJ and Notterman DA (2024) Recent insights from non-mammalian models of brain injuries: an emerging literature. *Front. Neurol.* 15:1378620. doi: 10.3389/fneur.2024.1378620

Recent insights from non-mammalian models of brain injuries: an emerging literature

Nicole J. Katchur[1,2]* and Daniel A. Notterman[1]

[1]Department of Molecular Biology, Princeton University, Princeton, NJ, United States, [2]Rutgers-Robert Wood Johnson Medical School, Piscataway, NJ, United States

Traumatic brain injury (TBI) is a major global health concern and is increasingly recognized as a risk factor for neurodegenerative diseases including Alzheimer's disease (AD) and chronic traumatic encephalopathy (CTE). Repetitive TBIs (rTBIs), commonly observed in contact sports, military service, and intimate partner violence (IPV), pose a significant risk for long-term sequelae. To study the long-term consequences of TBI and rTBI, researchers have typically used mammalian models to recapitulate brain injury and neurodegenerative phenotypes. However, there are several limitations to these models, including: (1) lengthy observation periods, (2) high cost, (3) difficult genetic manipulations, and (4) ethical concerns regarding prolonged and repeated injury of a large number of mammals. Aquatic vertebrate model organisms, including *Petromyzon marinus* (sea lampreys), zebrafish (*Danio rerio*), *and invertebrates, Caenorhabditis elegans* (*C. elegans*), and *Drosophila melanogaster* (*Drosophila*), are emerging as valuable tools for investigating the mechanisms of rTBI and tauopathy. These non-mammalian models offer unique advantages, including genetic tractability, simpler nervous systems, cost-effectiveness, and quick discovery-based approaches and high-throughput screens for therapeutics, which facilitate the study of rTBI-induced neurodegeneration and tau-related pathology. Here, we explore the use of non-vertebrate and aquatic vertebrate models to study TBI and neurodegeneration. *Drosophila*, in particular, provides an opportunity to explore the longitudinal effects of mild rTBI and its impact on endogenous tau, thereby offering valuable insights into the complex interplay between rTBI, tauopathy, and neurodegeneration. These models provide a platform for mechanistic studies and therapeutic interventions, ultimately advancing our understanding of the long-term consequences associated with rTBI and potential avenues for intervention.

KEYWORDS

repetitive brain injury, non-mammalian models, neurodegeneration, tauopathy, traumatic brain injury

1 Introduction

Traumatic brain injury (TBI) affects an estimated 69 million people each year (1) and impose an economic burden on the world economy of over $400 billion (2). In the United States, more than 472,000 military service members sustained at least one brain injury between 2000 and 2022, with many reporting head injuries before service (3). Studies have shown that TBI is an environmental risk factor for neurodegenerative diseases including Alzheimer's disease (AD) and other dementias (4, 5) while those with repeated head trauma

are at risk of developing chronic traumatic encephalopathy (CTE) (6). A previous head injury increases the risk for a subsequent head injury; thus, greater than 260 per 10,0000 military service members experience subsequent head injury within 1 year of an initial TBI (7). Athletes participating in high-contact sports are at risk for repeated head trauma, and exposure to repetitive TBIs (rTBIs) is common in professional athletes (8, 9). Some American football linemen experience nearly 2,000 impacts over the course of their career (8, 9). While repeated head trauma is commonly linked to contact sports such as football and boxing, it is also evident in the context of intimate partner violence (IPV). Thirty to 94% of women experiencing IPV report at least a single brain injury, with an estimated 80–90% of women sustaining injuries to the head and neck (10, 11). Those who experience brain injuries from IPV may report chronic cognitive impairments in memory and learning (12). Over time, the accumulation of these traumatic events may lead to the development of CTE, a progressive, neurodegenerative disease induced by repeated blows to or rapid displacement of the head, producing chronic changes in cognition, memory, and mood (6). Emerging literature suggests that neurodegenerative changes may occur in women who have experienced IPV, including a recent case study where CTE-like pathology was reported (13, 14). The link between CTE and repeated trauma in athletes is well-established. In a convenience sample of 202 deceased American football players, 87% were diagnosed post-mortem with CTE; the affected percentage was higher (99%) when the sample was restricted to NFL players (15). In a post-mortem study of rugby and soccer players, eleven experienced repeated head trauma, and CTE pathology was found in eight of eleven (16). Despite attempts to use neuroimaging as a mechanism to identify and diagnose CTE before death, the formal diagnosis of CTE occurs only upon autopsy and no effective therapeutic interventions exist to prevent or mitigate neurodegeneration following rTBI.

Mammalian species, such as rats, mice, and pigs, have been used to model TBI and other neurodegenerative diseases including CTE to elucidate long-term outcomes. Although they have provided key insight into numerous secondary injury mechanisms and therapy development (17–19), there are several limitations to the existing literature: (1) lengthy observation periods of the model organism, (2) high cost for experimentation and associated costs, (3) relatively difficult and lengthy genetic manipulations, and (4) ethical concerns regarding a large number of mammals experiencing pain and debilitating injury. For these reasons and others, over the past several decades, researchers have initiated non-mammalian models such as fruit flies (*Drosophila melanogaster; Drosophila*), nematodes (*Caenorhabditis elegans; C. elegans*), zebrafish (*Danio rerio*) and sea lampreys (*Petromyzon marinus*) to model human neurodegenerative diseases and to map the etiopathogenesis of aberrant tau formation after TBI (20). Lower-order vertebrate and invertebrate models offer important potential benefits to studying TBI-induced neurodegeneration, including shorter lifespans to study endpoints, vast genetic tools to manipulate the expression of genes of interest, high-throughput analysis to identify genetic and biochemical networks, screening techniques to identify potential therapeutics, and reduced cost. Here, we highlight the use of non-vertebrate and aquatic vertebrate organisms to define the basic mechanisms underlying repeated TBI and to model rTBI-induced neurodegeneration.

2 Mechanisms of acute and repeated traumatic brain injury

2.1 Primary injury

As a result of TBI, two separate injuries occur on impact, a primary injury which causes a secondary injury to unfold in the minutes to hours after the initial impact. Blast injury, penetrating injuries, direct impact, and rapid acceleration and deceleration forces can injure the brain, producing a primary injury (21, 22). Within milliseconds, the primary impact produces TBI causing brain tissue to undergo rapid movement and tissue deformation (23). The primary injury leads to the shearing of white matter tracts, resulting in the formation of focal contusions as well as intra-and extracerebral hematomas (22).

In closed-head trauma, mechanical force transmits energy to neurons and glia, which may cause traumatic disruption of CNS structures, disturbances in circulatory autoregulation, impairment of the blood–brain barrier (BBB), and acute cellular dysfunction (23–25). The brain is particularly vulnerable to mechanical force because of its viscoelastic nature and lack of structural support; therefore it is ineffective in withstanding the mechanical forces from a blow to the head (26). Linear acceleration forces exerted during traumatic events can lead to the formation of superficial brain lesions, whereas rotational forces rotate the brain around a fixed axis (27, 28). These rotational forces impart damage to deeper cortical structures (26, 29). Translational forces, specifically linear acceleration forces, impart damage to superficial gray matter, generating cerebral hemorrhages and cortical contusions (27, 30). In contrast, rotational forces mechanically and physiologically damage the deep cerebral white matter axons, resulting in diffuse axonal injury (27, 28). It is hypothesized that axons are further damaged when rapid acceleration and deceleration forces promote the dissociation of tau from microtubules by altering microtubule dynamics, leading to subsequent tau hyperphosphorylation and aggregation (31, 32). However, others suggest that tau hyperphosphorylation occurs first, altering microtubule dynamics, and affecting its association to microtubules (33, 34). Multiple exposures to blast force also result in an accumulation of pathological tau aggregates in the brain (35). Rapid distortion of neuron shape may also induce tau hyperphosphorylation, resulting in tau mislocalization (36). Collectively, these studies suggest that force from a primary injury, at least in part, contributes to the development of neurodegenerative tauopathies.

2.2 Secondary injury

The biochemical and cellular responses to the initial impact produce additional damage to the brain, resulting in a secondary injury. Following a primary injury, massive disturbances in brain metabolism, neuroinflammatory responses, microstructural changes, and behavioral changes occur reviewed in (37). Often a consequence of injury, disruption of neuronal and glia osmotic control drives cellular edema, the predominant form of brain edema immediately following TBI (38). Brain edema likely exacerbates injury by increasing cytotoxicity and promoting cell death (39). It is hypothesized that following trauma, extracellular glutamate rises, initiating activation of N-methyl-D-aspartate (NMDA) receptors which promotes the influx

of intracellular calcium ions (40). The large influx of calcium activates proteases, endonucleases, and other degradative enzymes and initiates cell death and apoptosis (41).

Oxidative stress damages brain tissue by supplying an excess of reactive oxygen species (ROS) and reactive nitrogen species (RNS) (42). These free radicals disrupt cellular function and preferentially lyse the hydrophobic portion of the lipid bilayer (42). Oxidative stress can oxidize amino acids, resulting in protein modification and loss of catalytic function (43). Protein modifications lead to severe protein aggregation within hours of post-ischemic injury (44). Endogenous antioxidants such as glutathione (GSH) play a vital role in protection against ROS and RNS. Depletion of GSH exacerbates brain infarction following cerebral ischemia (45, 46). After TBI in rodents, GSH decreases in the hippocampus, potentially leading to apoptotic neuronal death (46).

Neuroinflammation, while it can promote recovery during a limited period, also contributes to the pathophysiology of secondary injury by exacerbating damage. The normal BBB prevents the entry of hydrophilic molecules through tight and adherens junctions between endothelial cells (47, 48). Following TBI, the BBB can be disrupted, recruiting leukocytes (49). The damage also activates resident microglial cells, which can remain in an activated state for years following TBI (50, 51). Chronic inflammation following traumatic brain injury increases axonal degeneration and neuronal loss (52, 53), and the resulting injury and brain dysfunction may have a delayed onset and persist long-term, leading to dementia or CTE. Microglia, along with astrocytes, participate in "reactive gliosis," an aggressive response to neurotrauma involving enlarged glial cells in damaged brain areas (54). Microglial cells function like peripheral macrophages and secrete proinflammatory cytokines and chemokines (55). In both post-brain injury and neurodegenerative disease such as AD, resident immune cells like astrocytes and microglia are elevated (53), implicating inflammation as a potential link between the two phenomena.

Recent evidence suggests that activated microglia can have detrimental effects as they directly correlate with the extent of tau pathology (55, 56) and can increase amyloidogenic amyloid precursor protein (APP) production (57). Cherry and colleagues investigated the relationship between neuroinflammation and CTE and found that the duration of repeated head injury exposure predicted the activated microglial cell density and subsequent greater hyperphosphorylated tau pathology (58). The increase in aberrant APP proliferation eventually leads to the amyloid beta (Aβ) plaques that have been previously associated with AD (59), emphasizing the role of neuroinflammation in the development of continuing injury long after TBI occurs. However, several models of TBI in rodents demonstrate a reduction in amyloid beta plaques following TBI (60, 61), and one study showed that mice overexpressing amyloid precursor protein had a rise in unaggregated Aβ in the hippocampus with extensive hippocampal neuronal death, thereby suggesting that the plaques may be protective against unaggregated (Aβ) toxicity unclear (62), though it remains. Therefore, a more thorough understanding of the complex mechanistic underpinnings of amyloidogenesis and tauopathies must be explored.

2.3 Acute and repeated brain trauma

Several studies highlight the different responses to single as opposed to multiple or repeated head injuries by characterizing the immediate and delayed effects on brain metabolism, neuroinflammatory responses, microstructural changes, and behavioral changes. Following a single mild TBI in mice, glucose utilization in the hippocampus and sensorimotor cortex increased in the first 3 days following injury, while rTBI (a second injury 3 days following the first injury) failed to elicit the same immediate response (63). However, after 20 days, rTBI mirrored single head injury with respect to glucose utilization (63), indicating a delayed effect on brain metabolism after rTBI. Moreover, axonal degeneration, increased glial activation and proinflammatory cytokine gene expression were detected 40 days after initial *repeated* injuries, highlighting the prolonged neuroinflammatory responses present after repeated but not single injuries (63). Studies in mammals demonstrate that a single TBI is associated with *transient* increases in hyperphosphorylated tau (64), while depositions of hyperphosphorylated tau aggregates were associated with rTBI (58, 65). Additionally, chronic mild rTBI increased tau abundance within the gray matter up to 3 months following injury (66), and rTBI led to increased phosphorylated tau than a single mild TBI (67). This evidence suggests that acute and repeated injuries have distinct temporal patterns of glucose utilization, neuroinflammatory responses, and tau hyperphosphorylation. Since prolonged neuroinflammatory responses are associated with an increased risk of neurodegenerative disease (68), this evidence suggests particular mechanisms that might be invoked to explain neurodegeneration following repeated, non-disabling head trauma.

Microstructural and behavioral changes also occur after rTBI. Multiple head injuries resulted in more severe microstructural changes, cortical volume loss, behavioral deficits, and histopathological alterations compared to single injuries (69). Jamnia et al. (70) demonstrated persistent memory deficits and structural changes in the cortex and corpus callosum in rats exposed to repeated concussions--three injuries, 48 h apart (70). These rats also experienced deficits in behavior, exhibited anxiety and increased corticosterone levels following rTBI (70). When piglets experienced one high-level rotational injury versus one high-level rotational injury with four subsequent mid-level rotational injuries administered 8 min apart, the multiple rotation injury group experienced greater gait times 1 day post after injury (71). Overall, gait patterns were normal in the single rotation group but were abnormal following the additional rotations (71), suggesting the long-term effect of repeated rotational brain injury on locomotor behavior. Recent studies underscored the accumulating nature of symptoms in adolescents with repeated concussions, with higher symptom scores observed after the second concussion compared to the initial one (72). Following a second concussion, patients reported an increased burden of neuropsychiatric symptoms, particularly in cognitive, sleep, and neuropsychiatric domains (73). *Collectively, these studies emphasize the importance of considering the cumulative effects of repeated head injuries*, with potential long-term consequences on brain structure, function, and behavior.

3 Tau's role in neurodegenerative disease

A recent NINDS consensus document indicated that CTE is likely to occur in the years to decades following rTBI; pathognomonic lesions of tau hyperphosphorylation occur in the cortical sulci surrounding small blood vessels (74). While many areas of the brain may be affected by rTBI, the hippocampus, an important structure for

memory and cognition, may be particularly vulnerable to subsequent injuries following a concussion-like injury, leading to changes in mood, memory, and anxiety regulation (75–78). The exact mechanisms by which these cognitive changes are triggered by repeated concussion (rather than physical disruption of neural tissue) remain unclear, though several studies have suggested that neurotoxicity, functional impairment of neuronal synapses, and axonal stabilization by aberrant microtubule-associated protein (MAP) tau may contribute to memory impairment and loss (79, 80) (Figures 1A,B). Tau is a crucial protein in the central nervous system (CNS) involved in the stabilization of microtubules and regulation of axonal transport (81, 82), and its accumulation, hyperphosphorylation, and aberrant localization are recognized as hallmarks of CTE (74). In humans, six different isoforms of tau are produced in the adult brain. These arise via alternative splicing at its amino-and carboxy-terminal ends (Figure 2). Once phosphorylated on multiple sites (e.g., Ser^{356}, Ser^{396}, Thr^{231}), tau loses the ability to bind microtubules (33, 83, 84), thereby promoting microtubule depolymerization and instability.

Abnormal phosphorylation of human tau (hTau) by both non-proline and proline kinases results in insoluble and misfolded tau, leading to the aberrant accumulation and aggregation of filamentous tau polymers, known as paired helical filaments (PHFs) and neurofibrillary tangles (NFTs), two features of CTE (74). Following and perhaps due to the formation of NFTs, neuronal degeneration and death result in release of tau into the extracellular space (90). In turn, this promotes tau uptake into astroglia (91). Some studies have even suggested that the spread of tau through glia cells mirrors a prion-like spread, though whether the misfolded tau actually promotes subsequent local misfolding of the normal *trans* isomer of tau has not been investigated (84, 92).

As noted, the configuration of tau in the *trans* form is the physiological conformation. In contrast, the *cis* conformation of aberrantly phosphorylated tau (p-tau) has been linked to pathogenesis in neurodegenerative disease and of cognitive symptoms (65, 93, 94). In a rodent study of impact and blast injury, the appearance of the *cis* configuration of hyperphosphorylated tau was associated with neurotoxic effects and spread to regions contralateral to the injury, associated with cognitive impairment (65, 94). When targeted with a monoclonal antibody against *cis* p-tau, neuronal apoptosis was prevented, suggesting that accumulation of *cis* p-tau is very early in the pathogenic sequence of post-TBI neurodegeneration (94). PIN1, a peptidyl-prolyl isomerase, plays a role in isomerizing threonine proline bonds at multiple sites (95–97) including those in tau. However, only the isomerization at the phosphorylated Thr^{231}-Pro^{232} bond in tau is associated with a biological phenotype (98). The isomerization of p-tau at Thr^{231}-Pro^{232} from *cis* to *trans*, promotes both dephosphorylation of tau by PP2A and microtubule stabilization (99). Depletion of Pin1 results in apoptosis and mitotic arrest (100). In an AD model, paired helical filaments contribute to neuronal death (101). Several studies demonstrate that upon restoring the prolyl isomerase in a cell model, Pin1 promotes microtubule binding and stability *in vitro* as well as dephosphorylation at amino acid site Thr^{231} (101, 102). The specific anatomic sites of where tau hyperphosphorylation is found and the pattern of neuronal spread can

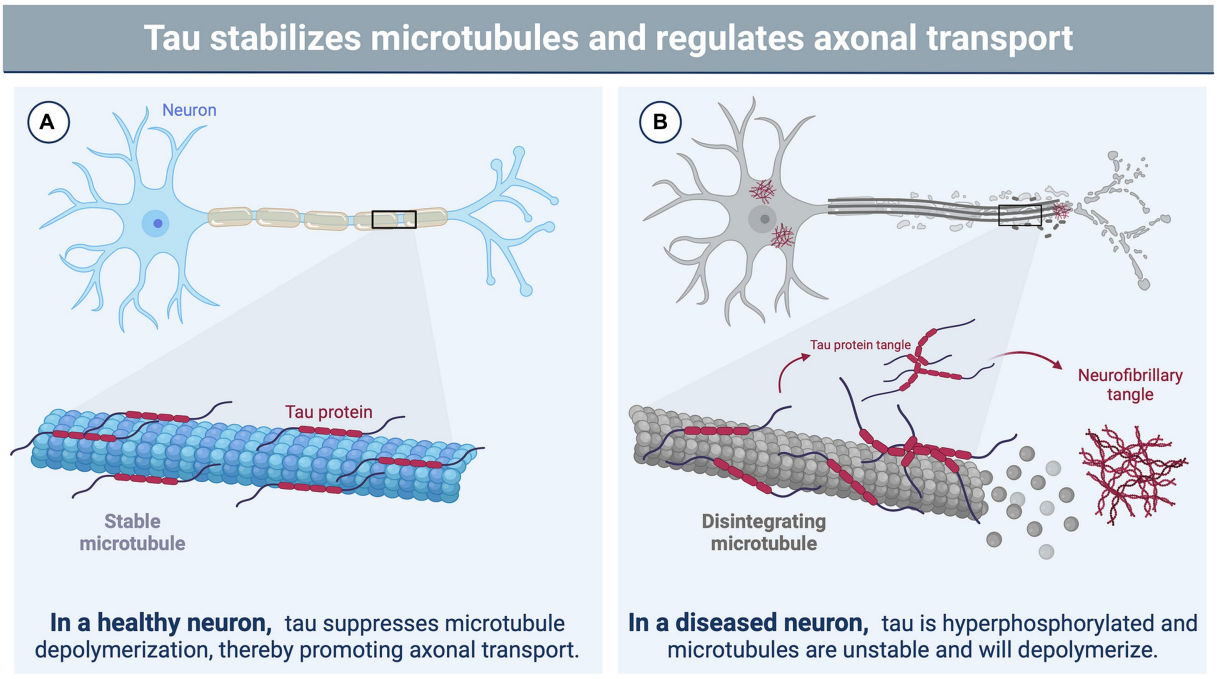

FIGURE 1
The function of tau in neurons and its role in brain injury. **(A)** In a healthy neuron, tau plays a vital role in stabilizing and supporting axonal transport by binding to microtubules and suppressing microtubule depolymerization (81, 82). The phosphorylation state of tau influences its binding affinity to the microtubule with hypophosphorylation supporting a tighter bind (33, 83, 84). **(B)** Brain injury triggers various cascades, leading to the hyperphosphorylation of tau by protein kinases (85). This hyperphosphorylated state disrupts the binding of tau to microtubules, causing microtubule instability and depolymerization (33, 83, 84). Consequently, tau undergoes filamentous aggregation, forming pathognomonic lesions characteristic of chronic traumatic encephalopathy (CTE), such as neurofibrillary tangles (86). Image created using BioRender.com.

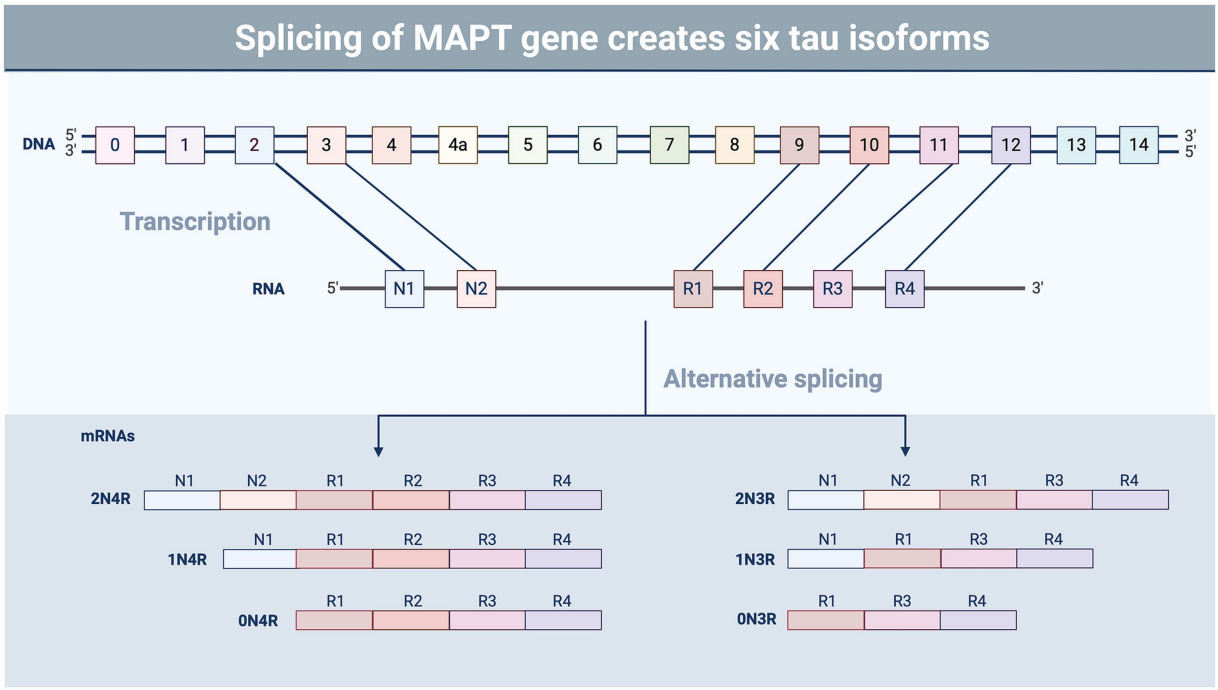

FIGURE 2
Splicing variants of tau. Tau undergoes alternative splicing involving exons 2, 3, and 10, resulting in six different isoforms of the protein containing the presence or absence of exons containing microtubule-binding domains (R) and N-terminal insertions (N) (87). The ratio of the different tau isoforms varies in different regions of the brain and during different stages of development (88). Tau isoform composition also varies in tauopathic diseases, such as CTE and Alzheimer's disease, which may impact aggregation and pathology (89). Image created using BioRender.

differentiate between different tauopathic neurodegenerative diseases. In AD, NFTs arise in the brainstem and entorhinal cortex before spreading to the medial temporal lobe and evenly distributing in the neocortex layers III and V (65, 103, 104). In contrast, CTE develops in the deep sulci of the superficial neocortical layers II and III of the cerebral cortex, focally and perivascularly (86). The spread continues irregularly to the neocortex, medial temporal lobe, diencephalon, basal ganglia, and brainstem (65, 105). Though the pathologic spread of tau differs, AD and CTE share at least two of the same tau phosphorylation sites including Thr^{231} and Ser^{199} which have been implicated in neurotoxicity and neuronal dysfunction (65). These common phosphorylation sites, in addition to patterns of deposition, allow AD models of tauopathy to inform CTE tauopathy studies. Throughout this review, "CTE-like" will be used to describe models that recapitulate the phosphorylation and aggregation profile of tau in human CTE, but for which meeting the criterion that tau aggregates occur in the sulci is not possible because the brain is lissencephalic.

Since there is currently no treatment to prevent or mitigate CTE or other forms of neurodegeneration after TBI, researchers have focused on two main drivers of injury-induced sequelae, Pin1 and tau. Lu et al. (101) have produced anti-Pin1 antibodies to restore the function of phosphorylated tau (101) *in vitro* but have not yet extended the studies to *in vivo* CTE-like models. In recent years, the literature has turned its focus to anti-*cis* tau antibodies that work to clear phosphorylated tau plaques in AD, CTE, and severe TBI animal models (93, 94, 106) and have reported improved outcomes *in vivo*. Albayram and colleagues found that repetitive mild injuries led to more severe phosphorylated *cis* tau and tangle-like structures which resemble CTE-like pathology. Treatment with anti-*cis* phosphorylated tau led to the elimination of *cis* phosphorylated tau and total tau accumulation (93). A clinical trial for the use of antibodies targeting *cis*-hyperphosphorylated tau at Thr^{231} is currently underway (107). Perhaps these promising developments in antibody-based therapies will result in effective treatments for CTE and other related tauopathies.

4 Non-mammalian models of neurodegenerative disease

For decades, researchers have used rodent models to recapitulate traumatic brain injury and its subsequent sequelae. Difficulties in modeling acceleration and deceleration forces limited the rodent models to specific features of TBI and led to the creation of contusion injury models, namely controlled cortical impact and fluid percussion models (108). The rapid increase in molecular and genetic techniques, in addition to the commercial availability of transgenic rodents and materials, make rodents an attractive substitute for large animal models of brain injury (109). However, large animal models of traumatic brain injury can model a more dynamic range of TBI, namely replicating features of acceleration/deceleration forces (110), which are limited in rodent models. Additionally, rodents have lissencephalic brains with no rigid tentorium cerebelli (109), which restrict the modeling of neurodegenerative diseases with pathology localized to the sulci in the brain. In particular, the pathognomonic lesions of human CTE are found in the sulci near perivascular regions, regions that are particularly vulnerable to mechanical stress from injury (86). Large animal models like primates, have gyrencephalic brains, increasing the translatability of this model to humans (109,

110). Like rodent models, primate models have drawbacks. However, primate models are limited by cost, lack of established post-TBI functional assays, are technically difficult, and raise ethical concerns (109, 110). Therefore, the use of non-mammalian models may be an attractive substitute for large animal and rodent models.

4.1 *Petromyzon marinus* (sea lampreys)

Harnessing lower vertebrates for the study of proteins implicated in human disease enables mechanistic studies in a large, identifiable neuron population while extending studies from invertebrates. The robust neuroregenerative capabilities and functional recuperation exhibited by the CNS in lower-order vertebrates make them an attractive experimental model for investigating the role and behavior of abnormal tau following TBI and neurodegeneration. In particular, the biochemical properties of tau have been studied in the lamprey. Hall et al. (111) utilized sea lamprey anterior bulbar cells (ABC) to demonstrate that chronic, full-length human tau overexpression resulted in fibrillary tangles reminiscent of the tau tangles present in neurodegenerative disease, particularly AD (111). They also demonstrated that proprietary small molecules prevented neurodegeneration in cells containing an accumulation of tau filaments (112) while Honson et al. (113) provided evidence for a small molecule inhibitor, N3 (a benzothiazole derivative) to arrest tau aggregate formation in sea lamprey neurons (113). Sea lampreys have also been used to study the movement and deposition of tau and its subsequent role in neurodegeneration. One study demonstrated that mutated tau, particularly the P301L form, migrates in a transneuronal manner, while wild-type tau does not (114, 115). Another study showed that extracellular human tau moves both synaptically and non-synaptically (116). Additionally, exonic mutations in human tau accelerated degeneration in lamprey ABCs (117). Interestingly, Le et al. (116) noted similarities between tau patterns in lampreys and tau patterns in humans. Over time, extracellular tau deposits in the lamprey mirrored the deposits indicative of human CTE and even resembled the perivascular halos that are pathognomonic of CTE in humans. (116). When taken together, these studies suggest that lampreys serve as an excellent model of some features of neurodegenerative disease, highlight its use as a rapid screening tool, and may be used to further investigate the mechanisms driving the formation of aberrant tau after TBI.

4.2 *Danio rerio* (zebrafish)

The zebrafish (*Danio rerio*) proteome exhibits a notable degree of homology with the human and they have similar anatomical structures and functions of the brain, thereby making it a suitable organism for investigating TBIs. There are several models that recapitulate closed-headed TBI in the zebrafish. McCutcheon et al. (118) employed a targeted, pulsed, high-intensity focused ultrasound (pHIFU) to induce damage to the brain by mechanical force (118). Zebrafish injured by pHIFU demonstrated increased expression of β-APP and β-III tubulin, a microtubule protein (118), suggesting that this model may be used to investigate the pathophysiology of TBI. Additionally, a non-invasive mild TBI model was developed in adult zebrafish using a laser to induce damage to neural tissue (119). Laser-induced damage to the brain resulted in dilated vessels, hemorrhage and edema, 1 day post-injury (119). These signs suggest that the laser-induced brain injury reproduces features of the pathophysiology associated with mild TBI (119). In the most recent study of zebrafish TBI models, Gill et al. (120) developed a method to model blast injury without the use of anesthetics by dropping a weight onto a fluid-filled plunger (120, 121). This method of injury produced cell death, hemorrhage, blood flow abnormalities, and tauopathy, consistent with TBI (121). The homology between zebrafish and humans in terms of TBI pathophysiology make zebrafish an excellent tool to advance our understanding of TBI and its underlying mechanisms.

In addition to modeling TBI pathophysiology, zebrafish have been used as a biosensor to investigate tauopathies. One study conducted a high-throughput screen for herbal extracts to reduce neuronal death initiated by aberrant tau. Of the 400 herbal extracts screened in the zebrafish, 45 were identified as having the potential to reduce tau-induced neuronal death (122). Additionally, Lopez et al. (123) investigated the clearance kinetics of an aberrant tau protein variant, p.A152T, and applied both pharmacological and genetic approaches to reduce the burden of p.A152T tau in zebrafish by upregulating autophagy (123). Reduction of p.A152T by upregulation of autophagy ameliorated morphological abnormalities and reduced hyperphosphorylated tau (123). In another study, Cosacak et al. (124) created a transgenic zebrafish to explore the aberrant human tau variant, P301L. P301L generates neurofibrillary tangles in mammalian models of tauopathies (125, 126), though did not produce neurofibrillary tangles in the zebrafish nor exacerbate Aβ42 toxicity (124), suggesting a protective mechanism in the zebrafish that may be exploited. These therapies aimed at reducing aberrant tau burden may serve as a strategy for treating tauopathies.

While aquatic vertebrates are useful models to study neurodegeneration and the mechanisms driving aberrant formation of tau, their inherent ability to regenerate neurons (127) following injury may confound the consequences of the secondary injury. However, understanding regeneration may provide key insights into pathways provoked by TBI and may lead to the development of therapeutics to mitigate the effects or potentially reverse TBI-induced pathology. Furthermore, these models provide a way to screen various interventions at relatively low cost while examining histological and biochemical correlates of TBI.

5 Invertebrate model organisms

5.1 *Caenorhabditis elegans* (roundworms)

In *C. elegans*, researchers have utilized blast injuries to model mild TBI. However, the existing blast methods have yielded heterogeneous outcomes. Angstman et al. developed a shock wave injury model that produces a consistent and quantifiable injury, but its predictive ability for individual outcomes remains limited. However, in 2019, Miansari et al. (128) demonstrated that high-frequency surface acoustic waves (SAW) in a *C. elegans* model of blast-induced mild TBI, confined within a narrow range of the substrate surface, induced mobility and short-term memory deficits in a more homogenous manner than previous models in the literature, suggesting that SAW may be an improved early-stage model for human TBI. Additionally, Angstman et al. have shown that their blast-related model of mild TBI in *C. elegans* recapitulates

essential characteristics of human TBI, including loss of consciousness and subsequent recovery (129, 130). This compelling evidence further strengthens the suitability of *C. elegans* as a viable non-mammalian model for TBI and a suitable alternative model organism for mitigating ethical concerns when using mammalian models to explore repetitive trauma.

Beyond inducing injuries, researchers have employed *C. elegans* as a model organism to investigate the effects of TBI-modified tau. Brain homogenates from mice with chronic TBI and or intracerebral inoculation of tau^{TBI}, a form of tau that aggregates after chronic TBI, impaired motility, and neuromuscular synaptic transmission in *C. elegans* (131, 132). Surprisingly, when naive mice were intracerebrally inoculated with tau^{TBI}, a prion-like spread of tau^{TBI} occurred, resulting in memory deficits and synaptic toxicity (131, 132). Moreover, Diomede et al. established the therapeutic potential of Aβ1-6A2V(D), an all-D-isomer synthetic peptide, to promote tau degradation by proteases and impede tau aggregation in a *C. elegans* model (114). Additionally, the average lifespan of *C. elegans* ranges from 9 to 23 days depending on the rearing temperature (133), highlighting the ability to track tau aggregation through the entire lifespan of the organism. Collectively, these studies demonstrate the potential of using *C. elegans* as biosensors to investigate and manipulate the biochemical properties of tau and its interactions with potential therapeutic peptides in a faster and less complex manner than mammalian models. Overall, *C. elegans* is a valuable alternative to mammalian models for studying neurodegenerative diseases, providing an array of genetic tools and simple mechanistic studies to understand tau in the context of dysfunction, such as TBI.

5.2 *Drosophila melanogaster* (fruit flies)

Drosophila melanogaster is an excellent model system to study the longitudinal effects of rTBI and its effect on endogenous tau protein. Using *Drosophila,* it is possible to study post-injury behavior, while interrogating histological features of injury and correlating these responses to proteomic and transcriptomic changes (e.g., mass spectroscopy and RNA seq) responses. While tau has been linked to neurodegeneration and neurotoxicity, there is only a rudimentary understanding of the upstream biochemical mediators of tau in the context of rTBI and CTE. Several studies have expressed wild-type and mutant human tau proteins in *Drosophila melanogaster* to model AD, although, *hTau* transgene expression in *Drosophila* is not an ideal functional model, in part because of poor binding to *Drosophila* microtubules. This, as well as differences in phosphorylation sites and uncertainty about whether hTau protein models endogenous NFT formation, limits the applicability of this model. *Drosophila* tau (dTau) contains five putative microtubule-binding repeats and lacks the N-terminal repeats seen in human tau, despite sharing 66% homology with hTau protein (134, 135). At least six CTE-associated phosphorylation sites are observed in human tau, and four of those, Thr^{231}, Ser^{202}, Thr^{205}, Ser^{199} are conserved in dTau, as Thr^{151}, Ser^{106}, Thr^{123}, Ser^{103}, respectively. While many studies express hTau in *Drosophila* to model tauopathic diseases, some have shown that dTau can confer the same neurotoxic and neurodegenerative effects as hTau (135). Thus, by investigating dTau in *Drosophila*, its endogenous properties can be readily understood and may represent an informative window into TBI-induced tauopathy (CTE-like) pathogenesis. Overexpression of dTau in *Drosophila* leads to neurotoxicity and eventual neurodegeneration similar to that observed with overexpression of hTau in *Drosophila* (135), though these overexpression models have not been studied in terms of the upstream and downstream mediators of tau-associated neurotoxicity. Neither dTau nor exogenous expression of hTau has been examined with respect to their roles in CTE in *Drosophila*, perhaps due to the lack of sulci and perivascular regions in *Drosophila* that are associated with human CTE pathogenesis. Instead, characterizing and exploring the vulnerable regions in the *Drosophila* brain in the context of repetitive TBI may help to establish a model of chronic traumatic encephalopathy, and evaluating endogenous dTau will provide valuable insights on the progression of tauopathy dysfunction after injury.

The current *Drosophila* models of head-specific TBI study acute changes (136, 137), while current models of rTBI are not head-specific. Traditional methods of TBI in flies utilize high-impact devices (138) or Omni-Bead Ruptor homogenizing platforms (139) that may be used for high-throughput injuries. The high-impact devices utilize a spring attached to a fly vial that, when stretched and released, generates an impact against a tabletop while the Omni-Bead Ruptor freely shakes a small screw cap tube in which the flies are placed. While these methods generate high-throughput injuries, the uncontrolled, full-body injury potentially results in confounding effects on climbing and walking assays, two paradigms commonly used to assess behavioral sequelae after TBI (136). To overcome this limitation, Sun and Chen developed a head-specific model that uses carbon dioxide to propel an impactor against the head (137). They explored walking distance and lifespan as potential markers of injury resulting from repeated head impacts in *Drosophila* (137). Despite this advancement, the use of a manual FlyBuddy switch system introduces variability in the timing of the impacts and the duration in which carbon dioxide propels the impactor. In addition, the underlying neurobiological changes that occur after multiple injuries have not been explored. The Bonini lab developed a fly impactor model using a piezoelectric striker to compress the fly head against a metal fly collar that fixes the head in place and demonstrated acute injury markers that progressed with increasing severity, establishing a more realistic single TBI model in *Drosophila* (136, 140).

6 Discussion and conclusion

In this review, we discuss the use of non-vertebrate animal models and vertebrate aquatic animals to explore the mechanisms driving tauopathies and other changes post-TBI. We highlight that these model organisms offer several advantages to research and will allow for cost-effective, rapid, discovery-based approaches and potential high-throughput screens for therapeutics, in addition to reviewing differences in behavioral and physiological response to acute and repeated brain injuries. It is important to note that while acute and repeated injuries differ in effects on glucose metabolism and even in temporal patterns of tau expression, several studies have shown that acute injuries may result in non-transient tau expression (141, 142). In rodents, exposure to a blast injury at 10.8 psi once per day for 3 days resulted in an accumulation of pathological tau aggregates in the brain (35). CTE pathology is also observed in some American football players with multiple concussive and

subconcussive blows to the head (143). However, CTE pathology was also found in military personnel who underwent a *single* IED blast injury (143), and a single moderate to severe brain injury resulted in tauopathic lesions in the brain (85). These studies suggest that the total mechanical force accumulated by the brain over time may represent one factor influencing the development of CTE, independent of the number of brain injuries. Severity of the injury, an indirect measure of the mechanical force sustained from a TBI, may also play a role in the development of CTE, with evidence of neuroinflammation in the brain 17 years after the initial injury (50). Several studies demonstrate that chronic neuroinflammation following an acute injury may serve as a contributing factor to neurodegeneration. Given the important role of neuroinflammation in TBI previously discussed and the recent studies that have revealed the powerful effects of microglial depletion strategies on modulating neuroinflammation after TBI, it will be critical to fully characterize the acute and chronic neuroinflammatory responses in a model organism that allows for rapid longitudinal and genetic studies (144–148). The emerging key role of age-related microglial phenotypes, recently described by (145), in this regard, and their link to neurodegeneration could represent a perfect opportunity for exploration in TBI models in *Drosophila*, given the relative ease and efficiency to study long-term effects and outcomes.

Author contributions

NK: Conceptualization, Writing – original draft, Writing – review & editing. DN: Supervision, Writing – original draft, Writing – review & editing.

Funding

The author(s) declare financial support was received for the research, authorship, and/or publication of this article. This publication was supported by the New Jersey Commission on Brain Injury Research CBIR23FEL005, the Center of Health and Well-being at Princeton University, the Brain Injury Association of America, and the Princeton Library Open Access Fund.

Acknowledgments

We thank Patrick Kochanek for his insightful comments and advice on the manuscription.

Conflict of interest

The authors declare that the research was conducted in the absence of any commercial or financial relationships that could be construed as a potential conflict of interest.

Publisher's note

References

1. Dewan MC, Rattani A, Gupta S, Baticulon RE, Hung Y-C, Punchak M, et al. Estimating the global incidence of traumatic brain injury. *J Neurosurg*. (2018) 130:1080–97. doi: 10.3171/2017.10.JNS17352

2. Maas AIR, Menon DK, Adelson PD, Andelic N, Bell MJ, Belli A, et al. Traumatic brain injury: integrated approaches to improve prevention, clinical care, and research. *Lancet Neurol*. (2017) 16:987–1048. doi: 10.1016/S1474-4422(17)30371-X

3. DOD TBI Worldwide Numbers (2023). Military health system. Available at: https://health.mil/Military-Health-Topics/Centers-of-Excellence/Traumatic-Brain-Injury-Center-of-Excellence/DOD-TBI-Worldwide-Numbers (Accessed July 24, 2023).

4. Kenney K, Iacono D, Edlow BL, Katz DI, Diaz-Arrastia R, Dams-O'Connor K, et al. Dementia after moderate-severe traumatic brain injury: coexistence of multiple Proteinopathies. *J Neuropathol Exp Neurol*. (2018) 77:50–63. doi: 10.1093/jnen/nlx101

5. Mortimer JA, van Duijn CM, Chandra V, Fratiglioni L, Graves AB, Heyman A, et al. Head trauma as a risk factor for Alzheimer's disease: a collaborative re-analysis of case-control studies. EURODEM risk factors research group. *Int J Epidemiol*. (1991) 20 Suppl 2:S28–35. doi: 10.1093/ije/20.Supplement_2.S28

6. McKee AC, Stein TD, Huber BR, Crary JF, Bieniek K, Dickson D, et al. Chronic traumatic encephalopathy (CTE): criteria for neuropathological diagnosis and relationship to repetitive head impacts. *Acta Neuropathol*. (2023) 145:371–94. doi: 10.1007/s00401-023-02540-w

7. Agimi Y, Earyes L, Deressa T, Stout K. Estimating repeat traumatic brain injury in the U.S. military, 2015-2017. *Mil Med*. (2022) 187:e360–7. doi: 10.1093/milmed/usab041

8. Crisco JJ, Fiore R, Beckwith JG, Chu JJ, Brolinson PG, Duma S, et al. Frequency and location of head impact exposures in individual collegiate football players. *J Athl Train*. (2010) 45:549–59. doi: 10.4085/1062-6050-45.6.549

9. Stern RA, Riley DO, Daneshvar DH, Nowinski CJ, Cantu RC, McKee AC. Long-term consequences of repetitive brain trauma: chronic traumatic encephalopathy. *PM R*. (2011) 3:S460–7. doi: 10.1016/j.pmrj.2011.08.008

10. Adhikari SP, Maldonado-Rodriguez N, Smiley SC, Lewis CD, Horst MD, Jeffrey Lai CW, et al. Characterizing possible acute brain injury in women experiencing intimate partner violence: a retrospective chart review. *Violence Against Women*. (2023) 10778012231159417:107780122311594. doi: 10.1177/10778012231159417

11. Kwako LE, Glass N, Campbell J, Melvin KC, Barr T, Gill JM. Traumatic brain injury in intimate partner violence: a critical review of outcomes and mechanisms. *Trauma Violence Abuse*. (2011) 12:115–26. doi: 10.1177/1524838011404251

12. Costello K, Greenwald BD. Update on domestic violence and traumatic brain injury: a narrative review. *Brain Sci*. (2022) 12. doi: 10.3390/brainsci12010122

13. Ayton D, Pritchard E, Tsindos T. Acquired brain injury in the context of family violence: a systematic scoping review of incidence, prevalence, and contributing factors. *Trauma Violence Abuse*. (2021) 22:3–17. doi: 10.1177/1524838018821951

14. Danielsen T, Hauch C, Kelly L, White CL. Chronic traumatic encephalopathy (CTE)-type neuropathology in a Young victim of domestic abuse. *J Neuropathol Exp Neurol*. (2021) 80:624–7. doi: 10.1093/jnen/nlab015

15. Mez J, Daneshvar DH, Kiernan PT, Abdolmohammadi B, Alvarez VE, Huber BR, et al. Clinicopathological evaluation of chronic traumatic encephalopathy in players of American football. *JAMA*. (2017) 318:360–70. doi: 10.1001/jama.2017.8334

16. Lee EB, Kinch K, Johnson VE, Trojanowski JQ, Smith DH, Stewart W. Chronic traumatic encephalopathy is a common co-morbidity, but less frequent primary dementia in former soccer and rugby players. *Acta Neuropathol*. (2019) 138:389–99. doi: 10.1007/s00401-019-02030-y

17. DeWitt DS, Hawkins BE, Dixon CE, Kochanek PM, Armstead W, Bass CR, et al. Pre-clinical testing of therapies for traumatic brain injury. *J Neurotrauma*. (2018) 35:2737–54. doi: 10.1089/neu.2018.5778

18. Kochanek PM, Dixon CE, Mondello S, Wang KKK, Lafrenaye A, Bramlett HM, et al. Multi-center pre-clinical consortia to enhance translation of therapies and biomarkers for traumatic brain injury: operation brain trauma therapy and beyond. *Front Neurol*. (2018) 9:640. doi: 10.3389/fneur.2018.00640

19. Smith DH, Hicks R, Povlishock JT. Therapy development for diffuse axonal injury. *J Neurotrauma*. (2013) 30:307–23. doi: 10.1089/neu.2012.2825

20. Zulazmi NA, Arulsamy A, Ali I, Zainal Abidin SA, Othman I, Shaikh MF. The utilization of small non-mammals in traumatic brain injury research: a systematic review. *CNS Neurosci Ther*. (2021) 27:381–402. doi: 10.1111/cns.13590

21. Dixon KJ. Pathophysiology of traumatic brain injury. *Phys Med Rehabil Clin N Am*. (2017) 28:215–25. doi: 10.1016/j.pmr.2016.12.001

22. Maas AIR, Stocchetti N, Bullock R. Moderate and severe traumatic brain injury in adults. *Lancet Neurol*. (2008) 7:728–41. doi: 10.1016/S1474-4422(08)70164-9

23. Wang F, Han Y, Wang B, Peng Q, Huang X, Miller K, et al. Prediction of brain deformations and risk of traumatic brain injury due to closed-head impact: quantitative analysis of the effects of boundary conditions and brain tissue constitutive model. *Biomech Model Mechanobiol*. (2018) 17:1165–85. doi: 10.1007/s10237-018-1021-z

24. Logsdon AF, Lucke-Wold BP, Turner RC, Huber JD, Rosen CL, Simpkins JW. Role of microvascular disruption in brain damage from traumatic brain injury. *Compr Physiol*. (2015) 5:1147–60. doi: 10.1002/cphy.c140057

25. McAllister TW. Neurobiological consequences of traumatic brain injury. *Dialogues Clin Neurosci*. (2011) 13:287–300. doi: 10.31887/DCNS.2011.13.2/tmcallister

26. McAllister TW, Stein MB. Effects of psychological and biomechanical trauma on brain and behavior. *Ann N Y Acad Sci*. (2010) 1208:46–57. doi: 10.1111/j.1749-6632.2010.05720.x

27. Greve MW, Zink BJ. Pathophysiology of traumatic brain injury. *Mt Sinai J Med*. (2009) 76:97–104. doi: 10.1002/msj.20104

28. Johnson VE, Stewart W, Smith DH. Axonal pathology in traumatic brain injury. *Exp Neurol*. (2013) 246:35–43.

29. Runnerstam M, Bao F, Huang Y, Shi J, Gutierrez E, Hamberger A, et al. A new model for diffuse brain injury by rotational acceleration: II. Effects on extracellular glutamate, intracranial pressure, and neuronal apoptosis. *J Neurotrauma*. (2001) 18:259–73. doi: 10.1089/08977150151070892

30. Ommaya AK, Goldsmith W, Thibault L. Biomechanics and neuropathology of adult and paediatric head injury. *Br J Neurosurg*. (2002) 16:220–42. doi: 10.1080/02688690220148824

31. Duquette A, Pernègre C, Veilleux Carpentier A, Leclerc N. Similarities and differences in the pattern of tau hyperphosphorylation in physiological and pathological conditions: impacts on the elaboration of therapies to prevent tau pathology. *Front Neurol*. (2020) 11:607680. doi: 10.3389/fneur.2020.607680

32. Tagge CA, Fisher AM, Minaeva OV, Gaudreau-Balderrama A, Moncaster JA, Zhang X-L, et al. Concussion, microvascular injury, and early tauopathy in young athletes after impact head injury and an impact concussion mouse model. *Brain*. (2018) 141:422–58. doi: 10.1093/brain/awx350

33. Lasagna-Reeves CA, Castillo-Carranza DL, Sengupta U, Sarmiento J, Troncoso J, Jackson GR, et al. Identification of oligomers at early stages of tau aggregation in Alzheimer's disease. *FASEB J*. (2012) 26:1946–59.

34. Liu F, Li B, Tung E-J, Grundke-Iqbal I, Iqbal K, Gong C-X. Site-specific effects of tau phosphorylation on its microtubule assembly activity and self-aggregation. *Eur J Neurosci*. (2007) 26:3429–36. doi: 10.1111/j.1460-9568.2007.05955.x

35. Dickstein DL, De Gasperi R, Gama Sosa MA, Perez-Garcia G, Short JA, Sosa H, et al. Brain and blood biomarkers of tauopathy and neuronal injury in humans and rats with neurobehavioral syndromes following blast exposure. *Mol Psychiatry*. (2021) 26:5940–54. doi: 10.1038/s41380-020-0674-z

36. Braun NJ, Yao KR, Alford PW, Liao D. Mechanical injuries of neurons induce tau mislocalization to dendritic spines and tau-dependent synaptic dysfunction. *Proc Natl Acad Sci USA*. (2020) 117:29069–79. doi: 10.1073/pnas.2008306117

37. Hashimoto Y, Kinoshita N, Greco TM, Federspiel JD, Jean Beltran PM, Ueno N, et al. Mechanical force induces phosphorylation-mediated signaling that underlies tissue response and robustness in Xenopus embryos. *Cell Syst*. (2019) 8:226–241.e7. doi: 10.1016/j.cels.2019.01.006

38. Marmarou A. A review of progress in understanding the pathophysiology and treatment of brain edema. *Neurosurg Focus*. (2007) 22:E1–E10. doi: 10.3171/foc.2007.22.5.2

39. Jha RM, Kochanek PM, Simard JM. Pathophysiology and treatment of cerebral edema in traumatic brain injury. *Neuropharmacology*. (2019) 145:230–46. doi: 10.1016/j.neuropharm.2018.08.004

40. Krishnamurthy K, Laskowitz DT. Cellular and molecular mechanisms of secondary neuronal injury following traumatic brain injury In: D Laskowitz and G Grant, editors. *Translational research in traumatic brain injury*. Boca Raton, FL: CRC Press/Taylor and Francis Group (n.d.)

41. Zhivotovsky B, Orrenius S. Calcium and cell death mechanisms: a perspective from the cell death community. *Cell Calcium*. (2011) 50:211–21. doi: 10.1016/j.ceca.2011.03.003

42. Shohami E., Kohen R. "The role of reactive oxygen species in the pathogenesis of traumatic brain injury," in: G Natan and H Hans, editors. *Göbel for Oxidative Stress and Free Radical Damage in Neurology*. Totowa, NJ: Humana Press, (2011) 99–118.

43. Sohal RS. Role of oxidative stress and protein oxidation in the aging process. *Free Radic Biol Med*. (2002) 33:37–44. doi: 10.1016/S0891-5849(02)00856-0

44. Kahl A, Blanco I, Jackman K, Baskar J, Milaganur Mohan H, Rodney-Sandy R, et al. Cerebral ischemia induces the aggregation of proteins linked to neurodegenerative diseases. *Sci Rep*. (2018) 8:2701. doi: 10.1038/s41598-018-21063-z

45. Ansari MA, Roberts KN, Scheff SW. Oxidative stress and modification of synaptic proteins in hippocampus after traumatic brain injury. *Free Radic Biol Med*. (2008) 45:443–52. doi: 10.1016/j.freeradbiomed.2008.04.038

46. Mizui T, Kinouchi H, Chan PH. Depletion of brain glutathione by buthionine sulfoximine enhances cerebral ischemic injury in rats. *Am J Phys*. (1992) 262:H313–7. doi: 10.1152/ajpheart.1992.262.2.H313

47. Daneman R, Prat A. The blood-brain barrier. *Cold Spring Harb Perspect Biol*. (2015) 7:a020412. doi: 10.1101/cshperspect.a020412

48. Sulhan S, Lyon KA, Shapiro LA, Huang JH. Neuroinflammation and blood-brain barrier disruption following traumatic brain injury: pathophysiology and potential therapeutic targets. *J Neurosci Res*. (2020) 98:19–28. doi: 10.1002/jnr.24331

49. Winkler EA, Minter D, Yue JK, Manley GT. Cerebral edema in traumatic brain injury: pathophysiology and prospective therapeutic targets. *Neurosurg Clin N Am*. (2016) 27:473–88. doi: 10.1016/j.nec.2016.05.008

50. Ramlackhansingh AF, Brooks DJ, Greenwood RJ, Bose SK, Turkheimer FE, Kinnunen KM, et al. Inflammation after trauma: microglial activation and traumatic brain injury. *Ann Neurol*. (2011) 70:374–83. doi: 10.1002/ana.22455

51. Smith C, Gentleman SM, Leclercq PD, Murray LS, Griffin WST, Graham DI, et al. The neuroinflammatory response in humans after traumatic brain injury. *Neuropathol Appl Neurobiol*. (2013) 39:654–66. doi: 10.1111/nan.12008

52. Ertürk A, Mentz S, Stout EE, Hedehus M, Dominguez SL, Neumaier L, et al. Interfering with the chronic immune response rescues chronic degeneration after traumatic brain injury. *J Neurosci*. (2016) 36:9962–75. doi: 10.1523/JNEUROSCI.1898-15.2016

53. Kokiko-Cochran ON, Godbout JP. The inflammatory continuum of traumatic brain injury and Alzheimer's disease. *Front Immunol*. (2018) 9:672. doi: 10.3389/fimmu.2018.00672

54. Verkhratsky A, Butt A, Li B, Illes P, Zorec R, Semyanov A, et al. Astrocytes in human central nervous system diseases: a frontier for new therapies. *Signal Transduct Target Ther*. (2023) 8:396. doi: 10.1038/s41392-023-01628-9

55. Ziebell JM, Morganti-Kossmann MC. Involvement of pro-and anti-inflammatory cytokines and chemokines in the pathophysiology of traumatic brain injury. *Neurotherapeutics*. (2010) 7:22–30. doi: 10.1016/j.nurt.2009.10.016

56. Odfalk KF, Bieniek KF, Hopp SC. Microglia: Friend and foe in tauopathy. *Prog Neurobiol*. (2022) 216:102306. doi: 10.1016/j.pneurobio.2022.102306

57. Griffin WS, Sheng JG, Gentleman SM, Graham DI, Mrak RE, Roberts GW. Microglial interleukin-1 alpha expression in human head injury: correlations with neuronal and neuritic beta-amyloid precursor protein expression. *Neurosci Lett*. (1994) 176:133–6. doi: 10.1016/0304-3940(94)90066-3

58. Cherry JD, Tripodis Y, Alvarez VE, Huber B, Kiernan PT, Daneshvar DH, et al. Microglial neuroinflammation contributes to tau accumulation in chronic traumatic encephalopathy. *Acta Neuropathol Commun*. (2016) 4:112. doi: 10.1186/s40478-016-0382-8

59. Kirouac L, Rajic AJ, Cribbs DH, Padmanabhan J. Activation of Ras-ERK signaling and GSK-3 by amyloid precursor protein and amyloid Beta facilitates neurodegeneration in Alzheimer's disease. *eNeuro*. (2017) 4:ENEURO.0149–16.2017. doi: 10.1523/ENEURO.0149-16.2017

60. Johnson VE, Stewart W, Smith DH. Traumatic brain injury and amyloid-β pathology: a link to Alzheimer's disease? *Nat Rev Neurosci*. (2010) 11:361–70. doi: 10.1038/nrn2808

61. Szczygielski J, Mautes A, Steudel WI, Falkai P, Bayer TA, Wirths O. Traumatic brain injury: cause or risk of Alzheimer's disease? A review of experimental studies. *J Neural Transm*. (2005) 112:1547–64. doi: 10.1007/s00702-005-0326-0

62. Smith DH, Nakamura M, McIntosh TK, Wang J, Rodríguez A, Chen XH, et al. Brain trauma induces massive hippocampal neuron death linked to a surge in beta-amyloid levels in mice overexpressing mutant amyloid precursor protein. *Am J Pathol*. (1998) 153:1005–10. doi: 10.1016/S0002-9440(10)65643-X

63. Weil ZM, Gaier KR, Karelina K. Injury timing alters metabolic, inflammatory and functional outcomes following repeated mild traumatic brain injury. *Neurobiol Dis*. (2014) 70:108–16. doi: 10.1016/j.nbd.2014.06.016

64. Mouzon B, Bachmeier C, Ojo J, Acker C, Ferguson S, Crynen G, et al. Chronic White matter degeneration, but no tau pathology at one-year post-repetitive mild traumatic brain injury in a tau transgenic model. *J Neurotrauma*. (2019) 36:576–88. doi: 10.1089/neu.2018.5720

65. Katsumoto A, Takeuchi H, Tanaka F. Tau pathology in chronic traumatic encephalopathy and Alzheimer's disease: similarities and differences. *Front Neurol*. (2019) 10:980. doi: 10.3389/fneur.2019.00980

66. Ojo JO, Mouzon B, Algamal M, Leary P, Lynch C, Abdullah L, et al. Chronic repetitive mild traumatic brain injury results in reduced cerebral blood flow, axonal injury, gliosis, and increased T-tau and tau oligomers. *J Neuropathol Exp Neurol*. (2016) 75:636–55. doi: 10.1093/jnen/nlw035

67. Ojo JO, Mouzon B, Greenberg MB, Bachmeier C, Mullan M, Crawford F. Repetitive mild traumatic brain injury augments tau pathology and glial activation in aged hTau mice. *J Neuropathol Exp Neurol*. (2013) 72:137–51. doi: 10.1097/NEN.0b013e3182814cdf

68. Chen W-W, Zhang X, Huang W-J. Role of neuroinflammation in neurodegenerative diseases (review). *Mol Med Rep*. (2016) 13:3391–6. doi: 10.3892/mmr.2016.4948

69. Kao Y-CJ, Lui YW, Lu C-F, Chen H-L, Hsieh B-Y, Chen C-Y. Behavioral and structural effects of single and repeat closed-head injury. *AJNR Am J Neuroradiol*. (2019) 40:601–8. doi: 10.3174/ajnr.A6014

70. Jamnia N, Urban JH, Stutzmann GE, Chiren SG, Reisenbigler E, Marr R, et al. A clinically relevant closed-head model of single and repeat concussive injury in the adult rat using a controlled cortical impact device. *J Neurotrauma*. (2017) 34:1351–63. doi: 10.1089/neu.2016.4517

71. Mull M, Aderibigbe O, Hajiaghamemar M, Oeur RA, Margulies SS. Multiple head rotations result in persistent gait alterations in piglets. *Biomedicines*. (2022) 10:2976. doi: 10.3390/biomedicines10112976

72. Wilson RJ, Bell MR, Giordano KR, Seyburn S, Kozlowski DA. Repeat subconcussion in the adult rat gives rise to behavioral deficits similar to a single concussion but different depending upon sex. *Behav Brain Res*. (2023) 438:114206. doi: 10.1016/j.bbr.2022.114206

73. Quinones A, Young T, Schupper AJ, Ali M, Hrabarchuk EI, Lamb CD, et al. Effects of repetitive head trauma on symptomatology of subsequent sport-related concussion. *J Neurosurg Pediatr*. (2023) 32:133–40. doi: 10.3171/2023.2.PEDS237

74. McKee AC, Cairns NJ, Dickson DW, Folkerth RD, Keene CD, Litvan I, et al. The first NINDS/NIBIB consensus meeting to define neuropathological criteria for the diagnosis of chronic traumatic encephalopathy. *Acta Neuropathol*. (2016) 131:75–86. doi: 10.1007/s00401-015-1515-z

75. Effgen G. B., Ong T., Nammalwar S., Ortuño A. I., Meaney D. F., 'Dale' Bass, C. R., et al. Primary blast exposure increases hippocampal vulnerability to subsequent exposure: reducing Long-term potentiation. *J Neurotrauma*. (2016) 33:1901–12. doi: 10.1089/neu.2015.4327

76. Meyer DL, Davies DR, Barr JL, Manzerra P, Forster GL. Mild traumatic brain injury in the rat alters neuronal number in the limbic system and increases conditioned fear and anxiety-like behaviors. *Exp Neurol*. (2012) 235:574–87. doi: 10.1016/j.expneurol.2012.03.012

77. Nawashiro H, Shima K, Chigasaki H. Selective vulnerability of hippocampal CA3 neurons to hypoxia after mild concussion in the rat. *Neurol Res*. (1995) 17:455–60. doi: 10.1080/01616412.1995.11740363

78. Tang Y-P, Noda Y, Hasegawa T, Nabeshima T. A concussive-like brain injury model in mice (II): selective neuronal loss in the cortex and Hippocampus. *J Neurotrauma*. (1997) 14:863–73. doi: 10.1089/neu.1997.14.863

79. Cheng JS, Craft R, Yu G-Q, Ho K, Wang X, Mohan G, et al. Tau reduction diminishes spatial learning and memory deficits after mild repetitive traumatic brain injury in mice. *PLoS One*. (2014) 9:e115765. doi: 10.1371/journal.pone.0115765

80. Schindowski K, Bretteville A, Leroy K, Bégard S, Brion J-P, Hamdane M, et al. Alzheimer's disease-like tau neuropathology leads to memory deficits and loss of functional synapses in a novel mutated tau transgenic mouse without any motor deficits. *Am J Pathol*. (2006) 169:599–616. doi: 10.2353/ajpath.2006.060002

81. Feinstein SC, Wilson L. Inability of tau to properly regulate neuronal microtubule dynamics: a loss-of-function mechanism by which tau might mediate neuronal cell death. *Biochim Biophys Acta (BBA) - Mol Basis Dis*. (2005) 1739:268–79. doi: 10.1016/j.bbadis.2004.07.002

82. Wang J-Z, Liu F. Microtubule-associated protein tau in development, degeneration and protection of neurons. *Prog Neurobiol*. (2008) 85:148–75. doi: 10.1016/j.pneurobio.2008.03.002

83. Alonso AC, Mederlyova A, Novak M, Grundke-Iqbal I, Iqbal K. Promotion of hyperphosphorylation by frontotemporal dementia tau mutations. *J Biol Chem*. (2004) 279:34873–81. doi: 10.1074/jbc.M405131200

84. Xia Y, Bell BM, Kim JD, Giasson BI. Tau mutation S356T in the three repeat isoform leads to microtubule dysfunction and promotes prion-like seeded aggregation. *Front Neurosci*. (2023) 17:1181804. doi: 10.3389/fnins.2023.1181804

85. Johnson VE, Stewart W, Smith DH. Widespread tau and amyloid-Beta pathology many years after a single traumatic brain injury in humans. *Brain Pathol*. (2012) 22:142–9. doi: 10.1111/j.1750-3639.2011.00513.x

86. McKee AC, Stein TD, Kiernan PT, Alvarez VE. The neuropathology of chronic traumatic encephalopathy. *Brain Pathol*. (2015) 25:350–64. doi: 10.1111/bpa.12248

87. Andreadis A. Tau gene alternative splicing: expression patterns, regulation and modulation of function in normal brain and neurodegenerative diseases. *Biochim Biophys Acta*. (2005) 1739:91–103. doi: 10.1016/j.bbadis.2004.08.010

88. Majounie E, Cross W, Newsway V, Dillman A, Vandrovcova J, Morris CM, et al. Variation in tau isoform expression in different brain regions and disease states. *Neurobiol Aging*. (2013) 34:1922.e7–1922.e12. doi: 10.1016/j.neurobiolaging.2013.01.017

89. Kovacs GG, Ghetti B, Goedert M. Classification of diseases with accumulation of tau protein. *Neuropathol Appl Neurobiol*. (2022) 48:e12792. doi: 10.1111/nan.12792

90. Metaxas A, Kempf SJ. Neurofibrillary tangles in Alzheimer's disease: elucidation of the molecular mechanism by immunohistochemistry and tau protein phospho-proteomics. *Neural Regeneration Res*. (2016) 11:1579–81. doi: 10.4103/1673-5374.193234

91. Piacentini R, Li Puma DD, Mainardi M, Lazzarino G, Tavazzi B, Arancio O, et al. Reduced gliotransmitter release from astrocytes mediates tau-induced synaptic dysfunction in cultured hippocampal neurons. *Glia*. (2017) 65:1302–16. doi: 10.1002/glia.23163

92. Vasconcelos B, Stancu I-C, Buist A, Bird M, Wang P, Vanoosthuyse A, et al. Heterotypic seeding of tau fibrillization by pre-aggregated Abeta provides potent seeds for prion-like seeding and propagation of tau-pathology in vivo. *Acta Neuropathol*. (2016) 131:549–69. doi: 10.1007/s00401-015-1525-x

93. Albayram O, Kondo A, Mannix R, Smith C, Tsai C-Y, Li C, et al. Cis P-tau is induced in clinical and preclinical brain injury and contributes to post-injury sequelae. *Nat Commun*. (2017) 8:1000. doi: 10.1038/s41467-017-01068-4

94. Kondo A, Shahpasand K, Mannix R, Qiu J, Moncaster J, Chen C-H, et al. Antibody against early driver of neurodegeneration cis P-tau blocks brain injury and tauopathy. *Nature*. (2015) 523:431–6. doi: 10.1038/nature14658

95. Kimura T, Tsutsumi K, Taoka M, Saito T, Masuda-Suzukake M, Ishiguro K, et al. Isomerase Pin1 stimulates dephosphorylation of tau protein at cyclin-dependent kinase (Cdk5)-dependent Alzheimer phosphorylation sites. *J Biol Chem*. (2013) 288:7968–77. doi: 10.1074/jbc.M112.433326

96. Smet C, Sambo A-V, Wieruszeski J-M, Leroy A, Landrieu I, Buée L, et al. The peptidyl prolyl cis/trans-isomerase Pin1 recognizes the phospho-Thr212-Pro213 site on tau. *Biochemistry*. (2004) 43:2032–40. doi: 10.1021/bi035479x

97. Smet C, Wieruszeski J-M, Buée L, Landrieu I, Lippens G. Regulation of Pin1 peptidyl-prolyl cis/trans isomerase activity by its WW binding module on a multi-phosphorylated peptide of tau protein. *FEBS Lett*. (2005) 579:4159–64. doi: 10.1016/j.febslet.2005.06.048

98. Nakamura K, Greenwood A, Binder L, Bigio EH, Denial S, Nicholson L, et al. Proline isomer-specific antibodies reveal the early pathogenic tau conformation in Alzheimer's disease. *Cell*. (2012) 149:232–44. doi: 10.1016/j.cell.2012.02.016

99. Albayram O, Herbert MK, Kondo A, Tsai C-Y, Baxley S, Lian X, et al. Function and regulation of tau conformations in the development and treatment of traumatic brain injury and neurodegeneration. *Cell Biosci*. (2016) 6:59. doi: 10.1186/s13578-016-0124-4

100. Lu KP, Hanes SD, Hunter T. A human peptidyl–prolyl isomerase essential for regulation of mitosis. *Nature*. (1996) 380:544–7. doi: 10.1038/380544a0

101. Lu PJ, Wulf G, Zhou XZ, Davies P, Lu KP. The prolyl isomerase Pin1 restores the function of Alzheimer-associated phosphorylated tau protein. *Nature*. (1999) 399:784–8. doi: 10.1038/21650

102. Hamdane M, Dourlen P, Bretteville A, Sambo A-V, Ferreira S, Ando K, et al. Pin1 allows for differential tau dephosphorylation in neuronal cells. *Mol Cell Neurosci*. (2006) 32:155–60. doi: 10.1016/j.mcn.2006.03.006

103. Hof PR, Bouras C, Buee L, Delacourte A, Perl DP, Morrison JH. Differential distribution of neurofibrillary tangles in the cerebral cortex of dementia pugilistica and Alzheimer's disease cases. *Acta Neuropathol*. (1992) 85:23–30. doi: 10.1007/bf00304630

104. Schmidt M, Zhukareva V, Newell K, Lee V, Trojanowski J. Tau isoform profile and phosphorylation state in dementia pugilistica recapitulate Alzheimer's disease. *Acta Neuropathol*. (2001) 101:518–24. doi: 10.1007/s004010000330

105. McKee AC, Stern RA, Nowinski CJ, Stein TD, Alvarez VE, Daneshvar DH, et al. The spectrum of disease in chronic traumatic encephalopathy. *Brain*. (2013) 136:43–64. doi: 10.1093/brain/aws307

106. Lu KP, Kondo A, Albayram O, Herbert MK, Liu H, Zhou XZ. Potential of the antibody against cis–phosphorylated tau in the early diagnosis, treatment, and prevention of Alzheimer disease and brain injury. *JAMA Neurol*. (2016) 73:1356–62. doi: 10.1001/jamaneurol.2016.2027

107. Foster K, Manca M, McClure K, Koivula P, Trojanowski JQ, Havas D, et al. Preclinical characterization and IND-enabling safety studies for PNT001, an antibody that recognizes cis-pT231 tau. *Alzheimers Dement*. (2023) 19:4662–74. doi: 10.1002/alz.13028

108. Marklund N. Rodent models of traumatic brain injury: methods and challenges. *Methods Mol Biol*. (2016) 1462:29–46. doi: 10.1007/978-1-4939-3816-2_3

109. Vink R. Large animal models of traumatic brain injury. *J Neurosci Res*. (2018) 96:527–35. doi: 10.1002/jnr.24079

110. Dai J-X, Ma Y-B, Le N-Y, Cao J, Wang Y. Large animal models of traumatic brain injury. *Int J Neurosci*. (2018) 128:243–54. doi: 10.1080/00207454.2017.1380008

111. Hall GF, Yao J, Lee G. Human tau becomes phosphorylated and forms filamentous deposits when overexpressed in lamprey central neurons in situ. *Proc Natl Acad Sci USA*. (1997) 94:4733–8. doi: 10.1073/pnas.94.9.4733

112. Hall GF, Lee S, Yao J. Neurofibrillary degeneration can be arrested in an in vivo cellular model of human tauopathy by application of a compound which inhibits tau filament formation in vitro. *J Mol Neurosci*. (2002) 19:253–60. doi: 10.1385/JMN:19:3:251

113. Honson NS, Jensen JR, Abraha A, Hall GF, Kuret J. Small-molecule mediated neuroprotection in an in situ model of tauopathy. *Neurotox Res*. (2009) 15:274–83. doi: 10.1007/s12640-009-9028-y

114. Diomede L, Zanier ER, Moro F, Vegliante G, Colombo L, Russo L, et al. Aβ1-6(D) peptide, effective on Aβ aggregation, inhibits tau misfolding and protects the brain after

traumatic brain injury. *Mol Psychiatry*. (2023) 28:2433–44. doi: 10.1038/s41380-023-02101-3

115. Kim W, Lee S, Jung C, Ahmed A, Lee G, Hall GF. Interneuronal transfer of human tau between lamprey central neurons in situ. *J Alzheimers Dis*. (2010) 19:647–64. doi: 10.3233/JAD-2010-1273

116. Le MN, Kim W, Lee S, McKee AC, Hall GF. Multiple mechanisms of extracellular tau spreading in a non-transgenic tauopathy model. *Am J Neurodegener Dis*. (2012) 1:316–33.

117. Lee S, Jung C, Lee G, Hall GF. Exonic point mutations of human tau enhance its toxicity and cause characteristic changes in neuronal morphology, tau distribution and tau phosphorylation in the lamprey cellular model of Tauopathy. *J Alzheimers Dis*. (2009) 16:99–111. doi: 10.3233/JAD-2009-0954

118. McCutcheon V, Park E, Liu E, Sobhebidari P, Tavakkoli J, Wen X-Y, et al. A novel model of traumatic brain injury in adult zebrafish demonstrates response to injury and treatment comparable with mammalian models. *J Neurotrauma*. (2017) 34:1382–93. doi: 10.1089/neu.2016.4497

119. Tikhonova MA, Maslov NA, Bashirzade AA, Nehoroshev EV, Babchenko VY, Chizhova ND, et al. A novel laser-based zebrafish model for studying traumatic brain injury and its molecular targets. *Pharmaceutics*. (2022) 14:1751. doi: 10.3390/pharmaceutics14081751

120. Gill T, Locskai LF, Burton AH, Alyenbaawi H, Wheeler T, Burton EA, et al. Delivering traumatic brain injury to larval zebrafish. *Methods Mol Biol*. (2024) 2707:3–22. doi: 10.1007/978-1-0716-3401-1_1

121. Alyenbaawi H, Kanyo R, Locskai LF, Kamali-Jamil R, DuVal MG, Bai Q, et al. Seizures are a druggable mechanistic link between TBI and subsequent tauopathy. *Elife*. (2021) 10. doi: 10.7554/eLife.58744

122. Wu BK, Yuan RY, Chang YP, Lien HW, Chen TS, Chien HC, et al. Epicatechin isolated from Tripterygium wilfordii extract reduces tau-GFP-induced neurotoxicity in zebrafish embryo through the activation of Nrf2. *Biochem Biophys Res Commun*. (2016) 477:283–9. doi: 10.1016/j.bbrc.2016.06.058

123. Lopez A, Lee SE, Wojta K, Ramos EM, Klein E, Chen J, et al. A152T tau allele causes neurodegeneration that can be ameliorated in a zebrafish model by autophagy induction. *Brain*. (2017) 140:1128–46. doi: 10.1093/brain/awx005

124. Cosacak MI, Bhattarai P, Bocova L, Dzewas T, Mashkaryan V, Papadimitriou C, et al. Human TAU overexpression results in TAU hyperphosphorylation without neurofibrillary tangles in adult zebrafish brain. *Sci Rep*. (2017) 7:12959. doi: 10.1038/s41598-017-13311-5

125. Bennett RE, Robbins AB, Hu M, Cao X, Betensky RA, Clark T, et al. Tau induces blood vessel abnormalities and angiogenesis-related gene expression in P301L transgenic mice and human Alzheimer's disease. *Proc Natl Acad Sci USA*. (2018) 115:E1289–98. doi: 10.1073/pnas.1710329115

126. Ramsden M, Kotilinek L, Forster C, Paulson J, McGowan E, SantaCruz K, et al. Age-dependent neurofibrillary tangle formation, neuron loss, and memory impairment in a mouse model of human tauopathy (P301L). *J Neurosci*. (2005) 25:10637–47. doi: 10.1523/JNEUROSCI.3279-05.2005

127. Maheras AL, Dix B, Carmo OMS, Young AE, Gill VN, Sun JL, et al. Genetic pathways of Neuroregeneration in a novel mild traumatic brain injury model in adult zebrafish. *eNeuro*. (2018) 5. doi: 10.1523/ENEURO.0208-17.2017

128. Miansari M, Mehta MD, Schilling JM, Kurashina Y, Patel HH, Friend J. Inducing mild traumatic brain injury in *C. elegans* via cavitation-free surface acoustic wave-driven ultrasonic irradiation. *Sci Rep*. (2019) 9:12775. doi: 10.1038/s41598-019-47295-1

129. Angstman NB, Frank H-G, Schmitz C. Hypothermia ameliorates blast-related lifespan reduction of *C. elegans*. *Sci Rep*. (2018) 8:10549. doi: 10.1038/s41598-018-28910-z

130. Angstman NB, Kiessling MC, Frank H-G, Schmitz C. High interindividual variability in dose-dependent reduction in speed of movement after exposing *C. elegans* to shock waves. *Front Behav Neurosci*. (2015) 9:12. doi: 10.3389/fnbeh.2015.00012

131. Zanier ER, Barzago MM, Vegliante G, Romeo M, Restelli E, Bertani I, et al. *C. elegans* detects toxicity of traumatic brain injury generated tau. *Neurobiol Dis*. (2021) 153:105330. doi: 10.1016/j.nbd.2021.105330

132. Zanier ER, Bertani I, Sammali E, Pischiutta F, Chiaravalloti MA, Vegliante G, et al. Induction of a transmissible tau pathology by traumatic brain injury. *Brain*. (2018) 141:2685–99. doi: 10.1093/brain/awy193

133. Riddle DL, Blumenthal T, Meyer BJ, Priess JR. *Aging in C. elegans*. *2nd* ed. New York: Cold Spring Harbor Laboratory Press (1997).

134. Heidary G, Fortini ME. Identification and characterization of the Drosophila tau homolog. *Mech Dev*. (2001) 108:171–8. doi: 10.1016/S0925-4773(01)00487-7

135. Ubhi KK, Shaibah H, Newman TA, Shepherd D, Mudher A. A comparison of the neuronal dysfunction caused by Drosophila tau and human tau in a Drosophila model of tauopathies. *Invertebr Neurosci*. (2007) 7:165–71. doi: 10.1007/s10158-007-0052-4

136. Saikumar J, Byrns CN, Hemphill M, Meaney DF, Bonini NM. Dynamic neural and glial responses of a head-specific model for traumatic brain injury in. *Proc Natl Acad Sci USA*. (2020) 117:17269–77. doi: 10.1073/pnas.2003909117

137. Sun M, Chen LL. A novel method to model chronic traumatic encephalopathy in Drosophila. *J Vis Exp*. (2017). doi: 10.3791/55602

138. Katzenberger RJ, Loewen CA, Bockstruck RT, Woods MA, Ganetzky B, Wassarman DA. A method to inflict closed head traumatic brain injury in Drosophila. *J Vis Exp*. (2015) 100:e52905. doi: 10.3791/52905

139. Barekat A, Gonzalez A, Mauntz RE, Kotzebue RW, Molina B, El-Mecharrafie N, et al. Using Drosophila as an integrated model to study mild repetitive traumatic brain injury. *Sci Rep*. (2016) 6:25252. doi: 10.1038/srep25252

140. Saikumar J, Kim J, Byrns CN, Hemphill M, Meaney DF, Bonini NM. Inducing different severities of traumatic brain injury in Drosophila using a piezoelectric actuator. *Nat Protoc*. (2021) 16:263–82. doi: 10.1038/s41596-020-00415-y

141. Huber BR, Meabon JS, Martin TJ, Mourad PD, Bennett R, Kraemer BC, et al. Blast exposure causes early and persistent aberrant phospho-and cleaved-tau expression in a murine model of mild blast-induced traumatic brain injury. *J Alzheimers Dis*. (2013) 37:309–23. doi: 10.3233/JAD-130182

142. Rubenstein R, McQuillan L, Wang KKW, Robertson C, Chang B, Yang Z, et al. Temporal profiles of P-tau, T-tau, and P-tau:tau ratios in cerebrospinal fluid and blood from moderate-severe traumatic brain injury patients and relationship to 6-12 month global outcomes. *J Neurotrauma*. (2023) 41:0479. doi: 10.1089/neu.2022.0479

143. Goldstein LE, Fisher AM, Tagge CA, Zhang X-L, Velisek L, Sullivan JA, et al. Chronic traumatic encephalopathy in blast-exposed military veterans and a blast neurotrauma mouse model. *Sci Transl Med*. (2012) 4:134ra60. doi: 10.1126/scitranslmed.3003716

144. Rice RA, Pham J, Lee RJ, Najafi AR, West BL, Green KN. Microglial repopulation resolves inflammation and promotes brain recovery after injury. *Glia*. (2017) 65:931–44. doi: 10.1002/glia.23135

145. Ritzel RM, Li Y, Jiao Y, Lei Z, Doran SJ, He J, et al. Brain injury accelerates the onset of a reversible age-related microglial phenotype associated with inflammatory neurodegeneration. *Sci Adv*. (2023) 9:eadd1101. doi: 10.1126/sciadv.add1101

146. Simon DW, McGeachy MJ, Bayır H, Clark RSB, Loane DJ, Kochanek PM. The far-reaching scope of neuroinflammation after traumatic brain injury. *Nat Rev Neurol*. (2017) 13:572. doi: 10.1038/nrneurol.2017.116

147. Wang C-F, Zhao C-C, Liu W-L, Huang X-J, Deng Y-F, Jiang J-Y, et al. Depletion of microglia attenuates dendritic spine loss and neuronal apoptosis in the acute stage of moderate traumatic brain injury in mice. *J Neurotrauma*. (2020) 37:43–54. doi: 10.1089/neu.2019.6460

148. Witcher KG, Bray CE, Chunchai T, Zhao F, O'Neil SM, Gordillo AJ, et al. Traumatic brain injury causes chronic cortical inflammation and neuronal dysfunction mediated by microglia. *J Neurosci*. (2021) 41:1597–616. doi: 10.1523/JNEUROSCI.2469-20.2020

frontiers | Frontiers in Immunology

TYPE Original Research
PUBLISHED 25 March 2024
DOI 10.3389/fimmu.2024.1349030

OPEN ACCESS

EDITED BY
Fawaz Alzaid,
Sorbonne Universités, France

REVIEWED BY
Natasja G. De Groot,
Biomedical Primate Research Centre (BPRC), Netherlands
Lisa Ellerby,
Buck Institute for Research on Aging, United States

*CORRESPONDENCE
Sulev Kõks
sulev.koks@perron.uwa.edu.au

RECEIVED 04 December 2023
ACCEPTED 06 March 2024
PUBLISHED 25 March 2024

CITATION
Kulski JK, Suzuki S, Shiina T, Pfaff AL and Kõks S (2024) Regulatory SVA retrotransposons and classical HLA genotyped-transcripts associated with Parkinson's disease.
Front. Immunol. 15:1349030.
doi: 10.3389/fimmu.2024.1349030

Regulatory SVA retrotransposons and classical HLA genotyped-transcripts associated with Parkinson's disease

Jerzy K. Kulski[1,2], Shingo Suzuki[1], Takashi Shiina[1], Abigail L. Pfaff[3,4] and Sulev Kõks[3,4]*

[1]Department of Molecular Life Science, Tokai University School of Medicine, Isehara, Kanagawa, Japan, [2]Health and Medical Science, Division of Immunology and Microbiology, School of Biomedical Sciences, The University of Western Australia, Nedlands, WA, Australia, [3]Perron Institute for Neurological and Translational Science, Perth, WA, Australia, [4]Centre for Molecular Medicine and Innovative Therapeutics, Murdoch University, Perth, WA, Australia

Introduction: Parkinson's disease (PD) is a neurodegenerative and polygenic disorder characterised by the progressive loss of neural dopamine and onset of movement disorders. We previously described eight SINE-VNTR-Alu (SVA) retrotransposon-insertion-polymorphisms (RIPs) located and expressed within the Human Leucocyte Antigen (HLA) genomic region of chromosome 6 that modulate the differential co-expression of 71 different genes including the HLA classical class I and class II genes in a Parkinson's Progression Markers Initiative (PPMI) cohort.

Aims and methods: In the present study, we (1) reanalysed the PPMI genomic and transcriptomic sequencing data obtained from whole blood of 1521 individuals (867 cases and 654 controls) to infer the genotypes of the transcripts expressed by eight classical HLA class I and class II genes as well as *DRA* and the *DRB3/4/5* haplotypes, and (2) examined the statistical differences between three different PD subgroups (cases) and healthy controls (HC) for the HLA and SVA transcribed genotypes and inferred haplotypes.

Results: Significant differences for 57 expressed HLA alleles (21 HLA class I and 36 HLA class II alleles) up to the three-field resolution and four of eight expressed SVA were detected at $p<0.05$ by the Fisher's exact test within one or other of three different PD subgroups (750 individuals with PD, 57 prodromes, 60 individuals who had scans without evidence of dopamine deficits [SWEDD]), when compared against a group of 654 HCs within the PPMI cohort and when not corrected by the Bonferroni test for multiple comparisons. Fourteen of 20 significant alleles were unique to the PD-HC comparison, whereas 31 of the 57 alleles overlapped between two or more different subgroup comparisons. Only the expressed *HLA-DRA*01:01:01* and *-DQA1*03:01:01* protective alleles (PD v HC), the *-DQA1*03:03:01* risk (HC v Prodrome) or protective allele (PD v Prodrome), the *-DRA*01:01:02* and *-DRB4*01:03:02* risk alleles (SWEDD v HC), and the *NR_SVA_381* present genotype (PD v HC) at a 5% homozygous insertion frequency near *HLA-DPA1*, were significant ($Pc<0.1$) after Bonferroni corrections. The homologous *NR_SVA_381* insertion significantly decreased the transcription levels of *HLA-DPA1* and *HLA-DPB1* in the PPMI cohort and its presence as a homozygous genotype is a risk factor ($Pc=0.012$) for PD. The most frequent

NR_SVA_381 insertion haplotype in the PPMI cohort was *NR_SVA_381/DPA1*02/DPB1*01* (3.7%). Although *HLA C*07/B*07/DRB5*01/DRB1*15/DQB1*06* was the most frequent HLA 5-loci phased-haplotype (n, 76) in the PPMI cohort, the *NR_SVA_381* insertion was present in only six of them (8%).

Conclusions: These data suggest that expressed SVA and HLA gene alleles in circulating white blood cells are coordinated differentially in the regulation of immune responses and the long-term onset and progression of PD, the mechanisms of which have yet to be elucidated.

KEYWORDS

major histocompatibility complex (MHC), human leucocyte antigen (HLA), SINE-VNTR-Alu (SVA), expression quantitative trait loci (eQTL), Parkinson's disease (PD), Parkinson's progression markers initiative (PPMI)

1 Introduction

Parkinson's disease (PD), familial and sporadic, is the second most common human neurodegenerative disease after Alzheimer's disease with almost 90,000 people in the USA diagnosed each year, and a 2019 world-wide prevalence rate of 8.5 million individuals that is increasing (1). PD pathology is age-related and characterised by progressive degeneration of dopaminergic neurons in the *substantia nigra* and other brainstem nuclei, with accumulation of tau and alpha-synuclein deposits (Lewy body inclusions) throughout the peripheral and central nervous systems (2–5). Essential differential observations accompanying PD subtypes include loss of dopamine, bradykinesia (movement disorders), rigidity, tremor and a range of non-motor symptoms such as cognitive impairment and sleep disturbance (6, 7). The primary and secondary causes of PD may involve genetic, environmental, metabolic and immunological factors with various non-neurological features and varying overlap with age-related autoimmune diseases such as multiple sclerosis, amyotrophic lateral sclerosis, thyroid diseases and rheumatoid myalgia (3, 8–11). In regard to the effect of the environment and immunogenetics, Braak et al. (12) postulated that an unknown viral or bacterial infection in the neurons of the gut and/or nasal cavity initiated the onset of sporadic PD with specific alpha-synuclein spreading and eventual Lewy body formation and glial neuroinflammatory activation. Considerable preclinical, clinical and laboratory evidence supports Braak's hypothesis of PD progression, although the specific mechanisms, stages and pathways still have to be elucidated (13, 14). Recent animal *in vitro* studies and human neuropathological examinations suggest that neuronal antigen presentation may have a role in PD and other neurodegenerative disorders (15).

Although the aetiology of sporadic PD remains unknown, the immune system has an important role in this disease (3, 8–11). The protective effect of nonsteroidal anti-inflammatory drugs in animal models and epidemiological studies underscores the role of neuroinflammation in PD (16). Large numbers of microglia expressing human leucocyte antigen (HLA)-DR have been detected in the brain of PD patients, particularly in areas of maximal neurodegeneration (15, 17). *Leucine-rich repeat kinase 2* (*LRRK2*), a risk gene of PD, is highly expressed in microglia, monocytes and other immune cells (18), and has been reported to be associated with an increasing risk of Crohn's disease, an inflammatory bowel disease and other autoimmune diseases (19–21). Alpha-synuclein specific T cell reactivity is associated with *HLA-DRB1*15:01* and *-DRB5*01:01* (22, 23), and with preclinical and early PD (24, 25), and the infiltration of CD4+ lymphocytes into the brain contributes to neurodegeneration in a mouse model of PD (15, 26). At least 90 genetic loci have been associated with PD risk in genome-wide association studies (GWAS), including the *HLA-DRA*, *-DRB*, and *-DQ* genes within the Major Histocompatibility Complex (MHC) class II region on the short arm of chromosome 6 at 6p21.3 (27, 28).

HLA class I and class II molecules are polymorphic cell-membrane-bound glycoproteins that present antigens to circulating CD8+ and CD4+ T-lymphocytes, and regulate the innate and adaptive immune responses including autoimmunity, infectious diseases and transplantation outcomes (29–31). The MHC or HLA genomic region encodes at least 160 genes within ~ 3 to 4 MB including three distinct structural regions designated as class I, class II and class III. Of the 32 HLA genes, the classical HLA class I genes, *HLA-A*, *-B* and *-C*, and the classical HLA class II genes, *HLA-DR*, *-DQ* and *-DP*, are characterised by an extraordinary large number of polymorphisms, whereas the non-classical HLA class I genes, such as *HLA-E*, *-F* and *-G*, are differentiated by their tissue-specific expression and limited polymorphism (32, 33). Several GWASs have shown an association between the HLA locus and the risk of PD especially involving the HLA class II gene SNPs of *HLA-DQA1*, *-DQA2*, *-DQB1*, *-DRB1*, and *-DRB5* (27, 34–36).

Most studies of PD association with HLA class I and class II alleles are limited in scope and power mainly because of small sample numbers and limited resolution of HLA typing methods. Studies with more than 500 PD cases suggest that HLA genes have a role in risk or protection in PD progression. The study by Saiki et al. (37) of a UK study group (528 PD cases and 3430 controls) revealed that *HLA-DRB1*03* and *-DQB1*05* allele groups were possible PD risk alleles whereas *HLA-DRB1*04* and *-DQB1*03* might be protective. Wissemann et al. (35) in an analysis of 2843 European PD cases from two separate cohorts including healthy controls found that the HLA class II risk alleles were *HLA-DRB1*15:01, -DQA1*01:02* and *-DQB1*06:02*, and the protective alleles were *-DRB1*04:04*, *-DQA1*03:01*, and *-DQA1*03:02*. They also suggested that *HLA-B*07:02* and *-C*07:02* are part of an HLA risk haplotype, whereas *HLA-B*40:01* and *-C*03:04* are protective alleles. Hollenbach et al. (38) in a sequencing and typing analysis of 11 classical HLA loci using 1597 PD and 1606 controls found strong protective effects of *HLA-DRB1*04:01* and *HLA-DQB1*03:02*, but no significant differences between cases and controls for alleles of any class I locus (*HLA-A*, *-B*, and *-C*) or class II loci *HLA-DPA1, -DPB1, -DRB3, -DRB4*, and *-DRB5*. They also proposed that HLA susceptibility to PD can be explained by a specific combination of amino acids at positions 70–74 on the HLA-DRB1 molecule referred to as the 'shared epitope' (SE) and that the SE in combination with valine at position 11 (11-V) is highly protective in PD, but a risk with the absence of 11-V. More recently, Yu et al. (34) used 13,770 European PD patients in a meta-analysis of multiple cohorts from eight independent sources to confirm that *HLA-DRB1*04:01, -DRB1*04:04*, *-DQA1*03:01* and *-DQB1*03:02* were protective. They concluded that the effect of the *HLA-DRB1* gene in susceptibility for PD is small and does not merit routine HLA typing in PD. An earlier study of Chinese Han (567 PD cases and 746 controls) indicated that *HLA-DRB1*03:01* was a risk allele, whereas *HLA-DRB1*04:06* was a protective allele in their study of only *HLA-DRB1* alleles (39). More studies of the association between HLA genotypes and PD are needed to understand the role of HLA in the disease processes of PD and how HLA genes and alleles might be interlinked with accompanying autoimmune diseases, especially those that show non-neurological symptoms associated with PD such as sleep disorder and a decrease in *HLA-DR* expression (40).

Apart from protein coding genes, numerous repeat elements (REs) within the human genome have been associated with PD including *SINE-R-VNTR-Alu* (SVA) retrotransposon insertion polymorphisms (RIPs), such as a SVA that is inserted in the *TAF1* gene that has been associated with the disease X-linked dystonia-parkinsonism, and at least five other SVA inserted within the PD (*PARK*) gene loci of different chromosomes (41, 42). Recently, expression quantitative trait loci (eQTL) of different SVAs and their effect on the regulation of gene expression were identified and described for a Parkinson's Progression Markers Initiative (PPMI) cohort using whole genome sequence and transcriptome data obtained from the blood of more than a thousand individuals (43). Also, there are SVAs within the MHC genomic region that are expressed and can regulate the expression of HLA genes (44). At least eighteen SVA polymorphic insertions were mapped previously within the MHC class I, II and III regions, and some were found to be haplotypic or haplospecific for particular HLA gene alleles that varied in frequency between European, Japanese and African American populations (45). For example, the *SVA-HF*, *SVA-HA*, and *SVA-HC* were inserted at a relatively low frequency (<0.2) in European populations and strongly associated with the HLA 7.1 ancestral haplotype, but not with the 8.1 haplotype (46, 47).

A PPMI clinical protocol was established in 2010 to acquire comprehensive longitudinal within-participant clinical, imaging, genomic, transcriptomic and biomarker data for three main cohorts, (1) PD with and without genetic risk variants, (2) prodromes (nonmotor features) at risk of PD, and (3) healthy controls with no neurological disorder and no first degree relative, currently aimed at enrolling 4000 participants at about 50 sites worldwide (48). We associated the regulatory properties of 8 SVA RIPs located within the class I and class II MHC regions of the PPMI cohort with the differential co-expression of 71 genes within and 75 genes outside of the MHC region, including all the classical class I and class II genes (44). A limitation of this SVA-HLA eQTL study was the absence of HLA allelic data to associate with the SVA genotypes and for stratifying the statistical differences between PD, prodromes and healthy controls within the PPMI cohort.

The purpose of our current study was to undertake an analysis of the expression of ten classical class I (*HLA-A, -B, -C*) and class II (*HLA-DRA, -DRB3/4/5 -DRB1, -DQB1, -DQA1, -DPA1, -DPB1*) gene alleles in the context of the eight regulatory SVA RIPs expressed within the MHC genomic region (Figure 1) that we had previously studied (44). The main aims of this study were to determine:

(a) the prevalence of the expressed HLA classical alleles and inferred haplotypes for the entire PPMI cohort, cases and controls.
(b) the HLA allelic and haplotypic statistical differences between PD, healthy controls (HC), prodromal PD and scans without evidence of dopamine deficits (SWEDD).
(c) the inferred SVA haplotypes and their association with HLA gene alleles.
(d) statistical differences between HLA & SVA alleles and PD, HC, prodromes and SWEDD.

Our RNA data analysis confirms that SVAs are eQTLs for classical HLA class I and class II alleles, and suggests that coordinated SVA and HLA gene expression might influence PD onset or progression via the adaptive immune system.

2 Materials and methods

2.1 Parkinson's progression markers initiative datasets

The PPMI and database is an ongoing longitudinal, observational, multicentre study of PD with an overall goal to identify biological and genetic markers of disease progression, accelerate therapeutic trials and reduce progression of PD

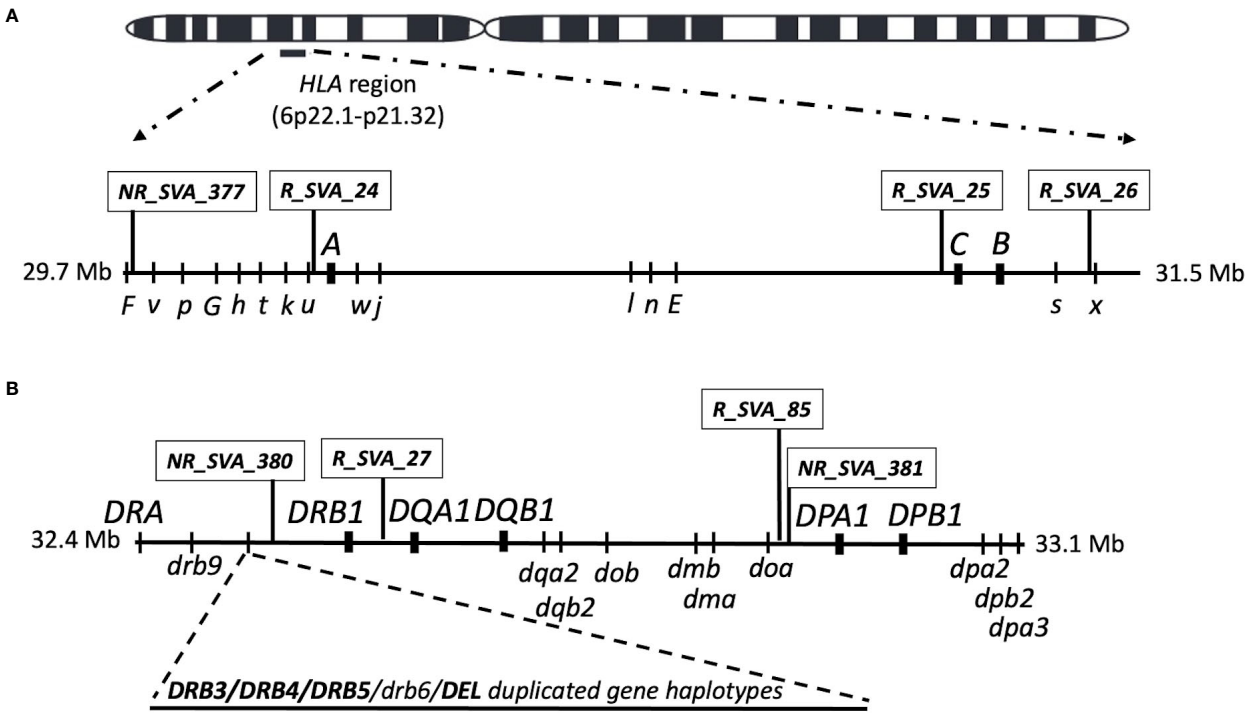

FIGURE 1
Location map of the SVA and classical HLA class I and class II genes on chromosome 6 that were transcribed in blood cells in this study. **(A)** is the HLA class I region showing the relative SVA and the three classical class I HLA gene loci above the horizontal line investigated in this study. The relative position of HLA nonclassical gene (capital letter) and pseudogene (lower case letters) loci are shown below the horizontal line. **(B)** is the classical class II region showing the relative SVA and five classical class II HLA gene loci above the horizontal line investigated in this study. The relative position of the HLA nonclassical class II genes and pseudogene loci are shown below the horizontal line. The region between *HLA-DRB9* and *-DRB1* that harbours the structural variants for the *HLA-DRB3, -DRB4, -DRB5,* and *-DRB6* genes and deletion are indicated by the dashed lines as an added horizontal extension. The Class III region that is located between the class I and class II regions is not shown in the figure. The location of all genes, pseudogenes and SVA are not shown to exact genomic scale.

disability (48). The PPMI cohort data were downloaded from http://www.ppmi-info.org/data (accessed on 19 January 2021) as previously described by Koks et al. (41). Transcriptome (RNAseq) data obtained from whole blood samples together with genetic and clinical data of 1521 individuals reported as mostly white Americans within the PPMI cohort consist of four subgroups, (1) 750 individuals with Parkinson disease (PD), (2) 57 with prodromal PD (Prodrome), (3) 60 individuals who had scans without evidence of dopamine deficits (SWEDD), and (4) 654 healthy controls (HC). The entire PPMI cohort with the four subgroups were analysed to determine the association between the transcribed SVA and classical HLA genes, each at eight loci, within the class I and class II regions of the human MHC (Figure 1).

2.2 SVA and HLA genotypes

Regulatory effects of SVA on HLA transcription levels were inferred statistically by eQTL analysis using the Matrix eQTL software (49) and described previously (44). Fastq files of whole-blood RNAseq were downloaded from the PPMI database and the referenced SVA (R_SVA) and non-referenced SVA (NR_SVA) (Figure 1) were located, genotyped and identified within or outside the MHC genomic region with the assistance of the software tools, *Delly2* structural variant caller and the transcript counters *Salmon* and *DESeq2*, as previously described (41, 44). All the transcripts' of 1521 individuals downloaded as PPMI blood RNAseq.bam files were used to identify the genotypes of ten classical class I and class II HLA genes using the *arcasHLA* software tool described by Orenbach et al. (50). *DRB3, DRB4* and *DRB5* were counted as a single locus or gene, including the designated '*DRB3DRB4DRB5 absent*', which is the haplotype with no *DRB3, DRB4, DRB5* locus. The HLA transcripts were 'genotyped' at least to the three-field resolution (eg., *A*02:01:01*) whereby the first field represents the ancestral allele group (e.g., *A*02*), the second field represents protein type and the third field represents synonymous changes in coding regions.

2.3 Statistical analysis

The p-values, odds ratios (OR), and 95% confidence intervals (CI) were calculated using Fisher's exact test using R software (R version 4.1.3). For multiple testing, the Bonferroni correction was applied, and the observed p-values were adjusted by multiplying them by the number of alleles at each HLA locus to obtain *Pc* values

(Bonferroni-corrected *Pc*-values). The estimation of haplotypes was performed using the PHASE program v2.1.1 (51) and are referred to in this study as phased-haplotypes.

3 Results

3.1 Common medical disorders associated between PD and HC

The aetiology of PD appears to be multifactorial involving aging, genetics, environmental factors (9), reflected by other inflammation-related disorders or autoimmune diseases (20, 52, 53). Table 1 shows a list of common diseases or disorders in 318 PD patients and 264 healthy controls (free of PD) in a subset of the PPMI cohort. The most significant risk factors (Pc<0.1) associated with PD in this subset of PD patients (average age of 61 years) is scoliosis (n, 9 v 0), and sleep disturbances (n, 72 v 33). Thyroid disease including hyperthyroidism is a risk factor in 75 of the PD patients by the Fisher's exact test with a *p*-value of 0.012.

3.2 HLA genotyped transcripts and statistical associations within case-control comparisons

The HLA genotypes of ten classical class I and class II genes of 1521 individuals within the PPMI cohort inferred from the transcription data are presented in Supplementary Table 1, and their overall frequencies are shown in Supplementary Table 2. The top six *HLA-A, -B, -C, -DRB1, -DQB1, -DQA1, -DPA1, -DPB1* allele frequencies in the PPMI cohort are shown in Table 2, confirming that the PPMI cohort consists mostly of white European or North American ancestry (33).

The significant differences at $p<0.05$ detected by the Fisher's exact test for 20 different HLA alleles (7 HLA class I and 13 HLA class II alleles) up to the three-field resolution in the statistical comparison between HC (n, 654) and PD (n, 750) are shown in Table 3. There are 8 risk alleles (3 HLA class I and 5 HLA class II alleles) and 12 protective alleles (4 HLA class I and 8 class II alleles) within this comparison. The protective alleles, *HLA-DRA*01:01:01* and *-DQA1*03:01:01*, are the only two significant (*Pc<0.1*) alleles

TABLE 1 Common medical diagnoses in 318 PD patients and 264 healthy controls (free of PD).

Common medical diagnoses	n		%			95% CI				
Available medical reports	PD	HC	PD	HC	OR	Lower	Upper	P-value	Pc-value	PD risk
allergy	6	68	1.9%	25.8%	0.06	0.02	0.13	< 2.20E-16	<7.26E-15	protective
arthritis	58	81	18.2%	30.7%	0.50	0.34	0.76	0.00060	0.01992	protective
asthma	12	14	3.8%	5.3%	0.70	0.29	1.67	0.42320	1	
atrial fibrillation	14	9	4.4%	3.4%	1.30	0.52	3.48	0.67030	1	
basal cell carcinoma	12	12	3.8%	4.5%	0.82	0.33	2.04	0.67940	1	
breast cancer	2	6	0.6%	2.3%	0.27	0.03	1.54	0.14980	1	
coronary artery disease	11	6	3.5%	2.3%	1.54	0.51	5.14	0.46500	1	
dermatitis	8	4	2.5%	1.5%	1.68	0.44	7.69	0.56050	1	
diabetes	29	34	9.1%	12.9%	0.68	0.39	1.19	0.17990	1	
Erectile Dysfunction	25	8	7.9%	3.0%	2.73	1.17	7.12	0.01197	0.39501	risk
fibromyalgia	3	6	0.9%	2.3%	0.41	0.07	1.94	0.31210	1	
genital herpes	5	3	1.6%	1.1%	1.39	0.27	9.03	0.73410	1	
gout	5	0	1.6%	0%	Inf	0.76	Inf	0.06681	1	
hypercholesterolemia	58	44	18.2%	16.7%	1.12	0.71	1.76	0.66200	1	
hyperlipidemia	45	57	14.2%	21.6%	0.60	0.38	0.94	0.02142	0.70686	protective
hypertension	109	88	34.3%	33.3%	1.04	0.73	1.50	0.86040	1	association
melanoma	8	5	2.5%	1.9%	1.34	0.38	5.26	0.78020	1	
Myasthenia Gravis	3	0	0.9%	0%	Inf	0.34	Inf	0.25520	1	
neck disorder or pain	5	13	1.6%	4.9%	0.31	0.09	0.94	0.02835	0.93555	protective
neuropathy	21	14	6.6%	5.3%	1.26	0.60	2.74	0.60050	1	
osteoporosis	26	23	8.2%	8.7%	0.93	0.50	1.76	0.88120	1	
prostate carcinoma	13	9	4.1%	3.4%	1.21	0.47	3.26	0.82790	1	

(Continued)

10.3389/fimmu.2024.1349030

TABLE 1 Continued

Common medical diagnoses	n		%			95% CI				
Available medical reports	PD	HC	PD	HC	OR	Lower	Upper	P-value	Pc-value	PD risk
psoriasis	10	14	3.1%	5.3%	0.58	0.23	1.43	0.21350	1	
restless leg syndrome	8	9	2.5%	3.4%	0.73	0.24	2.17	0.62350	1	
scoliosis	9	0	2.8%	0%	Inf	1.67	Inf	0.00487	0.16084	risk
shingles herpes	1	3	0.3%	1.1%	0.28	0.01	3.45	0.33390	1	
sleep disturbances, insomnia, sleep apnea	72	33	22.6%	12.5%	2.05	1.28	3.32	0.00164	0.05415	risk
squamous cell carcinoma	4	0	1.3%	0%	Inf	0.55	Inf	0.13020	1	
thyroid disease and hyperthyroidism	75	40	23.6%	15.2%	1.73	1.11	2.72	0.01205	0.39765	risk
urinary tract infection	8	8	2.5%	3.0%	0.83	0.27	2.56	0.80110	1	

665 listed diseases in 262 individuals (82.4%) with PD (average age of 61).
611 listed diseases 234 individuals (88.6%) without PD (average age of 60).
'Inf' is an infinite value due to a zero value in HC.

TABLE 2 Top six inferred allele frequencies for HLA-A, -B, -C, -DRB1, DQA1, -DQB1, -DPA1 and -DPB1 transcripts.

Locus	Allele name	Number of genotypes				
		PD	PRODROME	SWEDD	HC	% Total
HLA-A	A*02:01:01	308	35	28	250	20.41
HLA-A	A*01:01:01	237	13	19	183	14.86
HLA-A	A*03:01:01	170	11	18	139	11.11
HLA-A	A*24:02:01	119	9	12	136	9.07
HLA-A	A*26:01:01	80	7	4	93	6.05
HLA-A	A*11:01:01	64	4	2	55	4.11
HLA-B	B*08:01:01	136	8	15	100	8.51
HLA-B	B*07:02:01	108	5	17	97	7.46
HLA-B	B*38:01:01	81	8	5	102	6.44
HLA-B	B*14:02:01	94	1	2	96	6.34
HLA-B	B*44:02:01	90	11	10	78	6.21
HLA-B	B*35:01:01	90	5	6	69	5.59
HLA-C	C*04:01:01	204	12	10	190	13.68
HLA-C	C*07:01:01	203	14	20	140	12.39
HLA-C	C*06:02:01	147	12	7	134	9.86
HLA-C	C*12:03:01	130	9	8	134	9.24
HLA-C	C*07:02:01	130	7	19	108	8.68
HLA-C	C*08:02:01	100	3	2	98	6.67
HLA-DRB1	DRB1*07:01:01	207	14	16	192	14.10
HLA-DRB1	DRB1*03:01:01	145	13	15	107	9.20
HLA-DRB1	DRB1*15:01:01	131	11	14	91	8.12
HLA-DRB1	DRB1*11:04:01	118	6	5	108	7.79
HLA-DRB1	DRB1*01:01:01	100	7	6	90	6.67

(Continued)

10.3389/fimmu.2024.1349030

TABLE 2 Continued

Locus	Allele name	Number of genotypes				
		PD	PRODROME	SWEDD	HC	% Total
HLA-DRB1	DRB1*13:01:01	80	9	3	78	5.59
HLA-DQA1	DQA1*05:05:01	270	12	13	208	16.54
HLA-DQA1	DQA1*02:01:01	206	14	16	193	14.10
HLA-DQA1	DQA1*01:02:01	197	18	22	140	12.39
HLA-DQA1	DQA1*03:01:01	128	6	18	157	10.16
HLA-DQA1	DQA1*05:01:01	148	11	16	111	9.40
HLA-DQA1	DQA1*01:03:01	110	10	4	116	7.89
HLA-DQB1	DQB1*03:01:01	259	18	19	207	16.54
HLA-DQB1	DQB1*05:01:01	191	15	10	195	13.51
HLA-DQB1	DQB1*02:02:01	148	8	8	151	10.36
HLA-DQB1	DQB1*06:02:01	145	11	18	110	9.34
HLA-DQB1	DQB1*03:02:01	117	7	18	137	9.17
HLA-DQB1	DQB1*02:01:01	138	13	15	102	8.81
HLA-DPA1	DPA1*01:03:01	1151	83	92	1047	78.01
HLA-DPA1	DPA1*02:01:01	215	18	12	174	13.77
HLA-DPA1	DPA1*02:01:02	48	1	7	28	2.76
HLA-DPA1	DPA1*02:02:02	34	3	4	15	1.84
HLA-DPA1	DPA1*02:07:01	16	0	2	12	0.99
HLA-DPA1	DPA1*01:04:01	9	2	2	16	0.95
HLA-DPB1	DPB1*04:01:01	577	42	46	545	39.78
HLA-DPB1	DPB1*02:01:02	225	14	13	226	15.71
HLA-DPB1	DPB1*04:02:01	182	6	12	135	11.01
HLA-DPB1	DPB1*03:01:01	89	9	11	66	5.75
HLA-DPB1	DPB1*01:01:01	69	5	8	42	4.08
HLA-DPB1	DPB1*104:01:01	46	3	2	46	3.19
total number of genotypes		1500	114	120	1308	3042

after Bonferroni correction for multiple testing. Some notable allelic differences between PD and HC at the $p<0.05$ level are *HLA-B*40:02:01, -DRB1*11:02:01* and *-DPA1*02:02:02* with relatively high *OR* levels (3.68, 4.38 and 2, respectively) and *-DRB1*04:02:01, -DRB1*04:04:01, -DQA1*03:01:01, -DQB1*03:02:01, -DPA1*01:03:01* and *-DPB1*16:01:01* with relatively low *OR* levels (0.64, 0.56, 0.68, 0.72, 0.82, and 0.17).

The HLA alleles frequencies in the PD group (n, 750) compared statistically against those in the Prodrome (n, 57) and SWEDD (n, 60) groups are shown in Table 4. There are 11 and 17 allelic differences at $p<0.05$ in the PD-Prodrome, and PD-SWEDD comparisons respectively, but only the protective *HLA-DQA1*03:03:01* in the PD-Prodrome comparison is significant ($Pc=0.066$) after the Bonferroni correction. Although the expressed *HLA-DRA*01:01:01* and *-DQA1*03:01:01* are protective alleles in the PD-HC comparison at $Pc<0.1$ (Table 3), *HLA-DQA1*03:01:01* is significant only at the $p<0.05$ level and *HLA-DRA*01:01:01* is not significant ($p>0.05$) in the SWEDD-HC comparison (Table 4). Neither *HLA-DRA*01:01:01* nor *-DQA1*03:01:01* is significant ($p>0.05$) in the PD-Prodrome comparison (Table 4).

The significant differences at $p<0.05$ for 43 HLA alleles (25 HLA class I and 38 HLA class II alleles) up to the three-field resolution in two comparisons between HC and the two PD subgroups, Prodrome (A) and SWEDD (B), are shown in Table 5. There are 20 different alleles (18 risk and 2 protective) in the Prodrome-HC, and 23 (18 risk and five protective) in the SWEDD-HC comparisons, with five alleles (*HLA-A*02:844, -B*14:02:01, -B*40:01:02, -C*03:04:01, -DRB1*04:01:01*) overlapping between the two comparisons, (A) and (B). Only three alleles were significant ($Pc<0.1$) after Bonferroni correction, the *HLA-DQA1*03:03:01* risk allele in the Prodrome-HC comparison, and

10.3389/fimmu.2024.1349030

TABLE 3 Significantly expressed HLA genotypes in healthy controls (HC) versus Parkinson Disease (PD).

HC, n=654 v PD, n=750												
20 alleles	n		%		PD	HC	OR	95% CI		P < 0.05	P< 0.1	Risk or
Allele name	PD	HC	PD	HC	Other	Other		Lower	Upper	P-value	Pc-value	protective
A*31:01:02	32	14	2.13%	1.07%	1468	1294	2.01	1.04	4.11	0.035850	1	risk
B*40:02:01	25	6	1.67%	0.46%	1475	1302	3.68	1.47	10.99	0.001917	0.151443	risk
C*07:01:01	203	140	13.53%	10.70%	1297	1168	1.31	1.03	1.66	0.024200	1	risk
DRB5*01:01:01	136	90	9.1%	7.0%	1352	1204	1.35	1.01	1.80	0.03693	0.59088	risk
DRB1*11:02:01	10	2	0.67%	0.15%	1490	1306	4.38	0.93	41.21	0.043470	1	risk
DQB1*05:03:01	53	27	3.53%	2.06%	1447	1281	1.74	1.07	2.89	0.022560	0.879840	risk
DPA1*02:02:02	34	15	2.27%	1.15%	1466	1293	2.00	1.05	3.97	0.02939	0.529020	risk
DPB1*13:01:01	47	24	3.13%	1.83%	1453	1284	1.73	1.03	2.98	0.030210	1	risk
A*24:02:01	119	136	7.93%	10.40%	1381	1172	0.74	0.57	0.97	0.025160	1	protective
B*15:03:01	0	4	0%	0.31%	1500	1304	0	0	1.32	0.046970	1	protective
B*38:01:01	81	102	5.40%	7.80%	1419	1206	0.68	0.49	0.92	0.011340	0.895860	protective
C*02:10:01	0	4	0%	0.31%	1500	1304	0	0	1.32	0.046970	1	protective
DRA*01:01:01	949	889	63.3%	68.0%	551	419	0.81	0.69	0.95	0.0097	**0.0485**	protective
DRB4*01:03:01	283	289	19.0%	22.3%	1205	1005	0.82	0.68	0.99	0.03427	0.54832	protective
DRB1*04:02:01	59	79	3.93%	6.04%	1441	1229	0.64	0.44	0.91	0.011040	0.563040	protective
DRB1*04:04:01	24	37	1.60%	2.83%	1476	1271	0.56	0.32	0.96	0.027590	1	protective
DQA1*03:01:01	128	157	8.53%	12.00%	1372	1151	0.68	0.53	0.88	0.002612	**0.070524**	protective
DQB1*03:02:01	117	137	7.80%	10.47%	1383	1171	0.72	0.55	0.94	0.014650	0.571350	protective
DPA1*01:03:01	1151	1047	76.73%	80.05%	349	261	0.82	0.68	0.99	0.03489	0.628020	protective
DPB1*16:01:01	2	10	0.13%	0.76%	1498	1298	0.17	0.02	0.82	0.016570	0.712510	protective

Pc<0.1 are bold numbers.

the *HLA-DRA*01:01:02* and *-DRB4*01:03:02* risk alleles in the SWEDD-HC comparison.

The statistical analyses of the HLA allele frequency differences at the *p<0.05* level of significance show that the PD, Prodrome and SWEDD subgroups are markedly different from each other within the PPMI cohort (Tables 3–5). There are 57 significantly *(p<0.05)* different HLA alleles (21 class I and 36 class II) in the five statistical comparisons between the different PD subgroups (Tables 3–5). Twenty-six (9 class I and 17 class II) of the 57 different alleles are limited to a single subgroup comparison, mainly in the HC-PD (14 of 20 alleles), HC-Prodrome (6 of 20 alleles), HC-SWEDD (4 of 23 alleles) and PD-Prodrome (2 of 11 alleles) comparisons, whereas thirty-one (12 class I and 19 class II) of the 57 alleles overlap between two or more different subgroup comparisons (Supplementary Table 3). In addition, there are more protective alleles in the HC group than risk alleles in the PD group at a ratio of 12 to 8 (60%) in the PD-HC comparison (Table 3), whereas the Prodrome and SWEDD comparisons with HC have more risk alleles than protective alleles at ratios of 18 to 2 (90%), and 18 to 5 (78%), respectively (Table 5). In a statistical comparison between the HC group (n, 654) and the combined PD subgroups (PD, Prodrome and SWEDD, [n, 867]), presented in Supplementary Table 4, there are 17 risk and 15 protective HLA alleles (12 class I and 20 class II) with 8 of the 32 significant alleles (p<0.05) present only in this analysis, whereas the other 24 alleles are present in at least one of the other statistical comparisons (Tables 3–5). In this analysis, the *HLA-DRA*01:01:01* protective allele is significant (*P=0.0223*) after a Bonferroni correction.

In summary, only five of the expressed HLA alleles shown in Tables 3, 5 are significantly different (*Pc<0.1*) after Bonferroni corrections, *HLA-DRA*01:01:01* (HC v PD), *-DQA1*03:01:01* (HC v PD), *-DQA1*03:03:01* (PD v Prodrome, HC v Prodrome), *-DRA*01:01:02* and *-DRB4*01:03:02* (SWEDD v HC).

3.3 SVA genotyped transcripts and phased-haplotypes within case-control comparisons

The eQTL SVA transcripts expressed at eight MHC loci (*NR_SVA_377, R_SVA_24, R_SVA_25, R_SVA_26, NR_SVA_380, R_SVA_27, R_SVA_85, NR_SVA_381*) that are shown in Figure 1

TABLE 4 Significant expressed HLA genotypes in Parkinson Disease (PD) compared to (A) prodrome and (B) scans without evidenece of dopamine deficits (SWEDD).

(A) PD, n=750 v Prodrome, n=57												
11 alleles	n		%		PD	PRODROME	OR	95% CI		P < 0.05	P< 0.1	Risk or
Allele name	PD	PRODROME	PD	PRODROME	Other	Other		Lower	Upper	P-value	Pc-value	protective
B*14:02:01	94	1	6.3%	0.9%	1406	113	7.55	1.29	303.82	0.01195	0.87235	risk
DQA1*05:05:01	270	12	18.0%	10.5%	1230	102	1.87	1.004	3.78	0.04105	1	risk
DPB1*04:02:01	182	6	12.1%	5.3%	1318	108	2.48	1.08	7.02	0.02318	0.90402	risk
A*02:01:01	308	35	20.5%	30.7%	1192	79	0.58	0.38	0.91	0.01271	0.59737	protective
A*34:02:01	3	2	0.2%	1.8%	1497	112	0.11	0.01	1.36	0.04295	1	protective
B*51:01:01	57	9	3.8%	7.9%	1443	105	0.46	0.22	1.09	0.04573	1	protective
DRB5*01:02:01	32	6	2.2%	5.3%	1456	108	0.40	0.16	1.18	0.04813	0.81821	protective
DQA1*03:03:01	78	15	5.2%	13.2%	1422	99	0.36	0.20	0.70	0.00244	**0.06583**	protective
DPA1*02:01:08	4	3	0.3%	2.6%	1496	111	0.10	0.02	0.69	0.00974	0.17536	protective
DPB1*14:01:01	20	6	1.3%	5.3%	1480	108	0.24	0.09	0.76	0.00779	0.30369	protective
DPB1*16:01:01	2	2	0.1%	1.8%	1498	112	0.08	0.01	1.04	0.02701	1	protective
(B) PD, n=750 v SWEDD, n=60												
17 alleles	n		%		PD	SWEDD	OR	95% CI		P < 0.05	P< 0.1	Risk or protective
Allele name	PD	SWEDD	PD	SWEDD	Other	Other		Lower	Upper	P-value	Pc-value	
B*14:02:01	94	2	6.3%	1.7%	1406	118	3.94	1.04	33.44	0.04184	1	risk
C*08:02:01	100	2	6.7%	1.7%	1400	118	4.21	1.11	35.70	0.02929	1	risk
DRB absent	239	11	16.1%	9.2%	1249	109	1.90	0.999	3.97	0.04876	0.73140	risk
DQA1*05:05:01	270	13	18.0%	10.8%	1230	107	1.81	0.99	3.56	0.04590	1	risk
DQB1*06:03:01	130	3	8.7%	2.5%	1370	117	3.70	1.21	18.45	0.01442	0.47586	risk
A*02:972	1	2	0.1%	1.7%	1499	118	0.04	0.001	0.77	0.01554	0.73038	protective
B*07:02:01	108	17	7.2%	14.2%	1392	103	0.47	0.27	0.87	0.01138	0.84212	protective
C*07:02:01	130	19	8.7%	15.8%	1370	101	0.50	0.30	0.90	0.01332	0.57276	protective
C*07:19	0	2	0%	1.7%	1500	118	0	0	0.42	0.00545	0.23414	protective
DRB4*01:03:02	10	4	0.7%	3.3%	1478	116	0.20	0.06	0.87	0.01642	0.24630	protective

(Continued)

10.3389/fimmu.2024.1349030

10.3389/fimmu.2024.1349030

TABLE 4 Continued

(B) PD, n=750 v SWEDD, n=60													
17 alleles	n		%		PD	SWEDD	OR	95% CI		P < 0.05	P< 0.1	Risk or protective
Allele name	PD	SWEDD	PD	SWEDD	Other	Other		Lower	Upper	P-value	Pc-value	
DRB1*04:04:01	24	7	1.6%	5.8%	1476	113	0.26	0.11	0.74	0.00604	0.27789	protective
DQA1*03:01:01	128	18	8.5%	15.0%	1372	102	0.53	0.31	0.96	0.02923	0.75998	protective
DQB1*03:02:01	117	18	7.8%	15.0%	1383	102	0.48	0.28	0.87	0.00968	0.31941	protective
DQB1*03:03:02	54	9	3.6%	7.5%	1446	111	0.46	0.22	1.09	0.04577	1	protective
DPB1*06:01:01	13	5	0.9%	4.2%	1487	115	0.20	0.07	0.73	0.00803	0.29718	protective
DPB1*10:01:01	20	6	1.3%	5.0%	1480	114	0.26	0.10	0.80	0.00981	0.36286	protective
DPB1*20:01:01	3	3	0.2%	2.5%	1497	117	0.08	0.01	0.59	0.00672	0.24868	protective

had statistically inferred regulatory effects on classical class I and class II gene transcription levels and their different isoforms (44). The MHC SVA genotype frequencies and their influence on classical class I and class II HLA genes and transcripts based on a previous study (44) are shown in Supplementary Table 5. The number and percentage frequency of the 64 SVA-phased haplotypes with the eight MHC genotyped SVA as present or absent insertions in the present study are shown in Supplementary Table 6.

Significant differences for SVA genotypes were detected at $p<0.05$ by the Fisher's exact test between different subgroups (PD, Prodrome, SWEDD and HC) within the PPMI cohort for only four (*R_SVA_25, NR_SVA_380, R_SVA_85*, and *NR_SVA_381*) of the eight SVAs (Table 6). *R_SVA_25* when absent (A) on both chromosomes is a homozygous AA referred to as the *R_SVA_25 AA* genotype. In the PD-SWEDD comparison, the *R_SVA_25 AA* genotype is a PD risk, whereas the *R_SVA_25 PA* genotype is protective. The homozygous presence (*PP*) of the *NR_SVA_381* insertion is a significant risk in the PD-HC and HC-Combination comparisons both at the $p<0.05$ and $Pc<0.1$ levels, but only at the $p<0.05$ level in the HC-Prodrome comparison.

3.4 SVA and HLA phased-haplotypes within case-control comparisons

Phased haplotypes and statistical analysis (Fisher's exact test, *p*-value; and Bonferroni correction, *Pc*-value) of HLA genotypes at 10-loci and SVA genotypes at 8-loci are listed in Supplementary Table 7. In this haplotype analysis of 18 loci, we used the genotype data of only 1165 (66%) of the 1521 individuals because of missing or uncertain data at one or more loci in the excluded 365 cases. Of the 1540 different phased haplotypes (66%) from a total of 2330 haplotypes in this analysis, only six are significantly different between PD and HC at $p<0.05$ (Figure 2). However, none of these *p*-values are significant when corrected by Bonferroni for multiple testing. The two most frequent HLA/SVA haplotypes shown in Figure 2 and listed in Supplementary Table 7 are phased-haplotype ID-797 (n, 37, 2.4%) and phased-haplotype ID-105 (n, 35, 2.3%). Moreover, there is only one risk haplotype (ID-100, n, 23, 1.5%) detected by the Fisher's exact test at $p=0.025$ that is more frequent in PD than HC. In this haplotype, the high frequency R_SVA_85 is absent (*A*) and the low frequency SVA_381 is present (*P*). The high-risk HLA haplotype reported by Wissemann et al. (35) with the *B*07:02/C*07:02/DRB5*01/DRB1*15:01/DQA1*01:02/DQB1*06:02* alleles is split in our study between 30 different haplotypes by including the *HLA-A, -DPA, -DPB* alleles, and SVA genotypes, and therefore was not significant (Supplementary Table 8). In our study, the protective *HLA-DRB1*04:04* allele reported by Wissemann et al. (35) is part of the 'protective' HLA/SVA phased-haplotype ID-1258 (Supplementary Table 7).

The SVAs that associated with the HLA allele groups at >73% are listed in Table 7. For example, in the MHC class I region, the low frequency *NR_SVA_377* (6.9%) is associated almost exclusively with the *HLA-A*11* allele group, whereas the moderately low frequency *R_SVA_24* (26.5%) is associated mostly with three

TABLE 5 Significantly expressed HLA genotypes in healthy controls (HC) versus (A) prodrome, and (B) scans without evidence of dopamine deficits (SWEDD).

(A) HC, n=654 v PRODROME, n=57												
20 alleles	n		%		PRODROME	HC	OR	95% CI		P < 0.05	P< 0.1	Risk or
Allele name	PRODROME	HC	PRODROME	HC	Other	Other		Lower	Upper	P-value	Pc-value	protective
A*02:01:01	35	250	30.70%	19.11%	79	1058	1.87	1.19	2.90	0.004761	0.20472	risk
A*02:844	2	2	1.75%	0.15%	112	1306	11.61	0.83	161.53	0.034350	1	risk
A*34:02:01	2	0	1.75%	0%	112	1308	Inf	2.17	Inf	0.006375	0.27413	risk
B*40:01:02	7	30	6.14%	2.29%	107	1278	2.78	1.01	6.67	0.024140	1	risk
B*49:01:01	5	19	4.39%	1.45%	109	1289	3.11	0.89	8.83	0.037510	1	risk
B*51:01:01	9	42	7.89%	3.21%	105	1266	2.58	1.07	5.57	0.017110	1	risk
C*03:04:01	9	39	7.89%	2.98%	105	1269	2.79	1.15	6.05	0.011580	0.48636	risk
C*05:01:01	14	85	12.28%	6.50%	100	1223	2.01	1.02	3.73	0.032010	1	risk
DRB5*02:02:01	5	20	4.4%	1.5%	109	1274	2.92	0.84	8.22	0.04560	0.72960	risk
DRB1*04:01:01	10	46	8.77%	3.52%	104	1262	2.64	1.15	5.49	0.011140	0.52358	risk
DRB1*11:02:01	2	2	1.75%	0.15%	112	1306	11.61	0.83	161.53	0.034350	1	risk
DRB1*16:01:01	5	16	4.39%	1.22%	109	1292	3.70	1.04	10.82	0.021780	1	risk
DQA1*01:02:02	6	22	5.26%	1.68%	108	1286	3.24	1.05	8.48	0.020310	0.50775	risk
DQA1*03:03:01	15	71	13.16%	5.43%	99	1237	2.64	1.35	4.86	0.003018	**0.07545**	risk
DQB1*03:19:01	2	1	1.75%	0.08%	112	1307	23.19	1.20	1363.90	0.018120	0.56172	risk
DQB1*05:02:01	6	26	5.26%	1.99%	108	1282	2.74	0.90	6.99	0.037550	1	risk
DPA1*02:01:08	3	4	2.63%	0.31%	111	1304	8.78	1.27	52.62	0.01384	0.22144	risk
DPB1*14:01:01	6	16	5.26%	1.22%	108	1292	4.48	1.41	12.36	0.005985	0.20948	risk
B*14:02:01	1	96	0.88%	7.34%	113	1212	0.11	0.00	0.65	0.005414	0.33567	protective
DQA1*03:01:01	6	157	5.26%	12.00%	108	1151	0.41	0.14	0.94	0.030770	0.76925	protective
(B) HC, n=654 v SWEDD, n=60												
23 alleles	n		%		SWEDD	HC	OR	95% CI		P < 0.05	P< 0.1	Risk or
Allele name	SWEDD	HC	SWEDD	HC	Other	Other		Lower	Upper	P-value	Pc-value	protective
A*02:844	2	2	1.67%	0.15%	118	1306	11.03	0.79	153.62	0.03755	1	risk
A*02:972	2	0	1.67%	0%	118	1308	Inf	2.06	Inf	0.00701	0.30134	risk

(Continued)

10.3389/fimmu.2024.1349030

TABLE 5 Continued

(B) HC, n=654 v SWEDD, n=60												
23 alleles	n		%		SWEDD	HC	OR	95% CI		P < 0.05	P< 0.1	Risk or
Allele name	SWEDD	HC	SWEDD	HC	Other	Other		Lower	Upper	P-value	Pc-value	protective
B*07:02:01	17	97	14.17%	7.42%	103	1211	2.06	1.11	3.64	0.01342	0.87230	risk
B*40:01:02	8	30	6.67%	2.29%	112	1278	3.04	1.18	6.99	0.01121	0.72865	risk
C*03:04:01	9	39	7.50%	2.98%	111	1269	2.64	1.09	5.72	0.01558	0.65436	risk
C*07:02:01	19	108	15.83%	8.26%	101	1200	2.09	1.16	3.60	0.01067	0.44814	risk
C*07:19	2	0	1.67%	0%	118	1308	Inf	2.06	Inf	0.00701	0.29434	risk
DRA*01:01:02	7	27	5.8%	2.1%	113	1281	2.94	1.06	7.11	0.0197	**0.0983**	risk
DRB4*01:03:02	4	5	3.3%	0.4%	116	1289	8.86	1.73	41.79	0.00445	**0.06671**	risk
DRB5*01:01:01	15	90	12.5%	7.0%	105	1204	1.91	0.99	3.47	0.04241	0.63615	risk
DRB1*04:01:01	9	46	7.50%	3.52%	111	1262	2.22	0.93	4.75	0.04300	1	risk
DQA1*01:02:01	22	140	18.33%	10.70%	98	1168	1.87	1.09	3.11	0.01583	0.39575	risk
DQB1*03:03:02	9	32	7.50%	2.45%	111	1276	3.23	1.32	7.14	0.00539	0.15092	risk
DQB1*06:02:01	18	110	15.00%	8.41%	102	1198	1.92	1.05	3.34	0.02797	0.78316	risk
DPA1*02:01:02	7	28	5.83%	2.14%	113	1280	2.83	1.02	6.82	0.02291	0.32074	risk
DPB1*06:01:01	5	17	4.17%	1.30%	115	1291	3.30	0.93	9.53	0.03173	1	risk
DPB1*10:01:01	6	18	5.00%	1.38%	114	1290	3.77	1.20	10.16	0.01186	0.39138	risk
DPB1*20:01:01	3	5	2.50%	0.38%	117	1303	6.67	1.02	34.75	0.02369	0.78177	risk
B*14:02:01	2	96	1.67%	7.34%	118	1212	0.21	0.03	0.81	0.01330	0.86450	protective
C*08:02:01	2	98	1.67%	7.49%	118	1210	0.21	0.02	0.80	0.01353	0.56826	protective
DRB345 absent	11	239	9.2%	18.5%	109	1055	0.45	0.21	0.85	0.00849	0.12734	protective
DQA1*01:03:01	4	116	3.33%	8.87%	116	1192	0.35	0.09	0.96	0.03756	0.93900	protective
DQB1*06:03:01	3	122	2.50%	9.33%	117	1186	0.25	0.05	0.77	0.00670	0.18752	protective

'Inf' is an infinite value due to a zero in HC.
Pc<0.1 are bold numbers.

10.3389/fimmu.2024.1349030

TABLE 6 Significant SVA genotypes transcribed in healthy controls (HC) versus (A) Parkinson Disease (PD), (B) prodrome, (C) Scans Without Evidence of Dopamine Deficits (SWEDD), and (D) combination (A+B+C); and (E) PD versus SWEDD.

(A) HC (n, 654) v PD (n, 750)											
		n		%		OR	95% CI		P<0.05	P<0.1	Risk or
Locus	Genotype	PD	HC	PD	HC		Lower	Upper	P-value	Pc-value	protective
NR_SVA_380	PA	139	148	22.53%	27.82%	0.75	0.57	1.00	0.040530	1.0000	protective
NR_SVA_381	PP	39	10	6.31%	1.88%	3.51	1.70	7.97	0.000190	0.0124	risk
(B) HC (n, 654) v PRODROME (n, 57)											
		n		%		OR	95% CI		P<0.05	P<0.1	Risk or
Locus	Genotype	PRODROME	HC	PRODROME	HC		Lower	Upper	P-value	Pc-value	protective
R_SVA_85	AA	3	5	5.77%	0.97%	6.22	0.94	33.07	0.029170	1.0000	risk
NR_SVA_381	PP	5	10	9.09%	1.88%	5.19	1.34	17.48	0.008732	0.5414	risk
(C) HC (n, 654) v SWEDD (n, 60)											
		n		%		OR	95% CI		P<0.05	P<0.1	Risk or
Locus	Genotype	SWEDD	HC	SWEDD	HC		Lower	Upper	P-value	Pc-value	protective
R_SVA_25	PA	19	82	32.76%	15.50%	2.65	1.37	4.97	0.002712	0.1654	risk
R_SVA_25	AA	39	444	67.24%	83.93%	0.39	0.21	0.76	0.003253	0.1984	protective
NR_SVA_380	PA	9	148	15.25%	27.82%	0.47	0.20	0.99	0.042860	1.0000	protective
NR_SVA_380	AA	50	378	84.75%	71.05%	2.26	1.07	5.36	0.030620	1.0000	risk
(D) HC (n, 654) v Combination (A+B+C) (n, 867)											
		n		%		OR	95% CI		P<0.05	P<0.1	Risk or
Locus	Genotype	All	HC	All	HC		Lower	Upper	P-value	Pc-value	protective
NR_SVA_380	PA	163	148	22.30%	27.82%	0.74	0.57	0.97	0.028960	1.0000	protective
R_SVA_85	AA	19	5	2.70%	0.97%	2.84	1.02	9.78	0.036250	1.0000	risk
NR_SVA_381	PP	47	10	6.42%	1.88%	3.58	1.76	8.02	0.000090	0.0058	risk
(E) PD (n, 750) v SWEDD (n, 60)											
		n		%		OR	95% CI		P<0.05	P<0.1	Risk or
Locus	Genotype	PD	SWEDD	PD	SWEDD		Lower	Upper	P-value	Pc-value	protective
R_SVA_25	AA	510	39	83.1%	67.2%	2.39	1.25	4.43	0.00671	0.43596	risk
R_SVA_25	PA	96	19	15.6%	32.8%	0.38	0.20	0.73	0.00284	0.18441	protective

10.3389/fimmu.2024.1349030

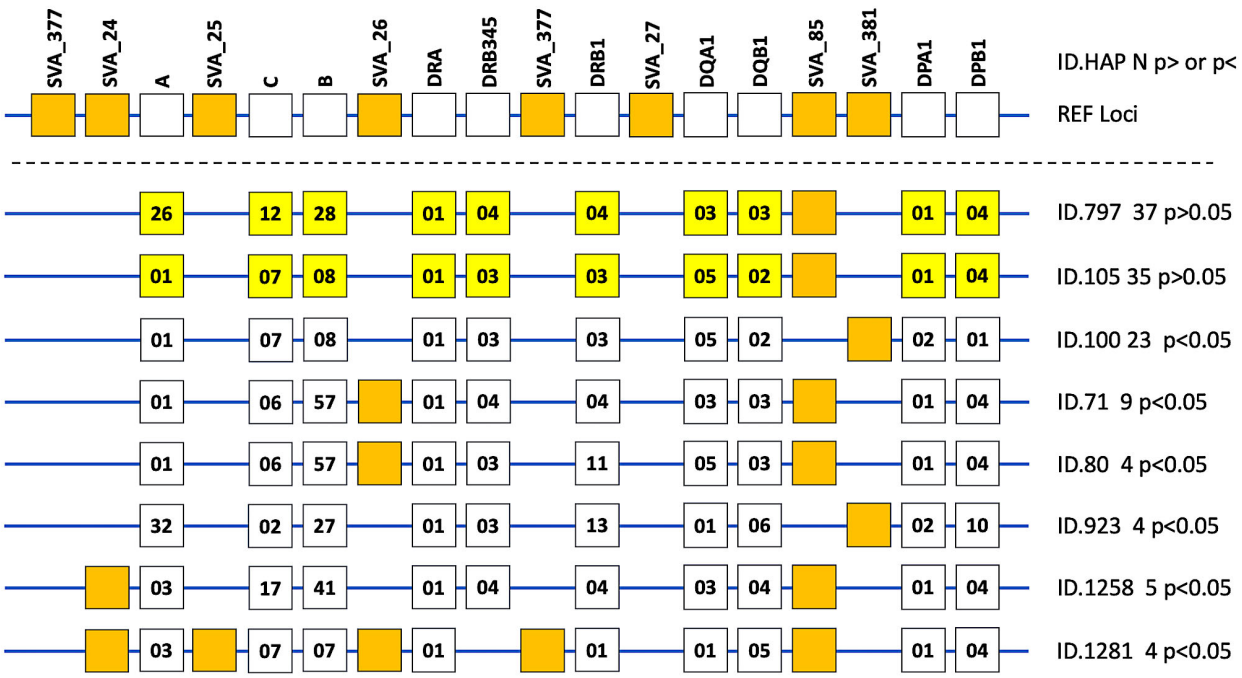

FIGURE 2
Phased haplotypes of HLA genotypes at 10-loci and the absence or presence of the SVA insertion at 8-loci are presented as line diagrams for eight examples of 1540 different haplotypes listed in Supplementary Table 7. The top horizontal line with 18 boxes represents the reference loci (REF loci) of a hypothetical haplotype with the ten labelled HLA genes (open boxes) and all the labelled SVA present at 8 loci. The R and NR designations were omitted from the labelled SVA loci. The next two horizontal lines from the top represent the two most frequent HLA/SVA haplotypes (ID.797 [n, 37] and ID.101 [n, 35], respectively) with ten yellow boxes representing the allelic groups of the HLA genes and the presence of only one SVA (closed orange box) represented by SVA-85. No other SVA was present in these two haplotypes that were not significantly different (p>0.05) between cases and healthy controls. The next six horizontal lines with ID numbers and n values beside them on their right side represent the haplotypes that were significantly different between PD and HC at *p<0.05*. The ten open boxes on each horizontal line represent the allelic groups of the HLA genes labelled on REF loci at the top. The SVA present in one or other of the particular haplotypes are represented by the closed orange boxes. For example, the bottom horizontal line represents the ID.1281 haplotype (n, 4) listed in Supplementary Table 7 and the orange closed boxes represent the presence of 5 SVA insertions that are SVA_24, SVA_25, SVA_26, SVA_377, and SVA_85. This haplotype does not have a DRB3, 4 or 5 gene, hence there is no open box in the DRB345 column. Also, there is no SVA_377 or SVA_27 insertion in any of these eight phased haplotype examples.

different HLA-A allelic groups, *A*03:01, A*11* and *A*30:01*. The low-frequency *R_SVA_25* (8.6%) is associated mostly with *C*07:02*, but also with *B*07:02, B*38:02*, and *B*39:06*. On the other hand, the moderately high-frequency *R_SVA_26* (46.2%) is strongly associated with at least 11 different *HLA-B* allelic groups and 6 different *HLA-C* allelic groups. *R_SVA_26* is associated at varying low levels (0-25%) with at least 19 different *HLA-B* allelic groups (*B*8, B*37, B*38, B*39, B*41, B*42, B*44, B*45, B*46, B*47, B*48, B*49, B*50, B*52, B*53, B*55, B*56, B*58, B*73*). In addition, there are various low and high-percentage associations within the same *HLA-B* allelic groups. For example, low percentage associations occur with *B*07:05* (but not *B*07:02, B*07:04, B*07:06*), *B*14:02* (but not *B*14:01*), *B*27:02, B*27:05* (but not *B*27:07*), and *B*35:01* (but not *B*35:02, B*35:03, B*35:08*). While *R_SVA_26* has high percentage associations with *HLA-C*03:04* (93.7%) and *C*07:02* (82.8%), it has little or no association with *HLA-C*03:02* and *-C*07:01*, respectively.

In the MHC class II region, *R_SVA_27* (11.9%) is associated with *DRB1*15* and *DRB1*16* allelic groups at 100% each. Although *R_SVA_27* is not significant (*p>0.05*) in the PPMI cohort subgroup comparisons, *DRB1*15:01* and *DRB1*16:01* are significant at *p<0.05* in the combination-HC, and Podromal-HC comparisons, respectively. Supplementary Table 9 shows the number of SVA*_27/DRB1*15 or DRB1*16/DQA1* haplotypes in the PPMI cohort, including *DRB1*15:01/DQA1*01:02*, which is associated with protection from T1D (54) and susceptibility for multiple sclerosis (55). Of the 194 *DRB1*15:01/SVA_27* haplotypes in PPMI, 178 (91.8%) are linked to *DQA1*01:02/DQB1*06:02*. Of the 50 *DRB1*16/SVA_27* haplotypes, 39 (78%) are linked to *DQA1*01:02:02/DQB1*05:02:01*.

The high frequency *R_SVA_85* insertion (82.2%) is associated strongly with three *DPA1* allele groups at 99.9% or 100% and with at least 13 *DPB1* allelic groups at >96%. The relatively low frequency *NR_SVA_381* (19.8%) that is significantly more prevalent in PD than healthy controls (Table 6) is strongly associated with the *HLA-DPA1*02* and *–DPA1*04* allele lineages, and with at least 9 *HLA-DPB1* allele lineages (Table 7). Of these *HLA-DPB1* allele groups, *DPB1*01, DPB1*10*, and *DPB1*14* appear to imply a disease risk based on *p<0.05* and high *OR* values >1 (Tables 3–5).

The HLA alleles *DRB1*01, DRB1*04, DRB1*11, DRB1*15, DRB1*16, DQA1*01, DQA1*03, -DQB1*03, -DQB1*05, -DQB1*06* (Tables 3–5) and *NR_SVA_380* (Table 6) are significant (*p<0.05*) in the PPMI cohort subgroup comparisons. In this regard, on the basis of the phase-haplotype inferences, we constructed twelve

10.3389/fimmu.2024.1349030

TABLE 7 SVA insertions and HLA allele associations (>70%).

SVA	HLA allele	% Association	Allele Fraction
NR_SVA _377	A*11:01:01	93.2	68 of 73
(n, 108, 6.9%)	A*11:303	88.1	37 of 42
R_SVA_24	A*03:01:01	100	193 of 193
(n, 418, 26.5%)	A*11:01:01	98.6	72 of 73
	A*11:303	100	42 of 42
	A*30:01:01	100	61 of 61
R_SVA_25	C*07:02:01	88.2	134 of 152
(n, 135, 8.6%)	C*07:02:80	100	1 of 1
	B*07:02:01	91.5	107 of 117
	B*07:02:45	100	1 of 1
	B*38:02:01	100	1 of 1
	B*39:06:02	100	12 of 12
R_SVA_26	B*07:02:01	98.3	123 of 126
(n, 727, 46.2%)	B*13:02:01	100	38 of 38
	B*14:01:01	83.3	10 of 12
	B*18:01:01	95.8	69 of 72
	B*27:07:01	100	5 of 5
	B*35	89.6	95 of 106
	B*40	96.8	90 of 93
	B*51:01:01	87.8	72 of 82
	B*52:01:01	93.3	28 of 30
	B*57	100	47 of 47
	B*81	100	3 of 3
	C*03:04	93.7	74 of 79
	C*07:02	82.8	111 of 134
	C*12:02	100	29 of 29
	C*14	93.3	14 of 15
	C*15	86.6	58 of 67
	C*18	100	4 of 4
NR_SVA _380	DRB1*01:01:01	93.8	181 of 194
(n, 206/ 1576, 13.1%)	DRB1*10:01:01	100	20 of 20
R_SVA_27	DRB1*15	100	145 of 145
(n, 188/ 1576, 11.9%)	DRB1*16	100	43 of 43
	DQA1*01:01:01	0.7	1 of 135
	DQA1*01:02:01	58.9	113 of 192
	DQA1*01:02:02	95.5	42 of 44
	DQA1*01:02:04	100	2 of 2
	DQA1*01:03:01	24.4	29 of 119
	DQB1*05:01:24	100	1 of 1
	DQB1*05:02:01	86.5	45 of 52
	DQB1*05:03:01	1.7	1 of 58
	DQB1*06:01:01	73.7	28 of 38
	DQB1*06:01:03	100	2 of 2
	DQB1*06:02:01	75.7	103 of 136
	DQB1*06:03:01	5.2	7 of 135
R_SVA_85	DPA1*01	99.9	1262 of 1263
(n, 1303/ 1586, 82.2%)	DPA1*03	100	5 of 5
	DPA1*04	100	1 of 1
	DPB1*02	96.5	278 of 288
	DPB1*03	100	101 of 101
	DRB1*04	97	731 of 754
	DPB1*06	100	26 of 26
	DPB1*15	100	20 of 20
	DPB1*16	100	16 of 16
	DPB1*18	100	4 of 4
	DPB1*20	100	10 of 10
	DPB1*23	100	10 of 10
	DPB1*34	100	3 of 3
	DPB1*104	100	50 of 50
	DPB1*105	100	5 of 5
	DPB1*124	100	5 of 5
NR_SVA _381	DPA1*02:01:01	98.1	205 of 209
(n, 313/ 1586, 19.8%)	DPA1*02:01:02	100	33 of 33
	DPA1*02:01:04	100	3 of 3
	DPA1*02:01:08	100	4 of 4
	DPA1*02:02:02	97.5	39 of 40
	DPA1*02:06	80	8 of 10
	DPA1*02:07:01	100	15 of 15
	DPA1*02:12:01	100	1 of 1
	DPA1*02:26:01	100	2 of 2
	DPA1*04:01:01	100	1 of 1
	DPA1*01:58	100	2 of 2
	DPB1*01	100	55 of 55
	DPB1*05	94.7	36 of 38

(Continued)

(Continued)

10.3389/fimmu.2024.1349030

TABLE 7 Continued

SVA	HLA allele	% Association	Allele Fraction
	DPB1*09	100	8 of 8
	DPB1*10	100	27 of 27
	DPB1*11	100	13 of 13
	DPB1*13	85.1	40 of 47
	DPB1*14	95.8	23 of 24
	DPB1*17	97.7	43 of 44
	DPB1*19	100	9 of 9

haplotypes of *NR_SVA_380*, and *HLA-DRB1, -DQA1* and *-DQB1* alleles to estimate their frequency and overall pattern of distribution (Table 8). There are 206 *NR_SVA_380* insertions associated with 395 *DRB1/DQA1/DQB1* haplotypes at 52.2%.

Because *HLA-DPA1*and *-DPB1* (Tables 3–5) and *R_SVA_85* and *NR_SVA_381* (Table 6) are significant in the PPMI cohort subgroup comparisons, we constructed fifty-five phased haplotypes of the *R_SVA_85, SVA_381* genotypes, and *HLA-DPA1* and *HLA-DPB1* allele lineages to estimate their frequency and overall distribution (Supplementary Table 10). Figure 3 shows that thirty-eight (1.6%) of the 2330 haplotypes have both SVA insertions (PP); 1893 (81.3%) have the R_SVA_85 insertion, but not NR_SVA_381 (PA); 396 (17%) have the NR_SVA_381 insertion, but not the R_SVA_85 (AP); and three (0.1%) have no R_SVA_85 and no NR_SVA_381 (AA). Supplementary Table 10 reveals that the three most frequent of the *R_SVA_85* insertion/DP haplotypes are *R_SVA_85/DPA1*01/DPB1*04* (50.3%), *R_SVA_85/DPA1*01/DPB1*02* (15.9%), and *R_SVA_85/DPA1*01/DPB1*03* (5.9%). The most frequent *NR_SVA_381* insertion/DP haplotype is *NR_SVA_381/DPA1*02/DPB1*01* (3.7%).

TABLE 8 Frequencies of twelve 3-loci HLA-DRB1/DQA1/DQB1 haplotypes with NR_SVA _380 insertions.

1	SVA_380/DRB1*01:01:01/ DQA1*01:01:01/DQB1*05:01:01	93.6%	117 of 125
2	SVA_380/DRB1*01:01:02/ DQA1*01:01:02/DQB1*05:01:01	94.8%	54 of 57
3	SVA_380/DRB1*10:01:01/ DQA1*01:05:01/DQB1*05:01:01	100%	19 of 19
4	SVA_380/DRB1*01:03:01/ DQA1*01:01:01/DQB1*05:01:01	80%	4 of 5
5	SVA_380/DRB1*01:03:01/ DQA1*05:05:01/DQB1*03:01:01	75%	3 of 4
6	SVA_380/DRB1*08:01:01/ DQA1*04:01:01/DQB1*04:02:01	10%	3 of 30
7	SVA_380/DRB1*10:01:01/ DQA1*01:05:01/DQB1*06:03:01	100%	1 of 1
8	SVA_380/DRB1*01:01:01/ DQA1*01:01:01/DQB1*05:23:01	100%	1 of 1
9	SVA_380/DRB1*01:01:01/ DQA1*01:01:04/DQB1*05:01:01	100%	1 of 1
10	SVA_380/DRB1*01:01:01/ DQA1*01:02:01/DQB1*05:04	100%	1 of 1
11	SVA_380/DRB1*08:01:01/ DQA1*04:02/DQB1*04:02:01	12.50%	1 of 8
12	SVA_380/DRB1*07:01:01/ DQA1*02:01:01/DQB1*02:02:01	0.7%	1 of 143

Total: 206 SVA_380 insertions associated with 395 DRB1/DQA1/DQB1 haplotypes at 52.2%

3.5 Modulation of *HLA-DPA1* and *-DPB1* by two MHC SVA RIPs in the PPMI cohort

Figure 4 shows box plots of the possible effects of *R_SVA_85* and *NR_SVA_381* on the expression of *HLA-DPA1* and *-DPB1* transcription. Homozygous *R_SVA_85* insertion (*PP*) significantly increases ($p=0.023$) the transcription of *HLA-DPB1*, but has no significant effect ($p=0.35$) on the transcription of *HLA-DPA1*. The absence of *R_SVA_85* appears to be a risk factor for the Prodrome cohort (Table 6). In contrast, homologous *NR_SVA_381* insertion (*PP*) (Table 6) significantly decreases the transcription levels of *HLA-DPA1* ($p=0.037$) and *HLA-DPB1* ($p=0.001$) in the PPMI cohort, and its presence as a homozygous genotype (*PP*) is a risk factor ($Pc=0.012$) for PD (Table 6A; Figure 4).

4 Discussion

The regulatory effects of eight transcribed SVA RIPs on the differential co-expression of 71 genes within the MHC genomic region including all the classical class I and class II genes of a PPMI cohort were previously identified by eQTL statistical analysis (41, 43, 44). In this study, the same PPMI RNAseq database was reused to genotype the transcripts encoded by classical class I and class II HLA genes in order to determine their frequency and estimate their haplotypic associations with each other and with the eight regulatory MHC SVAs. The *arcasHLA* software tool (50) was used to impute the genotypes of the transcripts expressed by the class I and class II HLA genes to at least the three-field resolution that included the ancestral allele group, the protein type and the synonymous changes in the coding regions. In a recent comparison of the seven best of 22 genotyping computation tools, *arcasHLA* was the fastest and among the top three most accurate (99.1% for MHC-I and 98.1% for MHC-II) for genotyping Caucasian American RNA data (56). The PPMI cohort HLA allele frequency and haplotype data confirmed that our cohort was mostly (>95%) Caucasian American or Caucasian European as expected (33, 48). Consequently, we have accepted the high accuracy and reliability of the *arcasHLA* imputations without resorting to the use of other genotyping tools.

Significant differences were detected at $p<0.05$ by the Fisher's exact test for 21 HLA class I alleles and 36 HLA class II alleles transcribed by 10 HLA genes that were different up to the three-field resolution within four subgroups (PD, Prodrome, SWEDD and HC) of the PPMI cohort when not corrected by multiple testing

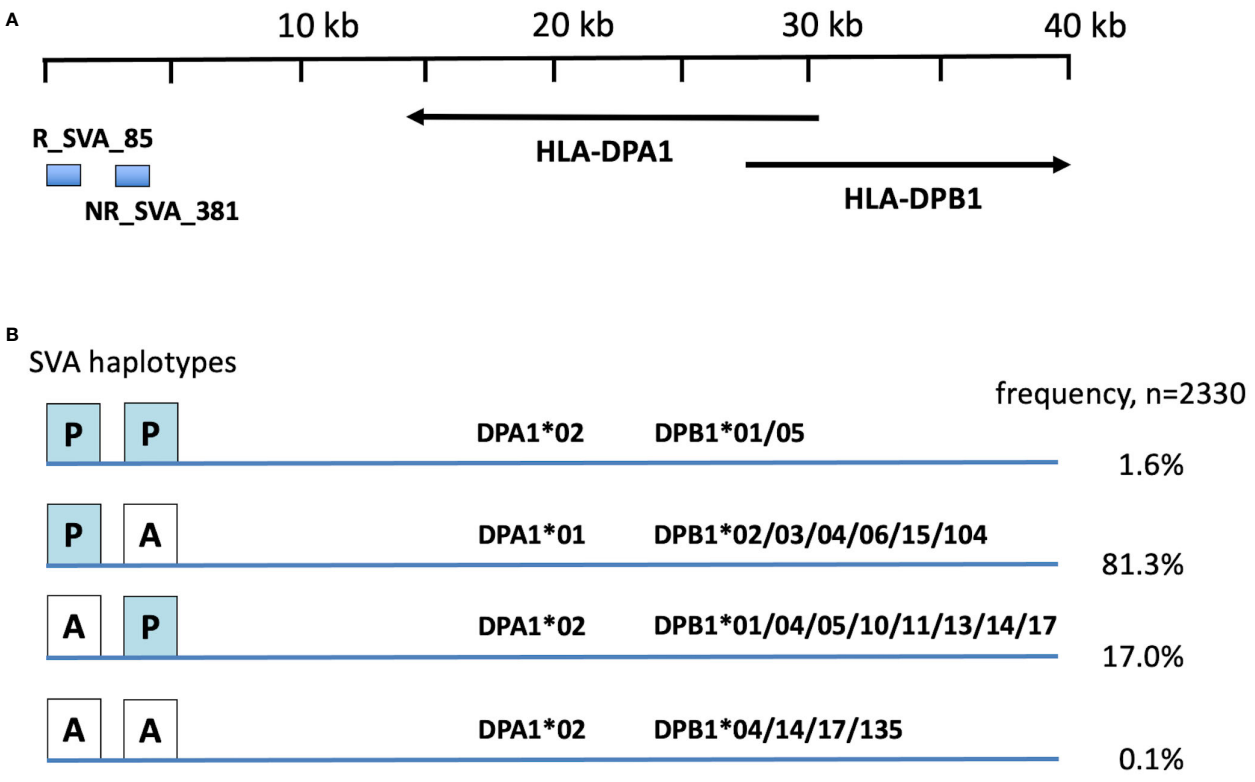

FIGURE 3
Frequency of R_SVA_85, SVA_381, DPA1, DPB1 haplotypes in PPMI cohort based on phased haplotypes in Supplementary Table 7. **(A)** relative position of SVA RIPs and HLA-DP genes at the centromeric end of the MHC class II gene cluster (Figure 1). Horizontal arrows show the 5′ prime to 3′ direction of the DPA1 and DPB1 gene coding. **(B)** Four main R_SVA_85, SVA_381 phased haplotype structures, PP, PA, AP and AA, of the 2330 haplotypes listing their percentage frequency association with the DPA1 and DPB1 haplotype allelic lineages.

(Tables 3–5). Only five alleles, all from the HLA class II region, were significant after the Bonferroni correction; the expressed protective alleles *HLA-DRA*01:01:01* and *-DQA1*03:01:01* within PD, the risk allele *HLA-DQA1*03:03:01* within the Prodrome cohort and the *HLA-DRA*01:01:02* and *-DRB4*01:03:02* risk alleles in the SWEDD group. Although *HLA-DQA1*03:01:01* differs from *-DQA1*03:03:01* by a single nucleotide substitution in exon 3 at codon 160 (c548.C<A), the OR calculations showed that the former was a protective allele and the later a risk allele. *HLA-DQA1*03:01:01* was more prevalent at 10.2% than *-DQA1*03:03* at 5.7% in the PPMI cohort (Supplementary Table 2). The 52 alleles that did not survive the Bonferroni statistical challenge, but had significant differences $p<0.05$ between the different cases and controls by the Fisher exact test were placed within a statistically marginal zone of 'possible' rather than 'strong' or 'definite' risk or protective effects. This lower level of statistical significance might have been confounded by various factors such as lack of statistical power due to insufficient sample numbers, unreliable disease and aetiological factors, or various comorbidities and other issues not accounted for in our analysis. However, many of the 57 possible protective or susceptibility HLA alleles ($p<0.05$ or $Pc<0.1$) were reported previously by others to be statistically significant in PD and various autoimmune disease studies. For example, we confirmed the results of previous studies that *HLA-DRA*01, -DRB4*01:03, -DRB5*01, -DQB1*05* and *-C*07:01:01* are predisposing alleles and that *HLA-DRB1*04:04, -DQA1*03:01, -DQA1*03:02*, and *-DQB1*03:02*, are protective in PD (34–37, 57). The *HLA-A*31:01:02*, and *-B*40:02:01* possible risk alleles in our PD cohort were not reported previously, although they were associated with the development of acquired aplastic anemia (58). Also, we found that the *HLA-DRB1*11:02:01* was a minor possible risk allele in the PD, Prodrome and combined cohorts, but not in the SWEDD cohort. This might be the first report to associate *HLA-DRB1*11:02:01* as a possible risk allele in PD, although it has been associated with systemic juvenile idiopathic arthritis (59), Graves' disease (60) and MS (57).

In our study, there was an overall greater number of possible protective alleles than risk alleles at a ratio of 12 to 8 (60%) in the PD group compared to healthy controls, whereas the Prodrome and SWEDD comparisons with HC had more possible risk alleles than protective alleles at ratios of 18 to 2 (90%), and 18 to 5 (78%), respectively. This greater ratio of HLA risk to protective alleles in Prodrome and SWEDD compared to HC might in part explain the gradual or variable progression to PD. Idiopathic, spasmodic and prodromal PD groups have a mixed population of different HLA haplotypes and HLA alleles that carry and present various peptides and antigens to T lymphocytes, which in turn are activated to regulate a diversity of immune responses including inappropriate and harmful autoimmune responses that can cause extensive tissue damage. In this study, we could not discern easily, which are the

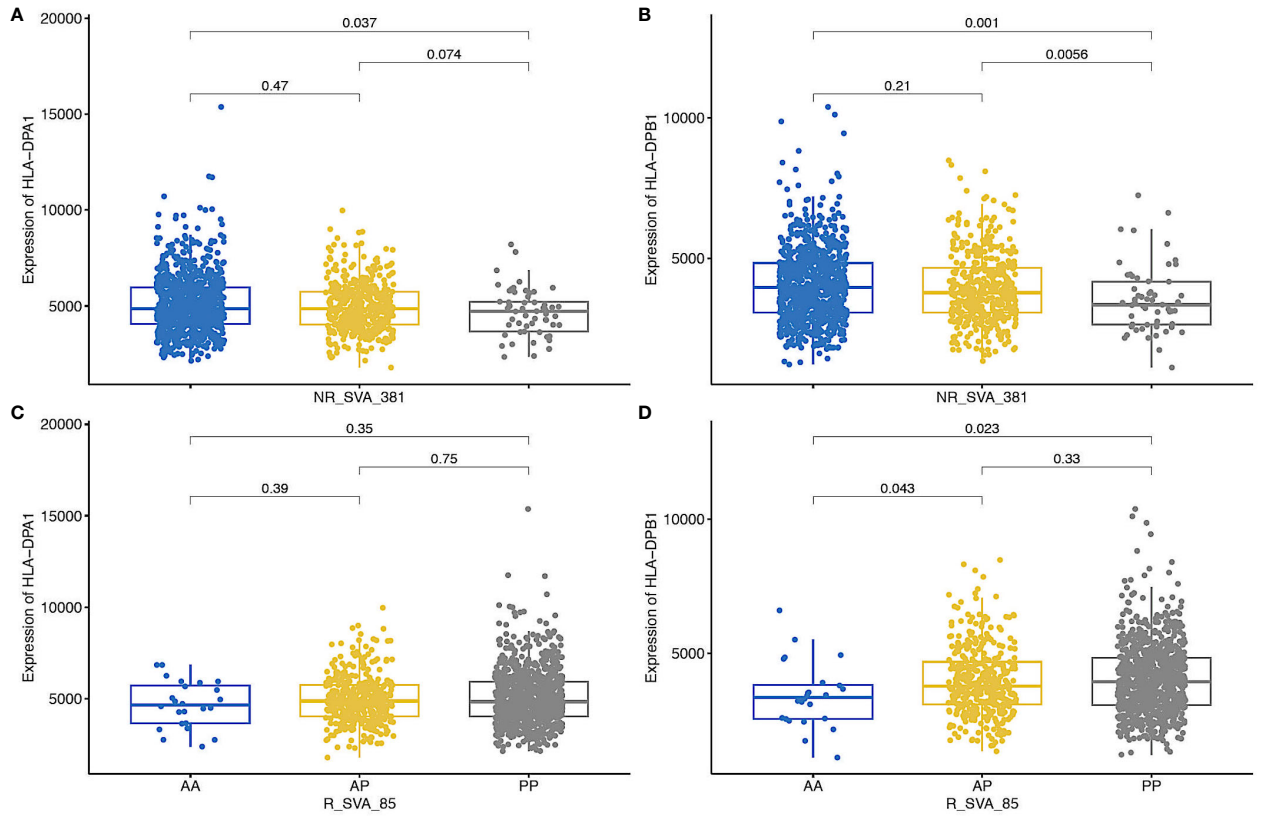

FIGURE 4
Box plots of regulation of the expression of HLA-DPA1 and HLA-DPB1 transcripts by NR_SVA_381 genotypes [**(A, B)**, respectively], and HLA-DPA1 and HLA-DPB1 transcripts by NR_SVA_85 genotypes (**C, D**, respectively) in PPMI cohort. The genotypes are absent-absent (AA), absent-present (AP), and present-present (PP). The number of genotypes (n) for NR_SVA_381 in each **(A, B)** are 805 for AA, 404 for AP, and 57 for PP in 1266 individuals. The number of genotypes for R_SVA_85 in each **(C, D)** are 24 for AA, 371 for AP and 826 for PP for 1221 individuals, data were not available for 45 individuals. The statistical p-values are shown above the box plots on horizontal lines between the genotypes.

possible high risk HLA haplotypes that lead to a faster rate of disease onset, and which are protective or low risk HLA alleles that slow down the disease rate. Wissemann et al. (35) on the basis of their study suggested that the 7.1 ancestral haplotype (AH) that consists of the linked HLA alleles *B*07:02/C*07:02/DRB5*01/DRB1*15:01/DQA1*01:02/DQB1*06:02* is a PD high risk haplotype and that the *C*03:04, DRB1*04:04* and *DQA1*03:01* alleles are part of low-risk haplotypes. We found that five of the alleles in the possible high risk 7.1AH were present in the SWEDD-HC comparison, but not in the PD-HC or Prodrome-HC comparisons. *DRB1*15:01* was a possible risk allele only in the Combination (all subgroups)-HC comparison. Also, these high-risk alleles were present in the SWEDD group at a frequency of between 14.2% and 18.3% relative to a frequency between 7% and 10.7% in the HC group. The low-risk alleles *DRB1*04:04* and *DQA1*03:01* were distributed as protective alleles in our PD-HC comparison. In contrast, *C*03:04* was a risk allele in the Prodrome-HC, and the SWEDD-HC comparisons. Furthermore, none of the HLA alleles of the frequent Caucasian 8.1AH haplotype: *HLA-A*0101/C*0701/B*0801/DRB1*0301/DQA1*0501/DQB1*0201*, except for *C*0701*, were significant in our study groups.

The statistical results for the *HLA-DRB1*04* alleles in previous studies of PD suggested both susceptibility (36) and protective associations (34, 35, 37–39). Our results revealed that the *HLA-DRB1*04* alleles were significant statistically at the 'possible' level (uncorrected Fisher's exact test, $p<0.05$) with *HLA-DRB1*04:02* and *-DRB1*04:04* protective in PD and PPMI (Table 3), whereas HLA-*DRB1*04:01* was a possible risk allele in the Prodrome and SWEDD groups, and the PPMI cohort (Table 5). This difference between the PD, Prodrome, and SWEDD groups might reflect that neither the Prodrome, nor SWEDD groups were an established PD with as yet degenerated dopaminergic neurons and large aggregates of alpha-synuclein or tau proteins (48). A recent study by Mignon et al. (61), reported in a preprint, suggested that HLA-DRB1*04 alleles strongly bound to an epitope sequence of tau in neurofibrillary tangles and mediated an adaptive immune response against tau to decrease PD risk. This protective effect of the HLA-DRB1*04 antigen was intermediary with HLA-DRB1*04:01 and HLA-DRB1*04:03, and absent for HLA-DRB1*04:05 (61), which might explain in part the differentiated statistical results that we obtained for the *HLA-DRB1*04* alleles in the PPMI cohort (Tables 3–5). In contrast, HLA-DRB1*04:01 might transport alpha-synuclein to the cell surface of T-cells (62) to become a risk factor for individuals in the Prodrome and SWEDD groups (Table 5). According to Hollenbach et al. (38), *HLA-DRB1*04:01* is part of the protective Caucasian haplotype *DRB1*04:01/DQA1*03:01/DQB1*03:02* and

that, along with *DRB1*01:01*, has the 'shared epitope' (SE) with the amino acid motif Q/RK/RRAA at positions 70–74 in combination with valine at position 11 (11-V) that are highly protective in PD. In our study, *HLA-DRB1*01:02* was a possible protective allele within the combined cohort-healthy controls comparison.

Four possible HLA risk alleles, *HLA-DRB5*01:01, -DRB1*04:01, -DRB1*15:01*, and *-DQB1*03:01*, are of particular interest because they have been associated with alpha-synuclein specific T cell reactivity in patients with PD (23–25). In this regard, Ozono et al. (62) showed experimentally that HLA class II molecules with the DRB5*01:01 allele captured and transported conformationally abnormal alpha-synuclein extracellularly, whereas HLA-DRB1*04:01 transported normal alpha-synuclein to the cell surface to present to circulating CD4-positive T cells, but did not translocate structurally abnormal alpha-synuclein. Moreover, alpha-synuclein32-46 peptide immunisation of mice that expressed *HLA-DRB1*15:01* triggered intestinal inflammation, enteric neurodegeneration, constipation, and weight loss (22), suggesting a critical role for alpha-synuclein autoimmunity in *HLA-DRB1*15:01* carriers in the combined PPMI cohort (Supplementary Table 4). The findings by Garretti et al. (22) are consistent with the hypothesis that alpha-synuclein-mediated pathology can originate in the enteric neural system and proceed into the brain via the vagus nerve (12, 52). In this context, Braak's hypothesis (12) connects the onset of PD to the alleles *HLA-DRB1*15:01, -DRB1*04:02:01, -DQA1*03*, and *-DQB1*03:02:01* that are associated with Crohn's disease, colitis or celiac disease (63–65), and that we found were significant ($p<0.05$) in the PPMI cohort (Tables 3–5; Supplementary Table 4). The question remains whether the CD4+ T lymphocytes that recognise and interact with the presented HLA class II bound alpha-synuclein antigens might in turn trigger cytotoxic CD8+ T lymphocytes and antibody producing B-lymphocytes to attack and destroy neurons that display HLA-bound alpha-synuclein antigen at the cell surface in the peripheral and central nervous systems. A dysfunctional blood brain barrier in PD patients can lead to increased levels of alpha-synuclein, autoantibodies against alpha-synuclein, and infiltrating T cells in the CSF and plasma (66). Consequently, more information is required about what subgroups of autoreactive T and B lymphocytes and other self-antigens beside alpha-synuclein might be generated by the adaptive immune system in PD pathogenesis.

Eight SVA eQTLs expressed within the MHC region were inferred to differentially modulate the transcription levels of classical class I and class II HLA genes within the PPMI cohort (43, 44). In the present study, four of the eight regulatory SVA-RIPs, *R_SVA_25, NR_SVA_380, R_SVA_85* and *NR_SVA_381*, are significant ($p<0.05$) by the Fisher's exact test within the different PPMI subgroups, but only the *SVA_381 PP* genotype is significant ($Pc<0.1$) after Bonferroni corrections for multiple testing (Table 6). *SVA_381 PP* is a significant ($p<0.05$) risk in the PD-HC, Prodrome-HC and combination-HC comparisons, but not significant ($p>0.05$) in the SWEDD-HC comparison. This result might be related to the observation that the homologous *NR_SVA_381* insertion (*PP*) is associated significantly with a decrease in the transcription levels of *HLA-DPA1* ($p=0.037$) and *HLA-DPB1* ($p=0.001$) in the PPMI cohort (Figure 4). The suppressed transcription rate might result in a reduced level of HLA-DPA1 and -DPB1 antigen presentation to the circulating CD4+ helper cells. Previously, *NR_SVA_381* was inferred to modulate only the allelic expression of the *HLA-DPA1, -DPB1* and *-B* genes, whereas *R_SVA_85* only modulates the *HLA-DPA1* and *-DPB1* genes (44). Thus, *R_SVA_85* and *NR_SVA_381* might have opposing regulatory effects on the *HLA-DPA1*, and *-DPB1* gene expression that together could have a small, but significant effect in some PD and Prodrome cases (Figures 3, 4).

The total absence of *R_SVA_85* (genotype *AA*) is a minor risk factor for the Prodrome cohort (Table 6), which suggests that its presence (genotype *PP*) might be protective. A possible protective role is supported by its presence in four significant protective haplotypes (Figure 2). Although *R_SVA_85* significantly increased ($p=0.023$) the transcription of *HLA-DPB1*, its presence (*PP*) had no significant statistical effect ($p>0.05$) on the levels of *HLA-DPA1* transcription (Figure 4). Therefore, the protective effect of the presence of *R_SVA_85* in PD or in the Prodrome cohort might be diluted out in a statistical analysis because of its overall high frequency (82.9%) in the PPMI cohort and strong association with many different *HLA-DPA1* alleles (Table 7; Figure 3). Although the *R_SVA_85* and *NR_SVA_381* loci are separated from each other by 1.7 kb in an intergenic region between the *HLA-DOA* and *HLA-DPA1* genes (Figure 1), they are together only at a low frequency of 1.6% (Figure 3). The effects of *R_SVA_85* and *NR_SVA_381* on the gene expression of *HLA-DPA1* and *-DPB1* genes (Figure 4), either separately or together, is of interest also for unrelated hematopoietic cell transplantation because the level of expression of HLA-DP in the recipient is an important prognostic indicator of donor-anti-host recognition and for evaluating the risk of graft-versus-host disease (67, 68).

Of the two other SVA-RIPs that had minor significance ($p<0.05$), *R_SVA_25* modulates the transcription of all the HLA class I genes and *HLA-DRB5, -DRB1 and -DQB1*, whereas *NR_SVA_380* modulates the transcription of the *HLA-C, HLA-DRB1* and the two *HLA-DQ* genes (44). *R_SVA_25* is inserted 23.4 kb telomeric of *HLA-C*, occurs at low frequency (8.6%), but upregulates the expression of 88.2% of the *C*07:02:01* risk alleles and 92% of the *B*07:02:01* risk alleles (Table 7) in the SWEDD-HC comparison (Table 4). *SVA_380 AA* is a minor risk genotype in the SWEDD-HC comparison, while *SVA_380 PA* is protective in the PD-HC comparison as well as in the SWEDD-HC comparison (Table 6). *NR_SVA_380*, inserted between *DRB5* and *DRB6*, up-regulates 93.8% of *DRB1*01:01:01* and 100% of *DRB1*10:01:01* neutral alleles (Table 7).

Our previous study was unable to discern whether *SVA_24, SVA_380* or *SVA_27* modulated the expression of *HLA-DQA1* protective or risk alleles (44). The present study revealed that of the 110 *HLA-DQA1*03:03:01* risk alleles in the PPMI cohort, 31 (28.2%) were associated with *SVA_24*, none with *SVA_380*, and none with *SVA_27*. Similarly, of 147 *DQA1*03:01:01* protective alleles, 35 (23.7%) were associated with *SVA_24*, none with *SVA_380*, and none with *SVA_27*. Although *SVA_24* is located near *HLA-A* within the alpha block of the MHC class I region and located 2.7 Mb from the *HLA-DQA1* locus, it appears to regulate the expression levels of the two most statistically significant ($Pc<0.1$) HLA class II alleles, *HLA-DQA1*03:01:01* and *-DQA1*03:03:01*, detected in our study (Tables 3, 5, respectively). If this is the case, then the statistical significance of *SVA_24* transcription and

regulation of HLA alleles in PD was not detected probably because it is associated more strongly with transcription modulation of the *HLA-A3, -A11* and *-A30* neutral alleles (Table 7). None of the other transcribed SVA RIPs were associated with the significant *HLA-DQA1*03* alleles.

SVAs have been inserted and translocated at different times of human evolutionary history (69). Consequently, the MHC SVA are associated more strongly with some HLA allele groups than others and could be used as evolutionary and disease markers (45). For example, *R_SVA_27*, although present in 11.9% of the PPMI cohort, is associated with all of the *HLA-DRB1*15* and *-DRB1*16* alleles, but with none of the other 11 *HLA-DRB1* allelic lineages (Table 7). We hypothesize that *R_SVA_27* was inserted originally into the MHC class II region in a location between *HLA-DRB1* and *HLA-DQA1* in an ancestor with either *HLA-DRB1*15* or *-DRB1*16* or a heterozygote individual who had both alleles. *R_SVA_27* is associated strongly also with some of the *HLA-DQB1*05* or *-DQB1*06* lineage alleles (Table 7). Therefore, *R_SVA_27* is an unique autoimmune disease marker because its linkage to the *DRB1*15:01/DQA1*01:02/DQB1*06:02* haplotype has been associated with multiple sclerosis (38, 70–72), and the *R_SVA_27/DRB1*16/DQB*05* haplotype was associated with other autoimmune diseases (73, 74). In the PPMI cohort, *R_SVA_27* is associated strongly with *HLA-DQA1*01:02* (96%), but weakly or not at all with the other *-DQA1*01* field-three alleles such as *HLA-DQA1*01:01:01* (0.7%), *-DQA1*01:02:01* (58.9%), or *-DQA1*01:03:01* (24.4%). These lower percentage associations suggest that *HLA-DQA1*01:01:01* was already fully established in the population before *R_SVA_27* was inserted, and that *HLA-DQA1*01:02:02* emerged probably at a time proximate to the *R_SVA_27* insertion event.

This study confirms and extends our previous reports that transcribed SVA elements inserted within the MHC genomic region can modulate certain HLA genes at the transcription level (41, 43, 44), and therefore, might regulate the expression of particular HLA risk and protective alleles, which in turn influence the onset and progression of PD via the immune response. For example, the upregulated or downregulated HLA transcription levels modulated by SVA transcripts could change the levels of foreign or autoreactive self-peptide presentation to CD4+ T helper lymphocytes or cytotoxic CD8+ T lymphocytes and influence the onset, development or progression of PD. In this regard, the SVA and HLA PD risk variants are likely additive causes with a complicated polygenic structure. Stronger statistical and molecular significance might be found in future studies with better stratification and compartmentalisation of the PD co-morbidities associated with autoimmune diseases and other age-related neurological diseases. The coordination of the adaptive and innate immunity by the HLA system in PD is highly complex and still poorly understood (3, 8, 66). The infiltration of peripheral CD4+ and CD8+ lymphocytes and monocytes into the brain across a dysfunctional blood brain barrier however suggests that the adaptive immune system contributes to neurodegeneration at different stages of PD pathogenesis (10, 14, 26, 66). While we limited our analysis to eight SVA within the MHC genomic region, it is noteworthy that there are many SVAs in other genomic regions that are strongly linked to PD (42, 43), including the SVA insertion within the *TAF1* gene that is associated with X-linked dystonia parkinsonism (75).

In conclusion, our study of the expressed *SVA* and *HLA* genes in circulating white blood cells confirms that the MHC genomic region has an important role in the coordinated regulation of immune responses possibly associated with the long-term onset and progression of PD, the mechanisms of which yet have to be elucidated. MHC SVA RIPs, by down or up regulating the antigen presenting HLA alleles at the proteomic level, might change the amount of risk or protective antigens presented to the CD4+ or CD8+T helper lymphocytes. Thus, co-expression of regulatory SVA RIPs and HLA class I and class II alleles adds another layer of biomolecular complication to the understanding of immune responses associated with PD.

Data availability statement

The original contributions presented in the study are included in the article/Supplementary Material. Further inquiries can be directed to the corresponding author.

Ethics statement

The studies involving humans were approved by University of Western Australia Human research ethics office. The studies were conducted in accordance with the local legislation and institutional requirements. The participants provided their written informed consent to participate in this study.

Author contributions

JK: Writing – original draft, Methodology, Writing – review & editing, Formal analysis, Conceptualization. SS: Writing – review & editing, Methodology. TS: Writing – review & editing. AP: Data curation, Writing – review & editing. SK: Project administration, Formal analysis, Conceptualization, Writing – review & editing.

Funding

The author(s) declare financial support was received for the research, authorship, and/or publication of this article. AP and SK are funded by MSWA and Perron Institute for Neurological and Translational 562 Science. The funding bodies played no role in the design of the study, the analysis and interpretation of the data, and the writing of the manuscript.

Acknowledgments

This work was supported by resources provided by the Pawsey Supercomputing Centre with funding from the Australian

Government and the Government of Western Australia. Data used in the preparation of this article was obtained from the Parkinson's Progression Markers Initiative (PPMI) database [www.ppmi-info.org/data (accessed on 19 January 2021)]. For up-to-date information on the study, visit www.ppmi-info.org. PPMI is sponsored and partially funded by The Michael J. Fox Foundation for Parkinson's Research.

Conflict of interest

The authors declare that the research was conducted in the absence of any commercial or financial relationships that could be construed as a potential conflict of interest.

Publisher's note

Supplementary material

The Supplementary Material for this article can be found online at: https://www.frontiersin.org/articles/10.3389/fimmu.2024.1349030/full#supplementary-material

References

1. Ou Z, Pan J, Tang S, Duan D, Yu D, Nong H, et al. Global trends in the incidence, prevalence, and years lived with disability of parkinson's disease in 204 countries/territories from 1990 to 2019. *Front Public Health*. (2021) 9:776847. doi: 10.3389/fpubh.2021.776847

2. Shulman JM, De Jager PL, Feany MB. Parkinson's disease: genetics and pathogenesis. *Annu Rev Pathol Mech Dis*. (2011) 6:193–222. doi: 10.1146/annurev-pathol-011110-130242

3. Kouli A, Williams-Gray CH. Age-related adaptive immune changes in parkinson's disease. *J Parkinson's Dis*. (2022) 12:S93–S104. doi: 10.3233/JPD-223228

4. Zhang X, Gao F, Wang D, Li C, Fu Y, He W, et al. Tau pathology in parkinson's disease. *Front Neurol*. (2018) 9:809. doi: 10.3389/fneur.2018.00809

5. Pan L, Meng L, He M, Zhang Z. Tau in the pathophysiology of parkinson's disease. *J Mol Neurosci*. (2021) 71:2179–91. doi: 10.1007/s12031-020-01776-5

6. Demaagd G, Philip A. Parkinson's disease and its management. Part 1: Disease entity, risk factors, pathophysiology, clinical presentation, and diagnosis. *PT*. (2015) 40:504–10. doi: 10.1136/gut.45.3.395

7. Greenland JC, Barker RA. *The differential diagnosis of parkinson's disease. In: Parkinson's disease: pathogenesis and clinical aspects*. Stoker TB, Greenland JC (Editors) (2018). Brisbane, Australia: Codon Publications. doi: 10.15586/codonpublications.parkinsonsdisease.2018.ch6

8. Kannarkat GT, Boss JM, Tansey MG. The role of innate and adaptive immunity in parkinson's disease. *J Parkinson's Dis*. (2013) 3:493–514. doi: 10.3233/JPD-130250

9. Pang SY-Y, Ho PW-L, Liu H-F, Leung C-T, Li L, Chang EES, et al. The interplay of aging, genetics and environmental factors in the pathogenesis of Parkinson's disease. *Transl Neurodegener*. (2019) 8:23. doi: 10.1186/s40035-019-0165-9

10. Tan E-K, Chao Y-X, West A, Chan L-L, Poewe W, Jankovic J. Parkinson disease and the immune system — associations, mechanisms and therapeutics. *Nat Rev Neurol*. (2020) 16:303–18. doi: 10.1038/s41582-020-0344-4

11. Weiss F, Labrador-Garrido A, Dzamko N, Halliday G. Immune responses in the Parkinson's disease brain. *Neurobiol Dis*. (2022) 168:105700. doi: 10.1016/j.nbd.2022.105700

12. Braak H, Rub U, Gai WP, Del Tredici K. Idiopathic Parkinson's disease: possible routes by which vulnerable neuronal types may be subject to neuroinvasion by an unknown pathogen. *J Neural Transm*. (2003) 110:517–36. doi: 10.1007/s00702-002-0808-2

13. Rietdijk CD, Perez-Pardo P, Garssen J, Van Wezel RJA, Kraneveld AD. Exploring braak's hypothesis of parkinson's disease. *Front Neurol*. (2017) 8:37. doi: 10.3389/fneur.2017.00037

14. Tansey MG, Wallings RL, Houser MC, Herrick MK, Keating CE, Joers V. Inflammation and immune dysfunction in Parkinson disease. *Nat Rev Immunol*. (2022) 22:657–73. doi: 10.1038/s41577-022-00684-6

15. Hobson BD, Sulzer D. Neuronal presentation of antigen and its possible role in parkinson's disease. *J Parkinson's Dis*. (2022) 12:S137–47. doi: 10.3233/JPD-223153

16. Ren L, Yi J, Yang J, Li P, Cheng X, Mao P. Nonsteroidal anti-inflammatory drugs use and risk of Parkinson disease: A dose–response meta-analysis. *Medicine*. (2018) 97:e12172. doi: 10.1097/MD.0000000000012172

17. McGeer PL, McGeer EG. Glial reactions in Parkinson's disease. *Mov Disord*. (2008) 23:474–83. doi: 10.1002/mds.21751

18. Zhang M, Li C, Ren J, Wang H, Yi F, Wu J, et al. The double-faceted role of leucine-rich repeat kinase 2 in the immunopathogenesis of parkinson's disease. *Front Aging Neurosci*. (2022) 14:909303. doi: 10.3389/fnagi.2022.909303

19. Herrick MK, Tansey MG. Is LRRK2 the missing link between inflammatory bowel disease and Parkinson's disease? *NPJ Parkinsons Dis*. (2021) 7:26. doi: 10.1038/s41531-021-00170-1

20. Li M, Wan J, Xu Z, Tang B. The association between Parkinson's disease and autoimmune diseases: A systematic review and meta-analysis. *Front Immunol*. (2023) 14:1103053. doi: 10.3389/fimmu.2023.1103053

21. Russo I, Bubacco L, Greggio E. LRRK2 as a target for modulating immune system responses. *Neurobiol Dis*. (2022) 169:105724. doi: 10.1016/j.nbd.2022.105724

22. Garretti F, Monahan C, Sloan N, Bergen J, Shahriar S, Kim SW, et al. Interaction of an α-synuclein epitope with HLA-DRB1∗15:01 triggers enteric features in mice reminiscent of prodromal Parkinson's disease. *Neuron*. (2023), 111(21):3397–413.e5. doi: 10.1016/j.neuron.2023.07.015

23. Sulzer D, Alcalay RN, Garretti F, Cote L, Kanter E, Agin-Liebes J, et al. T cells from patients with Parkinson's disease recognize α-synuclein peptides. *Nature*. (2017) 546:656–61. doi: 10.1038/nature22815

24. Lindestam Arlehamn CS, Dhanwani R, Pham J, Kuan R, Frazier A, Rezende Dutra J, et al. α-Synuclein-specific T cell reactivity is associated with preclinical and early Parkinson's disease. *Nat Commun*. (2020) 11:1875. doi: 10.1038/s41467-020-15626-w

25. Singhania A, Pham J, Dhanwani R, Frazier A, Rezende Dutra J, Marder KS, et al. The TCR repertoire of α-synuclein-specific T cells in Parkinson's disease is surprisingly diverse. *Sci Rep*. (2021) 11:302. doi: 10.1038/s41598-020-79726-9

26. Brochard V, Combadière B, Prigent A, Laouar Y, Perrin A, Beray-Berthat V, et al. Infiltration of CD4+ lymphocytes into the brain contributes to neurodegeneration in a mouse model of Parkinson disease. *J Clin Invest*. (2008), 119:182–92. doi: 10.1172/JCI36470

27. Hamza TH, Zabetian CP, Tenesa A, Laederach A, Montimurro J, Yearout D, et al. Common genetic variation in the HLA region is associated with late-onset sporadic Parkinson's disease. *Nat Genet*. (2010) 42:781–5. doi: 10.1038/ng.642

28. Bandres-Ciga S, Diez-Fairen M, Kim JJ, Singleton AB. Genetics of Parkinson's disease: An introspection of its journey towards precision medicine. *Neurobiol Dis*. (2020) 137:104782. doi: 10.1016/j.nbd.2020.104782

29. Kulski JK, Inoko H. Major Histocompatibility Complex (MHC) Genes. In: Cooper DN, editor. *Encyclopedia of the Human Genome*. (London, UK: Macmillan Publishers Ltd, Nature Publishing Group) (2003). p. 778–85. doi: 10.1038/npg.els.0005900

30. Chaplin DD. Overview of the immune response. *J Allergy Clin Immunol*. (2010) 125:S3–S23. doi: 10.1016/j.jaci.2009.12.980

31. Petersdorf EW. In celebration of Ruggero Ceppellini: HLA in transplantation. *HLA*. (2017) 89:71–6. doi: 10.1111/tan.12955

32. Shiina T, Hosomichi K, Inoko H, Kulski JK. The HLA genomic loci map: expression, interaction, diversity and disease. *J Hum Genet*. (2009) 54:15–39. doi: 10.1038/jhg.2008.5

33. Kulski JK, Suzuki S, Shiina T. Human leukocyte antigen super-locus: nexus of genomic supergenes, SNPs, indels, transcripts, and haplotypes. *Hum Genome Var*. (2022) 9:49. doi: 10.1038/s41439-022-00226-5

34. Yu E, Ambati A, Andersen MS, Krohn L, Estiar MA, Saini P, et al. Fine mapping of the HLA locus in Parkinson's disease in Europeans. *NPJ Parkinsons Dis*. (2021) 7:84. doi: 10.1038/s41531-021-00231-5

35. Wissemann WT, Hill-Burns EM, Zabetian CP, Factor SA, Patsopoulos N, Hoglund B, et al. Association of parkinson disease with structural and regulatory variants in the HLA region. *Am J Hum Genet*. (2013) 93:984–93. doi: 10.1016/j.ajhg.2013.10.009

36. Pandi S, Chinniah R, Sevak V, Ravi PM, Raju M, Vellaiappan NA, et al. Association of HLA–DRB1, DQA1 and DQB1 alleles and haplotype in Parkinson's disease from South India. *Neurosci Lett*. (2021) 765:136296. doi: 10.1016/j.neulet.2021.136296

37. Saiki M, Baker A, Williams-Gray CH, Foltynie T, Goodman RS, Taylor CJ, et al. Association of the human leucocyte antigen region with susceptibility to Parkinson's disease. *J Neurol Neurosurg Psychiatry*. (2010) 81:890–1. doi: 10.1136/jnnp.2008.162883

38. Hollenbach JA, Norman PJ, Creary LE, Damotte V, Montero-Martin G, Caillier S, et al. A specific amino acid motif of *HLA-DRB1* mediates risk and interacts with smoking history in Parkinson's disease. *Proc Natl Acad Sci USA*. (2019) 116:7419–24. doi: 10.1073/pnas.1821778116

39. Sun C, Wei L, Luo F, Li Y, Li J, Zhu F, et al. HLA-DRB1 alleles are associated with the susceptibility to sporadic parkinson's disease in chinese han population. *PloS One*. (2012) 7:e48594. doi: 10.1371/journal.pone.0048594

40. Farmen K, Nissen SK, Stokholm MG, Iranzo A, Østergaard K, Serradell M, et al. Monocyte markers correlate with immune and neuronal brain changes in REM sleep behavior disorder. *Proc Natl Acad Sci USA*. (2021) 118:e2020858118. doi: 10.1073/pnas.2020858118

41. Koks S, Pfaff AL, Bubb VJ, Quinn JP. Expression quantitative trait loci (eQTLs) associated with retrotransposons demonstrate their modulatory effect on the transcriptome. *Int J Mol Sci*. (2021) 22:6319. doi: 10.3390/ijms22126319

42. Savage AL, Bubb VJ, Quinn JP. What role do human specific retrotransposons play in mental health and behaviour? *Curr Trends Neurol*. (2013) 7:57–68.

43. Pfaff AL, Bubb VJ, Quinn JP, Koks S. Reference SVA insertion polymorphisms are associated with Parkinson's Disease progression and differential gene expression. *NPJ Parkinsons Dis*. (2021) 7:44. doi: 10.1038/s41531-021-00189-4

44. Kulski JK, Pfaff AL, Marney L, Frohlich A, Bubb VJ, Quinn J, et al. Regulation of expression quantitative trait loci by SVA retrotransposons within the major histocompatibility complex. *Exp Biol Med*. (2023) 248:2304–18. doi: 10.1177/15353702231209411

45. Kulski JK, Shigenari A, Inoko H. Polymorphic SVA retrotransposons at four loci and their association with classical HLA class I alleles in Japanese, Caucasians and African Americans. *Immunogenetics*. (2010) 62:211–30. doi: 10.1007/s00251-010-0427-2

46. Kulski JK, Suzuki S, Shiina T. Haplotype shuffling and dimorphic transposable elements in the human extended major histocompatibility complex class II region. *Front Genet*. (2021) 12:665899. doi: 10.3389/fgene.2021.665899

47. Kulski JK, Suzuki S, Shiina T. SNP-density crossover maps of polymorphic transposable elements and HLA genes within MHC class I haplotype blocks and junction. *Front Genet*. (2021) 11:594318. doi: 10.3389/fgene.2020.594318

48. Marek K, Chowdhury S, Siderowf A, Lasch S, Coffey CS, Caspell-Garcia C, et al. The Parkinson's progression markers initiative (PPMI) – establishing a PD biomarker cohort. *Ann Clin Transl Neurol*. (2018) 5:1460–77. doi: 10.1002/acn3.644

49. Shabalin AA. Matrix eQTL: ultra fast eQTL analysis via large matrix operations. *Bioinformatics*. (2012) 28:1353–8. doi: 10.1093/bioinformatics/bts163

50. Orenbuch R, Filip I, Comito D, Shaman J, Pe'er I, Rabadan R. arcasHLA: high-resolution HLA typing from RNAseq. *Bioinformatics*. (2020) 36:33–40. doi: 10.1093/bioinformatics/btz474

51. Stephens M, Smith NJ, Donnelly P. A new statistical method for haplotype reconstruction from population data. *Am J Hum Genet*. (2001) 68:978–89. doi: 10.1086/319501

52. Boyko A, Troyanova N, Kovalenko E, Sapozhnikov A. Similarity and differences in inflammation-related characteristics of the peripheral immune system of patients with parkinson's and alzheimer's diseases. *Int J Mol Sci*. (2017) 18:2633. doi: 10.3390/ijms18122633

53. Itoh Y, Voskuhl RR. Cell specificity dictates similarities in gene expression in multiple sclerosis, Parkinson's disease, and Alzheimer's disease. *PloS One*. (2017) 12:e0181349. doi: 10.1371/journal.pone.0181349

54. Pugliese A, Boulware D, Yu L, Babu S, Steck AK, Becker D, et al. HLA-DRB1*15:01-DQA1*01:02-DQB1*06:02 haplotype protects autoantibody-positive relatives from type 1 diabetes throughout the stages of disease progression. *Diabetes*. (2016) 65:1109–19. doi: 10.2337/db15-1105

55. Kaushansky N, Eisenstein M, Boura-Halfon S, Hansen BE, Nielsen CH, Milo R, et al. Role of a novel human leukocyte antigen-DQA1*01:02;DRB1*15:01 mixed isotype heterodimer in the pathogenesis of "Humanized" Multiple sclerosis-like disease. *J Biol Chem*. (2015) 290:15260–78. doi: 10.1074/jbc.M115.641209

56. Claeys A, Merseburger P, Staut J, Marchal K, Van Den Eynden J. Benchmark of tools for *in silico* prediction of MHC class I and class II genotypes from NGS data. *BMC Genomics*. (2023) 24:247. doi: 10.1186/s12864-023-09351-z

57. Misra MK, Damotte V, Hollenbach JA. The immunogenetics of neurological disease. *Immunology*. (2018) 153:399–414. doi: 10.1111/imm.12869

58. Zaimoku Y, Mizumaki H, Imi T, Hosokawa K, Maruyama H, Katagiri T, et al. The copy number of disease-associated HLA alleles predicts the response to immunosuppressive therapy in acquired aplastic anemia. *Blood*. (2021) 138:604–4. doi: 10.1182/blood-2021-148240

59. Ombrello MJ, Remmers EF, Tachmazidou I, Grom A, Foell D, Haas J-P, et al. *HLA-DRB1*11* and variants of the MHC class II locus are strong risk factors for systemic juvenile idiopathic arthritis. *Proc Natl Acad Sci USA*. (2015) 112:15970–5. doi: 10.1073/pnas.1520779112

60. Zawadzka-Starczewska K, Tymoniuk B, Stasiak B, Lewiński A, Stasiak M. Actual associations between HLA haplotype and Graves' disease development. *J Clin Med*. (2022) 11:2492. doi: 10.3390/jcm11092492

61. Mignot E, Guen YL, Luo G, Ambati A, Damotte V, Jansen I, et al. Protective association of HLA-DRB1*04 subtypes in neurodegenerative diseases implicates acetylated tau PHF6 sequences. *Res Square preprint*. (2022). doi: 10.21203/rs.3.rs-1285855/v1

62. Ozono T, Kimura Y, Suenaga T, Beck G, Jinno J, Aguirre C, et al. Extracellular transportation of α-synuclein by HLA class II molecules. *Biochem Biophys Res Comm*. (2023) 644:25–33. doi: 10.1016/j.bbrc.2022.12.082

63. Ahmad T. Genetics of inflammatory bowel disease: The role of the HLA complex. *World J Gastroenterol*. (2006) 12:3628. doi: 10.3748/wjg.v12.i23.3628

64. Degenhardt F, Mayr G, Wendorff M, Boucher G, Ellinghaus E, Ellinghaus D, et al. Transethnic analysis of the human leukocyte antigen region for ulcerative colitis reveals not only shared but also ethnicity-specific disease associations. *Hum Mol Genet*. (2021) 30:356–69. doi: 10.1093/hmg/ddab017

65. Mahdi BM. Role of HLA typing on Crohn's disease pathogenesis. *Ann Med Surg*. (2015) 4:248–53. doi: 10.1016/j.amsu.2015.07.020

66. Rickenbach C, Gericke C. Specificity of adaptive immune responses in central nervous system health, aging and diseases. *Front Neurosci*. (2022) 15:806260. doi: 10.3389/fnins.2021.806260

67. Petersdorf EW, Malkki M, O'hUigin C, Carrington M, Gooley T, Haagenson MD, et al. High HLA-DP expression and graft-versus-host disease. *N Engl J Med*. (2015) 373:599–609. doi: 10.1056/NEJMoa1500140

68. Fleischhauer K. Immunogenetics of HLA-DP — A new view of permissible mismatches. *N Engl J Med*. (2015) 373:669–72. doi: 10.1056/NEJMe1505539

69. Chu C, Lin EW, Tran A, Jin H, Ho NI, Veit A, et al. The landscape of human SVA retrotransposons. *Nucl Acids Res*. (2023), 51:11453–65. doi: 10.1093/nar/gkad821

70. Prat E, Tomaru U, Sabater L, Park DM, Granger R, Kruse N, et al. HLA-DRB5*0101 and -DRB1*1501 expression in the multiple sclerosis-associated HLA-DR15 haplotype. *J Neuroimmunol*. (2005) 167:108–19. doi: 10.1016/j.jneuroim.2005.04.027

71. Caillier SJ, Briggs F, Cree BAC, Baranzini SE, Fernandez-Vina M, Ramsay PP, et al. Uncoupling the roles of HLA-DRB1 and HLA-DRB5 genes in multiple sclerosis. *J Immunol*. (2008) 181:5473–80. doi: 10.4049/jimmunol.181.8.5473

72. Mosca L. HLA-DRB1*15 association with multiple sclerosis is confirmed in a multigenerational Italian family. *Funct Neurol*. (2017) 32:83. doi: 10.11138/FNeur/2017.32.2.083

73. Huang X, Liu G, Mei S, Cai J, Rao J, Tang M, et al. Human leucocyte antigen alleles confer susceptibility and progression to Graves' ophthalmopathy in a Southern Chinese population. *Br J Ophthalmol*. (2021) 105:1462–8. doi: 10.1136/bjophthalmol-2020-317091

74. Testi M, Terracciano C, Guagnano A, Testa G, Marfia GA, Pompeo E, et al. Association of HLA-DQB1*05:02 and DRB1*16 alleles with late-onset, nonthymomatous, AChR-Ab-Positive myasthenia gravis. *Autoimmune Dis*. (2012) 2012:1–3. doi: 10.1155/2012/541760

75. Makino S, Kaji R, Ando S, Tomizawa M, Yasuno K, Goto S, et al. Reduced neuron-specific expression of the TAF1 gene is associated with X-linked dystonia-parkinsonism. *Am J Hum Genet*. (2007) 80:393–406. doi: 10.1086/512129

frontiers | Frontiers in Immunology

TYPE Mini Review
PUBLISHED 26 March 2024
DOI 10.3389/fimmu.2024.1375453

OPEN ACCESS

EDITED BY
Fawaz Alzaid,
Sorbonne Universités, France

REVIEWED BY
Xavier Fioramonti,
INRA UMR1286 Laboratoire NutriNeuro, France
Jason M. Miska,
Northwestern University, United States

*CORRESPONDENCE
Kenneth K. Y. Ting
kenneth.ting@mail.utoronto.ca

RECEIVED 23 January 2024
ACCEPTED 18 March 2024
PUBLISHED 26 March 2024

CITATION
Ting KKY (2024) Fructose overconsumption-induced reprogramming of microglia metabolism and function.
Front. Immunol. 15:1375453.
doi: 10.3389/fimmu.2024.1375453

Fructose overconsumption-induced reprogramming of microglia metabolism and function

Kenneth K. Y. Ting[1,2]*

[1]Department of Immunology, University of Toronto, Toronto, ON, Canada, [2]Toronto General Hospital Research Institute, University Health Network, Toronto, ON, Canada

The overconsumption of dietary fructose has been proposed as a major culprit for the rise of many metabolic diseases in recent years, yet the relationship between a high fructose diet and neurological dysfunction remains to be explored. Although fructose metabolism mainly takes place in the liver and intestine, recent studies have shown that a hyperglycemic condition could induce fructose metabolism in the brain. Notably, microglia, which are tissue-resident macrophages (Mφs) that confer innate immunity in the brain, also express fructose transporters (GLUT5) and are capable of utilizing fructose as a carbon fuel. Together, these studies suggest the possibility that a high fructose diet can regulate the activation and inflammatory response of microglia by metabolic reprogramming, thereby altering the susceptibility of developing neurological dysfunction. In this review, the recent advances in the understanding of microglia metabolism and how it supports its functions will be summarized. The results from both *in vivo* and *in vitro* studies that have investigated the mechanistic link between fructose-induced metabolic reprogramming of microglia and its function will then be reviewed. Finally, areas of controversies and their associated implications, as well as directions that warrant future research will be highlighted.

KEYWORDS

microglia, immunometabolism, macrophages, fructose metabolism, GLUT5, inflammation, glycolytic reprogramming, neurological dysfunction

1 Introduction of microglia

Microglia, which are tissue resident macrophages (Mφs) of the central nervous system, constitute a major component of the innate immune system in the brain. Depending on the area, microglia can comprise 5% to 12% of the total cell populations in the brain (1). Although microglia are classified as tissue resident Mφs, their ontogeny is notably distinct when compared to other types of Mφs. Genetic fate-mapping studies have now demonstrated that microglia are derived from primitive Mφs, which are differentiated

from erythro-myeloid precursors in the yolk sac, and they colonize the developing brain as early as embryonic day 9.5 (2–4). Upon colonization, they retain their embryonic origin throughout adult life with no replacement from circulating monocytes.

To provide immune protection and maintain a healthy neural microenvironment, microglia are responsible for monitoring and scavenging the parenchyma continuously through its interaction with environmental cues, such as chemokines, cytokines, and other trophic factors (5–7). Upon detection of changes in the local environment, depending on the type of stimuli, microglia becomes activated and display a diverse profile of phenotypes. Similar to other tissue resident Mφs, microglia can also be divided into M1 and M2 Mφs. As M1 Mφs, they display cytotoxic and pro-inflammatory responses upon recognition of inflammatory stimulus, such as bacterial lipopolysaccharides (LPS). On other hand, they can also be alternatively activated into M2 Mφs, where they can perform repair and regeneration functions (M2a), immune-regulatory functions (M2b) or the acquisition of a deactivating phenotype (M2c) (8, 9). Overall, microglia demonstrate high phenotypic and functional plasticity in response to the wide spectrum of changes that take place in the brain (1, 10). Apart from its scavenging functions, microglia are also now recognized to be involved in other dynamic processes that can modulate brain functions, including the formation and maturation of synapse, brain homeostasis, neurogenesis and regulating neuronal excitability (11).

2 Metabolic reprogramming of microglia

Recent advances in the immunometabolism field have shown that the acquisition of altered metabolic adaptations due to the rewiring of metabolic circuits, known as metabolic reprogramming, is critical for the activation of immune cells and their functions. To support the heterogenous phenotypes and functions of microglia as described above, they are capable of metabolizing a variety of carbon sources, such as glucose (12), fructose (13), free fatty acids (14), lactate (15), and ketone bodies (16), in which the type of fuel it metabolizes can modulate its ability to perform its effector functions. In general, microglia express GLUT3 and GLUT5 to facilitate the uptake of glucose and fructose respectively (17–19). However, under inflammatory conditions, microglia can undergo metabolic reprogramming by transcriptionally activating the expression of glycolytic genes, such as glucose transporters (GLUT1) and lactate transporters (MCT1), to increase the breakdown of glucose (glycolysis) (15, 20, 21). More importantly, it has been shown that LPS-induced activation of microglia cell lines increased the rate of glycolysis while decreased the rate of oxidative phosphorylation (OXPHOS) (22). This shift from OXPHOS to aerobic glycolysis is known as the Warburg effect, which was first observed in cancer cells by Otto Warburg (23). Mechanistically, it is believed that this metabolic shift is due to the activation of mechanistic target of rapamycin (mTOR) complex 1 and hypoxia-induced factor 1α (HIF-1α) (24–26), which directly transactivate the expression of glycolytic and inflammatory genes, along with the activation of HIF-1α co-activators.

The increased flux of glycolysis in activated microglia is directly linked to its ability elicit an inflammatory response as blocking glycolysis with 2-deoxy-glucose impaired its production of pro-inflammatory cytokines, such as Tumor Necrosis Factor alpha (TNF-α) and Interleukin-6 (IL-6), in a NF-kB-dependent manner (27, 28). On the other hand, incubation of microglia with increased concentration of glucose further enhanced its production of TNF-α (29, 30). Although the direct link between the consequence of increased glycolytic flux and production of inflammatory cytokines is an ongoing investigation, recent reports have shown that the induction of glycolysis could lead to increased flux of the pentose phosphate pathway (PPP) and multiple disruptions in the tricarboxylic acid (TCA) cycle of Mφs in general (31–33). While the increased flux of PPP increased the production of NADPH, which is critical for regulating Mφ inflammatory responses (34), the disrupted TCA cycle had led to the accumulation of key metabolites that are linked to inflammation. For instance, the accumulation of succinate due to the inhibition of succinate dehydrogenase is important for the stabilization of HIF-1α and its direct transcription of *Il1b* transcripts (35, 36). On the other hand, the accumulation of citrate due to the inhibition of isocitrate dehydrogenase (36, 37) can be converted back to acetyl-CoA by ATP citrate lyase and it is critical for histone acetylation of inflammatory genes (38, 39), as well as *de novo* lipid synthesis, which supports the secretion of pro-inflammatory mediators (40). Apart from metabolites, the increased flux of the PPP also fuels the production of nitric oxide (NO) by nitric oxide synthase, in which the production of NO could inhibit the function of the electron transport chain (ETC) in Mφs (41, 42). The impaired activity of the ETC then induce the reversal of electron flow and drive the production of ROS, which is responsible to inhibit the activity of prolyl hydroxylases and thus stabilizing HIF-1α levels (43). More recently, it has also been revealed that blocking the activity of factor inhibiting HIF (FIH), an enzyme that inhibits the transactivation capacity of HIF-1α, is also critical for fully activating HIF-1α transcriptional function in Mφs (44). Collectively, these studies have shown that glucose metabolism plays a critical role in orchestrating the inflammatory response of activated microglia (Figure 1).

On the other hand, under anti-inflammatory conditions, such as stimulation by Interleukin-4 or Interleukin-13, microglia are metabolically adapted to utilize OXPHOS, which led to an attenuated uptake of glucose and production of lactate, and display similar oxygen consumption rate (OCR) and extracellular acidification rate (ECAR) levels as unstimulated microglia (14, 31). Finally, under homeostatic physiological conditions, microglia utilize a combination of oxidative catabolism of glucose and free fatty acids to fuel the TCA cycle and electron transport chain for generating large amounts of ATP, thereby sustaining the energetic needs for their basic surveyance functions (14, 45).

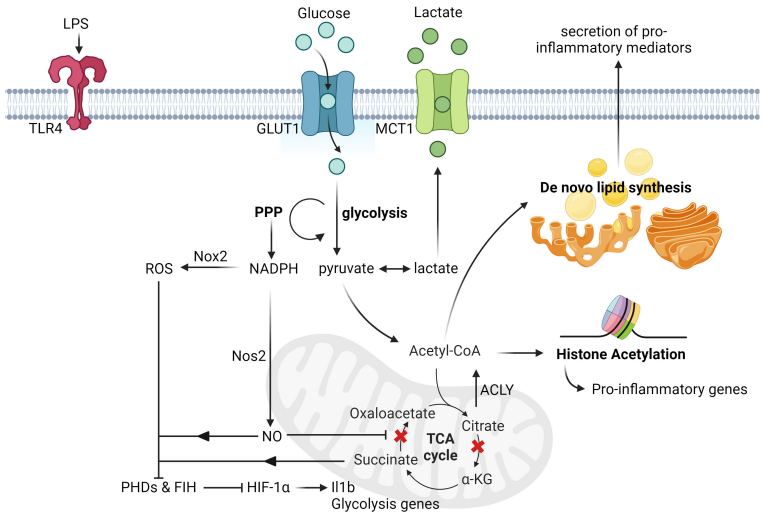

FIGURE 1
Glucose-induced metabolic reprogramming of activated microglia and macrophages. Upon LPS stimulation, microglia upregulate the expression of glucose transporters (GLUT1) and lactate transporters (MCT1) to increase the rate of glucose metabolism. This induction of glycolysis then leads to the increased rate of PPP, which is responsible for the synthesis of nucleotides and NADPH. The augmented production of NADPH subsequently drives the production of nitric oxide and ROS by Nos2 and Nox2 respectively. Upon nitric oxide-mediated inhibition of succinate dehydrogenase activity, it leads to the accumulation of succinate, which together with ROS, inhibit the activity of both FIH and PHDs. This eventually leads to the stabilization and activation of HIF-1α transactivation capacity, and the transcription of its targeted genes, such as *Il1b* and other glycolysis genes. Apart from this, another metabolic break happens at the isocitrate dehydrogenase level due to its suppressed expression post LPS stimulation, thereby leading to the accumulation of citrate. The rapid increased levels of citrate can then be converted to acetyl-CoA by ACLY and contribute to histone acetylation and *de novo* lipid biosynthesis (ex. synthesis of fatty acids), which can promote histone acetylation of pro-inflammatory genes and secretion of pro-inflammatory cytokines respectively. All figures are created with BioRender.com.

3 Fructose-induced metabolism in the brain and its reprogramming of microglia

It is well-established that glucose metabolism is vital to fuel the inflammatory functions of microglia, yet the role of fructose metabolism in modulating microglia inflammatory response is largely unexplored. In fact, it was previously unclear if dietary fructose consumption could even affect fructose metabolism in the brain as the breakdown of fructose mainly takes place in the intestine and liver (46–49). Until recently, Hwang et al. have used ^{1}H magnetic resonance spectroscopy (MRS) scanning to measure intracerebral fructose levels, and found it was rapidly increased in the human brain under hyperglycemic condition (intravenous injection of 20% dextrose in human subjects) (50). Specifically, the authors found the fructose levels in the brain rose significantly, as early as 20 minutes post dextrose injection, and maintained elevated until the end of the study (240 minutes), with the range of fructose concentration changing from 0 to 0.7mmol/L approximately (50). More importantly, the authors also discovered that the rapid rise of intracerebral fructose levels occurred prior to the increase of plasma fructose levels, suggesting that the hyperglycemic condition could induce endogenous fructose production in the brain (50). Similar findings were also observed in a previous study performed by Hwang et al, where the authors have used gas chromatography-mass spectroscopy to measure fructose concentration in cerebrospinal fluids (CSF) from pregnant women and found that CSF-derived fructose and sorbitol levels were much higher (9-20-fold) than the levels in plasma (51). Taken together, these findings collectively demonstrate that fructose could be produced endogenously in the brain and that the effects of intracerebral fructose extend beyond its dietary consumption.

Understanding that fructose can be endogenously produced in the brain under hyperglycemic condition, and that a high-fructose diet is known to induce hyperglycemia, this then raises the possibility that a high-fructose diet can potentially modulate the metabolic and inflammatory profiles in the brain. Indeed, past reports have already revealed that a high fructose diet increased the expression of GLUT5 (52), as well as pro-inflammatory mediators, such as *Tnfa*, in the hippocampus (53). Mechanistically, fructose-diet induced Toll-like receptor 4/NF-kB and p38 MAPK/ERK inflammatory phosphorylating signaling cascades in the hippocampus, which eventually led to the increased expression of pro-inflammatory cytokines (54).

To further investigate if dietary fructose-induced inflammation in the hippocampus is due to increased activation of microglia, recent effort has been invested to elucidate the link between fructose-mediated metabolic reprogramming in microglia and its effector functions. Using leptin receptor-deficient type 2 diabetes mellitus (db/db) mice, Li et al reported an upregulation of fructose-related metabolism in the hippocampus, as determined by metabolomic, proteomic, and transcriptomic analysis (13). Single-cell RNA sequencing of hippocampus also revealed that the expression of fructose metabolism-related genes, such as *Khk* and *Slc2a5*, as well as ROS generating enzymes, such as NADPH Oxidase 4 (Nox4), were increased in microglia in db/db mice compared to littermate control (13). Mechanistically, selective

knockdown of *Khk* in the hippocampus and microglia resulted in reduced expression of Nox4 in microglia (13). Fructose-mediated Nox4 regulation was also linked to its mitochondrial translocation and that Nox4-induced ROS impaired mitochondrial homeostasis, eventually leading to the damage of synaptic plasticity (13). Similar to this, another study done by Hyer et al also found that high fructose diet induced the activation of microglia in male, but interestingly not in female rats (55). Specifically, male rats fed on a high fructose diet had increased activation of microglia with reduction of their dendritic complexity, which correlated to an impairment of their reverse learning ability (55).

Although the studies above demonstrated that the metabolism and function of microglia *in vivo* was modulated in response to high fructose diet, *in vitro* studies that investigated the direct intrinsic effects of fructose on microglia remains to be controversial. For instance, Mizuno et al have treated primary microglia and SIM-A9 cells (murine microglia cell lines) with high concentration of fructose (7.5mM for 24h) and glucose (7.5mM for 24h) separately and found that only glucose has induced inflammation and expression of *Slc2a5* (GLUT5) (56). However, on the other hand, Xu et al have treated microglia BV-2 cells with high concentration of fructose (5mM for 24h) and found it induced TLR4/NF-κB activation, as well as pro-inflammatory gene expression, such as *Il1b*, *Il6* and *Tnfa* (57). Similar findings were also reported by Cigliano et al where they also incubated BV-2 cells with a range of concentration of fructose (0 to 10mM, 24h) and found it increased TNF-α production as measured by ELISA (54). Overall, these studies suggest that the intrinsic inflammatory effect of fructose appears to be dependent on specific experimental condition, and further experiments are needed to resolve the controversies.

Several important points of consideration need to be taken when comparing the results obtained from the presented *in vitro* and *in vivo* studies, one of which is the discrepancy between the intracerebral fructose levels quantified in the *in vivo* experiments, and the experimental fructose levels that were used in the *in vitro* experiments. For instance, as shown in the MRS scanning study performed by Hwang et al., the intracerebral fructose levels fluctuated only between 0 to 0.7mmol/L post dextrose injection (50). Yet, all the *in vitro* studies presented in this review have incubated microglia with fructose at a much higher concentration (at least 5mM). This not only raises concerns that the *in vitro* findings may not demonstrate physiological relevance, but also suggests the need of more *in vitro* studies that incubate microglia with physiologically relevant levels of fructose. Apart from this, the expression and function of proteins involved in fructose metabolism, such as GLUT5, is not always measured in the *in vitro* studies discussed in this review, thus making it difficult to draw a mechanistic link between the observed inflammatory phenotypes in microglia and their metabolism of fructose.

4 Conclusion and future perspectives

The overconsumption of dietary fructose has been associated with the rise of chronic inflammatory diseases, such as obesity, diabetes, cardiovascular disease, and cancer (58–60). Furthermore, epidemiological studies have now revealed that high fructose consumption can also induce brain disturbances and negatively affect the development of neural system (61, 62). Early studies that investigated the relationship between the effects of dietary fructose and neural functions have shown that microglia do express fructose transporter (GLUT5) (18) and that fructose metabolism in the brain was stimulated under hyperglycemic condition (50). Understanding that the type of carbon fuel in which microglia metabolize can profoundly shape their effector functions, the focus of recent research has now shifted to the elucidation of a mechanistic link between high fructose consumption and its metabolic effects on microglia activation and inflammatory response. While this topic is still currently under heavy investigation, recent completed studies have generally demonstrated that high fructose-diet induced fructose metabolism in microglia is linked to its increased activation and inflammatory response, which can possibly lead to cognitive dysfunction and impairment (Figure 2). Yet, *in vitro* studies that directly investigate the intrinsic inflammatory response of fructose in microglia remains to be controversial and warrants future research to further determine the inflammatory signaling cascades that fructose metabolism may enhance, as well as the transcriptional regulation that modulates the expression of fructose metabolism genes.

The controversial findings observed *in vitro* could also suggest the existence of other external factors derived from the high fructose diet that could enhance the inflammatory responses of microglia *in vivo*, such as circulating metabolites that can cross the blood brain barrier. Furthermore, external variables such as sex can also modulate the effects of dietary fructose on neural functions. As

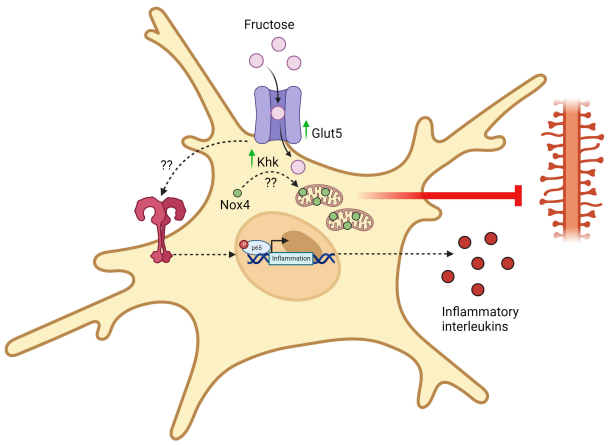

FIGURE 2
Fructose-induced metabolic reprogramming of activated microglia. Upon chronic exposure of high fructose, microglia upregulates the expression of fructose transporters (GLUT5) and keto-hexokinase (KHK). Through an unidentified mechanism, KHK promotes the translocation of Nox4 into the mitochondria and Nox4-mediated ROS synthesis disrupts mitochondrial homeostasis and eliminates dendrites. This eventually damages synaptic transmission and promotes the development of cognitive disorders. Apart from this, chronic exposure of high fructose also activates TLR4/NF-kB signaling pathways through an unidentified mechanism, thereby leading to the transcription and synthesis of pro-inflammatory mediators. All figures are created with BioRender.com.

described from the study by Hyer et al, cognitive flexibility was only impaired in male, but not female rats fed on high fructose diet, implicating that female sex hormones may play a role in the protection against fructose diets (55). Indeed, past research has shown that females do not develop hyperinsulinemia post fructose feeding with the exception of ovariectomy (63). Understanding the underlying differences between how high fructose consumption differentially affect the neural function of males and females may help to identify novel mechanisms that protect the deleterious effects of fructose in an *in vivo* setting.

Author contributions

KKYT: Conceptualization, Funding acquisition, Visualization, Writing – original draft, Writing – review & editing.

Funding

The author(s) declare financial support was received for the research, authorship, and/or publication of this article. KKYT was supported by fellowships from Canadian Institutes of Health Research, Ontario Graduate Scholarship, fellowships from the University of Toronto and The Peterborough K. M. Hunter Charitable Foundation.

Conflict of interest

The author declares that the research was conducted in the absence of any commercial or financial relationships that could be construed as a potential conflict of interest.

Publisher's note

References

1. Ransohoff RM. A polarizing question: do M1 and M2 microglia exist? *Nat Neurosci.* (2016) 19:987–91. doi: 10.1038/nn.4338

2. Ginhoux F, Greter M, Leboeuf M, Nandi S, See P, Gokhan S, et al. Fate mapping analysis reveals that adult microglia derive from primitive macrophages. *Science.* (2010) 330:841–5. doi: 10.1126/science.1194637

3. Gomez Perdiguero E, Klapproth K, Schulz C, Busch K, Azzoni E, Crozet L, et al. Tissue-resident macrophages originate from yolk-sac-derived erythro-myeloid progenitors. *Nature.* (2015) 518:547–51. doi: 10.1038/nature13989

4. Kierdorf K, Erny D, Goldmann T, Sander V, Schulz C, Perdiguero EG, et al. Microglia emerge from erythromyeloid precursors via Pu.1- and Irf8-dependent pathways. *Nat Neurosci.* (2013) 16:273–80. doi: 10.1038/nn.3318

5. Davalos D, Grutzendler J, Yang G, Kim JV, Zuo Y, Jung S, et al. ATP mediates rapid microglial response to local brain injury *in vivo*. *Nat Neurosci.* (2005) 8:752–8. doi: 10.1038/nn1472

6. Nimmerjahn A, Kirchhoff F, Helmchen F. Resting microglial cells are highly dynamic surveillants of brain parenchyma *in vivo*. *Science.* (2005) 308:1314–8. doi: 10.1126/science.1110647

7. Li Q, Barres BA. Microglia and macrophages in brain homeostasis and disease. *Nat Rev Immunol.* (2018) 18:225–42. doi: 10.1038/nri.2017.125

8. Chhor V, Le Charpentier T, Lebon S, Oré MV, Celador IL, Josserand J, et al. Characterization of phenotype markers and neuronotoxic potential of polarised primary microglia *in vitro*. *Brain Behav Immun.* (2013) 32:70–85. doi: 10.1016/j.bbi.2013.02.005

9. Boche D, Perry VH, Nicoll JA. Review: activation patterns of microglia and their identification in the human brain. *Neuropathol Appl Neurobiol.* (2013) 39:3–18. doi: 10.1111/nan.12011

10. Schwartz M, Butovsky O, Brück W, Hanisch UK. Microglial phenotype: is the commitment reversible? *Trends Neurosci.* (2006) 29:68–74. doi: 10.1016/j.tins.2005.12.005

11. Lenz KM, McCarthy MM. A starring role for microglia in brain sex differences. *Neuroscientist.* (2015) 21:306–21. doi: 10.1177/1073858414536468

12. Aldana BI. Microglia-specific metabolic changes in neurodegeneration. *J Mol Biol.* (2019) 431:1830–42. doi: 10.1016/j.jmb.2019.03.006

13. Li Y, Jiang T, Du M, He S, Huang N, Cheng B, et al. Ketohexokinase-dependent metabolism of cerebral endogenous fructose in microglia drives diabetes-associated cognitive dysfunction. *Exp Mol Med.* (2023) 55:2417–32. doi: 10.1038/s12276-023-01112-y

14. Orihuela R, McPherson CA, Harry GJ. Microglial M1/M2 polarization and metabolic states. *Br J Pharmacol.* (2016) 173:649–65. doi: 10.1111/bph.13139

15. Moreira TJ, Pierre K, Maekawa F, Repond C, Cebere A, Liljequist S, et al. Enhanced cerebral expression of MCT1 and MCT2 in a rat ischemia model occurs in activated microglial cells. *J Cereb Blood Flow Metab.* (2009) 29:1273–83. doi: 10.1038/jcbfm.2009.50

16. Huang C, Wang P, Xu X, Zhang Y, Gong Y, Hu W, et al. The ketone body metabolite β-hydroxybutyrate induces an antidepression-associated ramification of microglia via HDACs inhibition-triggered Akt-small RhoGTPase activation. *Glia.* (2018) 66:256–78. doi: 10.1002/glia.23241

17. Kalsbeek MJ, Mulder L, Yi CX. Microglia energy metabolism in metabolic disorder. *Mol Cell Endocrinol.* (2016) 438:27–35. doi: 10.1016/j.mce.2016.09.028

18. Payne J, Maher F, Simpson I, Mattice L, Davies P. Glucose transporter Glut 5 expression in microglial cells. *Glia.* (1997) 21:327–31. doi: 10.1002/(ISSN)1098-1136

19. Douard V, Ferraris RP. Regulation of the fructose transporter GLUT5 in health and disease. *Am J Physiol Endocrinol Metab.* (2008) 295:E227–37. doi: 10.1152/ajpendo.90245.2008

20. Wang L, Pavlou S, Du X, Bhuckory M, Xu H, Chen M. Glucose transporter 1 critically controls microglial activation through facilitating glycolysis. *Mol Neurodegener.* (2019) 14:2. doi: 10.1186/s13024-019-0305-9

21. Kong L, Wang Z, Liang X, Wang Y, Gao L, Ma C. Monocarboxylate transporter 1 promotes classical microglial activation and pro-inflammatory effect via 6-phosphofructo-2-kinase/fructose-2, 6-biphosphatase 3. *J Neuroinflamm.* (2019) 16:240. doi: 10.1186/s12974-019-1648-4

22. Voloboueva LA, Emery JF, Sun X, Giffard RG. Inflammatory response of microglial BV-2 cells includes a glycolytic shift and is modulated by mitochondrial glucose-regulated protein 75/mortalin. *FEBS Lett.* (2013) 587:756–62. doi: 10.1016/j.febslet.2013.01.067

23. Weinhouse S. On respiratory impairment in cancer cells. *Science.* (1956) 124:267–9. doi: 10.1126/science.124.3215.267

24. Sangineto M, Ciarnelli M, Cassano T, Radesco A, Moola A, Bukke VN, et al. Metabolic reprogramming in inflammatory microglia indicates a potential way of targeting inflammation in Alzheimer's disease. *Redox Biol.* (2023) 66:102846. doi: 10.1016/j.redox.2023.102846

25. Baik SH, Kang S, Lee W, Choi H, Chung S, Kim J-I, et al. A breakdown in metabolic reprogramming causes microglia dysfunction in Alzheimer's disease. *Cell Metab.* (2019) 30:493–507.e6. doi: 10.1016/j.cmet.2019.06.005

26. Bernier L-P, York EM, MacVicar BA. Immunometabolism in the brain: how metabolism shapes microglial function. *Trends Neurosci.* (2020) 43:854–69. doi: 10.1016/j.tins.2020.08.008

27. Wang Q, Zhao Y, Sun M, Liu S, Li B, Zhang L, et al. 2-Deoxy-d-glucose attenuates sevoflurane-induced neuroinflammation through nuclear factor-kappa B pathway *in vitro*. *Toxicol In Vitro.* (2014) 28:1183–9. doi: 10.1016/j.tiv.2014.05.006

28. Cheng J, Zhang R, Xu Z, Ke Y, Sun R, Yang H, et al. Early glycolytic reprogramming controls microglial inflammatory activation. *J Neuroinflamm.* (2021) 18:129. doi: 10.1186/s12974-021-02187-y

29. Quan Y, Jiang CT, Xue B, Zhu SG, Wang X. High glucose stimulates TNFα and MCP-1 expression in rat microglia via ROS and NF-κB pathways. *Acta Pharmacol Sin*. (2011) 32:188–93. doi: 10.1038/aps.2010.174

30. Zhang X, Dong H, Zhang S, Lu S, Sun J, Qian Y. Enhancement of LPS-induced microglial inflammation response via TLR4 under high glucose conditions. *Cell Physiol Biochem*. (2015) 35:1571–81. doi: 10.1159/000373972

31. Gimeno-Bayón J, López-López A, Rodríguez MJ, Mahy N. Glucose pathways adaptation supports acquisition of activated microglia phenotype. *J Neurosci Res*. (2014) 92:723–31. doi: 10.1002/jnr.23356

32. Tu D, Gao Y, Yang R, Guan T, Hong JS, Gao HM. The pentose phosphate pathway regulates chronic neuroinflammation and dopaminergic neurodegeneration. *J Neuroinflamm*. (2019) 16:255. doi: 10.1186/s12974-019-1659-1

33. Chausse B, Lewen A, Poschet G, Kann O. Selective inhibition of mitochondrial respiratory complexes controls the transition of microglia into a neurotoxic phenotype in situ. *Brain Behav Immun*. (2020) 88:802–14. doi: 10.1016/j.bbi.2020.05.052

34. Ting KKY, Jongstra-Bilen J, Cybulsky MI. The multi-faceted role of NADPH in regulating inflammation in activated myeloid cells. *Front Immunol*. (2023) 14. doi: 10.3389/fimmu.2023.1328484

35. Tannahill GM, Curtis AM, Adamik J, Palsson-McDermott EM, McGettrick AF, Goel G, et al. Succinate is an inflammatory signal that induces IL-1β through HIF-1α. *Nature*. (2013) 496:238–42. doi: 10.1038/nature11986

36. Jha AK, Huang SC, Sergushichev A, Lampropoulou V, Ivanova Y, Loginicheva E, et al. Network integration of parallel metabolic and transcriptional data reveals metabolic modules that regulate macrophage polarization. *Immunity*. (2015) 42:419–30. doi: 10.1016/j.immuni.2015.02.005

37. Williams NC, O'Neill LAJ. A role for the Krebs cycle intermediate citrate in metabolic reprogramming in innate immunity and inflammation. *Front Immunol*. (2018) 9:141. doi: 10.3389/fimmu.2018.00141

38. Lauterbach MA, Hanke JE, Serefidou M, Mangan MSJ, Kolbe CC, Hess T, et al. Toll-like receptor signaling rewires macrophage metabolism and promotes histone acetylation via ATP-citrate lyase. *Immunity*. (2019) 51:997–1011.e7. doi: 10.1016/j.immuni.2019.11.009

39. Ting KKY, Yu P, Iyayi M, Dow R, Hyduk SJ, Floro E, et al. Oxidized low-density lipoprotein accumulation in macrophages impairs lipopolysaccharide-induced activation of AKT2, ATP citrate lyase, acetyl–coenzyme A production, and inflammatory gene H3K27 acetylation. *ImmunoHorizons*. (2024) 8:57–73. doi: 10.4049/immunohorizons.2300101

40. Yang S, Qin C, Hu Z-W, Zhou L-Q, Yu H-H, Chen M, et al. Microglia reprogram metabolic profiles for phenotype and function changes in central nervous system. *Neurobiol Dis*. (2021) 152:105290. doi: 10.1016/j.nbd.2021.105290

41. Clementi E, Brown GC, Feelisch M, Moncada S. Persistent inhibition of cell respiration by nitric oxide: crucial role of S-nitrosylation of mitochondrial complex I and protective action of glutathione. *Proc Natl Acad Sci USA*. (1998) 95:7631–6. doi: 10.1073/pnas.95.13.7631

42. Van den Bossche J, Baardman J, Otto Natasja A, van der Velden S, Neele Annette E, van den Berg Susan M, et al. Mitochondrial dysfunction prevents repolarization of inflammatory macrophages. *Cell Rep*. (2016) 17:684–96. doi: 10.1016/j.celrep.2016.09.008

43. Van den Bossche J, O'Neill LA, Menon D. Macrophage immunometabolism: where are we (Going)? *Trends Immunol*. (2017) 38:395–406. doi: 10.1016/j.it.2017.03.001

44. Ting KKY, Yu P, Dow R, Floro E, Ibrahim H, Scipione CA, et al. Oxidized low-density lipoprotein accumulation suppresses glycolysis and attenuates the macrophage inflammatory response by diverting transcription from the HIF-1α to the Nrf2 pathway. *J Immunol*. (2023) 211:1561–77. doi: 10.4049/jimmunol.2300293

45. Biswas SK, Mantovani A. Orchestration of metabolism by macrophages. *Cell Metab*. (2012) 15:432–7. doi: 10.1016/j.cmet.2011.11.013

46. Jang C, Hui S, Lu W, Cowan AJ, Morscher RJ, Lee G, et al. The small intestine converts dietary fructose into glucose and organic acids. *Cell Metab*. (2018) 27:351–61.e3. doi: 10.1016/j.cmet.2017.12.016

47. Lanaspa MA, Ishimoto T, Li N, Cicerchi C, Orlicky DJ, Ruzycki P, et al. Endogenous fructose production and metabolism in the liver contributes to the development of metabolic syndrome. *Nat Commun*. (2013) 4:2434. doi: 10.1038/ncomms3929

48. Ishimoto T, Lanaspa MA, Rivard CJ, Roncal-Jimenez CA, Orlicky DJ, Cicerchi C, et al. High-fat and high-sucrose (western) diet induces steatohepatitis that is dependent on fructokinase. *Hepatology*. (2013) 58:1632–43. doi: 10.1002/hep.26594

49. Ishimoto T, Lanaspa MA, Le MT, Garcia GE, Diggle CP, Maclean PS, et al. Opposing effects of fructokinase C and A isoforms on fructose-induced metabolic syndrome in mice. *Proc Natl Acad Sci USA*. (2012) 109:4320–5. doi: 10.1073/pnas.1119908109

50. Hwang JJ, Jiang L, Hamza M, Dai F, Belfort-DeAguiar R, Cline G, et al. The human brain produces fructose from glucose. *JCI Insight*. (2017) 2:e90508. doi: 10.1172/jci.insight.90508

51. Hwang JJ, Johnson A, Cline G, Belfort-DeAguiar R, Snegovskikh D, Khokhar B, et al. Fructose levels are markedly elevated in cerebrospinal fluid compared to plasma in pregnant women. *PLoS One*. (2015) 10:e0128582. doi: 10.1371/journal.pone.0128582

52. Shu HJ, Isenberg K, Cormier RJ, Benz A, Zorumski CF. Expression of fructose sensitive glucose transporter in the brains of fructose-fed rats. *Neuroscience*. (2006) 140:889–95. doi: 10.1016/j.neuroscience.2006.02.071

53. Ho CY, Lin YT, Chen HH, Ho WY, Sun GC, Hsiao M, et al. CX3CR1-microglia mediates neuroinflammation and blood pressure regulation in the nucleus tractus solitarii of fructose-induced hypertensive rats. *J Neuroinflamm*. (2020) 17:185. doi: 10.1186/s12974-020-01857-7

54. Cigliano L, Spagnuolo MS, Crescenzo R, Cancelliere R, Iannotta L, Mazzoli A, et al. Short-term fructose feeding induces inflammation and oxidative stress in the hippocampus of young and adult rats. *Mol Neurobiol*. (2018) 55:2869–83. doi: 10.1007/s12035-017-0518-2

55. Hyer MM, Dyer SK, Kovalchick LV, Targett I, Burns CM, Kloster A, et al. Fructose-induced cognitive impairment co-occurs with morphological changes in dendrites and microglia of male rats. *Psychoneuroimmunol J*. (2022) 3:1–12. doi: 10.32371/pnij/246142

56. Mizuno TM, Lew PS, Jhanji G. Regulation of the fructose transporter gene slc2a5 expression by glucose in cultured microglial cells. *Int J Mol Sci*. (2021) 22. doi: 10.3390/ijms222312668

57. Xu MX, Yu R, Shao LF, Zhang YX, Ge CX, Liu XM, et al. Up-regulated fractalkine (FKN) and its receptor CX3CR1 are involved in fructose-induced neuroinflammation: Suppression by curcumin. *Brain Behav Immun*. (2016) 58:69–81. doi: 10.1016/j.bbi.2016.01.001

58. Hannou SA, Haslam DE, McKeown NM, Herman MA. Fructose metabolism and metabolic disease. *J Clin Invest*. (2018) 128:545–55. doi: 10.1172/JCI96702

59. Herman MA, Birnbaum MJ. Molecular aspects of fructose metabolism and metabolic disease. *Cell Metab*. (2021) 33:2329–54. doi: 10.1016/j.cmet.2021.09.010

60. Febbraio MA, Karin M. "Sweet death": Fructose as a metabolic toxin that targets the gut-liver axis. *Cell Metab*. (2021) 33:2316–28. doi: 10.1016/j.cmet.2021.09.004

61. Beecher K, Alvarez Cooper I, Wang J, Walters SB, Chehrehasa F, Bartlett SE, et al. Long-term overconsumption of sugar starting at adolescence produces persistent hyperactivity and neurocognitive deficits in adulthood. *Front Neurosci*. (2021) 15:670430. doi: 10.3389/fnins.2021.670430

62. Lien L, Lien N, Heyerdahl S, Thoresen M, Bjertness E. Consumption of soft drinks and hyperactivity, mental distress, and conduct problems among adolescents in Oslo, Norway. *Am J Public Health*. (2006) 96:1815–20. doi: 10.2105/AJPH.2004.059477

63. Galipeau D, Verma S, McNeill JH. Female rats are protected against fructose-induced changes in metabolism and blood pressure. *Am J Physiol Heart Circ Physiol*. (2002) 283:H2478–84. doi: 10.1152/ajpheart.00243.2002

frontiers | Frontiers in Neurology

TYPE Case Report
PUBLISHED 16 April 2024
DOI 10.3389/fneur.2024.1352779

OPEN ACCESS

EDITED BY
Ayman ElAli,
Laval University, Canada

REVIEWED BY
Judith Theresia Bellmann-Strobl,
Charite University Medicine Berlin, Germany
Nicolas Collongues,
Hôpitaux Universitaires de Strasbourg, France

*CORRESPONDENCE
Michael Levy
✉ mlevy11@mgh.harvard.edu

RECEIVED 08 December 2023
ACCEPTED 02 April 2024
PUBLISHED 16 April 2024

CITATION
Osborne B, Romanow G, Hemphill JM, Zarif M, DeAngelis T, Kaplan T, Oh U, Pinkhasov J, Patterson K and Levy M (2024) Case report: Transition from anti-CD20 therapy to inebilizumab for 14 cases of neuromyelitis optica spectrum disorder. *Front. Neurol.* 15:1352779. doi: 10.3389/fneur.2024.1352779

Case report: Transition from anti-CD20 therapy to inebilizumab for 14 cases of neuromyelitis optica spectrum disorder

Benjamin Osborne[1], Gabriela Romanow[2], J. Michael Hemphill[3], Myassar Zarif[4], Tracy DeAngelis[5], Tyler Kaplan[6], Unsong Oh[7], Johnathan Pinkhasov[8], Kristina Patterson[8] and Michael Levy[2]*

[1]Department of Neurology, Georgetown University Medical Center, Washington, DC, United States, [2]Department of Neurology, Massachusetts General Hospital and Harvard Medical School, Boston, MA, United States, [3]Savannah Neurology Specialists, Savannah, GA, United States, [4]South Shore Neurologic Associates, Patchogue, NY, United States, [5]Neurological Associates of Long Island, New Hyde Park, NY, United States, [6]Department of Neurology, Rush University Medical Center, Chicago, IL, United States, [7]Department of Neurology, Virginia Commonwealth University, Richmond, VA, United States, [8]Medical Affairs, Horizon Therapeutics, Deerfield, IL, United States

Neuromyelitis optica spectrum disorder (NMOSD) is a rare autoimmune disorder of the central nervous system characterized by recurrent, disabling attacks that affect the optic nerve, spinal cord, and brain/brainstem. While rituximab, targeting CD20-positive B-cells, is used as an off-label therapy for NMOSD, some patients continue to exhibit breakthrough attacks and/or adverse reactions. Inebilizumab, a humanized and glycoengineered monoclonal antibody targeting CD19-positive B-cells, has been FDA approved for the treatment of NMOSD in adult patients who are anti-aquaporin-4 (AQP4) antibody positive. Given the limited real-world data on the efficacy and safety of inebilizumab, especially in those transitioning from rituximab, a retrospective chart review was conducted on 14 NMOSD patients from seven centers. Of these, 71.4% (n=10) experienced a combined 17 attacks during rituximab treatment, attributed to either breakthrough disease (n=10) or treatment delay (n=7). The mean duration of rituximab treatment was 38.4months (3.2years). Notably, no subsequent attacks were observed during inebilizumab treatment [mean duration of inebilizumab treatment was 19.3months (1.6years)], underscoring its potential as an effective treatment for NMOSD. Our data suggest that inebilizumab provides clinical benefit with effective disease control and a favorable safety profile for patients transitioning from rituximab.

KEYWORDS

neuromyelitis optica spectrum disorder, aquaporin-4 antibody, inebilizumab, rituximab, treatment transition, clinical outcome, case report

1 Introduction

Neuromyelitis optica spectrum disorder (NMOSD) is a rare, debilitating autoimmune disorder of the central nervous system characterized by recurrent attacks affecting the optic nerve and spinal cord (1). However, NMOSD can also involve various other regions of the CNS, including the brainstem, area postrema, diencephalon, and cerebral white matter.

NMOSD predominantly affects women and frequently leads to severe neurological disability, encompassing not only visual impairment and motor dysfunction but also symptoms such as sensory disturbances, cognitive deficits, and autonomic dysfunction. In one study of untreated NMOSD patients, it was found that 50% required wheelchairs, 50% were blind in at least one eye, and 33% had died within 5 years of their first attack (2). The identification of aquaporin-4 antibodies ($AQP4^+$) as a precise diagnostic biomarker for NMOSD has advanced our knowledge of its disease pathophysiology, underscoring the pathogenesis of autoimmunity against the AQP4 water channel protein present on astrocytes in the central nervous system (3).

Over the past decade, the management of NMOSD has evolved significantly with the advent of targeted immunotherapies aimed at reducing the frequency and severity of attacks. Among several off-label therapies for NMOSD, rituximab is widely used as a therapeutic intervention as a chimeric monoclonal antibody that targets CD20-positive B-cells (4). However, not all patients respond adequately to rituximab, and some may experience breakthrough attacks, adverse events, develop resistance, or encounter reimbursement challenges (5).

Inebilizumab, a humanized and glycoengineered monoclonal antibody targeting CD19-positive B-cells, was approved for the treatment of $AQP4^+$ NMOSD based on the results of the N-MOmentum (NCT02200770) trial (6). As the largest global study ever conducted for NMOSD, this double-blind, placebo-controlled, randomized phase III trial enrolled 230 patients across multiple international sites to assess the efficacy and safety of inebilizumab in NMOSD patients.

With a primary endpoint focused on assessing the time to an adjudicated NMOSD attack, and secondary endpoints centered on disability progression, hospitalization rate, and quality of life, the randomized control period (RCP) of the N-MOmentum trial demonstrated a 77% reduction in the risk of attacks compared to placebo in the first 6.5 months. Notably, enrollment in the trial was halted prematurely based on the recommendation of the data-monitoring committee, which, recognizing clear evidence of efficacy, advised the early cessation of the study due to a conditional power exceeding 99% (6). The long-term data of the optional open label extension period (OLP) demonstrated a 97% attack risk reduction in patients that received ≥2.5 years of inebilizumab treatment compared to the placebo group in the RCP (6). An additional *post-hoc* analysis assessed the efficacy and safety in a small cohort of patients ($n = 17/230$) who were previously exposed to rituximab prior to initiating inebilizumab, with seven out of 17 having recorded breakthrough NMOSD attacks despite rituximab treatment, and four out of those seven experiencing more than one attack during their rituximab treatment course (7). The annualized attack rate of this cohort of participants with prior rituximab use decreased from 0.78 at baseline to 0.08 with inebilizumab treatment and was similar to the annualized attack rate of participants without prior rituximab use (0.10). Furthermore, none of the seven participants in the study who experienced breakthrough attacks while previously being treated with rituximab went on to experience an attack while taking inebilizumab. Inebilizumab may be effective in preventing attacks in NMOSD patients regardless of prior rituximab experience, and patients who experienced treatment failure or sub-optimal treatment with rituximab may still experience significant clinical benefits after initiating inebilizumab treatment (7). However, limited real-world data exist on the efficacy and safety of inebilizumab, particularly in patients who have transitioned from other treatments, such as rituximab.

This retrospective analysis evaluates the characteristics of patients who have transitioned from rituximab to inebilizumab and assesses the clinical changes that occur during and after the transition in a cohort of 14 NMOSD patients. We also examine the diagnosis, referral pathway, and medical history of these patients to better understand the potential characteristics of viable transition candidates in real-world utilization. Through this retrospective case series, our objective is to identify the drivers for switching from rituximab to inebilizumab treatment, to provide insights into the effectiveness and safety of inebilizumab in a real-world clinical setting, and to evaluate inebilizumab as a therapeutic alternative for NMOSD patients who do not adequately respond to or experience adverse events with rituximab.

2 Case presentation

A retrospective study of patients with NMOSD who had transitioned from rituximab to inebilizumab was designed. De-identified patient data including demographics (e.g., age, gender, and diagnoses), disease characteristics, referral pathways, treatment history, drivers of treatment decision making, and safety and efficacy outcomes were collected. The original case intake form is available (Supplementary material S1). Supporting magnetic resonance imaging (MRI) were aggregated for analysis. The study population was drawn from seven institutions in the United States (Supplementary material S2). A total of 14 patients met the inclusion criteria of being 18 years of age or older and having a diagnosis of NMOSD with a transition from rituximab to inebilizumab treatment (either immediately or after a treatment gap) with at least one dose of administered inebilizumab.

Permissible conditions included patients who were on a combination of rituximab and other treatments [e.g., mycophenolate mofetil (MMF)] prior to transitioning to inebilizumab, and treatment gaps between rituximab and inebilizumab were permissible provided no *new* long-term immunosuppressants or biologics were introduced during the gap. Any dosing intervals extending beyond 6 months after rituximab cessation were documented but did not lead to exclusion. In addition, AQP4 antibody status was not a factor for exclusion. Patients who, *after* discontinuing rituximab, started and remained on other long-term immunosuppressants [e.g., azathioprine (AZA), MMF] or biologics (e.g., eculizumab) before starting inebilizumab were excluded from further analysis.

Descriptive statistics summarized patient characteristics and clinical outcomes. Continuous variables were reported as means, while categorical variables were reported as frequencies and percentages. Outcome measures included changes in NMOSD attack rate, expanded disability status scale (EDSS) score, and transition-related adverse events. Clinical evaluation, patient medical history, clinical course, patient symptoms/neurological deficits, treatment and monitoring with rituximab or inebilizumab, and patient-reported outcomes and clinical observations were all recorded for each case report.

2.1 Patient demographics

Of the 14 patients examined, the majority identified as female (78.6%, $n = 11$) and Black or African American (57.1%, $n = 8$). Two (14.3%) reported to be of Hispanic or Latino ethnicity. The mean age at the onset of the first NMOSD symptom was 37.8 years, ranging between 18 and 62 years; however, details for four patients remain undisclosed (Table 1).

2.2 Referral patterns

Referrals to the treating physician were predominant (85.7%) and primarily from general neurologists (42.8%, $n = 6$) and emergency room visits (21.4%, $n = 3$). Half of the patients (50%, $n = 7$) were already receiving treatment at the time of referral (Table 1).

2.3 Clinical characteristics

Among the patients, 92.9% ($n = 13$) were AQP4 seropositive. While 78.6% ($n = 11$) were diagnosed using a cell-based assay (CBA), one patient (7.1%, $n = 1$) was identified as seropositive through the enzyme-linked immunosorbent assay (ELISA). The remaining patient, identified as AQP4 seronegative with indeterminate myelin oligodendrocyte glycoprotein (MOG) test results, met the criteria outlined by the International Panel for Neuromyelitis Optica Diagnosis (IPND) for seronegative NMOSD, and the physician made the decision to treat the patient off-label with inebilizumab. This diversity in serological profiles underscores the nuanced diagnostic landscape within the study cohort (Table 1).

Diagnoses were made between January 2011 and November 2021. Optic neuritis (ON) and transverse myelitis (TM) emerged as the leading clinical features, present in 42.9% ($n = 6$) and 71.4% ($n = 10$) of patients, respectively. Among TM diagnoses, more than three vertebral segments were involved in 80.0% ($n = 8$). Cases also included Area Postrema Syndrome (APS) in 14.3% ($n = 2$) and Acute Brainstem Syndrome in 7.1% ($n = 1$, Table 1).

2.4 Historical treatment (excluding rituximab)

From symptom onset, the average time to NMOSD diagnosis was 2.4 years (28.8 months), with some diagnosed at time of first attack and others taking up to 10.2 years (ranging from 0 to 122 months). Notable autoimmune comorbidities were found in two patients: Hashimoto's thyroiditis ($n = 1$) and systemic lupus erythematosus ($n = 1$). Other patients had histories of varied treatments, including corticosteroids, plasma exchange (PLEX), intravenous immunoglobulin (IVIG) ($n = 7$), oral immunosuppressants such as AZA or MMF ($n = 7$), and one with a prior CD20 therapy ($n = 1$, Table 1).

Between 2008 and 2022, the cohort recorded a total of 31 attacks. These comprised ON only ($n = 7$), TM only ($n = 11$), both ON and TM ($n = 7$), APS ($n = 1$), APS combined with TM ($n = 1$), and other manifestations like seizure, encephalopathy, ataxia, brainstem syndrome, and lower extremity leg weakness ($n = 4$, Table 1). The manifestation of lower extremity leg weakness was distinct and not attributed to transverse myelitis (TM).

2.5 Treatment and monitoring with rituximab

Five patients were treatment naïve prior to initiating rituximab. For those on prior therapy ($n = 9$), the average time from diagnosis to first rituximab infusion was 23.6 months. The average duration of rituximab treatment was 38.6 months (approximately 3.2 years), with individual durations spanning from 3 to 84 months (0.3–7 years). All patients ($n = 14$) underwent rituximab infusions biannually at a dosage of 1,000 mg every 6 months (Table 2).

Two patients received rituximab in conjunction with other immunosuppressive therapies, which included IVIG due to hypogammaglobulinemia ($n = 1$) or MMF ($n = 1$). Corticosteroids were utilized concurrently by 28.6% ($n = 4$) of the cohort, with durations spanning from less than 4 weeks ($n = 3$) to over 12 weeks ($n = 1$, Table 2).

Throughout the rituximab treatment period, 17 total attacks were documented in 71.4% ($n = 10$) of the patients. These attacks were primarily attributed to breakthrough disease ($n = 10$) and treatment delays ($n = 7$, Table 2). Across the six patients who experienced breakthrough disease on rituximab treatment, the average duration of rituximab treatment at the time of any NMOSD attack was about 26.5 months. However, when focusing on the final attack only (considering patients may have experienced more than one attack), the average duration was approximately 22.5 months. The average duration of treatment delay with rituximab was approximately 48 months among the four patients included in the analysis. In total, seven treatment delays were recorded, with an average treatment delay of 27 months (range: 2–55 months) across all patients. Breakthrough disease events and treatment delays are elaborated upon in Supplementary material S3, S4.

Overall, two patients were reported to have experienced rituximab infusion-related reactions despite the administration of pre-infusion medications, which included symptoms such as encephalopathy, brain fog, headache, itchy throat, and itchy face. Infections were reported in one patient, specifically mild urinary tract infections, which were resolved with appropriate antibiotic treatment.

Monitoring of patients involved routine assessments of IgG, IgM, and B-cell depletion, complemented by occasional evaluations like complete blood count (CBC) and a comprehensive metabolic panel (CMP). The frequency of these tests varied, ranging from an "as-needed" basis to annual assessments.

Imaging techniques, including MRI of the brain, spine, optic orbits, and computed tomography (CT) scans of the spine and brain, were employed to track disease progression and evaluate treatment efficacy (Figure 1). The frequency of these imaging assessments was patient-specific, occurring either annually, biannually, or as needed.

Clinical symptomatology was monitored, encompassing motor, visual, and sensory functions, and specific symptoms like leg spasms, clonus, hemiparesis, numbness, burning sensations, and vision complications. Some patients underwent additional ophthalmological exams and standard neurological evaluations, including the Timed 25-Foot Walk (T25-FW) and the 9-Hole Peg Test.

TABLE 1 Patient demographics, journey to diagnosis, clinical evaluation, and medical history; $N = 14$.

Demographics		Patients *n* (%)
Gender	Female	11 (78.6%)
	Male	1 (7.1%)
	N/A (not available)	2 (14.3%)
Age at first symptom onset	Range: 18–62 years old	10 (71.4%)
	Mean: 37.8 years	
	N/A (not available)	4 (28.6%)
Race	Black or African American	8 (57.1%)
	White	5 (35.7%)
	Other	1 (7.1%)
Residence (state)	Maine (ME)	1 (7.1%)
	Kentucky (KY)	1 (7.1%)
	Georgia (GA)	1 (7.1%)
	Washington D.C. (D.C.)	3 (21.4%)
	New York (NY)	4 (28.6%)
	Illinois (IL)	2 (14.3%)
	Virginia (VA)	2 (14.3%)
Occupation	Retired/Disability	1 (7.1%)
	Nursing/Disability	1 (7.1%)
	Retail/Cashier	1 (7.1%)
	Unemployed	1 (7.1%)
	N/A (not available)	10 (71.4%)
Journey to NMOSD diagnosis		Patients *n* (%)
Referred to treating HCP	Referred	12 (85.7%)
	Referral sources:	
	General Neurologists	6 (42.8%)
	Primary Care Physicians	2 (14.3%)
	Emergency Rooms	3 (21.4%)
	Neuro-ophthalmologists	1 (7.1%)
	N/A (not available)	2 (14.3%)
Patient already diagnosed upon referral	Yes	11 (78.6%)
	General Neurologist	7 (50.0%)
	Ophthalmologist	1 (7.1%)
	Neuro-ophthalmologist	1 (7.1%)
	Neuro-oncologist	1 (7.1%)
	MS Specialist	1 (7.1%)
	No	1 (7.1%)
	N/A (not available)	2 (14.3%)
Referred for a second opinion	Referred	5 (35.7%)
	Not referred	7 (50.0%)
	N/A (not available)	2 (14.3%)
Treatment status at the time of referral	Already receiving treatment	7 (50.0%)
	Not receiving treatment	7 (50.0%)
Continuity of care	Patients that have their case report-submitting physician continuing as their current treating physician	14 (100%)

(Continued)

TABLE 1 (Continued)

Demographics		Patients *n* (%)
Clinical evaluation		Patients *n* (%)
AQP4 seropositivity	Seropositive	13 (92.9%)
	Seronegative	1 (7.1%)
Serologic testing dates	Ranged from 01/01/2011 to 12/20/2022	9 (64.3%)
	Not available	5 (35.7%)
AQP4 test method	Cell based assay (CBA)	11 (78.6%)
	ELISA and CBA	1 (7.1%)
	ELISA	1 (7.1%)
	Not available	1 (7.1%)
MOG testing results	Seronegative/indeterminate/low titer	1 (7.1%)
	Not available	13 (92.9%)
NMOSD diagnoses	Occurred between 01/01/2011 and 11/01/2021	14 (100%)
Core clinical characteristics	Optic neuritis (ON)	6 (42.9%)
	Transverse myelitis (TM)	10 (71.4%)
	TM involving ≥3 vertebral segments	8 (80.0%)
	Area postrema Syndrome (APS)	2 (14.3%)
	Acute brainstem syndrome	1 (7.1%)
Imaging files taken	Yes	11 (78.6%)
	No	3 (21.4%)
Medical history (Prior to transitioning to rituximab)		Patients *n* (%)
Time from symptom onset to diagnosis	Mean: 28.8 months (2.4 years)	14 (100%)
	Range: 0–122 months (0–10.2 years)	
Autoimmune comorbidities	Hashimoto's thyroiditis disease	1 (7.1%)
	Systemic lupus erythematosus	1 (7.1%)
Previous NMOSD treatment history	No previous treatment	5 (35.7%)
	Previously treated with Steroid, PLEX, or IVIG	7 (50.0%)
	Previously treated with oral ISTs (AZA or MMF)	7 (50.0%)
	CD20 Agent	1 (7.1%)
First-line treatment (Mean duration: 2.9 years)	Intravenous Methylprednisolone	3 (21.4%)
	Azathioprine (AZA)	2 (14.3%)
	Mycophenolate Mofetil (MMF)	2 (14.3%)
	Intravenous immunoglobulin (IVIG)	1 (7.1%)
	Plasma exchange (PLEX)	1 (7.1%)
Second-line treatment (Mean duration: 3.22 years; 0–9.54 years)	Prednisone	3 (21.4%)
	Plasma exchange (PLEX)	1 (7.1%)
	Mycophenolate Mofetil (MMF)	1 (7.1%)
Reasons for discontinuation of treatment	Breakthrough disease	5 (35.7%)
	Worsening symptoms	2 (14.3%)
	Insurance	1 (7.1%)

(Continued)

TABLE 1 (Continued)

Demographics		Patients *n* (%)
Attacks between 2008 and 2022	Total number of attacks	31 (100%)
	Optic neuritis (ON)	7 (22.6%)
	Transverse myelitis (TM)	11 (35.5%)
	ON and TM	1 (7.1%)
	Area postrema syndrome (APS)	1 (7.1%)
	APS combined with TM	7 (22.6%)
	Other (encephalopathy, ataxia, brainstem syndrome, and lower extremity leg weakness)	4 (12.9%)
Patient symptoms/neurological deficits; *N* = 14		
Symptoms	Category	Patients *n* (%)
Visual Acuity (OD, right eye)	Visual	5 (35.7%)
Visual Acuity (OS, left eye)	Visual	2 (14.3%)
Double vision	Visual	1 (7.1%)
Neuropathic pain	Motor/Sensory	9 (64.3%)
Gait impairment	Motor/Sensory	11 (78.6%)
Numbness	Motor/Sensory	4 (28.6%)
Paresis/Paralysis	Motor/Sensory	6 (42.9%)
Spasticity	Motor/Sensory	4 (28.6%)
Spasms	Motor/Sensory	4 (28.6%)
Fatigue	Other	6 (42.9%)
Headache	Other	4 (28.6%)
Depression	Other	3 (21.4%)
Anxiety	Other	2 (14.3%)
Speech deficiencies	Other	1 (7.1%)
Loss of coordination	Other	1 (7.1%)
Loss bowel/ bladder control	Other	3 (21.4%)
Brain fog	Other	2 (14.3%)
Seizure	Other	1 (7.1%)
Difficulty swallowing	Other	1 (7.1%)
Vitamin B12 deficiency	Other	1 (7.1%)
Mood changes*	Other	1 (7.1%)

*Mood changes refers to a case of paranoid delusional disorder confirmed by psychiatry. n, number; %, percentage; HCP, Health care professional; NMOSD, Neuromyelitis optica spectrum disorder; AQP4, Aquaporin 4; MOG, Myelin oligodendrocyte glycoprotein; ELISA, Enzyme-linked immunosorbent assay; CBA, Cell-based assay; ON, Optic neuritis; TM, Transverse myelitis; PLEX, Plasma exchange; IVIG, Intravenous immunoglobulin; ISTs, Immunosuppressants; AZA, Azathioprine; MMF, Mycophenolate mofetil.

Lastly, adverse events such as hypogammaglobulinemia, infusion-related reactions, coagulopathies, and infections were monitored. The monitoring frequencies for these adverse events were patient-specific, with intervals ranging from quarterly to annual assessments.

2.6 Treatment and monitoring with inebilizumab

Among the 14 patients transitioning from rituximab to inebilizumab, 42.9% ($n = 6$) did so due to breakthrough disease. For 50.0% ($n = 7$), personal preference was the deciding factor, with one patient specifically valuing inebilizumab for its home infusion option. Among these, the Federal Drug Administration (FDA) approval of inebilizumab for AQP4$^+$ NMOSD influenced the decision for 42.9% ($n = 6$). Treatment delay with rituximab prompted the change to inebilizumab for one patient (Table 2).

When transitioning from rituximab to inebilizumab, 21.4% ($n = 3$) did so within 3 months, 50.0% ($n = 7$) transitioned between 4 and 6 months, and 28.6% ($n = 4$) transitioned after 6 months relative to their prior rituximab infusion. For inebilizumab loading doses, four patients (28.6%) received one dose while 10 patients (71.4%) received two doses (Table 3). For context, the dosing regimen in the N-MOmentum trial prescribed a 300 mg IV dose on day 1 and another on day 15 as part of the loading phase, followed by 300 mg maintenance doses every 6 months thereafter. On average, inebilizumab treatment duration spanned approximately 19.3 months, with a median of 19 months and individual treatment durations ranging from 9 to 35 months.

Apart from the pre-infusion steroid administration, there were no reports of concurrent corticosteroid administration or corticosteroid tapering during the initiation of the inebilizumab loading phase. Among the 14 participants, no infusion-related reactions or infections were reported. Notably, one patient continued with MMF during the transition (but discontinued after the second dose of inebilizumab, Supplementary material S4).

Laboratory assessments were performed on various immunological markers, with IgG, IgM, and B-cells being the most common. Assessments were conducted either once to date, every 6 months (most common), or every 6 months to 1 year. All of the patients (100%, $n = 4$) who tested for B-cell enumeration reported undetectable levels of CD19+ B-cells (Table 3).

During treatment, neurological symptoms were evaluated such as visual acuity, eye pain, headaches, weakness, numbness, leg spasms, clonus, left-side weakness, burning sensations, vision issues, hemiparesis, tongue paralysis, and dysphagia. Diagnostic tests including the T25-FW and the 9-Hole Peg Test were administered to assess neurological function and mobility. Additionally, imaging studies, predominantly MRI scans of the brain and thoracic regions, were conducted using varied protocols to evaluate structural changes and abnormalities. The frequency of imaging ranged from once to date to once annually, with some patients receiving imaging on an as-needed basis.

Adverse events monitored during treatment included infusion reactions, opportunistic infections, hypogammaglobulinemia, and coagulopathies. The frequency of adverse event evaluations varied but were reported to be with each infusion ($n = 1$), every 6 months ($n = 2$), or every 8–9 months ($n = 1$). For 10 patients, adverse event information was either not evaluated or unavailable at the time of the survey, as determined from the retrospective chart review (Table 3).

2.7 Patient reported outcomes and clinical observations with inebilizumab

Upon evaluating 14 NMOSD patients who transitioned to inebilizumab, we found that none experienced attacks during the

inebilizumab treatment phase. Additionally, there were no reported modifications to ongoing treatments after the initiation of inebilizumab.

To highlight the therapeutic impact of inebilizumab, we systematically documented relevant clinical observations. Regarding disability assessments, three patients (21.4%) underwent evaluations using EDSS, and all three documented a 0.5-point improvement. Evaluations using the T25-FW and the 36-Item Short Form Survey (SF-36) scales, were each conducted for two patients (14.3%) with varied results. A notable case involved a patient who exhibited a pronounced improvement in the T25-FW assessment, while two others showed minimal or indeterminate changes on the SF-36 scale. Moreover, a majority of the cohort (71.4%, $n = 10$) were assessed for Activities of Daily Living and Quality of Life (ADL/QOL). Of these, six patients (60.0%) exhibited improved daily life quality and functionality (Table 3).

Subsequently, we documented patient-reported outcomes. Seven of the participants (50.0%) indicated alterations in their NMOSD symptoms after the transition. Six of the seven patients reported marked symptomatic improvements. For instance, one patient highlighted enhanced gait symptoms after a 5-month period, while another noted a considerable improvement in gait over 20 months. One patient (7.1%) reported exacerbated symptoms such as neuropathic pain, burning, spasticity, and sleepiness. However, their SF-36 score was improved at the 12-month mark. This patient was uniquely diagnosed with seronegative NMOSD with a complex medical history (Table 3).

TABLE 2 NMOSD patients on rituximab: clinical outcomes and treatment experiences; $N = 14$.

Clinical outcomes and treatment experiences		
Category	Details/Notes	Patients *n* (%)
Average treatment duration (months)	Mean: 38.6 months (3.2 years)	14 (100%)
	Range: 3 months–84 months (0.3–7 years)	
Infusion reactions	Encephalopathy, brain fog, headache, itchy throat, itchy left face	2 (14.3%)
Dosing changes due to incomplete B-cell depletion	Yes	0 (0%)
	No	14 (100%)
Infections	None	12 (85.7%)
	Unknown	1 (7.1%)
	Mild urinary tract infections	1 (7.1%)
Rituximab + Other IST	No	12 (85.7%)
	IVIG for low antibody levels	1 (7.1%)
	Mycophenolate mofetil (MMF)	1 (7.1%)
Concurrent steroid use	Yes	4 (28.6%)
	Treatment duration <4 weeks	3 (75.0%)
	Treatment duration >12 weeks	1 (25.0%)
Attacks	Reported patients	10 (71.4%)
	Total attacks across reported patients	17
	Reported causes:	
	Breakthrough disease	10 (58.8%)
	Treatment delay	7 (41.2%)
Catalyst for transitioning to inebilizumab	Breakthrough disease	6 (42.9%)
	Patient preference	7 (50.0%)
	Requested home infusion	1 (7.1%)
	FDA approved and superior clinical efficacy	6 (42.9%)
	Treatment delays	1 (7.1%)

n, number; %, percentage; OS, Oculus sinister-left eye; OD, Oculus dexter-right eye; Min, Minimum; Max, Maximum; IST, Immunosuppressant; IVIG, Intravenous immunoglobulin; MMF, Mycophenolate mofetil.

3 Discussion

The advent of targeted therapies has significantly transformed the treatment paradigm for NMOSD. While rituximab is frequently used off-label for NMOSD, inebilizumab, which targets CD19-positive B-cells and is FDA-approved for AQP4$^+$ NMOSD, has proven efficacy in reducing NMOSD attacks as evidenced in a pivotal randomized controlled trial (6). Recent research underscores the central role of CD19+ plasmablasts in neuroimmunology disorders, suggesting that their migration into the central nervous system and function as auto-antibody producers could have implications for the observed therapeutic response in NMOSD patients transitioning from rituximab to inebilizumab (8).

Genetic considerations further differentiate rituximab from inebilizumab. Specifically, rituximab-treated patients carrying the *FCGR3A-F* allele have been shown to have a heightened risk of relapse (9). In contrast, inebilizumab-treated participants in the N-MOmentum trial displayed consistent outcomes irrespective of the *FCGR3A* genotype, reinforcing the drug's targeted efficacy (10). The absence of neutralizing anti-drug antibodies (ADA) with inebilizumab additionally offers a significant advantage, ensuring sustained drug activity and reduced immunogenic reactions.

Our comprehensive analysis of 14 patients transitioning from rituximab to inebilizumab provides valuable insights into its real-world application, efficacy, and safety. Notably, none of these patients, even those who previously had disease breakthroughs on rituximab, experienced attacks under inebilizumab, echoing findings from the N-MOmentum trial. Prior real-world studies reporting on the treatment transition to inebilizumab in NMOSD are scarce. A published retrospective study of medical records in 164 AQP4+ NMOSD patients revealed that transitions from one therapy to the next may be associated with an increased relapse rate if done for "non-medical" reasons; however, these patients had an average of approximately 3 months of washout between medications (range 1–2,810 days) (11).

As a promising and versatile therapeutic agent, the introduction of inebilizumab has shown optimistic results for NMOSD patients. Most patients reported symptom relief and stable disability scores, underscoring the need for individualized care and consistent monitoring. The preference expressed by patients toward inebilizumab underlines the importance of patient-centric care in decision making. As the NMOSD therapeutic landscape evolves, ensuring patients are well-informed and involved in treatment

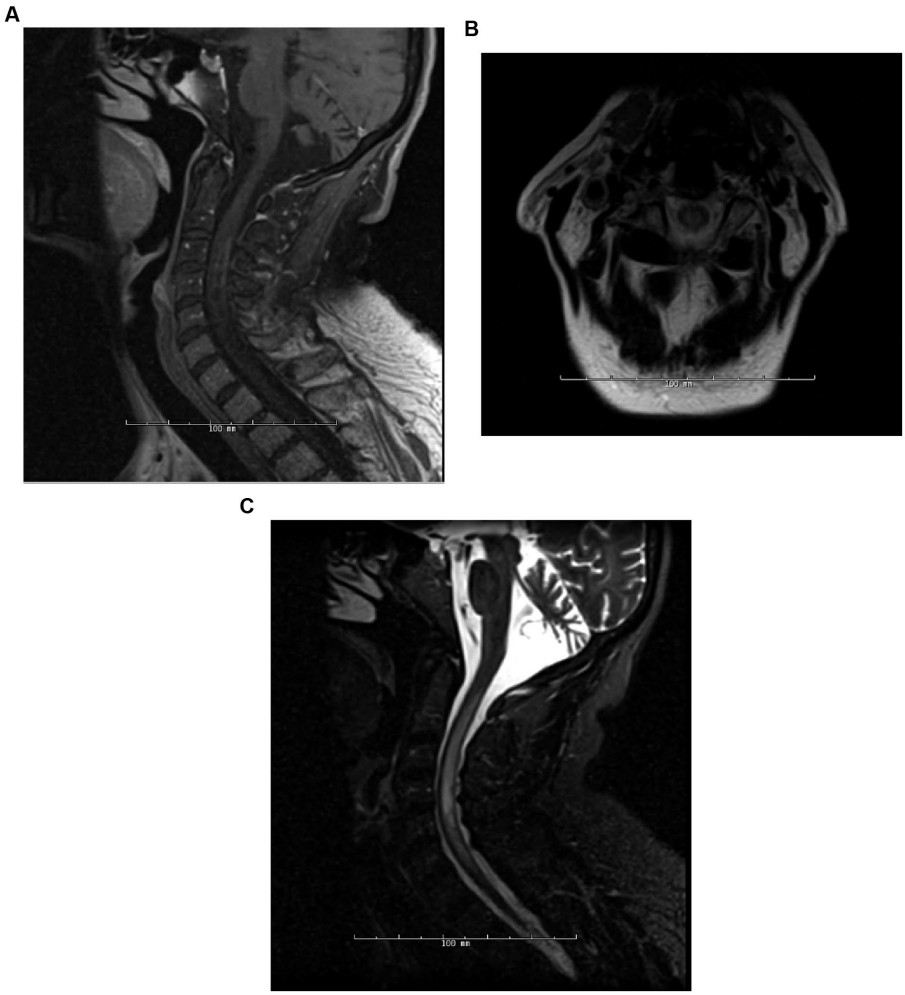

FIGURE 1
Patient 5 (*detailed under "breakthrough disease"* in Supplementary material S3), 6 months post-initiation of rituximab treatment, the patient manifested an attack, encompassing both TM and encephalopathy, with a concurrent CD19+ B-cell count of 3%. MRI assessments during this episode included Sagittal T1-post contrast **(A)**, Axial T2 **(B)**, and Sagittal STIR **(C)** of the spine.

decisions is critical. This sentiment suggests that beyond mere clinical outcomes, factors such as administration methods, treatment frequency, side effects, and individual perceptions significantly influence treatment choices. Furthermore, our study spotlighted a pressing real-world challenge: treatment disruptions due to insurance complications. Such disruptions can have severe ramifications on patient health and can inflate healthcare costs, emphasizing the need for uninterrupted access to transformative therapies and comprehensive discussions between healthcare providers, insurers, and policymakers.

Though insightful, our study possesses limitations characteristic of retrospective analyses, such as potential selection biases and the absence of a control group. It is important to note that the dataset used is partially incomplete, which may affect the robustness of our conclusions. Additionally, the modest sample size and the relatively short follow-up duration necessitate a careful interpretation of the findings. Furthermore, monitoring of B cell depletion and quantitative serum immunoglobulin levels are important during treatment with inebilizumab and this information would have provided additional support for our findings of the response to treatment.

4 Conclusion

Neuromyelitis optica spectrum disorder is a debilitating neurological condition that demands effective and consistent therapeutic strategies. Our retrospective analysis highlights the potential of inebilizumab as a valuable treatment option, especially for patients who may not derive optimal outcomes with rituximab.

However, as with all therapies, individualized care is paramount. The variability in patient responses emphasizes the importance of continued monitoring and patient-centric decision-making. Furthermore, challenges such as treatment interruptions due to insurance barriers highlight the need for a more integrated approach to patient care, encompassing both clinical and socio-economic facets.

In conclusion, while inebilizumab offers potential advantages for NMOSD patients, achieving optimal patient outcomes is a multi-dimensional endeavor. This journey mandates the concerted efforts of clinicians, researchers, patients, and policymakers. The pursuit for more comprehensive data and a deeper understanding persists, all aimed at enhancing the quality of life for those impacted by NMOSD.

TABLE 3 NMOSD patients on inebilizumab: treatment and monitoring, patient reported outcomes, and clinical observations; $N = 14$.

Treatment and monitoring		
Category	Subcategory	Patients *n* (%)
Transition period: time from last rituximab dose to first inebilizumab dose (months)	< 3 months	3 (21.4%)
	4–6 months	7 (50.0%)
	>6 months	4 (28.6%)
Other treatment between transition?	Yes—MMF	1 (7.1%)
	No	13 (92.9%)
Number of loading doses	One loading dose	4 (28.6%)
	Two loading doses	10 (71.4%)
Duration of inebilizumab use	< 6 months	0 (0.0%)
	6–12 months	1 (7.1%)
	13–24 months	11 (78.6%)
	> 24 months	2 (14.3%)
Infusion reactions	Yes	0 (0.0%)
	No	14 (100.0%)
Combined with immunosuppressants?	Yes—MMF	1 (7.1%)
	No	13 (92.9%)
Concurrent steroid use (including corticosteroid taper)?	Yes	0 (0.0%)
	No	14 (100.0%)
Frequency of lab assessments (IgG, IgM, and B-cell counts)	Once to date	1 (7.1%)
	Every 6 months	4 (28.6%)
	Every 6–12 months	3 (21.4%)
	Unknown	6 (42.9%)
CD19+ B cell levels	Negligible/Zero	14 (100.0%)
Frequency of imaging (MRI of brain, thoracic, cervical, and orbits)	As needed	1 (7.1%)
	Once to date	4 (28.6%)
	Every 6 months	1 (7.1%)
	Every 12 months	1 (7.1%)
	Unknown	7 (50.0%)
Frequency of adverse event evaluations (hypogammaglobulinemia, infusion-related reactions, infections, and coagulopathies)	Every infusion	1 (7.1%)
	Every 6 months	2 (14.3%)
	Every 8–9 months	1 (7.1%)
	Not mentioned/unknown	10 (71.4%)
Attacks while on inebilizumab treatment	Yes	0 (0.0%)
	No	14 (100.0%)
Chronic treatment adjustments made	Yes	0 (0.0%)
	No	14 (100.0%)
Patient reported outcomes and clinical observations; $N = 14$		
Category	Description	Patients *n* (%)
Patients reporting NMOSD changes	Reported patients	7 (50.0%)
	Improvement of symptoms[a]	6 (42.9%)
	Worsening of symptoms[b]	1 (7.1%)
Disability scales measured	EDSS	3 (21.4%)
	T25-FW	2 (14.3%)
	SF-36	2 (14.3%)
Patients with improved disability	EDSS	3 (21.4%)
	T25-FW	1 (7.1%)
	SF-36	0 (0.0%)
Patients with minimal/uncertain disability change	T25-FW	1 (7.1%)
	SF-36	2 (14.3%)
Activities of daily living/Quality of life (ADL/QOL) outcomes measured	Reported patients	10 (71.4%)
	Positive trends	6 (42.9%)
	Uncertain trends	4 (28.6%)
Improvements in symptoms[a]	Gait symptoms	4 (28.6%)
	General comfort and no new weakness	1 (7.1%)
	Upper extremity function	1 (7.1%)
Worsening symptoms[b]	Neuropathic pain, burning, spasticity, and sleepiness	1 (7.1%)

[a]Improvements in symptoms; Patient 1: saw mild improvement of gait symptoms after 5 months of inebilizumab exposure (EDSS baseline: 6.5, follow up: 6). Patient 2: saw mild improvement of gait symptoms after 7 months of inebilizumab exposure (EDSS baseline; 6, follow up 5.5). Patient 3: saw mild improvement of gait symptoms after 11 months of inebilizumab exposure (EDSS baseline: 6.5, follow up 6). Patient 4: noted improved symptomatology after 9 months of inebilizumab exposure—general feeling well, no new weakness. Patient is pleased with being on it and noted more comfortable than being on RTX. Patient 5: noted improved function in upper extremities after 4 months of inebilizumab exposure. Patient 6: noted improvement of gait symptoms after 20 months of inebilizumab exposure [T25-FW; Baseline: 33.7; Follow Up: 6.7 (11/2022)]. [b]Worsening symptoms; despite a slight improvement recorded in SF-36 (baseline: 6; follow up: 5) after 12 months of inebilizumab exposure, one patient case reported subjective worsening of symptoms including neuropathic pain, burning, spasticity, and sleepiness. Of note, the patient was diagnosed with seronegative NMOSD (the only seronegative participant in this case series) and has been reported to include the following medical history: stroke, CKD, migraines, Hepatitis B, depression, anxiety, obesity (gastric bypass), MGUS, hypothyroidism (thyroidectomy 2000), COPD, and myelodysplastic syndrome. n, number; %, percentage; NMOSD, Neuromyelitis optica spectrum disorder; EDSS, Expanded disability status scale; T25-FW, Timed 25-foot walk test; SF-36, 36-item short-form health survey; ADL, Activities of daily living; and QOL, Quality of life.

Data availability statement

The datasets presented in this article are not readily available because of ethical and privacy restrictions. Requests to access the datasets should be directed to the corresponding author.

Ethics statement

Ethical review and approval was not required for the study on human participants in accordance with the local legislation and institutional requirements. Written informed consent from the patients/participants or patients/participants' legal guardian/next of kin was not required to participate in this study in accordance with the national legislation and the institutional requirements. Written informed consent was obtained from the individual(s) and/or

minor(s)' legal guardian/next of kin for the publication of any potentially identifiable images or data included in this article.

Author contributions

BO: Data curation, Writing – review & editing. GR: Data curation, Writing – review & editing. JH: Data curation, Writing – review & editing. MZ: Data curation, Writing – review & editing. TD: Data curation, Writing – review & editing. TK: Data curation, Writing – review & editing. UO: Data curation, Writing – review & editing. JP: Conceptualization, Data curation, Formal Analysis, Investigation, Methodology, Project administration, Supervision, Writing – original draft, Writing – review & editing. KP: Conceptualization, Data curation, Formal Analysis, Investigation, Methodology, Project administration, Resources, Supervision, Writing – original draft, Writing – review & editing. ML: Data curation, Investigation, Writing – review & editing.

Funding

The author(s) declare financial support was received for the research, authorship, and/or publication of this article.

Acknowledgments

Medical writing and editorial support were provided by Amy Cohen, PhD of Horizon Therapeutics (now Amgen). Support for data reconciliation was provided by Delisa Clay of Horizon Therapeutics (now Amgen).

Conflict of interest

BO is currently compensated as a speaker for Alexion, Genentech, and Horizon Therapeutics (now Amgen); has received personal compensation from Biogen as a speaker; currently receives royalties from UpToDate for chapters authored on optic neuritis; has received personal compensation for participation in advisory boards from both Alexion and Horizon Therapeutics. MH has received research support from Sanofi, Roche, and Novartis; has served on scientific advisory boards for Horizon Therapeutics, Alexion, EMD Serono, and Roche/Genentech; currently a speaker for Horizon Therapeutics (now Amgen), Alexion, EMD Serono, Biogen, and TG Therapeutics. MZ currently receives personal compensation as a speaker for Horizon Therapeutics (now Amgen) and Biogen. TD has received personal compensation as a speaker for Teva; currently receives personal compensation as a speaker for Horizon Therapeutics (now Amgen) and Biogen. TK has received personal compensation as a speaker for Horizon Therapeutics, Biogen, TG Therapeutics, and EMD Serono; for participating in advisory boards for Horizon Therapeutics, TG Therapeutics, Sanofi, Genentech, Bristol Myers Squibb, Octave Bio, and Genzyme. UO has received consulting fees from Horizon Therapeutics and Genentech. ML currently receives personal compensation for advising the following companies: Alexion, Horizon Therapeutics (now Amgen), Genentech/Roche, UCB, Sanofi, and Mitsubishi. Through Mass General, ML received grants from Alexion, Horizon, Genentech, Roche, UCB, and Sanofi for research projects. JP and KP are employees of Horizon Therapeutics and own stock.

The remaining author declares that the research was conducted in the absence of any commercial or financial relationships that could be construed as a potential conflict of interest.

The authors declare that the N-MOmentum trial was funded by MedImmune/AstraZeneca and Viela Bio (now part of Horizon Therapeutics). The funder had the following involvement in the study: Horizon Therapeutics (now Amgen) supported the development of this manuscript and provided data analyses according to the direction of the authors.

Publisher's note

Supplementary material

The Supplementary material for this article can be found online at: https://www.frontiersin.org/articles/10.3389/fneur.2024.1352779/full#supplementary-material

References

1. Wingerchuk DM, Banwell B, Bennett JL, Cabre P, Carroll W, Chitnis T, et al. International consensus diagnostic criteria for neuromyelitis optica spectrum disorders. *Neurology*. (2015) 85:177–89. doi: 10.1212/WNL.0000000000001729

2. Huda S, Whittam D, Bhojak M, Chamberlain J, Noonan C, Jacob A. Neuromyelitis optica spectrum disorders. *Clin Med*. (2019) 19:169–76. doi: 10.7861/clinmedicine.19-2-169

3. Lennon VA, Kryzer TJ, Pittock SJ, Verkman AS, Hinson SR. IgG marker of optic-spinal multiple sclerosis binds to the aquaporin-4 water channel. *J Exp Med*. (2005) 202:473–7. doi: 10.1084/jem.20050304

4. Kim SM, Kim SJ, Lee HJ, Kuroda H, Palace J, Fujihara K. Differential diagnosis of neuromyelitis optica spectrum disorders. *Ther Adv Neurol Disord*. (2017) 10:265–89. doi: 10.1177/1756285617709723

5. Damato V, Evoli A, Iorio R. Efficacy and safety of rituximab therapy in Neuromyelitis Optica Spectrum disorders: a systematic review and Meta-analysis. *JAMA Neurol*. (2016) 73:1342–8. doi: 10.1001/jamaneurol.2016.1637

6. Cree BAC, Bennett JL, Kim HJ, Weinshenker BG, Pittock SJ, Wingerchuk DM, et al. Inebilizumab for the treatment of neuromyelitis optica spectrum disorder (N-MOmentum): a double-blind, randomised placebo-controlled phase 2/3 trial. *Lancet*. (2019) 394:1352–63. doi: 10.1016/S0140-6736(19)31817-3

7. Flanagan EP, Levy M, Katz E, Cimbora D, Drappa J, Mealy MA, et al. Inebilizumab for treatment of neuromyelitis optica spectrum disorder in patients with prior rituximab use from the N-MOmentum study. *Mult Scler Relat Disord*. (2022) 57:103352. doi: 10.1016/j.msard.2021.103352

8. Chihara N, Matsumoto R, Yamamura T. Plasmablasts and neuroimmunological disorders. *Immunol Med*. (2019) 42:103–7. doi: 10.1080/25785826.2019.1659476

9. Kim SH, Jeong IH, Hyun JW, Joung A, Jo HJ, Hwang SH, et al. Treatment outcomes with rituximab in 100 patients with Neuromyelitis Optica: influence of FCGR3A polymorphisms on the therapeutic response to rituximab. *JAMA Neurol*. (2015) 72:989–95. doi: 10.1001/jamaneurol.2015.1276

10. Weinshenker BG, Bennett JL, Cree BAC, Paul F, Kim HJ, Hartung HP, et al. Inebilizumab reduces attack risk independent of low affinity IgG fc region receptor III-A gene polymorphisms in neuromyelitis optica spectrum disorder (P13.5.015). *Neurology*. (2023) 100:1755. doi: 10.1212/WNL.0000000000202099

11. Okuda DT, Moog TM, McCreary M, Cook K, Burgess KW, Smith AD. Treatment transitions in neuromyelitis optica spectrum disorder increase risk for disease advancement. *Mult Scler Relat Disord*. (2023) 79:105041. doi: 10.1016/j.msard.2023.105041

frontiers | Frontiers in Immunology

TYPE Original Research
PUBLISHED 29 April 2024
DOI 10.3389/fimmu.2024.1370276

OPEN ACCESS

EDITED BY
Fawaz Alzaid,
Sorbonne Universités, France

REVIEWED BY
Xiaokuang Ma,
The University of Arizona College of Medicine – Phoenix, United States
Roopali Rajput,
Jamia Hamdard University, India

*CORRESPONDENCE
Hao Zhang
crrczh2020@163.com

RECEIVED 14 January 2024
ACCEPTED 16 April 2024
PUBLISHED 29 April 2024

CITATION
Long J, Dang H, Su W, Moneruzzaman M and Zhang H (2024) Interactions between circulating inflammatory factors and autism spectrum disorder: a bidirectional Mendelian randomization study in European population. *Front. Immunol.* 15:1370276. doi: 10.3389/fimmu.2024.1370276

Interactions between circulating inflammatory factors and autism spectrum disorder: a bidirectional Mendelian randomization study in European population

Junzi Long[1,2,3], Hui Dang[2,4], Wenlong Su[1,2], Md. Moneruzzaman[1,2] and Hao Zhang[1,2,3,4]*

[1]School of Rehabilitation, Capital Medical University, Beijing, China, [2]Department of Neurorehabilitation, China Rehabilitation Research Center, Beijing, China, [3]Division of Brain Sciences, Changping Laboratory, Beijing, China, [4]Cheeloo College of Medicine, Shandong University, Jinan, Shandong, China

Background: Extensive observational studies have reported an association between inflammatory factors and autism spectrum disorder (ASD), but their causal relationships remain unclear. This study aims to offer deeper insight into causal relationships between circulating inflammatory factors and ASD.

Methods: Two-sample bidirectional Mendelian randomization (MR) analysis method was used in this study. The genetic variation of 91 circulating inflammatory factors was obtained from the genome-wide association study (GWAS) database of European ancestry. The germline GWAS summary data for ASD were also obtained (18,381 ASD cases and 27,969 controls). Single nucleotide polymorphisms robustly associated with the 91 inflammatory factors were used as instrumental variables. The random-effects inverse-variance weighted method was used as the primary analysis, and the Bonferroni correction for multiple comparisons was applied. Sensitivity tests were carried out to assess the validity of the causal relationship.

Results: The forward MR analysis results suggest that levels of sulfotransferase 1A1, natural killer cell receptor 2B4, T-cell surface glycoprotein CD5, Fms-related tyrosine kinase 3 ligand, and tumor necrosis factor-related apoptosis-inducing ligand are positively associated with the occurrence of ASD, while levels of interleukin-7, interleukin-2 receptor subunit beta, and interleukin-2 are inversely associated with the occurrence of ASD. In addition, matrix metalloproteinase-10, caspase 8, tumor necrosis factor-related activation-induced cytokine, and C-C motif chemokine 19 were considered downstream consequences of ASD.

Conclusion: This MR study identified additional inflammatory factors in patients with ASD relative to previous studies, and raised a possibility of ASD-caused immune abnormalities. These identified inflammatory factors may be potential biomarkers of immunologic dysfunction in ASD.

KEYWORDS

autism spectrum disorder, inflammatory factors, inflammation, Mendelian randomization, single nucleotide polymorphisms, genome-wide association study

1 Introduction

Autism spectrum disorders (ASD) are defined as a group of neurodevelopmental conditions of childhood with environmental causes that are still not fully understood. Most environmental factors during the perinatal stage appear to converge into a series of inflammatory conditions, such as bacterial and viral infections and inflammatory bowel disease (1, 2), suggesting that inflammatory responses could be an underlying factor in the etiology of ASD. Large population-based epidemiological studies have linked ASD with autoimmune disease and abnormal blood levels of various inflammatory cytokines and immunological biomarkers (3, 4). For instance, previous studies on inflammatory biomarkers have found increased concentrations of pro-inflammatory factors IL-1β, IL-4, IL-6, IL-8, and TNF-α (5–8), as well as decreased concentrations of anti-inflammatory factors IL-10 and IL-1Ra (9) in the peripheral blood of patients with ASD. These abnormal inflammatory cytokine levels are linked to greater impairments in language function and social interaction in children with ASD (6, 8). Therefore, it is necessary to further identify inflammatory biomarkers in ASD and uncover the causality between ASD and changes in the levels of inflammatory factors.

Observational studies are often susceptible to confounding, reverse causation, and multiple biases, which can lead to unreliable findings regarding the causal effects of exposures on outcomes. The Mendelian randomization (MR) method provides an alternative approach to investigate causality in epidemiological research, by utilizing genetic variants as instrumental variables to determine whether a risk factor has a causal effect on a health outcome. As an individual's genotype is determined at conception and cannot be altered, this method avoids the reverse causality between genotype and outcome. In general, MR analysis rests on 3 assumptions: (1) genetic variants are associated with the risk factor; (2) genetic variants are not associated with confounders; and (3) genetic variants affect the outcome only through the risk factor (10). The advent of large-scale genome-wide association studies (GWAS) increases the accessibility of single-nucleotide polymorphisms (SNPs) as instrumental variables to infer causality in MR studies.

Based on the GWAS summary statistics, previous studies have examined causal relationships between 41 circulating inflammatory factors (11) and various complex diseases, including depression (12), epilepsy (13), and Alzheimer's disease (14). Recently, Zhao et al. (15) extended previous works by conducting a genome-wide protein quantitative trait locus study which identified the genetic architecture of 91 circulating inflammatory factors in 14,824 European-ancestry participants. Several recent studies have included these 91 inflammatory factors for MR analysis, which further extends the use of inflammatory factors in MR studies (16, 17). Although previous observational studies have found a strong association between changes in levels of some circulating inflammatory proteins and ASD (5–9), their causal relationships remain undefined. The number of inflammatory factors analyzed in these studies is also relatively limited. Based on the knowledge above, we conducted the first bidirectional two-sample MR analysis (SNPs associated with the exposure and outcome are individually obtained from two independent samples) to determine the causal relationship between 91 inflammatory factors and ASD. The inflammatory biomarkers identified in this work may provide the basis for an objective test for early and accurate diagnosis of ASD and may shed light on the etiology and pathogenesis of ASD.

2 Materials and methods

2.1 Study design and data sources

Figure 1 displays a schematic presentation of the study design. The data were obtained from the GWAS database and all included subjects had provided written informed consent in original research. The GWAS data sets for 91 circulating inflammatory factors are available in the GWAS Catalog (accession numbers from GCST90274758 to GCST90274848). These results come from a recent genome-wide protein quantitative trait locus study of 91 inflammation-related plasma factors in 14,824 European-ancestry participants (15). The genetic data on ASD were obtained from a genome-wide association meta-analysis of 18,381 ASD cases and 27,969 controls by Grove et al. (18) (OpenGWAS: ieu-a-1185). All participants were children born in Denmark between 1981 and 2005, diagnosed with ASD according to the 10th Revision of the International Classification of Diseases before 2014.

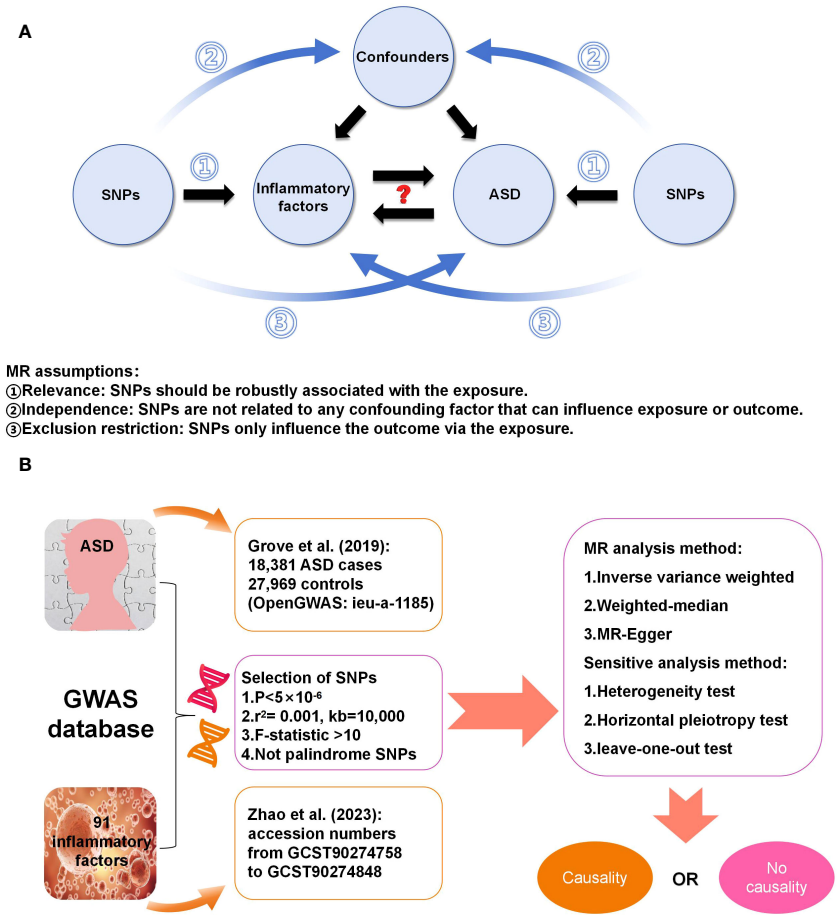

FIGURE 1
(A) Three assumptions in this MR study; **(B)** Workflow of this MR study.

2.2 Instrument selection

The SNPs strongly associated with inflammatory factors ($p < 5e{-}06$) were selected as instrumental variables. The linkage disequilibrium of these SNPs was removed using the clumping procedure in PLINK software (version v1.90), with the linkage disequilibrium parameter (r^2) < 0.001 and a distance threshold of 10,000 kilobases. The r^2 was calculated based on the 1000 Genomes Projects reference panel (Genomes Project C et al., 2012) (19). Additionally, we excluded palindrome SNPs and weak instrumental SNPs (F-statistics < 10). The F statistic was calculated by the following equation: $F = R^2 \times (N{-}k{-}1)/k \times (1 - R^2)$, where N is the sample size of the exposure factor, K is the number of instrumental variables, and R^2 is the proportion of variance explained by each instrumental variable. An F-statistic >10 typically indicates a strong correlation between instrumental variables and exposure factors (20).

2.3 Statistical analysis

Both statistical and sensitive analyses were conducted using the R software (version 4.2.1) and the "TwoSampleMR" R package (21, 22). The random-effects inverse variance weighted (IVW) method was employed as the main MR analysis to estimate causal effects, complemented by the weighted-median (WM) and MR-Egger methods to investigate potential pleiotropic effects. The IVW method can analyze individual Wald-type ratios of causal effects for each SNP, which provides the most accurate and unbiased causal estimates in the absence of horizontal pleiotropy (23). In the presence of horizontal pleiotropy, the WM method provides a consistent estimate even though half of the genetic variants are invalid instrumental variables (24). The estimation of causal effects of modifiable phenotypes on an outcome relies on the assumption of no pleiotropy, wherein genes solely influence the outcome via the given phenotype. If the genetic variants have a pleiotropic effect on the outcome, then the causal estimates may be biased. The MR-Egger regression intercept test was used to assess residual horizontal pleiotropy – intercepts around the zero indicate that SNPs do not have a direct effect on the outcome via the exposure (25). The Cochran's Q statistic was utilized to evaluate the heterogeneity of SNPs in both the IVW and MR Egger methods (21). The core assumption of MR is not contradicted even if there is significant heterogeneity in the instrumental variables. A p-value of less than 0.05 suggests the presence of horizontal pleiotropy and heterogeneity. The association of

individual SNPs was determined using leave-one-out sensitivity analysis to investigate whether the results were driven by any single SNP (26). For binary exposures, causal estimates were presented as odds ratio (OR) and 95% confidence interval (CI) per log-odds increment of genetic exposure risk. To account for multiple testing, a p-value of 0.00055 (0.05/91) was considered robust significance after the Bonferroni correction. A p-value between 0.00055 and 0.05 was deemed as suggestive evidence of potential causation. All statistical analyses were two-sided.

3 Results

3.1 Basic information about instrumental variables and exposures

After the selection of SNPs based on the criteria, a total of 1,815 SNPs related to 91 circulating inflammatory factors extracted from the GWAS database were used as instrumental variables (Supplementary Table S1). The basic information on 91 circulating inflammatory factors is summarized in Supplementary Table S2. Due to the large number of inflammatory factors and associated SNPs, in this section, we focus on the presentation of positive results in MR analysis. SNPs used in the positive results of both forward and reverse MR analysis are shown in Supplementary Tables S3, S4. This compilation includes information on chromosome location, effect allele, and effect allele frequency. Moreover, all SNPs had F statistics greater than 10, indicating that they were free of weak instrumental bias.

3.2 The causative impact of circulating inflammatory factors on ASD

The analysis results from IVW showed a statistically significant negative correlation between levels of interleukin-7 (IL-7) and ASD (OR = 0.858, 95% CI = 0.796 to 0.925, p = 6.69e-05). The results also showed possible positive associations between elevated levels of sulfotransferase 1A1 (SULT1A1) (OR = 1.109, 95% CI = 1.0423 to 1.181, p = 0.001), natural killer cell receptor 2B4 (CD244) (OR = 1.144, 95% CI = 1.040 to 1.259, p = 0.006), T-cell surface glycoprotein CD5 (CD5) (OR = 1.126, 95% CI = 1.028 to 1.233, p = 0.011), Fms-related tyrosine kinase 3 ligand (FLT3LG) (OR = 1.120, 95% CI = 1.013 to 1.238, p = 0.027), and tumor necrosis factor-related apoptosis-inducing ligand (TNFSF10) (OR = 1.093 95% CI = 1.009 to 1.184, p = 0.029) and an increased occurrence of ASD. Levels of interleukin-2 receptor subunit beta (IL2Rβ) (OR = 0.838, 95% CI = 0.749 to 0.936, p = 0.002), and interleukin-2 (IL-2) (OR = 0.874, 95% CI = 0.785 to 0.972, p = 0.013) were inversely associated with the risk of ASD. The results of the WM analysis for CD244 (OR = 1.150, 95% CI = 1.026 to 1.289, p = 0.016) and CD5 (OR = 1.181, 95% CI = 1.028 to 1.355, p = 0.018) also indicate a causal relationship with ASD, consistent with the trend observed in the IVW method. MR Egger analysis of all the inflammatory factors did not find any significant causal relationship with ASD. Figure 2 provide the results of the IVW, WM, and MR Egger analysis. None of the intercepts in the MR-Egger regression analysis significantly deviated from the zero (p > 0.05), suggesting no horizontal pleiotropy. Heterogeneity was observed only in TNFSF10 with a Cochran's Q-derived p <0.05, but the causal estimate was acceptable when utilizing the random-effects IVW method (Table 1). The MR leave-one-out sensitivity analysis indicated that sequentially excluding individual SNP did not significantly influence the results, and all the estimates of the error lines were on the same side (Figure 3). The results of the IVW, WM, and MR Egger mode for all circulating inflammatory factors on ASD are displayed in Supplementary Table S5.

3.3 The causative impact of ASD on circulating inflammatory factors

When considering functional outcomes of ASD as exposures and the 91 circulating inflammatory factors as outcomes, the IVW results indicate that adverse functional outcomes following ASD may lead to increased levels of matrix metalloproteinase-10 (MMP10) and caspase 8 (CASP8) (OR = 1.067, 95% CI = 1.006 to 1.131, p = 0.032; OR = 1.064, 95% CI = 1.003-1.128, p = 0.040), as well as decreased levels of tumor necrosis factor-related activation-induced cytokine (TNFSF11) and C-C motif chemokine 19 (CCL19) (OR = 0.942, 95% CI = 0.888 to 0.998, p = 0.044; OR = 0.942 95% CI = 0.888 to 0.999, p = 0.047). The analysis results from both WM and MR Egger did not reveal any significant causality between ASD and the four inflammatory factors. Figure 4 provide the results of the IVW, WM, and MR Egger analysis. Cochran's Q-test results showed no evidence of heterogeneity in the causal relationship between these SNPs. The p-value of the MR-Egger intercept was greater than 0.05, indicating that horizontal pleiotropy was not possible for these four associations (Table 2). Furthermore, the sensitivity analysis proved the robustness of these observed causal associations (Figure 5). The results of the IVW,

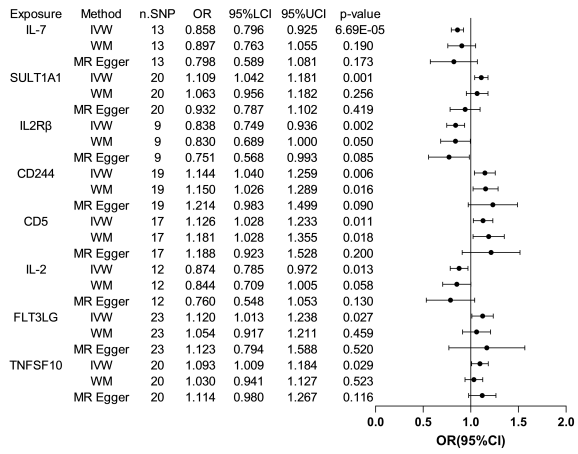

FIGURE 2
Forest plots of the pooled OR results between 8 inflammatory factors and ASD in the forward MR analysis.

TABLE 1 The heterogeneity and horizontal pleiotropy results of the 8 inflammatory factors and ASD in the forward MR analysis.

Exposure	Heterogeneity test						Pleiotropy test		
	MR Egger			IVW			MR Egger		
	Q-value	Q-df	p-value	Q-value	Q-df	p-value	Intercept	SE	p-value
IL-7	4.28	11	0.961	4.54	12	0.971	0.0072	0.014	0.616
SULT1A1	8.55	18	0.969	13.68	19	0.802	0.0201	0.010	0.061
IL2Rβ	4.14	7	0.763	4.93	8	0.765	0.0130	0.015	0.405
CD244	25.00	17	0.094	25.60	18	0.109	-0.0066	0.011	0.546
CD5	14.10	15	0.521	14.30	16	0.579	-0.0056	0.012	0.657
IL-2	6.56	10	0.766	7.40	11	0.766	0.0165	0.018	0.382
FLT3LG	29.10	21	0.111	29.10	22	0.142	-0.0002	0.015	0.989
TNFSF10	34.9	18	0.010	35.5	19	0.013	-0.0042	0.011	0.708

MR, Mendelian randomization; Q, heterogeneity statistic Q; df, degree of freedom; SE, standard error.

WM, and MR Egger mode for ASD on all circulating inflammatory factors are displayed in Supplementary Table S6.

4 Discussion

Although recent observational studies have suggested an association between inflammatory factors and ASD (27–29), it is important to note that these results may be influenced by confounding factors, and the causal relationship between the two remains inconclusive. Using novel data and approaches, this bidirectional MR study offers a genetic insight into the potential causal relationship between circulating inflammatory factors and ASD. The findings of this study suggest that levels of SULT1A1, CD244, CD5, FLT3LG, and TNFSF10 are positively associated with the risk of ASD, while levels of IL-7, IL2Rβ, and IL-2 are inversely associated with the risk of ASD. Furthermore, the genetic susceptibility to ASD exhibited suggestive evidence of increased levels of MMP10 and CASP8, and decreased levels of TNFSF11 and CCL19. Importantly, sensitivity analyses supported the robustness of these results.

Individuals with ASD show alterations in circulating inflammatory factors along with abnormal peripheral blood levels

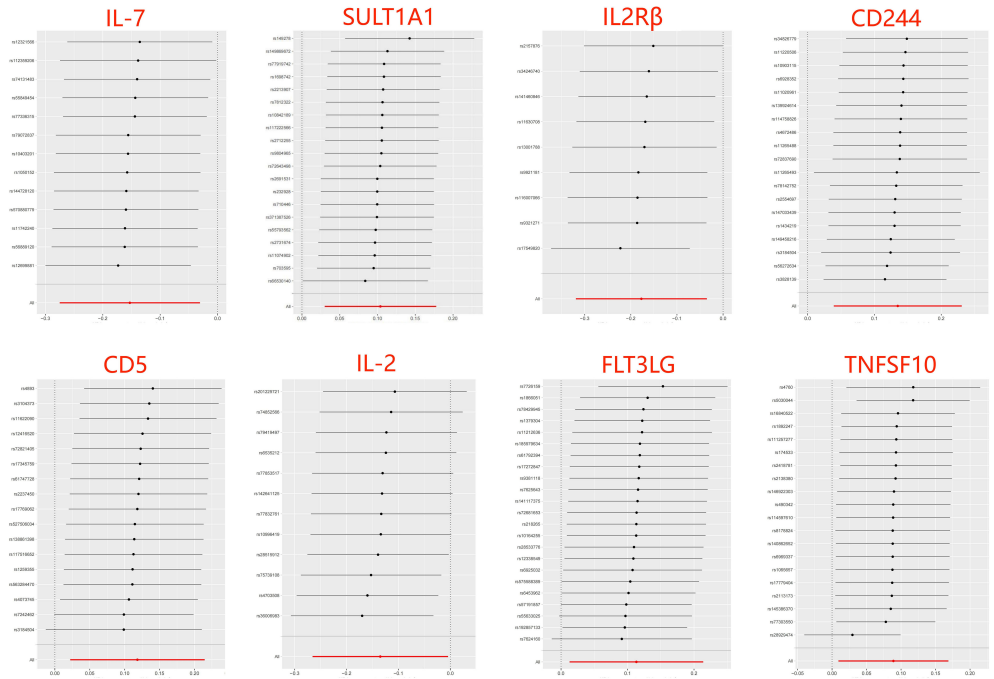

FIGURE 3
Leave-one-out of SNPs results between 8 inflammatory factors and ASD in the forward MR analysis. Each black point indicates the MR result of all remaining SNPs after removing the SNP in this line. The MR results estimated by all SNPs are depicted by the red point. No single SNP strongly drives the overall causal effect in these sensitivity analyses.

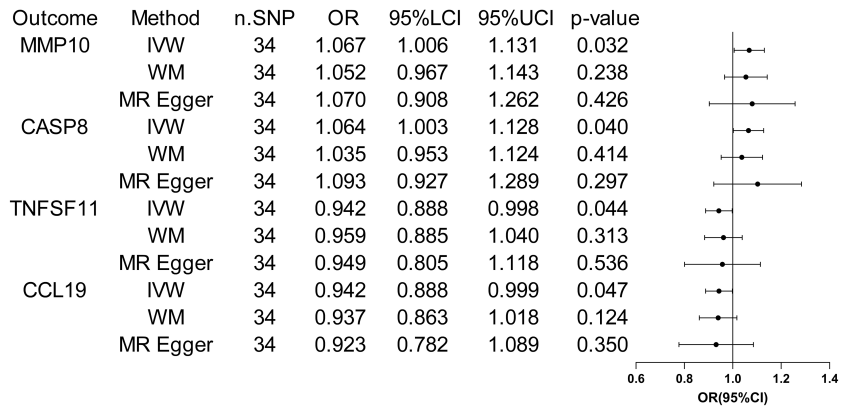

FIGURE 4
Forest plots of the pooled OR results between ASD and 4 inflammatory factors in the reverse MR analysis.

of lymphocytes and macrophages across the lifespan (30). Inflammatory factor profiling can reveal the progression and status of immune system dysregulation in ASD, offering therapeutic targets for improving core autistic symptoms. Current results in the forward MR analysis demonstrated a strong causal association between a decreased level of circulating IL-7 and a higher liability of ASD based on the Bonferroni correction. IL-7 is mainly produced by stromal cells in lymphoid tissues and has pleiotropic effects on the development of T and B cells, as well as T-cell homeostasis. The administration or neutralization of IL-7 may enable the modulation of immune function in individuals with lymphocyte depletion or autoimmunity (31). Data from several studies have shown that plasma levels of IL-7 were higher in children with ASD than those observed in typically developing controls, but these differences did not reach statistical significance after correction for multiple comparisons (32–34). By contrast, Napolioni and colleagues (35) found that plasma levels of IL-7 were inversely correlated with full intelligence quotient in children with ASD using Spearman's rank correlation analysis. Similarly, a large observational study on the risk of psychopathology found that decreased IL-7 levels in cord serum were linked to emotional symptoms and abnormal pro-social behavior in 5-year-old children (36). Overall, this MR analysis based on large populations replicates and extends these findings, highlighting a causal protective role of genetically encoded higher IL-7 levels against ASD.

Other results did not show robust causality after Bonferroni correction, which can only be regarded as suggestive evidence of potential causality. IL-2 functions as an essential immunoregulatory factor produced primarily by T cells, exerting its effects via binding to the high-affinity IL-2R comprising of α (IL-2Rα), β (IL-2Rβ), and γ (IL-2Rγ) subunits. Both IL-2 and IL-2Rβ have been implicated in clonal expansion and functional differentiation of T cells and natural killer cells (37, 38). Vojdani et al. have found that children with ASD appeared to suffer from decreased blood natural killer cell activity due to their low intracellular IL-2 levels (39). In patients with ASD, the proportion of DR+ (activated) T lymphocytes is abnormally increased, whereas the proportion of IL-2 receptor+ lymphocytes remains unchanged or even decreases. This is inversely proportional to the severity of autistic symptoms and similar to that seen in autoimmune diseases (40–42). In addition, previous studies have observed lower mRNA expression levels of IL-2 and percentages of IL-2 synthesizing CD4+ and CD8+ T cells in the peripheral blood of ASD children as compared to controls (43, 44). To sum up, our findings further support these observations and provide evidence of immune dysfunction and autoimmunity in patients with ASD.

Preliminary results suggest that there may be a positive association between levels of SULT1A1, CD244, CD5, FLT3LG, and TNFSF10 and risk of ASD. However, much of the research up to now has not dealt with the relationship between these inflammatory factors and ASD. SULT1A1 is responsible for the

TABLE 2 The heterogeneity and horizontal pleiotropy results of the ASD and 4 inflammatory factors in the reverse MR analysis.

Outcome	Heterogeneity test						Pleiotropy test		
	MR Egger			IVW			MR Egger		
	Q-value	Q-df	p-value	Q-value	Q-df	p-value	Intercept	SE	p-value
MMP10	28.34	32	0.652	28.34	33	0.698	-0.0003	0.008	0.965
CASP8	27.00	32	0.718	27.12	33	0.754	-0.0007	0.007	0.922
TNFSF11	24.04	32	0.843	24.05	33	0.872	-0.0002	0.015	0.989
CCL19	25.78	32	0.773	25.84	33	0.808	0.0020	0.0076	0.798

MR, Mendelian randomization; Q, heterogeneity statistic Q; df, degree of freedom; SE, standard error.

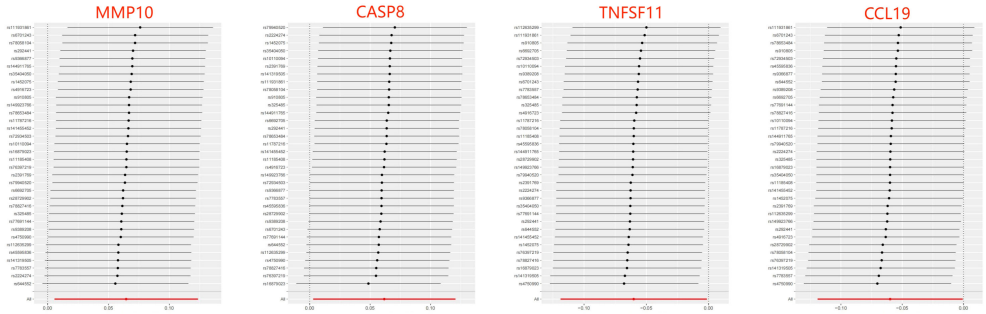

FIGURE 5
Leave-one-out of SNPs results between ASD and 4 inflammatory factors in the reverse MR analysis. Each black point indicates the MR result of all remaining SNPs after removing the SNP in this line. The MR results estimated by all SNPs are depicted by the red point. No single SNP strongly drives the overall causal effect in these sensitivity analyses.

sulfonation of xenobiotics and has been implicated in several cancers by activating carcinogens (45). During autoimmune neuroinflammation, SULT1A is highly expressed in astrocytes, hindering the anti-inflammatory activity of endogenous estrogens (46). CD244 is an immune regulation receptor presented in all NK cells, which can stimulate NK cell cytotoxicity and IFN-γ production by interacting with CD48 on neighboring lymphocytes (47, 48). It has previously been observed that children with ASD had significantly higher serum and plasma levels of CD5 than those of normal controls, which is positively correlated with Childhood Autism Rating Scale score (49, 50). As a pan T cell marker, CD5 is highly expressed in a variety of autoimmune diseases, and this MR study provides new evidence that elevated levels of circulating CD5 may directly promote the development of ASD. In premature infants following respiratory viral infections, hyperoxia-induced high FLT3LG expression can lead to expansion and activation of lung CD103+ dendritic cells. The FLT3LG level is positively correlated with the level of proinflammatory cytokines (51). In addition, chronic HIV-1 patients also displayed significantly high levels of FLT3LG expression (52). TNFSF10 a proapoptotic member of the tumor necrosis factor family, has been shown to be highly up-regulated in patients with inflammatory bowel disease (53) and neurodegenerative diseases (54). The previous findings suggest a positive outcome for our MR results, indicating the need for further research on the current topic.

The occurrence of ASD may increase the levels of MMP10 and CASP8 and decrease the levels of TNFSF11 and CCL19 in the results of reverse MR analyses, suggesting that they may act as downstream factors in ASD. A recent proteomics analysis on plasma inflammation-related protein changes found that MMP-10 expression was significantly up-regulated in the ASD group compared with healthy children (29). Mild cognitive impairment individuals with elevated cerebrospinal fluid levels of MMP-10 had a higher likelihood of progression to Alzheimer's type dementia and faster cognitive decline (55). CASP8 is a protease with both pro-death and pro-survival functions by mediating extrinsic apoptosis and suppressing necroptosis. Postmortem analysis results showed that the apoptosis was increased in the prefrontal cortex, hippocampus, and cerebellum of the autistic brain, as characterized by significantly increased levels of cleaved CASP8 (56). TNFSF11 exerts essential roles in lymph node organogenesis, cellular immunity, and osteoclastogenesis. For example, TNFSF11 can signal the augmentation of IFN-γ secretion and inhibit apoptosis of human monocyte-derived dendritic cells (57, 58). CCL19 has shown significant potential in the regulation of adaptive immune responses by coordinating dendritic cell migration and increasing interactions between dendritic cells, T cells, and B cells in secondary lymphoid tissues (59, 60). Hence, ASD-induced decreases in peripheral blood CCL19 and TNFSF11 levels may further exacerbate immune system disorders.

This MR study employed a large sample size and instrumental variables obtained from the GWAS database, ensuring statistical robustness in estimating causal associations and enhancing the credibility of results. By addressing the bias introduced by confounding factors and reverse causality through MR analysis, this study provides stronger evidence for assessing the causal relationship between inflammatory factor levels and the risk of ASD compared to traditional observational studies. Nevertheless, several limitations of the present study should be considered. Firstly, the present MR study can only provide statistical evidence for the causal association between circulating inflammatory factors and ASD, and further research is needed to investigate the potential mechanisms involved. Secondly, although current sensitivity analyses did not reveal any significant pleiotropy between SNPs, the effect of pleiotropy on the MR results cannot be completely ruled out. Thirdly, this MR study utilized pooled data from the GWAS database and did not analyze stratified risk factors related to ASD duration, severity, treatment, and comorbidities. Finally, the genetic data were mainly collected from individuals of European descent, and it is uncertain whether these findings are applicable to individuals of other ancestries.

5 Conclusion

Overall, this study provide novel ideas that IL-7, SULT1A1, IL2Rβ, CD244, CD5, IL-2, FLT3LG, and TNFSF10 may be upstream factors in the pathogenesis of ASD, while levels of MMP10, CASP8, TNFSF11, and CCL19 may act as downstream

factors in ASD. These inflammatory factors could potentially serve as biomarkers for early diagnosis and treatment of ASD.

Data availability statement

The original contributions presented in the study are included in the article/Supplementary Material. Further inquiries can be directed to the corresponding author.

Ethics statement

Ethical approval was not required for the study involving humans in accordance with the local legislation and institutional requirements. Written informed consent to participate in this study was not required from the participants or the participants' legal guardians/next of kin in accordance with the national legislation and the institutional requirements.

Author contributions

JL: Writing – review & editing, Writing – original draft, Resources, Methodology, Investigation, Formal Analysis, Data curation, Conceptualization. HD: Writing – review & editing, Writing – original draft, Visualization, Software, Investigation, Formal Analysis. WS: Writing – review & editing, Visualization, Software, Methodology, Investigation. MM: Writing – review & editing, Validation, Resources, Methodology. HZ: Writing – review & editing, Writing – original draft, Supervision, Project administration, Investigation, Conceptualization.

Funding

The author(s) declare financial support was received for the research, authorship, and/or publication of this article. This work was supported by National Key Research and Development Program of China (2018YFC2001703), China Disabled Persons Federation (CDPF2023KF00001), and Changping laboratory (2021B-01-01-1).

Conflict of interest

The authors declare that the research was conducted in the absence of any commercial or financial relationships that could be construed as a potential conflict of interest.

Publisher's note

Supplementary material

The Supplementary Material for this article can be found online at: https://www.frontiersin.org/articles/10.3389/fimmu.2024.1370276/full#supplementary-material

References

1. Careaga M, Murai T, Bauman MD. Maternal immune activation and autism spectrum disorder: from rodents to nonhuman and human primates. *Biol Psychiatry*. (2017) 81:391–401. doi: 10.1016/j.biopsych.2016.10.020

2. Sadik A, Dardani C, Pagoni P, Havdahl A, Stergiakouli EiPSYCH Autism Spectrum Disorder Working Group, et al. Parental inflammatory bowel disease and autism in children. *Nat Med*. (2022) 28:1406–11. doi: 10.1038/s41591-022-01845-9

3. Gesundheit B, Rosenzweig JP, Naor D, Lerer B, Zachor DA, Procházka V, et al. Immunological and autoimmune considerations of Autism Spectrum Disorders. *J Autoimmun*. (2013) 44:1–7. doi: 10.1016/j.jaut.2013.05.005

4. Hughes HK, Mills Ko E, Rose D, Ashwood P. Immune dysfunction and autoimmunity as pathological mechanisms in autism spectrum disorders. *Front Cell Neurosci*. (2018) 12:405. doi: 10.3389/fncel.2018.00405

5. Kordulewska NK, Kostyra E, Piskorz-Ogórek K, Moszyńska M, Cieślińska A, Fiedorowicz E, et al. Serum cytokine levels in children with spectrum autism disorder: Differences in pro- and anti-inflammatory balance. *J Neuroimmunol*. (2019) 337:577066. doi: 10.1016/j.jneuroim.2019.577066

6. Ashwood P, Krakowiak P, Hertz-Picciotto I, Hansen R, Pessah I, Van de Water J. Elevated plasma cytokines in autism spectrum disorders provide evidence of immune dysfunction and are associated with impaired behavioral outcome. *Brain Behav Immun*. (2011) 25:40–5. doi: 10.1016/j.bbi.2010.08.003

7. Zhao H, Zhang H, Liu S, Luo W, Jiang Y, Gao J. Association of peripheral blood levels of cytokines with autism spectrum disorder: A meta-analysis. *Front Psychiatry*. (2021) 12:670200. doi: 10.3389/fpsyt.2021.670200

8. Krakowiak P, Goines PE, Tancredi DJ, Ashwood P, Hansen RL, Hertz-Picciotto I, et al. Neonatal cytokine profiles associated with autism spectrum disorder. *Biol Psychiatry*. (2017) 81:442–51. doi: 10.1016/j.biopsych.2015.08.007

9. Saghazadeh A, Ataeinia B, Keynejad K, Abdolalizadeh A, Hirbod-Mobarakeh A, Rezaei N. Anti-inflammatory cytokines in autism spectrum disorders: A systematic review and meta-analysis. *Cytokine*. (2019) 123:154740. doi: 10.1016/j.cyto.2019.154740

10. Emdin CA, Khera AV, Kathiresan S. Mendelian randomization. *JAMA*. (2017) 318:1925–6. doi: 10.1001/jama.2017.17219

11. Ahola-Olli AV, Würtz P, Havulinna AS, Aalto K, Pitkänen N, Lehtimäki T, et al. Genome-wide association study identifies 27 loci influencing concentrations of circulating cytokines and growth factors. *Am J Hum Genet*. (2017) 100:40–50. doi: 10.1016/j.ajhg.2016.11.007

12. Wang M, Jin G, Cheng Y, Guan SY, Zheng J, Zhang SX. Genetically predicted circulating levels of cytokines and the risk of depression: a bidirectional Mendelian-randomization study. *Front Genet*. (2023) 14:1242614. doi: 10.3389/fgene.2023.1242614

13. Sun H, Ma D, Hou S, Zhang W, Li J, Zhao W, et al. Exploring causal correlations between systemic inflammatory cytokines and epilepsy: A bidirectional Mendelian randomization study. *Seizure*. (2023) 114:44–9. doi: 10.1016/j.seizure.2023.11.006

14. Yeung CHC, Schooling CM. Systemic inflammatory regulators and risk of Alzheimer's disease: a bidirectional Mendelian-randomization study. *Int J Epidemiol*. (2021) 50:829–40. doi: 10.1093/ije/dyaa241

15. Zhao JH, Stacey D, Eriksson N, Macdonald-Dunlop E, Hedman ÅK, Kalnapenkis A, et al. Genetics of circulating inflammatory proteins identifies drivers of immune-mediated disease risk and therapeutic targets. *Nat Immunol*. (2023) 24:1540–51. doi: 10.1038/s41590-023-01588-w

16. Huang H, Fu Z, Yang M, Hu H, Wu C, Tan L. Levels of 91 circulating inflammatory proteins and risk of lumbar spine and pelvic fractures and peripheral

ligament injuries: a two-sample mendelian randomization study. *J Orthop Surg Res*. (2024) 19:161. doi: 10.1186/s13018-024-04637-8

17. Shi W, Xu Y, Zhang A, Jia X, Liu S, Hu Z. Inflammatory cytokines and their potential role in Sjogren's syndrome risk: insights from a mendelian randomization study. *Adv Rheumatol*. (2024) 64:14. doi: 10.1186/s42358-024-00354-2

18. Grove J, Ripke S, Als TD, Mattheisen M, Walters RK, Won H, et al. Identification of common genetic risk variants for autism spectrum disorder. *Nat Genet*. (2019) 51:431–44. doi: 10.1038/s41588-019-0344-8

19. 1000 Genomes Project Consortium, Abecasis GR, Auton A, Brooks LD, DePristo MA, Durbin RM, et al. An integrated map of genetic variation from 1,092 human genomes. *Nature*. (2012) 491:56–65. doi: 10.1038/nature11632

20. Burgess S, Thompson SGCRP CHD Genetics Collaboration. Avoiding bias from weak instruments in Mendelian randomization studies. *Int J Epidemiol*. (2011) 40:755–64. doi: 10.1093/ije/dyr036

21. Hemani G, Zheng J, Elsworth B, Wade KH, Haberland V, Baird D, et al. The MR-Base platform supports systematic causal inference across the human phenome. *Elife*. (2018) 7:e34408. doi: 10.7554/eLife.34408

22. Yavorska OO, Burgess S. MendelianRandomization: an R package for performing Mendelian randomization analyses using summarized data. *Int J Epidemiol*. (2017) 46:1734–9. doi: 10.1093/ije/dyx034

23. Burgess S, Small DS, Thompson SG. A review of instrumental variable estimators for Mendelian randomization. *Stat Methods Med Res*. (2017) 26:2333–55. doi: 10.1177/0962280215597579

24. Bowden J, Davey Smith G, Haycock PC, Burgess S. Consistent estimation in mendelian randomization with some invalid instruments using a weighted median estimator. *Genet Epidemiol*. (2016) 40:304–14. doi: 10.1002/gepi.21965

25. Bowden J, Davey Smith G, Burgess S. Mendelian randomization with invalid instruments: effect estimation and bias detection through Egger regression. *Int J Epidemiol*. (2015) 44:512–25. doi: 10.1093/ije/dyv080

26. Liang Z, Zhao L, Lou Y, Liu S. Causal effects of circulating lipids and lipid-lowering drugs on the risk of epilepsy: a two-sample Mendelian randomization study. *QJM*. (2023) 116:421–8. doi: 10.1093/qjmed/hcad048

27. Gesundheit B, Zisman PD, Hochbaum L, Posen Y, Steinberg A, Friedman G, et al. Autism spectrum disorder diagnosis using a new panel of immune- and inflammatory-related serum biomarkers: A case-control multicenter study. *Front Pediatr*. (2023) 11:967954. doi: 10.3389/fped.2023.967954

28. Than UTT, Nguyen LT, Nguyen PH, Nguyen XH, Trinh DP, Hoang DH, et al. Inflammatory mediators drive neuroinflammation in autism spectrum disorder and cerebral palsy. *Sci Rep*. (2023) 13:22587. doi: 10.1038/s41598-023-49902-8

29. Bao XH, Chen BF, Liu J, Tan YH, Chen S, Zhang F, et al. Olink proteomics profiling platform reveals non-invasive inflammatory related protein biomarkers in autism spectrum disorder. *Front Mol Neurosci*. (2023) 16:1185021. doi: 10.3389/fnmol.2023.1185021

30. Arteaga-Henríquez G, Gisbert L, Ramos-Quiroga JA. Immunoregulatory and/or anti-inflammatory agents for the management of core and associated symptoms in individuals with autism spectrum disorder: A narrative review of randomized, placebo-controlled trials. *CNS Drugs*. (2023) 37:215–29. doi: 10.1007/s40263-023-00993-x

31. Fry TJ, Mackall CL. Interleukin-7: from bench to clinic. *Blood*. (2002) 99:3892–904. doi: 10.1182/blood.v99.11.3892

32. Inga Jácome MC, Morales Chacòn LM, Vera Cuesta H, Maragoto Rizo C, Whilby Santiesteban M, Ramos Hernandez L, et al. Peripheral inflammatory markers contributing to comorbidities in autism. *Behav Sci*. (2016) 6:29. doi: 10.3390/bs6040029

33. Suzuki K, Matsuzaki H, Iwata K, Kameno Y, Shimmura C, Kawai S, et al. Plasma cytokine profiles in subjects with high-functioning autism spectrum disorders. *PloS One*. (2011) 6:e20470. doi: 10.1371/journal.pone.0020470

34. Pecorelli A, Cervellati F, Belmonte G, Montagner G, Waldon P, Hayek J, et al. Cytokines profile and peripheral blood mononuclear cells morphology in Rett and autistic patients. *Cytokine*. (2016) 77:180–8. doi: 10.1016/j.cyto.2015.10.002

35. Napolioni V, Ober-Reynolds B, Szelinger S, Corneveaux JJ, Pawlowski T, Ober-Reynolds S, et al. Plasma cytokine profiling in sibling pairs discordant for autism spectrum disorder. *J Neuroinflamm*. (2013) 10:38. doi: 10.1186/1742-2094-10-38

36. Barbosa S, Khalfallah O, Forhan A, Galera C, Heude B, Glaichenhaus N, et al. Immune activity at birth and later psychopathology in childhood. *Brain Behav Immun Health*. (2020) 8:100141. doi: 10.1016/j.bbih.2020.100141

37. Fernandez IZ, Baxter RM, Garcia-Perez JE, Vendrame E, Ranganath T, Kong DS, et al. A novel human IL2RB mutation results in T and NK cell-driven immune dysregulation. *J Exp Med*. (2019) 216:1255–67. doi: 10.1084/jem.20182015

38. Henney CS, Kuribayashi K, Kern DE, Gillis S. Interleukin-2 augments natural killer cell activity. *Nature*. (1981) 291:335–8. doi: 10.1038/291335a0

39. Vojdani A, Mumper E, Granpeesheh D, Mielke L, Traver D, Bock K, et al. Low natural killer cell cytotoxic activity in autism: the role of glutathione, IL-2 and IL-15. *J Neuroimmunol*. (2008) 205:148–54. doi: 10.1016/j.jneuroim.2008.09.005

40. Denney DR, Frei BW, Gaffney GR. Lymphocyte subsets and interleukin-2 receptors in autistic children. *J Autism Dev Disord*. (1996) 26:87–97. doi: 10.1007/BF02276236

41. Plioplys AV, Greaves A, Kazemi K, Silverman E. Lymphocyte function in autism and Rett syndrome. *Neuropsychobiology*. (1994) 29:12–6. doi: 10.1159/000119056

42. Warren RP, Yonk J, Burger RW, Odell D, Warren WL. DR-positive T cells in autism: association with decreased plasma levels of the complement C4B protein. *Neuropsychobiology*. (1995) 31:53–7. doi: 10.1159/000119172

43. Eftekharian MM, Ghafouri-Fard S, Noroozi R, Omrani MD, Arsang-Jang S, Ganji M, et al. Cytokine profile in autistic patients. *Cytokine*. (2018) 108:120–6. doi: 10.1016/j.cyto.2018.03.034

44. Gupta S, Aggarwal S, Rashanravan B, Lee T. Th1- and Th2-like cytokines in CD4 + and CD8+ T cells in autism. *J Neuroimmunol*. (1998) 85:106–9. doi: 10.1016/s0165-5728(98)00021-6

45. Gamage NU, Duggleby RG, Barnett AC, Tresillian M, Latham CF, Liyou NE, et al. Structural and kinetic implications of substrate inhibition. *J Biol Chem*. (2003) 278:7655–62. doi: 10.1074/jbc.M207246200

46. Guillot F, Garcia A, Salou M, Brouard S, Laplaud DA, Nicot AB. Transcript analysis of laser capture microdissected white matter astrocytes and higher phenol sulfotransferase 1A1 expression during autoimmune neuroinflammation. *J Neuroinflamm*. (2015) 12:130. doi: 10.1186/s12974-015-0348-y

47. Sun L, Gang X, Li Z, Zhao X, Zhou T, Zhang S, et al. Advances in understanding the roles of CD244 (SLAMF4) in immune regulation and associated diseases. *Front Immunol*. (2021) 12:648182. doi: 10.3389/fimmu.2021.648182

48. Messmer B, Eissmann P, Stark S, Watzl C. CD48 stimulation by 2B4 (CD244)-expressing targets activates human NK cells. *J Immunol*. (2006) 176:4646–50. doi: 10.4049/jimmunol.176.8.4646

49. Desoky T, Hassan MH, Fayed HM, Sakhr HM. Biochemical assessments of thyroid profile, serum 25-hydroxycholecalciferol and cluster of differentiation 5 expression levels among children with autism. *Neuropsychiatr Dis Treat*. (2017) 13:2397–403. doi: 10.2147/NDT.S146152

50. Halepoto DM, Alhowikan AM, Ayadhi LA. Cluster of differentiation 5 (CD5) levels in the plasma of children with autism spectrum disorder (ASD). *J Coll Physicians Surg Pak*. (2017) 27:149–52.

51. Cui TX, Brady AE, Zhang YJ, Fulton CT, Goldsmith AM, Popova AP. Early-life hyperoxia-induced Flt3L drives neonatal lung dendritic cell expansion and proinflammatory responses. *Front Immunol*. (2023) 14:1116675. doi: 10.3389/fimmu.2023.1116675

52. Ling L, Tang X, Huang X, Li J, Wang H, Chen Z. AAV-vectored fms-related tyrosine kinase 3 ligand inhibits CD34+ Progenitor cell engraftment in humanized mice. *J Neuroimmune Pharmacol*. (2018) 13:541–50. doi: 10.1007/s11481-018-9819-0

53. Begue B, Wajant H, Bambou JC, Dubuquoy L, Siegmund D, Beaulieu JF, et al. Implication of TNF-related apoptosis-inducing ligand in inflammatory intestinal epithelial lesions. *Gastroenterology*. (2006) 130:1962–74. doi: 10.1053/j.gastro.2006.03.022

54. Huang Y, Erdmann N, Peng H, Zhao Y, Zheng J. The role of TNF related apoptosis-inducing ligand in neurodegenerative diseases. *Cell Mol Immunol*. (2005) 2:113–22.

55. Martino Adami PV, Orellana A, García P, Kleineidam L, Alarcón-Martín E, Montrreal L, et al. Matrix metalloproteinase 10 is linked to the risk of progression to dementia of the Alzheimer's type. *Brain*. (2022) 145:2507–17. doi: 10.1093/brain/awac024

56. Dong D, Zielke HR, Yeh D, Yang P. Cellular stress and apoptosis contribute to the pathogenesis of autism spectrum disorder. *Autism Res*. (2018) 11:1076–90. doi: 10.1002/aur.1966

57. Chen NJ, Huang MW, Hsieh SL. Enhanced secretion of IFN-gamma by activated Th1 cells occurs via reverse signaling through TNF-related activation-induced cytokine. *J Immunol*. (2001) 166:270–6. doi: 10.4049/jimmunol.166.1.270

58. Wong BR, Josien R, Lee SY, Sauter B, Li HL, Steinman RM, et al. TRANCE (tumor necrosis factor [TNF]-related activation-induced cytokine), a new TNF family member predominantly expressed in T cells, is a dendritic cell-specific survival factor. *J Exp Med*. (1997) 186:2075–80. doi: 10.1084/jem.186.12.2075

59. Marsland BJ, Bättig P, Bauer M, Ruedl C, Lässing U, Beerli RR, et al. CCL19 and CCL21 induce a potent proinflammatory differentiation program in licensed dendritic cells. *Immunity*. (2005) 22:493–505. doi: 10.1016/j.immuni.2005.02.010

60. Liu X, Wang B, Li Y, Hu Y, Li X, Yu T, et al. Powerful anticolon tumor effect of targeted gene immunotherapy using folate-modified nanoparticle delivery of CCL19 to activate the immune system. *ACS Cent Sci*. (2019) 5:277–89. doi: 10.1021/acscentsci.8b00688

frontiers | Frontiers in Immunology

TYPE Original Research
PUBLISHED 21 May 2024
DOI 10.3389/fimmu.2024.1374301

OPEN ACCESS

EDITED BY
Fawaz Alzaid,
Sorbonne Universités, France

REVIEWED BY
Fabrícia Lima Fontes-Dantas,
Rio de Janeiro State University, Brazil
Courtney Bouchet,
Colorado State University, United States
Kwang-Mook Jung,
University of California, Irvine, United States

*CORRESPONDENCE
Alexis F. League
leagueaf@protonmail.com
Sylvia Fitting
sfitting@email.unc.edu

RECEIVED 21 January 2024
ACCEPTED 25 April 2024
PUBLISHED 21 May 2024

CITATION
League AF, Yadav-Samudrala BJ, Kolagani R, Cline CA, Jacobs IR, Manke J, Niphakis MJ, Cravatt BF, Lichtman AH, Ignatowska-Jankowska BM and Fitting S (2024) A helping HAND: therapeutic potential of MAGL inhibition against HIV-1-associated neuroinflammation. *Front. Immunol.* 15:1374301. doi: 10.3389/fimmu.2024.1374301

A helping HAND: therapeutic potential of MAGL inhibition against HIV-1-associated neuroinflammation

Alexis F. League[1*], Barkha J. Yadav-Samudrala[1], Ramya Kolagani[1], Calista A. Cline[1], Ian R. Jacobs[1], Jonathan Manke[2], Micah J. Niphakis[3], Benjamin F. Cravatt[3], Aron H. Lichtman[4], Bogna M. Ignatowska-Jankowska[5] and Sylvia Fitting[1*]

[1]Department of Psychology and Neuroscience, University of North Carolina at Chapel Hill, Chapel Hill, NC, United States, [2]Department of Pharmaceutical Sciences, Skaggs School of Pharmacy and Pharmaceutical Sciences, University of Colorado Anschutz Medical Campus, Aurora, CO, United States, [3]Department of Chemistry, Scripps Research, La Jolla, CA, United States, [4]Department of Pharmacology and Toxicology, Virginia Commonwealth University, Richmond, VA, United States, [5]Neuronal Rhythms in Movement Unit, Okinawa Institute of Science and Technology, Okinawa, Japan

Background: Human immunodeficiency virus (HIV) affects nearly 40 million people globally, with roughly 80% of all people living with HIV receiving antiretroviral therapy. Antiretroviral treatment suppresses viral load in peripheral tissues but does not effectively penetrate the blood-brain barrier. Thus, viral reservoirs persist in the central nervous system and continue to produce low levels of inflammatory factors and early viral proteins, including the transactivator of transcription (Tat). HIV Tat is known to contribute to chronic neuroinflammation and synaptodendritic damage, which is associated with the development of cognitive, motor, and/or mood problems, collectively known as HIV-associated neurocognitive disorders (HAND). Cannabinoid anti-inflammatory effects are well documented, but therapeutic utility of cannabis remains limited due to its psychotropic effects, including alterations within brain regions encoding reward processing and motivation, such as the nucleus accumbens. Alternatively, inhibiting monoacylglycerol lipase (MAGL) has demonstrated therapeutic potential through interactions with the endocannabinoid system.

Methods: The present study utilized a reward-related operant behavioral task to quantify motivated behavior in female Tat transgenic mice treated with vehicle or MAGL inhibitor MJN110 (1 mg/kg). Brain tissue was collected to assess dendritic injury and neuroinflammatory profiles, including dendritic microtubule-associated protein (MAP2ab) intensity, microglia density, microglia morphology, astrocyte density, astrocytic interleukin-1ß (IL-1ß) colocalization, and various lipid mediators.

Results: No significant behavioral differences were observed; however, MJN110 protected against Tat-induced dendritic injury by significantly upregulating MAP2ab intensity in the nucleus accumbens and in the infralimbic cortex of Tat(+) mice. No or only minor effects were noted for Iba-1$^+$ microglia density and/or microglia morphology. Further, Tat increased GFAP$^+$ astrocyte density in the infralimbic cortex

and GFAP$^+$ astrocytic IL-1ß colocalization in the nucleus accumbens, with MJN110 significantly reducing these measures in Tat(+) subjects. Lastly, selected HETE-related inflammatory lipid mediators in the striatum were downregulated by chronic MJN110 treatment.

Conclusions: These findings demonstrate anti-inflammatory and neuroprotective properties of MJN110 without cannabimimetic behavioral effects and suggest a promising alternative to cannabis for managing neuroinflammation.

KEYWORDS

HIV-1, inflammation, transactivator of transcription (Tat), endocannabinoids, HETE, monoacylglycerol lipase (MAGL)

1 Introduction

Human immunodeficiency virus (HIV) remains a major global public health issue, with 39.0 million (33.1-45.7 million) people living with HIV (PLWH) worldwide at the end of 2022, out of which 76% (65-89%) received combination antiretroviral therapy (cART) (1). The overall prevalence rate of HIV-1 infection is higher among adult women than men, with 15% more women living with HIV-1 relative to men in 2019 (2). Importantly, HIV-1 affects women differently than men, with greater immune activation observed in women despite lower overall viral load (3). Given the historical underrepresentation of females across human and animal models of HIV infection, the present study centers specifically on females to better characterize the effects of HIV and novel intervention strategies in this statistically underrepresented population.

While cART successfully reduces viral load in peripheral tissues and significantly improves life expectancy of PLWH (4–6), these treatments are largely incapable of effectively crossing the blood-brain barrier (BBB) to suppress replication of viral proteins, such as transactivator of transcription (Tat), which enters the central nervous system (CNS) within two weeks of infection both directly and through peripherally infected monocytes and macrophages (7–10). Secretion and synthesis of viral protein reservoirs persist in the CNS, where they alter the cellular environment, contributing to chronic neuropathy and HIV-associated neurocognitive disorders (HAND), even in patients actively undergoing treatment (7). Underlying HAND are several dysfunctional immunomodulatory mechanisms within the CNS, including persistent inflammation and immune activation (11–14), which ultimately lead to dendritic injury and damage to neurons (15–17). Notably, cART itself also contributes to both neuroinflammation and altered neuronal connectivity with prolonged exposure (18, 19). In preclinical animal studies, the HIV Tat transgenic mouse model is a well-established model for neuroHIV since their neuropathology and behavioral deficits tend to mirror those observed in cART-treated PLWH with HAND (20–22). These include structural abnormalities in neurons/dendrites, such as reduced spine density and changes in synaptic proteins (21–23), disrupted frontostriatal circuitry (24), and glial abnormalities including microglial activation and micro/astrogliosis (20, 21, 25). Further, these mice and related neuroHIV rodent models also develop changes in learning/memory, motor activity, and motivated behaviors (24, 26–30) relevant for cART-treated PLWH. As dopaminergic neurocircuitry is highly susceptible to disruption by HIV proteins, including HIV Tat (29, 31–34), motivational alterations remain problematic neurobehavioral manifestations in cART-treated PLWH, including apathy (35, 36) which parallels lack of motivation.

The endogenous cannabinoid (endocannabinoid) system is a critical line of defense against neurodegenerative and inflammatory conditions (37). It is well established that endocannabinoids, such as 2-arachidonoylglycerol (2-AG) and N-arachidonoylethanolamine (AEA) upregulate in certain disorders (e.g., Parkinson's disease, Alzheimer's disease, multiple sclerosis) and reduce or abolish unwanted effects of these disorders or slow their progression (38, 39). Recent work has demonstrated therapeutic potential of inhibiting monoacylglycerol lipase (MAGL), the primary enzyme that hydrolyzes 2-AG. 2-AG, is an endogenous ligand at neuronal cannabinoid type-1 receptors (CB_1R) and, importantly, also an agonist at cannabinoid type-2 receptors (CB_2R) in immune cells throughout the brain and body (40). Activation of CB_2R has shown protective properties against neuroinflammation and neurodegenerative disorders (41). MAGL-focused strategies are of great interest because targeting enzymatic breakdown is more beneficial relative to phytocannabinoids, as 2-AG tone is affected locally on-demand where its breakdown is dysregulated, thus reducing off-target effects relative to exogenous agonists (42). Because the downstream products of 2-AG hydrolysis, including arachidonic acid (AA), are themselves broken down into proinflammatory eicosanoid lipid mediators such as prostaglandins, hydroxyeicosatetraenoic acids (HETEs), and epoxyeicosatrienoic acids (EETs), inhibiting 2-AG breakdown also stands to reduce proinflammatory processes (43, 44).

Previous studies have demonstrated the neuroprotective properties of MAGL inhibition across numerous models of brain damage and inflammation (45–48), including suppressed astrocytic

and microglial activation in models of Alzheimer's disease (49, 50) and reduced HIV-1 envelope glycoprotein (gp120)-associated synapse loss and IL-1β (51). Further, as 2-AG plays a significant role in modulating mesolimbic dopamine release and associated behaviors (52), inhibiting 2-AG degradation by targeting MAGL has been shown to enhance dopamine signaling, reward-related behavior, and motivation with the MAGL inhibitor JZL184 (53, 54). While JZL184 targets 2-AG more potently and selectively (55) compared to earlier-generation MAGL inhibitors such as URB602 (56), studies have shown desensitization of CB_1R, which can contribute to physical dependency (57), as well as cross-reactivity with other serine hydrolases including α/β hydrolase domain (ABHD) (55). Newer-generation MAGL inhibitors such as MJN110 confer greater 2-AG selectivity with adequate potency to effectively inhibit MAGL *in vivo* at doses as low as 1 mg/kg (58). MJN110, in particular has shown antinociceptive, anti-inflammatory, and neurorestorative effects previously (59, 60). While MJN110 has also previously been shown to increase reward-directed behavior, this observation was specific to doses of 5 and 10 mg/kg (61). Given these findings, we were interested in characterizing whether Tat or lower-dose MJN110 may affect motivated behavior in the present model.

Thus, the present study used the HIV-1 Tat transgenic mouse model to investigate the chronic effects of MAGL inhibitor MJN110 (1 mg/kg) on reward-related motivated behavior. Immunohistochemical and lipid mediator analyses were conducted to assess potential anti-inflammatory and neuroprotective effects of chronic MJN110 exposure against Tat-induced toxicity on the CNS system, with focusing on the ventral striatum (nucleus accumbens) and infralimbic cortex. It is hypothesized that MJN110 will reduce Tat-driven dysregulation in motivated behavior and exert protective effects against Tat-driven neuroinflammation and neuronal injury.

2 Materials and methods

2.1 Subjects

Brain-specific, astrocyte-driven HIV-1 Tat_{1-86} expression was induced in a Tet-on system using doxycycline in transgenic female mice (N = 34) as previously described (62). Briefly, mice were developed on a hybrid C57BL/6J background wherein Tat(+) subjects expressed both glial fibrillary acidic protein (GFAP)-reverse tetracycline-controlled transactivator (rtTa) and tetracycline-responsive element (TRE)-tat genes, while control Tat(−) subjects expressed only the GFAP-rtTA gene (20). Genotyping was performed 7-10 days post-weaning to confirm Tat transgene expression. Subjects at ~ 4 months of age (age range: 3-6 months) were provided ad libitum access to water and doxycycline-containing chow (6 mg/g; Envigo, NJ, USA; #TD.09282) for three months preceding and throughout behavioral assays to establish and maintain a chronic exposure model (63). Note that estrous cycle was not monitored due to the concern that stress associated with daily vaginal lavage could confound our dependent measures (64). Subjects were maintained on a 12-hour reversed light/dark cycle, and behavioral data were collected during the dark phase only. Experimenters were blind to genotype throughout data collection. All procedures were conducted in strict accordance with the ethical guidelines outlined in the NIH Guide for the Care and Use of Laboratory Animals (NIH Publication No. 85-23) and approved by the Institutional Animal Care and Use Committee (IACUC, Protocol#: 23-056.0) at the University of North Carolina at Chapel Hill.

2.2 Drug treatment

Drug assignment (MJN110/vehicle) was randomized and counterbalanced across genotype groups [Tat(−) and Tat(+) mice] to yield four total genotype/drug groups with 8-9 subjects each [Tat(−) Vehicle, n = 9; Tat(−) MJN110, n = 8; Tat(+) Vehicle, n = 8; Tat(+) MJN110, n = 9]. MJN110 (1 mg/kg) was dissolved in a vehicle solution containing a 1:1:18 ratio of Kolliphor (Sigma-Aldrich, #C5135), ethanol (Decon Laboratories, #64174), and 0.9% sodium chloride (Braun Medical, #J8K944) as described previously (58). Mice assigned to the vehicle group received the vehicle solution without the MJN110 drug. MJN110 dosage was chosen based on prior studies which demonstrated 1 mg/kg oral MJN110 administration was sufficient to partially block MAGL in the brain, precluding tolerance development which occurs with full blockade via CB_1R desensitization (58). Additionally, subcutaneous 1 mg/kg MJN110 injections 2 hours prior to an intraperitoneal acid injection showed a prominent antinociceptive profile that tended to be greater in female rats compared to males (65). Subcutaneous injections (10 μL/g) were performed daily for two weeks preceding and throughout behavioral assessments (3-22 days, depending on animal's performance). This method of delivery was chosen to most closely mimic oral administration and preclude complications associated with intraperitoneal injections (e.g., lower full-blockade dose, faster absorption, and greater potential for intestinal irritation) (66). Injections were administered at the same time each day, approximately two hours before data collection to ensure maximal effect during the testing window (58). Subject weight was recorded daily for dosing accuracy and to ensure body mass remained stable across the treatment time course.

2.3 Reward-related operant behavioral task

2.3.1 Experimental design

Subjects were trained to nose poke for 25% sucrose solution (w/v), similar in concentration to that used in previous studies (67, 68). The procedural design described herein was adapted from Nam and colleagues (69) (Figure 1). Subjects first underwent habituation and magazine training to acclimate to test procedures and stimuli. After successfully making the association between nose poke behaviors and sucrose availability and learning to respond consistently, subjects advanced to a motivation test, which assessed

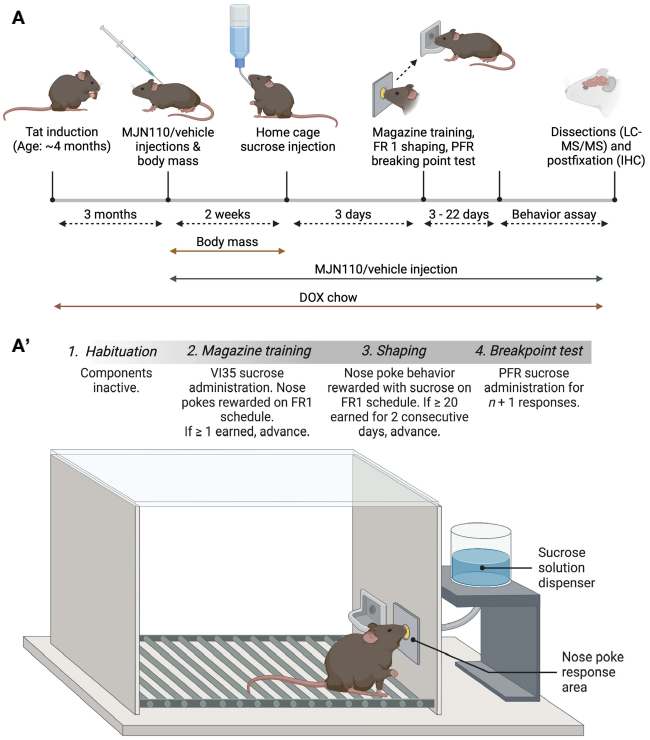

FIGURE 1
Schematic representation of the experimental timeline **(A)** and the behavioral assay **(A')**. **(A)** After mice received DOX-containing chow for 3 months, mice were subcutaneously injected with vehicle/MJN110 for 2 weeks. DOX food and drug injections continued throughout the experimental study. Body mass was recorded daily when drug injections started. After 2 weeks of drug injections, subjects were habituated for 3 days in their home cage to the 25% sucrose solution (w/v). The behavioral assay started the next day and lasted between 3-22 days depending on animal's performance **(A')**. Figure created with BioRender.com. DOX, doxycycline; FR1, fixed-ratio 1; PFR, progressive fixed-ratio; VI35, variable-interval schedule (30-45 seconds).

how many nose poke behaviors they would perform to earn a single sucrose reward.

2.3.2 Apparatus

Behavior was recorded in operant chambers (MED Associates, #ENV-307W) containing a nose poke response port and adjacent reward dispenser (MED Associates, #ENV-302W-S). To reduce potential visual and auditory distractions, operant chambers were contained within sound-attenuating cubicles providing 80 dB white noise (MED Associates, #ENV-022MD). MED-PC computer interface software was used to automate sessions and record behavior. To ensure testing environment consistency across training and test phases, subjects were randomly assigned an operant chamber in which they were tested throughout all sessions.

2.3.3 Habituation

Subjects were habituated to experimenter handling for two weeks preceding behavioral training. Three days before operant chamber habituation, water in home cages was replaced with 10% sucrose (w/v) on days 1 and 2, then 20% sucrose (w/v) on day 3. Sucrose concentration was increased across the habituation period to allow subjects time to adapt and develop consummatory behaviors towards the solution. To increase reward salience for magazine training, sucrose solution was replaced with water on the day of test environment habituation (day 4), wherein subjects were exposed to operant chambers and white noise for 30 minutes, with nose poke response ports and reward dispensing components inactive.

2.3.4 Magazine training

The following day, subjects underwent a one-hour training session wherein all operant chamber components were active. During this phase of training, 25% sucrose solution (w/v) was made available for 20 seconds at a time on a variable-interval (VI) schedule (30-45 seconds, VI35). Sucrose solution was also made available for each nose poke response initiated by subjects. If the number of recorded nose pokes and earned reinforcers equaled at least one by the end of the session, the subject was advanced to fixed-ratio (FR) 1 shaping sessions. If no responses were made to earn reinforcers, magazine training sessions were repeated for up to two additional consecutive days as necessary. Session advancement was determined on an individual basis.

2.3.5 Fixed-ratio 1 shaping sessions

Subjects then underwent daily one-hour training sessions utilizing an FR 1 schedule of reinforcement to strengthen the association between nose poke behaviors and reinforcer availability. In these sessions, a reinforcer was made available for each nose poke response. Once subjects demonstrated consistent reward-related behavior by earning at least 20

reinforcers per session across two consecutive sessions, they were advanced individually to the progressive fixed-ratio (PFR) motivation test. If no responses were made across three consecutive sessions, subjects were individually returned to magazine training for one day before resuming FR 1 shaping.

2.3.6 Progressive fixed-ratio breakpoint test

On the final day of the behavioral assay, subjects underwent a single session that utilized a PFR schedule of reinforcement, wherein reinforcers were administered with $n + 1$ responses where n represents the number of responses required to earn a reinforcer in the previous trial (i.e., 1 nose poke yields reinforcer availability on trial 1, 2 nose pokes yield reinforcer availability on trial 2, etc.). The breakpoint, or the point at which subjects stopped responding for a reinforcer, was measured as a proxy for motivation. A measure of average response effort was also derived by dividing the total number of nose pokes by the duration of time subjects engaged with the task. The session terminated after three hours or 20 minutes without an earned reinforcer, whichever occurred first.

2.4 Immunohistochemistry

2.4.1 Tissue collection

Two hours after injections on the day after completion of the PFR breakpoint test, subjects were deeply anesthetized with isoflurane and sacrificed by rapid decapitation. Brains were removed and sagittally bisected for one hemisphere to be used in immunohistochemical analyses and the other to be used for lipidomic analyses with liquid chromatography-tandem mass spectrometry. The left hemisphere was postfixed in 4% paraformaldehyde (PFA) for 24 hours at room temperature, then an additional 24 hours at 4°C. Brains were agitated on a rocker for all steps to maximize tissue penetration. Following postfixation, brains were submerged in phosphate buffered saline (PBS) for three 20-minute washes, then transferred to 30% sucrose solution for 24 hours at 4°C. Prior to sectioning, brains were embedded with Tissue-Tek OCT compound, frozen with dry ice, and stored at -80°C. Sagittal sections 30 µm in thickness were cut with a Leica CM300 cryostat (Leica, Deerfield, IL). Sections for each subject were contained in sealed 12-well plates and stored in PBS at 4°C for immunolabeling. Three-four sections per subject were taken for each analysis.

2.4.2 Tissue processing for histological analysis: neuronal dendrites (MAP2ab), microglia (Iba-1), astrocytes (GFAP), colocalization of IL-1β with astrocytes (GFAP/IL-1β)

All immunohistochemistry (IHC) wash and incubation procedures were performed at room temperature unless otherwise specified, and free-floating tissue was rocked at 27 rpm for all steps in 12-well plates fitted with 74 µm mesh inserts (Corning Life Sciences, Netwell Inserts, # 29442-132). All washes, as described, consist of three 5-minute rinses in phosphate buffer saline (PBS).

For MAP2ab and Iba-1 IHC, free-floating sections were first incubated in 0.5% H_2O_2 for 30 min, in 1% H_2O_2 for 60 min, and again in 0.5% H_2O_2 for 30 min, then washed, and followed by exposure to blocking buffer for 1 hour (PBS with 3% normal goat serum and 0.5% Triton X-100). Tissue was then incubated in primary antibodies, including microtubule-associated protein 2, ab (MAP2ab, mouse, Millipore, #MAB378; 1:500) for the detection of neuronal dendrites and ionized calcium-binding adapter molecule 1 (Iba-1, rabbit, Wako, #019-19741; 1:500) for the detection of microglia, mixed into blocking solution for 24 hours at 4°C. The primary antibodies were detected using secondary antibodies as follows: goat-anti-rabbit Alexa 594 (ThermoFisher, #A11012, red,1:500) and goat-anti-mouse Alexa 488 (ThermoFisher, #A21121, green, 1:500). The secondary antibodies were diluted in goat blocking buffer and applied to the sections for one hour. Cell nuclei were visualized with Hoechst 33342 (1:200, Molecular Probes, H3570, exposed for 3 minutes). Tissue sections were triple-rinsed in distilled water, mounted on Superfrost Plus glass microscopic slides (Fisher Scientific, #12-550-15), and coverslipped with antifade mounting medium (VectaShield, #H-1400).

For GFAP and IL-1β IHC, sections were washed and incubated in a permeability solution for 30 minutes [0.1% bovine serum albumin (BSA), 0.1% Triton X-100]. Samples were washed again and incubated in a blocking solution for 30 minutes (5% normal goat serum, 5% BSA, 0.1% Triton X-100). Tissue was then incubated in chicken anti-GFAP (1:1000; Thermo Fisher, #PA110004) and rabbit anti-IL-1β (1:250; Abcam, #AB9722) mixed into blocking solution for 24 hours at 4°C. Tissue was washed, covered, and incubated for one hour in goat anti-chicken Alexa Fluor 594 (1:500; Thermo Fisher, #A-11042) and goat anti-rabbit Alexa Fluor 488 (1:500; Thermo Fisher, #A-11034) diluted in blocking solution, washed, incubated for 3 minutes in Hoechst fluorescent stain (1:200 Hoechst:distilled water), then triple-rinsed in distilled water. Samples were then mounted on Superfrost Plus glass microscope slides and coverslipped with antifade mountant (Invitrogen ProLong Gold, #P36930).

2.4.3 Confocal microscopy: mean fluorescence intensity, cell quantification, cell morphology, and colocalization analysis

Immunolabeled tissue was imaged at 20x or 63x using a Zeiss LSM800 T-PMT laser scanning confocal microscope and ZEN 2018 Blue Edition software (Carl Zeiss, Inc., Thornwood, NY). The collection, processing and analyses of all images were conducted by experimenters blind to genotype and drug conditions. Images were acquired by using identical parameters for all groups (i.e., identical objective, zoom, laser intensity, gain, offset, and scan speed) optimized for control tissues. For both brain regions (i.e., nucleus accumbens and infralimbic cortex), images were sampled from 3-4 sagittal sections, spaced 300 µm apart, per animal.

For $MAP2ab^+$ immunoreactive neuronal dendrites, one image per brain region was taken per section, and the entire image (20x objective, 0.3 mm^2) was used as region of interest and processed using ImageJ (70) to quantify the intensity of staining per pixel in each image. Mean fluorescent intensity (MFI) was determined with ImageJ without digital manipulation. Data represent individual subject data (MAP2ab MFI) averaged across all images taken per brain region.

For microglia activity, one image per brain region was taken per section and Iba-1$^+$ microglial cell bodies containing Hoechst-stained nuclei were counted by two experimenters blinded to treatment groups (20x objective, 0.3 mm^2). Interrater reliability was assessed using Cronbach's alpha (nucleus accumbens α = .798; infralimbic cortex α = .814), and data from both raters were averaged to represent microglia counts. Data represent individual subject data (Iba-1$^+$ microglia counts) averaged across all images taken per brain region. Furthermore, microglia morphology was assessed for the nucleus accumbens via Sholl analysis following published procedures (63, 71, 72). In brief, z-stack images were collected at 63x magnification of immunodetected Iba-1$^+$ microglia stained with Hoechst (n = 4 mice per group/3-4 sections each). Orthogonal projection images were generated from the slide z-stack images, resulting in one z-plane, using ZEN 2018 Blue Edition software, and exported to Fiji build of ImageJ. Per animal a total of 5-6 microglia were individually isolated for analysis by random selection (72). The soma size was measured in Fiji using the freehand selection tool. The images were cleaned, and the background noise was removed using the despeckle tool. The processed images were overlayed with the original image, and the tracing tool was used to select the microglia of interest, and the background was cleared. The images were converted to binary images, and the line segment tool was used to draw a line from the center of each soma to the tip of its longest process, providing the maximum branch length (µm). The Sholl analysis plugin software was used to assess additional measures, with the first shell set at 10 µm and subsequent shells set at 2 µm sizes, to determine intersections at each Sholl radius. This provided the critical radius (radius value with the highest number of intersections), the process maximum (the highest number of intersections regardless of radius value), the number of primary processes (intersections at the first Sholl radius), and the process total (total number of intersections). Individual microglia were treated as individual data points.

For GFAP$^+$ astrocytes and colocalization with IL-1β, three z-stack images per brain region were taken per section (20x objective, 0.3 mm^2), and ImageJ software was used for astrocyte quantification and analyses of colocalization with IL-1β. GFAP$^+$ astrocyte cell bodies containing Hoechst-stained nuclei were manually quantified by two experimenters blinded to treatment groups. Interrater reliability was assessed using Cronbach's alpha (α = 0.993) (nucleus accumbens α = .994; infralimbic cortex α = .992), and data from both raters were averaged to represent astrocyte counts. Data represent individual subject data (GFAP$^+$ astrocyte counts) averaged across all images taken per brain region. For GFAP$^+$ colocalization with IL-1β, the JACoP plugin was used for colocalization measures (73). Herein, absolute intensity thresholds were defined manually for both channels to control for any background fluorescence. Voxels that exceeded thresholds across both channels were considered colocalized, and the corresponding Pearson's correlation coefficient (PCC) was recorded. Generated cytofluorograms were also reviewed to ensure accurate colocalization thresholds. Data represent individual subject data (GFAP/IL-1β colocalization) averaged across all images taken per brain region. Note, that we lost the brain sections of one vehicle-treated Tat(−) mouse due to a processing error during IHC labeling, and thus, only 8 individual subject data points are shown for GFAP$^+$ astrocyte counts and GFAP/IL-1β colocalization.

2.5 Liquid chromatography-tandem mass spectrometry

2.5.1 Metabolo-lipidomic sample preparation

Whole tissue striatal and hippocampal samples dissected from the hemisphere that were not used for IHC were prepared as previously described (74). All standards and internal standards used for LC-MS/MS analysis (referred to collectively as lipidomic analyses elsewhere) of arachidonic acid, docosahexaenoic acid, and linoleic acid-derived lipid mediators were purchased from Cayman Chemical (Ann Arbor, Michigan, USA). All high-performance liquid chromatography (HPLC) solvents and extraction solvents were HPLC grade or better.

Tissue samples were massed into pre-chilled (-20°C) Qiagen homogenizer tubes containing a 5mm stainless steel homogenizing bead (Qiagen, Germantown, MD, USA). An aliquot of 500 µL pre-chilled methanol was added to each tube before homogenizing at 50 Hz for 2 minutes. Samples were then centrifuged at 14,000 rpm and 4°C for ten minutes. The supernatant was extracted into a 1.5 mL centrifuge tube and spiked with 10 µL of the internal standard solution (10 pg/µL each of 5(S)-HETE-d8, 8-iso-PGF2a-d4, 9(S)-HODE-d4, LTB4-d4, LTD4-d5, LTE4-d5, PGE2-d4, PGF2a-d9 and RvD2-d5 in ethanol), followed by vortexing. The sample was then dried in a vacuum centrifuge at 55°C until dry. The sample was then immediately reconstituted in 1.0 mL of 90:10 water:methanol before purification by solid phase extraction (SPE).

Lipid mediators were isolated using Strata-X 33 µm 30 mg/1 mL SPE columns (Phenomenex, Torrance, CA) on a Biotage positive pressure SPE manifold (Biotage, Charlotte, NC). SPE columns were pre-washed with 2 mL of methanol (MeOH) followed by 2 mL of H_2O. After applying the entire 1 mL of reconstituted sample, the columns were washed with 1 mL of 10% MeOH. The lipid mediators were then eluted sequentially with 1 mL of methyl formate followed by 1 mL of MeOH directly into a reduced surface activity/maximum recovery glass autosampler vial (MicroSolv Technology Corp. Leland, NC), drying after each solvent elution with a steady stream of nitrogen directly on the SPE manifold. The sample was then immediately reconstituted with 20 µL of ethanol and analyzed immediately or stored at –70°C until analysis for no more than 1 week.

2.5.2 Liquid chromatography-mass spectrometry

Quantitation of lipid mediators was performed using 2-dimensional reverse phase HPLC tandem mass spectrometry (LC-MS/MS). The HPLC system consisted of an Agilent 1260 autosampler (Agilent Technologies, Santa Clara, CA), an Agilent 1260 binary loading pump (pump 1), an Agilent 1260 binary analytical pump (pump 2), and a 6-port switching valve. Pump 1 buffers consisted of 0.1% formic acid in water (solvent A) and 9:1 v:v acetonitrile:water with 0.1% formic acid (solvent B). Pump 2 buffers consisted of 0.01% formic acid in water (solvent C) and 1:1 v:v acetonitrile:isopropanol (solvent D).

Five µL of extracted sample was injected onto an Agilent SB-C18 2.1 X 5 mm 1.8 µm trapping column using pump 1 at 2 mL/minute for 0.5 minutes with a solvent composition of 97% solvent A: 3% solvent B. At 0.51 minutes, the switching valve changed the flow to the trapping column from pump 1 to pump 2. The flow was reversed and the trapped lipid mediators were eluted onto an Agilent Eclipse Plus C-18 2.1 X 150 mm 1.8 µm analytical column using the following gradient at a flow rate of 0.3 mL/minute: hold at 75% solvent A:25% solvent D from 0-0.5 minutes, then a linear gradient from 25-75% D over 20 minutes followed by an increase from 75-100% D from 20-21 minutes, then holding at 100% D for 2 minutes. During the analytical gradient, pump 1 washed the injection loop with 100% B for 22.5 minutes at 0.2 mL/minute. Both the trapping column and the analytical column were re-equilibrated at starting conditions for 5 minutes before the next injection.

Mass spectrometric analysis was performed on an Agilent 6490 triple quadrupole mass spectrometer in negative ionization mode. The drying gas was 250°C at a 15 mL/minute flow rate. The sheath gas was 350°C at 12 mL/minute. The nebulizer pressure was 35 psi. The capillary voltage was 3500 V. Data for lipid mediators was acquired in dynamic MRM mode using experimentally optimized collision energies obtained by flow injection analysis of authentic standards. Calibration standards for each lipid mediator were analyzed over a range of concentrations from 0.25 – 250 pg on column. Calibration curves for each lipid mediator were constructed using Agilent Masshunter Quantitative Analysis software. Tissue samples were quantitated using the calibration curves to obtain the on-column concentration, followed by multiplication of the results by the appropriate dilution factor to obtain the concentration in pg/mL.

2.6 Statistical analyses

All statistical analyses were performed using SPSS (IBM SPSS Statistics, Version 28, Chicago, IL, USA) and represented visually using GraphPad Prism (GraphPad Software, Inc., Version 9, San Diego, CA, USA) and OriginPro (OriginLab Corporation, Version 2022b, Northampton, MA, USA). Biorender was also utilized to create the experimental schematic depicted in Figure 1. Data are reported as mean ± standard error. Two-way analyses of variance (ANOVAs) with follow-up Tukey's *post hoc* tests when appropriate were conducted with genotype [2 levels: Tat(−), Tat(+)] and drug (2 levels: vehicle, MJN110) as between-subjects factors for all but three measures (exceptions detailed as follows). For assessments of body mass, three-way mixed ANOVAs were conducted with time (14 levels: 14 days) as a within-subjects factor and genotype and drug as between-subjects factors. This was then followed up by two-way ANOVAs with genotype and drug as between-subjects factors for each day and Tukey's *post hoc* tests when appropriate. For assessments of PFR breakpoint and number of days to acquisition, Shapiro Wilk tests demonstrated residuals failed to meet normality assumptions; as such, Mann-Whitney U nonparametric tests were run to assess the effects of genotype and drug. Pearson correlation coefficients were calculated for three behavioral measures and all striatal-related CNS measures, except for Iba-1$^+$ microglial morphology due to the chosen smaller sample size, and potential relationships between variables were explored. Data were subdivided by genotype and drug groups to obtain the correlation matrices. Pearson's correlation coefficients were calculated for each pair of continuous variables for each group. This allowed the assessment of the strength and direction of the linear relationship between variables within each group separately. An alpha of $p \leq 0.05$ was considered significant for all analyses.

3 Results

3.1 Body mass was not affected by chronic MJN110 treatment

Body mass (g) was taken daily from the start of drug injections until the end of the study. Body mass data are reported for the first two weeks of drug injections prior to the start of behavioral assessment. No significant effects were noted, with only a trend toward a significant genotype effect [$F(1, 30) = 3.7$, $p = 0.063$; Figure 2]. Separate two-way ANOVAs for each day revealed Tat expression significantly decreasing body mass for day 5 [$F(1, 30) = 4.3$, $p = 0.047$], day 9 [$F(1, 30) = 4.7$, $p = 0.038$], day 13 [$F(1, 30) = 4.5$, $p = 0.042$], and day 14 [$F(1, 30) = 4.2$, $p = 0.050$]. Follow-up Tukey's *post hoc* tests demonstrated no significant group differences.

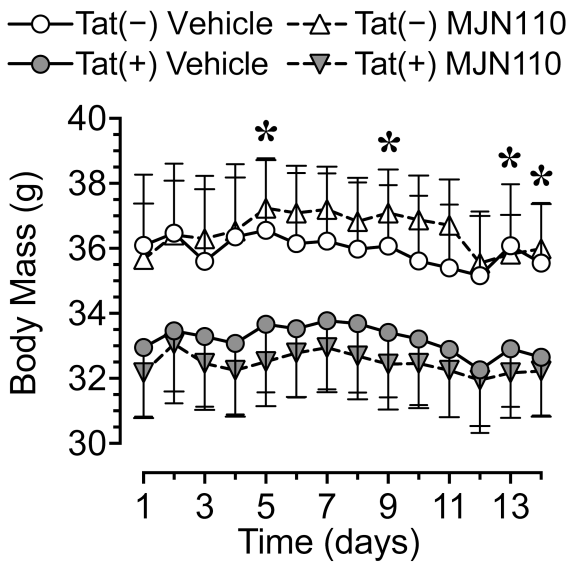

FIGURE 2
Body mass data for the two weeks of MJN110/vehicle injections prior to the start of behavioral assessment. Tat expression showed a trend for decreased body mass (g) over the two-week period, with lower body mass for Tat(+) mice compared to Tat(−) mice on days 5, 9, 13, and 14. Follow-up Tukey's *post hoc* test demonstrated no significant group differences. No effects were noted for MJN110 treatment. All data are expressed as mean ± the standard error of the mean (SEM). Statistical significance was assessed by ANOVAs followed by Tukey's *post hoc* tests when appropriate; *$p < 0.05$ main effect of genotype.

3.2 No behavioral alterations were observed following Tat induction or MJN110 treatment

No baseline performance differences were observed between Tat(−) and Tat(+) subjects across drug groups during FR 1 shaping trials, either in the number of sessions required to learn the task (Figure 3A) or the number of reinforcers earned during sessions wherein criteria for advancement to the PFR breakpoint test were met (Figure 3A'). Additionally, no significant differences were observed between Tat(−) and Tat(+) subjects across drug groups during the PFR breakpoint test in measures of breakpoint (Figure 3B), total session time (Figure 3B'), number of nose pokes (Figure 3C), or nose pokes per minute (Figure 3C'). These results indicate that Tat and 1 mg/kg MJN110 demonstrate no significant effects on either reward-related task learning or motivation to exert additional effort to receive a salient reinforcer.

3.3 MJN110 reversed Tat-induced dendritic injury, but only minor effects were noted on microglia

3.3.1 Neuronal dendritic density

MJN110 significantly increased neuronal dendritic density in the nucleus accumbens [$F(1, 29) = 4.4$, $p = 0.044$; Figure 4A], which was significantly altered by genotype [$F(1, 29) = 4.5$, $p = 0.042$]. A follow-up Tukey's *post hoc* test revealed vehicle-treated Tat(+) mice showing lower neuronal dendritic density compared to vehicle-treated Tat(−) mice ($p = 0.050$) and MJN110-treated Tat(+) mice ($p = 0.027$). Within the infralimbic cortex, significant effects of both Tat and MJN110 were observed [$F(1, 29) = 5.2$, $p = 0.030$ and $F(1, 29) = 4.0$, $p = 0.054$, respectively; Figure 4A']. A follow-up Tukey's *post hoc* test revealed vehicle-treated Tat(+) mice showing lower neuronal dendritic density compared to MJN110-treated Tat(−)

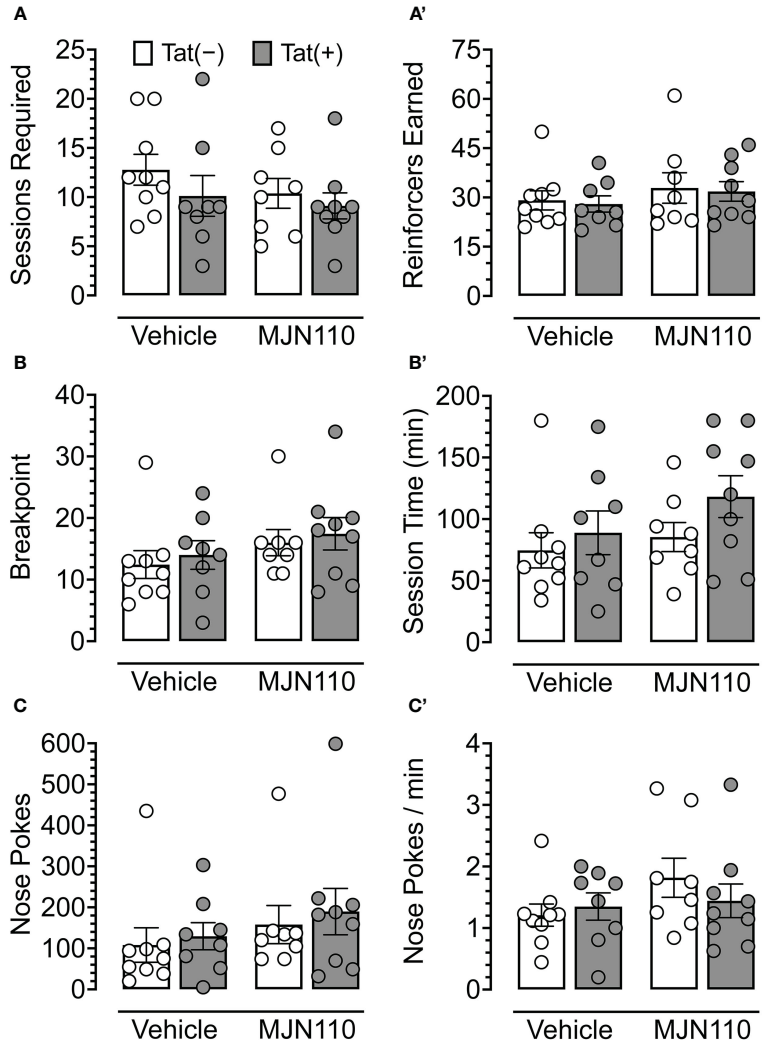

FIGURE 3
Behavioral data for fixed-ratio (FR) 1 shaping sessions and progressive fixed-ratio (PFR) breakpoint test. For FR 1 shaping **(A, A')**, no significant differences were observed between genotype or drug groups for the number of sessions required to advance to the PFR breakpoint test **(A)** or the number of reinforcers earned in sessions wherein criteria for advancement were met **(A')**. In the PFR breakpoint test **(B-C')**, no significant differences were observed for breakpoint **(B)**, session length **(B')**, total number of nose poke behaviors **(C)**, or nose pokes per minute **(C')**. All data are expressed as mean ± the standard error of the mean (SEM). Statistical significance was assessed by ANOVAs or Mann-Whitney U nonparametric tests. Individual subject data are represented by open circles.

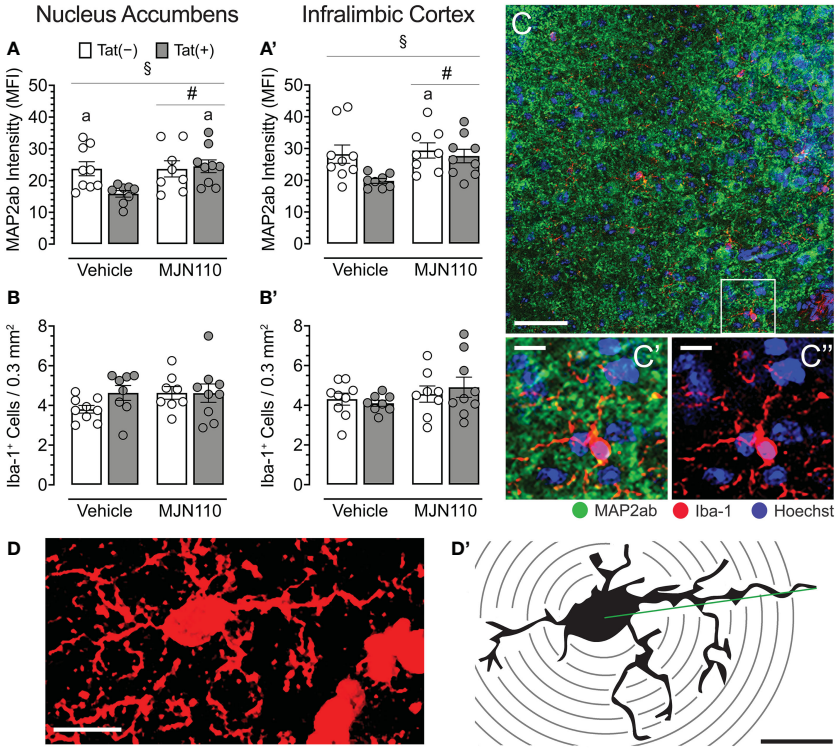

FIGURE 4
Neuronal dendritic intensity and microglia density/morphology in the nucleus accumbens and infralimbic cortex. **(A)** In the nucleus accumbens, MJN110 increased neuronal dendritic intensity based on Tat expression, with decreased MAP2ab intensity in vehicle-treated Tat(+) mice compared to MJN110-treated Tat(+) mice and vehicle-exposed Tat(–) mice. **(A')** In the infralimbic cortex, the same main effect for drug and drug x genotype interaction was noted, with decreased MAP2ab intensity in vehicle-treated Tat(+) mice compared to MJN110-treated Tat(–) mice. **(B, B')** Microglia density was not affected by genotype or drug in the nucleus accumbens or infralimbic cortex. **(C)** Brain section from the nucleus accumbens of a vehicle-treated Tat(+) mouse taken at 20x (0.3 mm^2, Scale bar = 50 µm) and at a higher magnification of MAP2ab intensity and/or microglia Iba-1 (**C'** and **C''**, Scale bars = 10 µm). **(D)** Example of an orthogonal projection Iba-1-stained image from the nucleus accumbens used for Sholl analysis (63x, Scale bar = 10 µm, image processed with ImageJ). **(D')** Example of a single microglial cell with concentric Sholl radii (black circles) superimposed on the image (Scale bar = 10 µm). All data are expressed as mean ± the standard error of the mean (SEM). Statistical significance was assessed by ANOVAs followed by Tukey's *post hoc* tests when appropriate; $^{\#}p < 0.05$ main effect of drug, $^{\S}p < 0.05$ genotype x drug interaction, $^{a}p < 0.05$ vs. vehicle-treated Tat(+) mice. Individual subject data (averaged across 3-4 images per region) represented by open circles.

mice ($p = 0.030$). No other group comparisons were significant, with only trending towards significance for vehicle-treated Tat(+) mice compared to MJN110-treated Tat(+) mice ($p = 0.057$).

3.3.2 Microglia density and morphology

For both brain regions, the nucleus accumbens and the infralimbic cortex, Tat and MJN110 had no significant effects on microglia density (Figure 4B, B', C, C', C''). Sholl analyses were conducted in the nucleus accumbens to assess microglia morphology ($n = 4$ mice per group with 3-4 sections/5-6 microglia, Figures 4D, D' and Table 1). Tat expression significantly increased the soma area (Table 1), which is associated with amoeboid morphology (71) and has been reported previously for Tat(+) male mice (63). Tukey's *post hoc* test revealed no significant differences between groups. Additionally, MJN110 increased the number of primary processes (intersections at the first Sholl radius), whereas no other measure was affected by the drug, and Tukey's *post hoc* test revealed no significant differences between groups. Overall, microglia morphology appears to be altered by Tat and MJN110 treatment only to a minimal extent.

3.4 MJN110 reversed some Tat-induced alterations to astrocyte density and IL-1β recruitment

3.4.1 Astrocyte density

Tat significantly increased astrocyte density in the nucleus accumbens [$F(1, 29) = 5.1$, $p = 0.032$; Figure 5A]. Subjects treated with MJN110 trended towards a significant decrease in this region [$F(1, 29) = 3.0$, $p = 0.096$]. A follow-up Tukey's *post hoc* test revealed vehicle-treated Tat(+) mice showing higher astrocyte density compared to MJN110-treated Tat(–) mice ($p = 0.045$). In the infralimbic cortex (Figure 5A'), Tat significantly increased the number of GFAP-positive astrocytes [$F(1, 29) = 6.5$, $p = 0.017$], whereas MJN110 significantly decreased this measure [$F(1, 29) = 8.7$, $p = 0.006$]. Importantly, a significant interaction was observed between genotype and drug [$F(1, 29) = 6.8$, $p = 0.015$], in which vehicle-treated Tat(+) subjects showed higher astrocyte density compared to all other groups [vehicle-treated Tat(–) mice, $p = 0.006$; MJN110-treated Tat(–) mice, $p = 0.003$; MJN110-treated Tat(+) mice, $p = 0.002$].

TABLE 1 Effect of Tat and MJN110 on microglia morphology in the nucleus accumbens of Tat transgenic mice.

Measure	Genotype	Repeated vehicle	Repeated MJN110	Genotype effect		Drug effect		Genotype x drug	
		mean ± SEM	mean ± SEM	$F_{1,80}$	p	$F_{1,80}$	p	$F_{1,80}$	p
Soma area (μm^2)	Tat(−)	30.85 ± 1.16	30.87 ± 1.02	3.92	**0.05**	0.86	0.35	0.90	0.34
	Tat(+)	33.82 ± 0.99	31.92 ± 0.85						
Maximum branch length (μm)	Tat(−)	29.24 ± 1.26	30.06 ± 1.33	0.18	0.66	0.17	0.68	0.04	0.84
	Tat(+)	30.08 ± 1.32	30.36 ± 1.39						
Critical radius (μm)	Tat(−)	12.76 ± 0.56	12.60 ± 0.63	1.94	0.16	0.003	0.95	0.02	0.86
	Tat(+)	13.64 ± 0.81	13.71 ± 0.78						
Number of primary process	Tat(−)	4.95 ± 0.34	5.90 ± 0.53	0.13	0.71	4.64	**0.03**	0.004	0.95
	Tat(+)	5.09 ± 0.53	6.10 ± 0.35						
Process maximum	Tat(−)	6.71 ± 0.44	7.65 ± 0.47	0.04	0.82	2.88	0.09	0.08	0.77
	Tat(+)	6.95 ± 0.44	7.62 ± 0.34						
Process total	Tat(−)	38.19 ± 3.84	38.95 ± 2.22	0.51	0.47	0.48	0.48	0.20	0.65
	Tat(+)	39.00 ± 3.23	42.57 ± 2.77						

Sholl analysis of microglia morphology in the nucleus accumbens of repeated (2-week) vehicle- or MJN110-treated Tat(−) and Tat(+) female mice. Data are expressed as the mean ± SEM. The parameters measured by Sholl analysis are indicated in parentheses in the first column. Two-way ANOVAs for each measurement were conducted with genotype and drug as between-subject factors. F values and p values are presented from ANOVA results. Bolded values denote significant differences at $p < 0.05$; mean ± SEM, $n = 4$ mice per group with 3-4 sections/5-6 microglia.

3.4.2 Astrocytic IL-1β colocalization

Within the nucleus accumbens, significant effects of both, Tat and MJN110 were observed [$F(1, 29) = 6.7$, $p = 0.015$ and $F(1, 29) = 12.0$, $p = 0.002$, respectively], as well as a trend towards a significant interaction [$F(1, 29) = 3.3$, $p = 0.078$; Figure 5B). Notably, a follow-up Tukey's *post hoc* test revealed that vehicle-treated Tat(+) subjects showed higher colocalization of IL-1β with GFAP compared to all

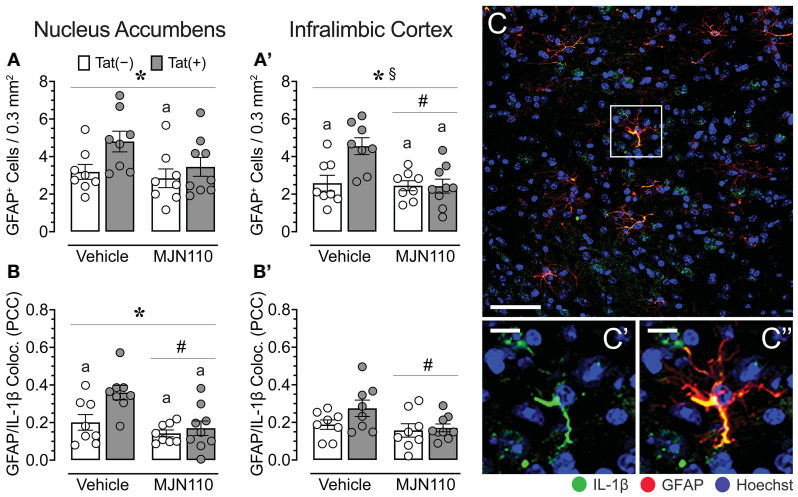

FIGURE 5
Astrocyte density and astrocytic IL-1β colocalization in the nucleus accumbens and infralimbic cortex. **(A)** Tat increased astrocyte density in the nucleus accumbens, with increased GFPA$^+$ counts for vehicle-treated Tat(+) mice compared to MJN110-treated Tat(−) mice. **(A')** In the infralimbic cortex, MJN110 downregulated Tat-driven increases in astrocyte density based on Tat expression, with increased GFPA$^+$ counts for vehicle-exposed Tat(+) mice compared to all other groups. **(B)** Colocalization of IL-1β with GFAP$^+$ cells in the nucleus accumbens was significantly affected by Tat and MJN110, with vehicle-exposed Tat(+) mice showing higher colocalization of IL-1β with GFAP$^+$ cells compared to all other groups. **(B')** In the infralimbic cortex, colocalization of IL-1β with GFAP$^+$ cells was downregulated by MJN110. **(C)** Brain section of GFAP$^+$ astrocytes with colocalization of IL-1β from the nucleus accumbens of a vehicle-treated Tat(+) mouse taken at 20x (0.3 mm^2, Scale bar = 50 μm) and at a higher magnification (**C'** and **C''**, Scale bars = 10 μm). All data are expressed as mean ± the standard error of the mean (SEM). Statistical significance was assessed by ANOVAs followed by Tukey's *post hoc* tests when appropriate; *$p < 0.05$ main effect of genotype, $^{\#}p < 0.01$ main effect of drug, $^{\S}p < 0.05$ genotype x drug interaction, $^{a}p < 0.05$ vs. vehicle-treated Tat(+) mice. Individual subject data (averaged across 3-4 images per region) are represented by open circles. Note that the brain sections of one vehicle-treated Tat(−) mouse were lost due to a processing error during IHC labeling and thus, only 8 individual subject data points are shown for the vehicle-treated Tat(−) mouse group. PCC, Pearson's colocalization coefficient.

other groups [vehicle-treated Tat(−) mice, p = 0.022; MJN110-treated Tat(−) mice, p = 0.001; MJN110-treated Tat(+) mice, p = 0.004]. While in the infralimbic cortex (Figure 5B'), no main effect of Tat was observed for colocalization of IL-1β with GFAP, MJN110 significantly decreased colocalization across genotypes [$F(1, 29)$ = 4.5, p = 0.042]. A follow-up Tukey's *post hoc* test demonstrated no significant group differences. Figures 5C-C" shows a representative image from the nucleus accumbens of colocalization of IL-1ß with GFAP$^+$ astrocytes.

3.5 Contrasting effects of Tat and MJN110 on proinflammatory lipid mediator expression

Due to the more prominent astrocytic IL-1β colocalization observed in the nucleus accumbens relative to the infralimbic cortex and our focus of interest on associated inflammatory lipid mediators, lipidomic analyses with LC-MS/MS centered primarily on further characterizing these profiles within the striatum. These analyses revealed a significant main effect of MJN110 treatment in reducing striatal 12-HETE [$F(1, 30) = 5.0$, $p = 0.033$; Figure 6A], 15-HETE [$F(1, 30) = 5.3$, $p = 0.029$; Figure 6B], 5-HETE/14(15)-epoxyeicosatrienoic acid [EET; $F(1, 30) = 4.9$, $p = 0.035$; Figure 6C], and 11-HETE [$F(1, 30) = 4.7$, $p = 0.038$; Figure 6D). Follow-up Tukey's *post hoc* tests revealed decreased 15-HETE striatal levels for MJN110-treated Tat(+) mice compared to vehicle Tat(−) mice (p = 0.023). Additional alterations were observed in the hippocampus (see Supplementary Figure S1). These analyses revealed a significant genotype x drug interaction for 12-HETE [$F(1, 30) = 4.6$, $p = 0.040$], with follow-up Tukey's *post hoc* revealing no significant group differences. Further, significant main effects of MJN110 treatment in reducing hippocampal 15-HETE [$F(1, 30) = 4.5$, $p = 0.042$] and 5-HETE/14(15)-epoxyeicosatrienoic acid [EET; $F(1, 30) = 6.7$, p = 0.015] were noted. Further, Tat expression increased 11-HETE [$F(1, 30) = 4.4$, $p = 0.046$] that was altered by drug [genotype x drug interaction, $F(1, 30) = 4.1$, $p = 0.051$]. Follow-up Tukey's *post hoc* tests revealed increased 11-HETE hippocampal levels for vehicle-treated Tat(+) mice compared to vehicle Tat(−) mice (p = 0.032).

3.6 Subgroup-specific relationships between measures

Associations between CNS and behavioral measures differed among subgroups and were only found in vehicle-treated Tat(−) mice and MJN110-treated Tat(+) subjects (Figure 7). In vehicle-treated Tat(−) subjects, low striatal 5-HETE/14(15)-EET was strongly associated with higher breakpoints and a larger number of reinforcers earned during FR1 shaping sessions (Figure 7A). In contrast, for MJN110-treated Tat(+) subjects, increased astrocyte density and higher astrocytic IL-1β colocalization in the nucleus accumbens was strongly associated with a larger number of reinforcers earned during FR1 shaping sessions and a greater number of shaping sessions required to advance to the PFR test, respectively (Figure 7D).

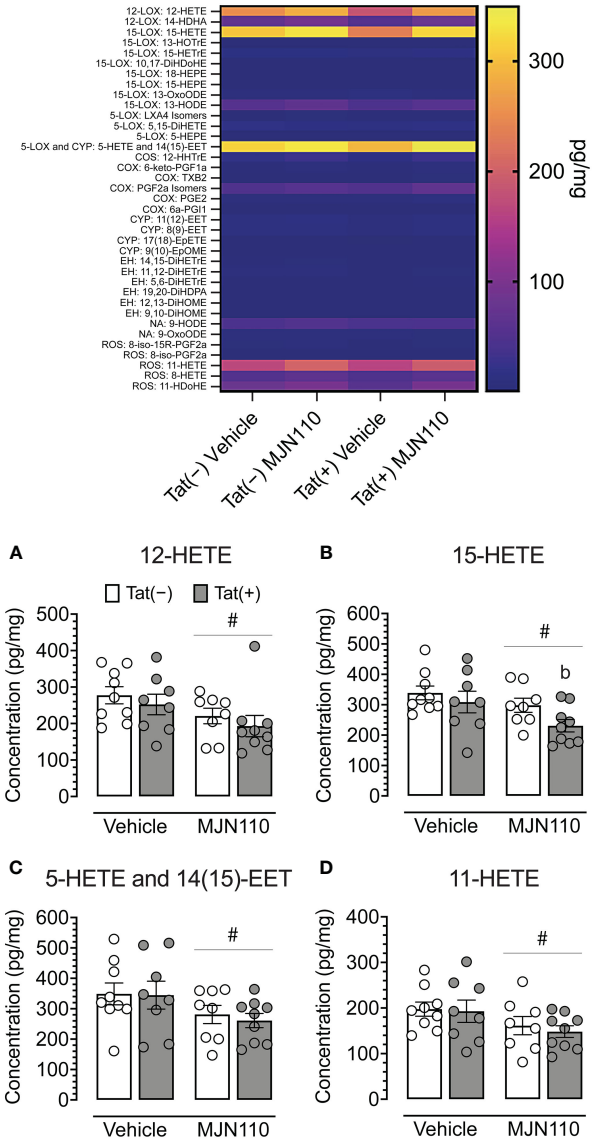

FIGURE 6
Quantification of striatal lipid mediators. Heatmap of all lipid mediators assessed (top). Summary data from significant findings **(A–D)**. MJN110 treatment significantly decreased striatal 12-HETE **(A)**, 15-HETE **(B)**, 5-HETE/14(15)-EET **(C)**, and 11-HETE **(D)**. All data are expressed as mean ± the standard error of the mean (SEM). Statistical significance was assessed by ANOVAs followed by Tukey's *post hoc* tests when appropriate; $^{\#}p < 0.05$ main effect of drug, $^{b}p = 0.023$ vs. vehicle-treated Tat(−) mice. Individual subject data are represented by open circles.

Behavioral predictors of PFR breakpoint also varied between groups. For all groups, except MJN110-treated Tat(+) mice, a larger number of reinforcers earned during FR1 shaping sessions was strongly associated with higher PFR breakpoints (Figures 7A-C). Further, in vehicle-treated Tat(+) subjects, a lower number of required FR1 shaping sessions was strongly associated with higher PFR breakpoints (Figure 7C).

Associations between CNS measures demonstrated that the four striatal HETE mediators showed high positive correlations within each other for all groups, except for the vehicle-treated Tat(−) mice (Figures 7B-D). In vehicle-treated Tat(−) mice, only higher striatal

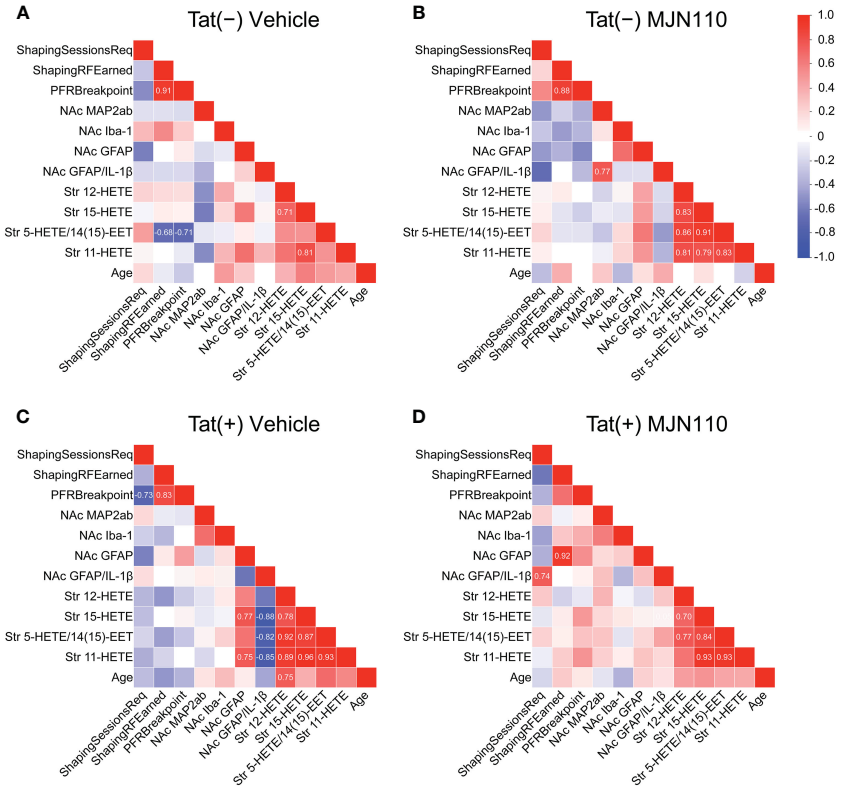

FIGURE 7
Correlation matrices of quantified variables across groups. Association patterns between behavior, nucleus accumbens MAP2ab+ dendritic intensity, microglia density, astrocyte density, astrocytic IL-1β colocalization, and striatal inflammatory lipid mediator expression differ between subgroups. Among other distinctions, predictors of PFR breakpoint varied between genotype and treatment groups. Additionally, vehicle-treated Tat(+) subjects **(C)** show stronger associations between astrocyte density and proinflammatory lipid mediator expression relative to the other groups, vehicle-treated Tat(−) mice **(A)**, MJN110-treated Tat(−) subjects **(B)**, and MJN110-treated Tat(+) mice **(D)**. Pearson's correlation coefficients (*r*) are indicated for significant values at $p \leq 0.05$. NAc, nucleus accumbens.

15-HETE levels were associated with higher 11-HETE and 12-HETE levels (Figure 7A). Interestingly, in vehicle-treated Tat(+) subjects, higher striatal 15-HETE and 11-HETE levels were strongly associated with increased astrocyte density in the nucleus accumbens, whereas higher striatal HETEs were also associated with less IL-1β colocalization with GFAP (Figure 7C).

4 Discussion

While no behavioral effects were observed, the present study demonstrated that in the infralimbic cortex and nucleus accumbens, MJN110 successfully reduced Tat-induced dendritic injury and Tat-induced astrocyte-related neuroinflammation, as shown by decreasing Tat-induced upregulated astrocyte density or astrocytic IL-1β colocalization. Notably, Tat induced region-specific inflammatory effects such that astrocyte recruitment was increased in the infralimbic cortex, whereas instead, astrocytic IL-1β was increased in the nucleus accumbens. No effects were noted for Iba-1$^+$ microglia density in either brain region, and only minor effects were noted for microglia morphology assessed in the nucleus accumbens. Further, selected HETE-related inflammatory lipid mediators in the striatum were downregulated by chronic MJN110 treatment.

The absence of behavioral differences, while contrary to hypothesized outcomes, may indeed be of some significance insofar as these results demonstrate MJN110 lacks cannabimimetic effects. Tetrahydrocannabinol (THC), a major CB_1R agonist component of cannabis, has been shown to increase dopamine signaling in the nucleus accumbens as well as the ventral tegmental area (75–77), with both regions being critical components of the mesocorticolimbic system involved in reward-related behaviors and salience processing. These THC-mediated dopamine alterations underlie commonly observed increases in food intake, often referred to as the "munchies" (78). While other studies of chronic THC use have contrastingly found decreases in dopamine synthesis and activity (79), it is important to note these results are largely driven by cannabis-dependent individuals with high-severity use (80, 81). The limited existing data available for MJN110 effects on motivated behavior demonstrate that acute treatment increases reward-directed response; however, this effect was only observed at doses five- and tenfold higher than the 1 mg/kg dose used in the present study (61).

The lack of behavioral alterations across groups may also be explained by compensatory mechanisms such as homeostatic scaling (82). Specifically, excitatory synapse loss and increased inhibitory tone have previously been observed, both of which function to protect neurons from increased N-methyl-D-

aspartate (NMDA) receptor activity in the presence of Tat-induced excitotoxicity (26, 83). Previous work has also found immune tolerance driven by Tat when assessing microglia activity [65]. As these compensatory changes in excitability and immune response are evident in the context of chronic rather than acute Tat exposure (63, 84), it could be speculated that more robust behavioral alterations may have been observed earlier after Tat induction than the time period presently investigated. Immune tolerance may also contribute to the lack of Tat-induced effects on lipid metabolite expression observed presently; while Tat initially induces inflammation, potentially contributing to dendritic injury seen in vehicle-exposed Tat(+) mice, the immune system becomes desensitized to its effects after about three months of exposure (63). Reduction in lipid metabolite expression following MJN110 treatment may suggest the potential to modulate immune responses in the chronic phase of HIV-1-associated neuroinflammation wherein observable inflammatory insult is diminished, but immune priming remains present (85). While no differences were observed between Tat(+) and Tat(−) subjects, the lipid metabolites assessed may not be as sensitive to Tat exposure in chronic conditions. MJN110 may exert effects through other mechanisms (e.g., modulation of immune cell activity or regulation of downstream signaling pathways associated with neuroinflammation).

Another plausible alternative explanation for behavioral similarity across groups is the growing body of research demonstrating biological sex-specific effects of HIV-1 and constituent viral proteins, including Tat, on both peripheral and CNS outcomes (86). Homeostatic scaling through upregulation of inhibitory activity by γ-aminobutyric acid (GABA)ergic neurons in the hippocampus (26, 83) and the prefrontal cortex have been established in the context of Tat expression, with the latter particularly in females (87). In accordance with these neurophysiological data, studies focused on neurocognitive outcomes of infection have shown worsened behavioral profiles among infected females in domains of spatial memory, learning, and motor skills (88, 89). Data have also shown female-specific hypersensitivity to pain (90), slower recovery from nerve injury, and heightened inflammatory responses to local injury (91). As sex-specific findings regarding executive function have historically been inconsistent (92, 93) and relatively little has been established for motivational deficits, the addition of male subjects in the present work would have provided valuable insight into potential sex differences in these domains. In addition to between-sex variation, there may be within-sex variation due to estrous cycle. Previous studies employing similar models have demonstrated that HIV-1 affects motivation, including reduced response vigor and increased reward threshold (28, 94); however, female subjects were not included in those studies. Prior work has also shown decreased motivation for food rewards (92, 95), even under food-restricted conditions when in estrus, during which time attention is diverted preferentially to sexual motivation (95). It has been posited that this decrease in consumption during estrus occurs due to reductions in positive-feedback signals elicited by natural reinforcers (96), potentially a result of increased striatal dopamine turnover and decreased dopamine concentrations during this phase of the estrous cycle (97). Tracking estrous cycles during assessment or phase-locking assessments to one estrous stage would better elucidate the effects of hormones on motivated behavior and potentially reduce variability.

Though this study did not directly observe the effects of MJN110 against HAND in terms of behavioral outcomes, it provides insights into its potential for neuroprotection and as a modulator of neuroinflammatory responses in the frontostriatal circuitry. The MJN110 observed increase of Tat-induced downregulation of MAP2ab$^+$ dendritic intensity and reduction of neuroinflammatory markers demonstrates promise for curbing the underlying inflammatory priming linked with HIV-1, potentially diminishing the emergence or persistence of additional behavioral sequelae associated with HAND. To better clarify the involvement of other cytokines in these effects, further quantification of TNF-α would be advantageous. Because TNF-α inhibits astrocytic glutamate uptake and increases reactive oxygen species (ROS) (98, 99), characterizing HIV-1-associated effects on this measure would enable elucidation of additional mechanisms by which these cells become dysfunctional in infection and may be restored with MJN110. Notably, biomarkers of oxidative stress are elevated in PLWH treated with highly active antiretroviral drugs (100). This increased oxidative stress contributes to neurotoxicity, HAND, and premature aging (100, 101). The observed upregulation of MAP2ab$^+$ dendritic signal by MJN110 in Tat(+) mice and MJN110-induced reduction in ROS-derived 11-HETE in the present study suggests a mechanism apart from other enzymatic pathways by which this treatment may be neuroprotective, and collecting data for TNF-α would provide insight into whether the reduction in oxidative stress biomarkers is related to possible additional MJN110-driven immunoreactivity-suppressing effects. Assessing lipid mediator expression in the infralimbic cortex would also provide valuable data to determine whether the effects of Tat and MJN110 may be distinct from those observed in the striatum. As hippocampal lipid mediator expression analyses revealed Tat-induced upregulation of 11-HETE (Supplementary Figure S1D), additional region-specific effects may also be observed elsewhere. Given the differences in neuroinflammatory phenotypes between the infralimbic cortex and striatum in astrocyte density and colocalization with IL-1β, it remains possible that diverse cellular mechanisms are recruited to drive distinct inflammatory responses across regions.

In contrast to previous studies of MAGL inhibition, which have shown reductions in prostaglandin expression (102), no such alteration was observed in our analyses (see Figure 6 and Supplementary Figure S1 heatmap panel sections for COX pathway). However, the underlying difference may involve which specific MAGL inhibitor is administered, what dosage is used, or a combination of the two factors. MJN110 is a newer-generation drug relative to those used in prior work, with benefits over previous-generation drugs as described earlier, including fewer off-target effects. Despite the similarity in that prostaglandins and HETEs are both inflammatory metabolites of arachidonic acid (AA), their derived mechanisms differ in their metabolizing enzyme. Prostaglandins are derived from cyclooxygenase (COX), whereas

HETEs are largely derived from lipoxygenases (LOX) and cytochrome P450 (CYP) enzymes (103). That MJN110 decreased HETEs without affecting prostaglandins suggests a more COX-independent pathway for MJN110's profile of anti-inflammatory effects. This finding is important because while COX-targeting therapeutics such as non-steroidal anti-inflammatory drugs (NSAIDs) are effective against inflammation and pain, they can also increase the risk of adverse cardiovascular events (104–106). MJN110 confers anti-inflammatory effects while more specifically targeting pathways beneficial to cardiac, respiratory, and cerebrovascular health, including LOX and CYP (107, 108), with the exception of 5-HETE, which is derived from AA through the LOX system but metabolized through the COX system (109). Given predispositions of PLWH to cardiovascular disease and related complications (110, 111), this therapeutic strategy may improve quality of life across more domains relative to earlier-developed MAGL inhibitors, which interact with COX pathways. Of note, HIV-1 gp120 is more strongly linked to increases in signaling within the COX pathway, particularly through induction of COX-2 expression (112), so using subjects who express more constituent proteins of the HIV-1 viral genome may provide a more complete understanding of virus-associated inflammatory profiles as well as therapeutic potential of MJN110 across signaling pathways.

Within astrocytic mechanisms, assessing other factors, such as neurotrophin synthesis and hypertrophy, could further elucidate additional contrasting effects of Tat and MJN110 on astrogliosis. Astrocyte density was assessed presently as increased astrocyte counts are widely understood to indicate increased proliferation associated with astrogliosis (113); however, a limitation remains in the inability to distinguish between normal and activated astrocytes. There also remains the question of other cellular mechanisms potentially driving independent inflammatory responses. While number of microglia and microglia morphology was not altered by Tat and MJN110, microglia are recognized as a productive viral reservoir that contributes to IL-1β upregulation through stimulation of nucleotide-binding domain leucine-rich repeat-containing proteins (NLRs) (114). The present study could not further probe microglial activation-induced IL-1β upregulation due to technical difficulties with triple-immunolabeling, but these contributions to inflammatory tone remain important to consider.

While the expression and distribution of MAGL were not assessed in the current study, recently published work specifically examined MAGL expression in our transgenic mouse model, and demonstrated Tat induction does not alter MAGL expression (87). Based on these findings, it can reasonably be inferred that MAGL expression was not a confounding factor in the data observed presently. Additionally, a previous paper authored by our lab provides relevant insights into MJN110's effects in the brain (62). This study, which utilized the same subject preparation methods, including dosage, frequency of MJN110 administration, and duration of Tat induction as the present study, investigated the effect of MJN110 on endocannabinoid levels in various brain regions and showed that treatment with MJN110 increased levels of 2-AG in multiple brain regions. These findings suggest that this MAGL inhibitor effectively modulated endocannabinoid signaling in the brain without baseline MAGL alteration driven by Tat. Nevertheless, to directly conclude that MJN110 effects are due to increases in 2-AG levels, mice should be administered a 2-AG synthesis blocker, such as DO34, similar to what has been published previously (60).

Several limitations of this study should be considered when applying current findings to the therapeutic potential of targeting MAGL in the context of HIV. First, despite the Tat transgenic mouse model being a well-established neuroHIV model, only one of the many viral proteins is expressed. It is known that viral proteins can interact and target various signaling pathways (115); thus they can modify CNS and behavior in different ways compared to a single viral protein. Second, the use of doxycycline for inducing Tat expression is not ideal, as doxycycline has neuroprotective effects on its own (116). Nevertheless, both Tat(−) and Tat(+) mouse groups received doxycycline chow throughout the study to control for this confound and minimize bias. Third, only females were used in the current study without monitoring estrous cycle. Future studies should monitor estrous cycle as hormones can alter motivated behavior associated with a food reward (94), as well as include male mice for comparison, especially due to the known sex-specific differences in immune response to the virus (117). Lastly, ART medication was not considered in the study, as the HIV Tat transgenic mouse model mimics individuals on ART because no virus replication/entry/integration is present, similar to what is seen in PLWH on ART with undetectable viral load. Nevertheless, it is known that cannabinoids and ART drugs are metabolized through the CYP450 system, thus leading to potential drug-drug interaction (118). Interestingly, no significant interactions have been reported between cannabinoids and HIV protease inhibitors in previous studies (119, 120), but additional pharmacokinetic studies remain necessary to increase our understanding of cannabinoid-ART interactions.

5 Conclusion

A wide body of evidence indicates while HIV-1 treatment has improved life expectancy and quality over the years, supplemental strategies and studies are needed to address persistent issues with patient health, shortcomings of cART, and historically problematic research design. Ultimately, understanding the specific virus-associated vulnerabilities across different subpopulations – and especially the therapeutic potential of novel adaptogenic compounds like MJN110, as demonstrated here – will enhance the foundation of knowledge upon which similar future studies are built and improve management strategies for HIV-1 and other inflammatory diseases.

Data availability statement

The raw data supporting the conclusions of this article will be made available by the authors, without undue reservation.

Ethics statement

The animal study was approved by University of North Carolina at Chapel Hill Institutional Animal Care and Use Committee. The study was conducted in accordance with the local legislation and institutional requirements.

Author contributions

AFL: Writing – review & editing, Writing – original draft, Visualization, Validation, Project administration, Methodology, Investigation, Funding acquisition, Formal analysis, Data curation, Conceptualization. BJY-S: Formal analysis, Data curation, Writing – review & editing. RK: Data curation, Writing – review & editing, Investigation. CAC: Investigation, Formal analysis, Writing – review & editing. IRJ: Methodology, Writing – review & editing. JM: Writing – original draft, Validation, Formal analysis, Data curation, Writing – review & editing, Resources. MJN: Writing – review & editing, Resources. BFC: Writing – review & editing, Resources. AHL: Writing – review & editing, Resources. BMI-J: Writing – review & editing, Resources. SF: Writing – review & editing, Writing – original draft, Validation, Supervision, Resources, Project administration, Methodology, Investigation, Funding acquisition, Formal analysis, Conceptualization.

Funding

The author(s) declare financial support was received for the research, authorship, and/or publication of this article. This research was funded by the National Institute on Drug Abuse (NIDA) R01 DA055523 (SF), R01 DA045596 (SF), P30 DA033934 (AHL), and F31 DA056299-01 (AFL). BMI-J was supported by Japan Society for Promotion of Science (JSPS) Fellowship for Overseas Researchers (P17388), Kakenhi Grant-in-Aid for JSPS Fellows (17F17388), and Kakenhi Grant for Scientific Research (21K06399). Further, we gratefully acknowledge the mass spectrometry work that generated lipidomic data, performed at the Skaggs School of Pharmacy and Pharmaceutical Sciences, University of Colorado Anschutz.

Acknowledgments

The authors would like to thank animal technician DeVeda Eubanks and surgical technician Leslie Whitfield for their work maintaining the welfare of our animals throughout these studies.

Conflict of interest

The authors declare that the research was conducted in the absence of any commercial or financial relationships that could be construed as a potential conflict of interest.

Publisher's note

All claims expressed in this article are solely those of the authors and do not necessarily represent those of their affiliated organizations, or those of the publisher, the editors and the reviewers. Any product that may be evaluated in this article, or claim that may be made by its manufacturer, is not guaranteed or endorsed by the publisher.

Supplementary material

The Supplementary Material for this article can be found online at: https://www.frontiersin.org/articles/10.3389/fimmu.2024.1374301/full#supplementary-material

References

1. Who. *HIV and AIDS: Key facts* (2023). Available online at: https://www.who.int/news-room/fact-sheets/detail/hiv-aids.

2. Collaborators GH. Global, regional, and national sex-specific burden and control of the HIV epidemic 1990-2019, for 204 countries and territories: the Global Burden of Diseases Study 2019. *Lancet HIV*. (2021) 8:e633–51. doi: 10.1016/S2352-3018(21)00152-1

3. Scully EP. Sex differences in HIV infection. *Curr HIV/AIDS Rep*. (2018) 15:136–46. doi: 10.1007/s11904-018-0383-2

4. May MT, Sterne JA, Costagliola D, Sabin CA, Phillips AN, Justice AC, et al. HIV treatment response and prognosis in Europe and North America in the first decade of highly active antiretroviral therapy: a collaborative analysis. *Lancet*. (2006) 368:451–8. doi: 10.1016/S0140-6736(06)69152-6

5. Harrison KM, Song R, Zhang X. Life expectancy after HIV diagnosis based on national HIV surveillance data from 25 states, United States. *J Acquir Immune Defic Syndr*. (2010) 53:124–30. doi: 10.1097/QAI.0b013e3181b563e7

6. Marcus JL, Chao CR, Leyden WA, Xu L, Quesenberry CP Jr., Klein DB, et al. Narrowing the gap in life expectancy between HIV-infected and HIV-uninfected individuals with access to care. *J Acquir Immune Defic Syndr*. (2016) 73:39–46. doi: 10.1097/QAI.0000000000001014

7. Hudson L, Liu J, Nath A, Jones M, Raghavan R, Narayan O, et al. Detection of the human immunodeficiency virus regulatory protein tat in CNS tissues. *J Neurovirol*. (2000) 6:145–55. doi: 10.3109/13550280009013158

8. Eisfeld C, Reichelt D, Evers S, Husstedt I. CSF penetration by antiretroviral drugs. *CNS Drugs*. (2013) 27:31–55. doi: 10.1007/s40263-012-0018-x

9. Calcagno A, Cusato J, Simiele M, Motta I, Audagnotto S, Bracchi M, et al. High interpatient variability of raltegravir CSF concentrations in HIV-positive patients: a pharmacogenetic analysis. *J Antimicrob Chemother*. (2014) 69:241–5. doi: 10.1093/jac/dkt339

10. Zhang YL, Ouyang YB, Liu LG, Chen DX. Blood-brain barrier and neuro-AIDS. *Eur Rev Med Pharmacol Sci*. (2015) 19:4927–39.

11. Gartner S. HIV infection and dementia. *Science*. (2000) 287:602–4. doi: 10.1126/science.287.5453.602

12. Kaul M, Garden GA, Lipton SA. Pathways to neuronal injury and apoptosis in HIV-associated dementia. *Nature*. (2001) 410:988–94. doi: 10.1038/35073667

13. Harezlak J, Buchthal S, Taylor M, Schifitto G, Zhong J, Daar E, et al. Persistence of HIV-associated cognitive impairment, inflammation, and neuronal injury in era of highly active antiretroviral treatment. *AIDS*. (2011) 25:625–33. doi: 10.1097/QAD.0b013e3283427da7

14. Sreeram S, Ye F, Garcia-Mesa Y, Nguyen K, El Sayed A, Leskov K, et al. The potential role of HIV-1 latency in promoting neuroinflammation and HIV-1-associated neurocognitive disorder. *Trends Immunol.* (2022) 43:630–9. doi: 10.1016/j.it.2022.06.003

15. Ellis R, Langford D, Masliah E. HIV and antiretroviral therapy in the brain: neuronal injury and repair. *Nat Rev Neurosci.* (2007) 8:33–44. doi: 10.1038/nrn2040

16. Saylor D, Dickens AM, Sacktor N, Haughey N, Slusher B, Pletnikov M, et al. HIV-associated neurocognitive disorder - pathogenesis and prospects for treatment. *Nat Rev Neurol.* (2016) 12:234–48. doi: 10.1038/nrneurol.2016.27

17. Irollo E, Luchetta J, Ho C, Nash B, Meucci O. Mechanisms of neuronal dysfunction in HIV-associated neurocognitive disorders. *Cell Mol Life Sci.* (2021) 78:4283–303. doi: 10.1007/s00018-021-03785-y

18. Gonzalez H, Podany A, Al-Harthi L, Wallace J. The far-reaching HAND of cART: cART effects on astrocytes. *J Neuroimmune Pharmacol.* (2021) 16:144–58. doi: 10.1007/s11481-020-09907-w

19. Zulu SS, Abboussi O, Simola N, Mabandla MV, Daniels WMU. Effects of combination antiretroviral drugs (cART) on hippocampal neuroplasticity in female mice. *J Neurovirol.* (2021) 27:325–33. doi: 10.1007/s13365-021-00967-z

20. Bruce-Keller AJ, Turchan-Cholewo J, Smart EJ, Geurin T, Chauhan A, Reid R, et al. Morphine causes rapid increases in glial activation and neuronal injury in the striatum of inducible HIV-1 Tat transgenic mice. *Glia.* (2008) 56:1414–27. doi: 10.1002/glia.20708

21. Hauser KF, Hahn YK, Adjan VV, Zou S, Buch SK, Nath A, et al. HIV-1 tat and morphine have interactive effects on oligodendrocyte survival and morphology. *Glia.* (2009) 57:194–206. doi: 10.1002/glia.20746

22. Fitting S, Xu R, Bull C, Buch SK, El-Hage N, Nath A, et al. Interactive comorbidity between opioid drug abuse and HIV-1 Tat: chronic exposure augments spine loss and sublethal dendritic pathology in striatal neurons. *Am J Pathol.* (2010) 177:1397–410. doi: 10.2353/ajpath.2010.090945

23. Nass SR, Hahn YK, Ohene-Nyako M, Mclane VD, Damaj MI, Thacker LR 2nd, et al. Depressive-like behavior is accompanied by prefrontal cortical innate immune fatigue and dendritic spine losses after HIV-1 tat and morphine exposure. *Viruses.* (2023) 15:590. doi: 10.3390/v15030590

24. Nass SR, Hahn YK, Mclane VD, Varshneya NB, Damaj MI, Knapp PE, et al. Chronic HIV-1 Tat exposure alters anterior cingulate cortico-basal ganglia-thalamocortical synaptic circuitry, associated behavioral control, and immune regulation in male mice. *Brain Behavior Immun - Health.* (2020) 5:100077. doi: 10.1016/j.bbih.2020.100077

25. Leibrand CR, Paris JJ, Jones AM, Ohene-Nyako M, Rademeyer KM, Nass SR, et al. Independent actions by HIV-1 Tat and morphine to increase recruitment of monocyte-derived macrophages into the brain in a region-specific manner. *Neurosci Lett.* (2022) 788:136852. doi: 10.1016/j.neulet.2022.136852

26. Fitting S, Ignatowska-Jankowska BM, Bull C, Skoff RP, Lichtman AH, Wise LE, et al. Synaptic dysfunction in the hippocampus accompanies learning and memory deficits in human immunodeficiency virus type-1 Tat transgenic mice. *Biol Psychiatry.* (2013) 73:443–53. doi: 10.1016/j.biopsych.2012.09.026

27. Hahn YK, Podhaizer EM, Farris SP, Miles MF, Hauser KF, Knapp PE. Effects of chronic HIV-1 Tat exposure in the CNS: heightened vulnerability of males versus females to changes in cell numbers, synaptic integrity, and behavior. *Brain Struct Funct.* (2015) 220:605–23. doi: 10.1007/s00429-013-0676-6

28. Bertrand SJ, Mactutus CF, Harrod SB, Moran LM, Booze RM. HIV-1 proteins dysregulate motivational processes and dopamine circuitry. *Sci Rep.* (2018) 8:7869. doi: 10.1038/s41598-018-25109-0

29. Mclaurin KA, Cook AK, Li H, League AF, Mactutus CF, Booze RM. Synaptic connectivity in medium spiny neurons of the nucleus accumbens: A sex-dependent mechanism underlying apathy in the HIV-1 transgenic rat. *Front Behav Neurosci.* (2018) 12:285. doi: 10.3389/fnbeh.2018.00285

30. Denton AR, Mactutus CF, Lateef AU, Harrod SB, Booze RM. Chronic SSRI treatment reverses HIV-1 protein-mediated synaptodendritic damage. *J Neurovirol.* (2021) 27:403–21. doi: 10.1007/s13365-021-00960-6

31. Midde NM, Gomez AM, Zhu J. HIV-1 Tat protein decreases dopamine transporter cell surface expression and vesicular monoamine transporter-2 function in rat striatal synaptosomes. *J Neuroimmune Pharmacol.* (2012) 7:629–39. doi: 10.1007/s11481-012-9369-9

32. Gaskill PJ, Miller DR, Gamble-George J, Yano H, Khoshbouei H. HIV, Tat and dopamine transmission. *Neurobiol Dis.* (2017) 105:51–73. doi: 10.1016/j.nbd.2017.04.015

33. Schier CJ, Marks WD, Paris JJ, Barbour AJ, Mclane VD, Maragos WF, et al. Selective vulnerability of striatal D2 versus D1 dopamine receptor-expressing medium spiny neurons in HIV-1 tat transgenic male mice. *J Neurosci.* (2017) 37:5758–69. doi: 10.1523/JNEUROSCI.0622-17.2017

34. Zhu J, Quizon PM, Wang Y, Adeniran CA, Strauss MJ, Jimenez-Torres AC, et al. SRI-32743, a novel allosteric modulator, attenuates HIV-1 Tat protein-induced inhibition of the dopamine transporter and alleviates the potentiation of cocaine reward in HIV-1 Tat transgenic mice. *Neuropharmacology.* (2022) 220:109239. doi: 10.1016/j.neuropharm.2022.109239

35. Kamat R, Woods SP, Marcotte TD, Ellis RJ, Grant IGroup H.I.V.N.R.P. Implications of apathy for everyday functioning outcomes in persons living with HIV infection. *Arch Clin Neuropsychol.* (2012) 27:520–31. doi: 10.1093/arclin/acs055

36. Bryant VE, Whitehead NE, Burrell LE2nd, Dotson VM, Cook RL, Malloy P, et al. Depression and apathy among people living with HIV: implications for treatment of HIV associated neurocognitive disorders. *AIDS Behav.* (2015) 19:1430–7. doi: 10.1007/s10461-014-0970-1

37. Cristino L, Bisogno T, Di Marzo V. Cannabinoids and the expanded endocannabinoid system in neurological disorders. *Nat Rev Neurol.* (2020) 16:9–29. doi: 10.1038/s41582-019-0284-z

38. Scotter EL, Abood ME, Glass M. The endocannabinoid system as a target for the treatment of neurodegenerative disease. *Br J Pharmacol.* (2010) 160:480–98. doi: 10.1111/j.1476-5381.2010.00735.x

39. Pertwee RG. Elevating endocannabinoid levels: pharmacological strategies and potential therapeutic applications. *Proc Nutr Soc.* (2014) 73:96–105. doi: 10.1017/S0029665113003649

40. Pertwee RG, Howlett AC, Abood ME, Alexander SP, Di Marzo V, Elphick MR, et al. International Union of Basic and Clinical Pharmacology. LXXIX. Cannabinoid receptors and their ligands: beyond CB(1) and CB(2). *Pharmacol Rev.* (2010) 62:588–631. doi: 10.1124/pr.110.003004

41. Kibret BG, Ishiguro H, Horiuchi Y, Onaivi ES. New insights and potential therapeutic targeting of CB2 cannabinoid receptors in CNS disorders. *Int J Mol Sci.* (2022) 23:975. doi: 10.3390/ijms23020975

42. Ignatowska-Jankowska B, Wilkerson JL, Mustafa M, Abdullah R, Niphakis M, Wiley JL, et al. Selective monoacylglycerol lipase inhibitors: antinociceptive versus cannabimimetic effects in mice. *J Pharmacol Exp Ther.* (2015) 353:424–32. doi: 10.1124/jpet.114.222315

43. Powell WS, Rokach J. Biosynthesis, biological effects, and receptors of hydroxyeicosatetraenoic acids (HETEs) and oxoeicosatetraenoic acids (oxo-ETEs) derived from arachidonic acid. *Biochim Biophys Acta.* (2015) 1851:340–55. doi: 10.1016/j.bbalip.2014.10.008

44. Yui K, Imataka G, Nakamura H, Ohara N, Naito Y. Eicosanoids derived from arachidonic acid and their family prostaglandins and cyclooxygenase in psychiatric disorders. *Curr Neuropharmacol.* (2015) 13:776–85. doi: 10.2174/1570159X13666151102103305

45. Nomura DK, Long JZ, Niessen S, Hoover HS, Ng SW, Cravatt BF. Monoacylglycerol lipase regulates a fatty acid network that promotes cancer pathogenesis. *Cell.* (2010) 140:49–61. doi: 10.1016/j.cell.2009.11.027

46. Nomura DK, Lombardi DP, Chang JW, Niessen S, Ward AM, Long JZ, et al. Monoacylglycerol lipase exerts dual control over endocannabinoid and fatty acid pathways to support prostate cancer. *Chem Biol.* (2011) 18:846–56. doi: 10.1016/j.chembiol.2011.05.009

47. Ye L, Zhang B, Seviour EG, Tao KX, Liu XH, Ling Y, et al. Monoacylglycerol lipase (MAGL) knockdown inhibits tumor cells growth in colorectal cancer. *Cancer Lett.* (2011) 307:6–17. doi: 10.1016/j.canlet.2011.03.007

48. Choi SH, Arai AL, Mou Y, Kang B, Yen CC, Hallenbeck J, et al. Neuroprotective effects of MAGL (Monoacylglycerol lipase) inhibitors in experimental ischemic stroke. *Stroke.* (2018) 49:718–26. doi: 10.1161/STROKEAHA.117.019664

49. Chen R, Zhang J, Wu Y, Wang D, Feng G, Tang YP, et al. Monoacylglycerol lipase is a therapeutic target for Alzheimer's disease. *Cell Rep.* (2012) 2:1329–39. doi: 10.1016/j.celrep.2012.09.030

50. Piro JR, Benjamin DI, Duerr JM, Pi Y, Gonzales C, Wood KM, et al. A dysregulated endocannabinoid-eicosanoid network supports pathogenesis in a mouse model of Alzheimer's disease. *Cell Rep.* (2012) 1:617–23. doi: 10.1016/j.celrep.2012.05.001

51. Zhang X, Thayer SA. Monoacylglycerol lipase inhibitor JZL184 prevents HIV-1 gp120-induced synapse loss by altering endocannabinoid signaling. *Neuropharmacology.* (2018) 128:269–81. doi: 10.1016/j.neuropharm.2017.10.023

52. Everett TJ, Gomez DM, Hamilton LR, Oleson EB. Endocannabinoid modulation of dopamine release during reward seeking, interval timing, and avoidance. *Prog Neuropsychopharmacol Biol Psychiatry.* (2021) 104:110031. doi: 10.1016/j.pnpbp.2020.110031

53. Covey DP, Dantrassy HM, Yohn SE, Castro A, Conn PJ, Mateo Y, et al. Inhibition of endocannabinoid degradation rectifies motivational and dopaminergic deficits in the Q175 mouse model of Huntington's disease. *Neuropsychopharmacology.* (2018) 43:2056–63. doi: 10.1038/s41386-018-0107-8

54. Covey DP, Hernandez E, Lujan MA, Cheer JF. Chronic augmentation of endocannabinoid levels persistently increases dopaminergic encoding of reward cost and motivation. *J Neurosci.* (2021) 41:6946–53. doi: 10.1523/JNEUROSCI.0285-21.2021

55. Long JZ, Li W, Booker L, Burston JJ, Kinsey SG, Schlosburg JE, et al. Selective blockade of 2-arachidonoylglycerol hydrolysis produces cannabinoid behavioral effects. *Nat Chem Biol.* (2009) 5:37–44. doi: 10.1038/nchembio.129

56. Vandevoorde S, Jonsson KO, Labar G, Persson E, Lambert DM, Fowler CJ. Lack of selectivity of URB602 for 2-oleoylglycerol compared to anandamide hydrolysis in *vitro*. *Br J Pharmacol.* (2007) 150:186–91. doi: 10.1038/sj.bjp.0706971

57. Schlosburg JE, Blankman JL, Long JZ, Nomura DK, Pan B, Kinsey SG, et al. Chronic monoacylglycerol lipase blockade causes functional antagonism of the endocannabinoid system. *Nat Neurosci.* (2010) 13:1113–9. doi: 10.1038/nn.2616

58. Niphakis MJ, Cognetta AB3rd, Chang JW, Buczynski MW, Parsons LH, Byrne F, et al. Evaluation of NHS carbamates as a potent and selective class of endocannabinoid hydrolase inhibitors. *ACS Chem Neurosci.* (2013) 4:1322–32. doi: 10.1021/cn400116z

59. Wilkerson JL, Niphakis MJ, Grim TW, Mustafa MA, Abdullah RA, Poklis JL, et al. The selective monoacylglycerol lipase inhibitor MJN110 produces opioid-sparing effects in a mouse neuropathic pain model. *J Pharmacol Exp Ther*. (2016) 357:145–56. doi: 10.1124/jpet.115.229971

60. Selvaraj P, Tanaka M, Wen J, Zhang Y. The novel monoacylglycerol lipase inhibitor MJN110 suppresses neuroinflammation, normalizes synaptic composition and improves behavioral performance in the repetitive traumatic brain injury mouse model. *Cells*. (2021) 10:3454. doi: 10.3390/cells10123454

61. Feja M, Leigh MPK, Baindur AN, Mcgraw JJ, Wakabayashi KT, Cravatt BF, et al. The novel MAGL inhibitor MJN110 enhances responding to reward-predictive incentive cues by activation of CB1 receptors. *Neuropharmacology*. (2020) 162:107814. doi: 10.1016/j.neuropharm.2019.107814

62. League AF, Gorman BL, Hermes DJ, Johnson CT, Jacobs IR, Yadav-Samudrala BJ, et al. Monoacylglycerol lipase inhibitor MJN110 reduces neuronal hyperexcitability, restores dendritic arborization complexity, and regulates reward-related behavior in presence of HIV-1 tat. *Front Neurol*. (2021) 12:651272. doi: 10.3389/fneur.2021.651272

63. Hermes DJ, Jacobs IR, Key MC, League AF, Yadav-Samudrala BJ, Xu C, et al. Escalating morphine dosing in HIV-1 Tat transgenic mice with sustained Tat exposure reveals an allostatic shift in neuroinflammatory regulation accompanied by increased neuroprotective non-endocannabinoid lipid signaling molecules and amino acids. *J Neuroinflamm*. (2020) 17:345. doi: 10.1186/s12974-020-01971-6

64. Varol AB, Esen EC, Kocak EE. Repeated collection of vaginal smear causes stress in mice. *Noro Psikiyatr Ars*. (2022) 59:325–9. doi: 10.29399/npa.28099

65. Diester CM, Lichtman AH, Negus SS. Behavioral battery for testing candidate analgesics in mice. II. Effects of endocannabinoid catabolic enzyme inhibitors and Δ9-tetrahydrocannabinol. *J Pharmacol Exp Ther*. (2021) 377:242–53. doi: 10.1124/jpet.121.000497

66. Turner PV, Brabb T, Pekow C, Vasbinder MA. Administration of substances to laboratory animals: routes of administration and factors to consider. *J Am Assoc Lab Anim Sci*. (2011) 50:600–13.

67. Sclafani A. Enhanced sucrose and Polycose preference in sweet "sensitive" (C57BL/6J) and "subsensitive" (129P3/J) mice after experience with these saccharides. *Physiol Behav*. (2006) 87:745–56. doi: 10.1016/j.physbeh.2006.01.016

68. Togo J, Hu S, Li M, Niu C, Speakman JR. Impact of dietary sucrose on adiposity and glucose homeostasis in C57BL/6J mice depends on mode of ingestion: liquid or solid. *Mol Metab*. (2019) 27:22–32. doi: 10.1016/j.molmet.2019.05.010

69. Nam HW, Hinton DJ, Kang NY, Kim T, Lee MR, Oliveros A, et al. Adenosine transporter ENT1 regulates the acquisition of goal-directed behavior and ethanol drinking through A2A receptor in the dorsomedial striatum. *J Neurosci*. (2013) 33:4329–38. doi: 10.1523/JNEUROSCI.3094-12.2013

70. Schneider CA, Rasband WS, Eliceiri KW. NIH Image to ImageJ: 25 years of image analysis. *Nat Methods*. (2012) 9:671–5. doi: 10.1038/nmeth.2089

71. Mcgill BE, Barve RA, Maloney SE, Strickland A, Rensing N, Wang PL, et al. Abnormal microglia and enhanced inflammation-related gene transcription in mice with conditional deletion of ctcf in camk2a-cre-expressing neurons. *J Neurosci*. (2018) 38:200–19. doi: 10.1523/JNEUROSCI.0936-17.2017

72. Young K, Morrison H. Quantifying microglia morphology from photomicrographs of immunohistochemistry prepared tissue using imageJ. *J Vis Exp*. (2018) 5(136):57648. doi: 10.3791/57648-v

73. Bolte S, Cordelieres FP. A guided tour into subcellular colocalization analysis in light microscopy. *J Microsc*. (2006) 224:213–32. doi: 10.1111/j.1365-2818.2006.01706.x

74. Armstrong M, Manke J, Nkrumah-Elie Y, Shaikh SR, Reisdorph N. Improved quantification of lipid mediators in plasma and tissues by liquid chromatography tandem mass spectrometry demonstrates mouse strain specific differences. *Prostaglandins Other Lipid Mediat*. (2020) 151:106483. doi: 10.1016/j.prostaglandins.2020.106483

75. Melis M, Gessa GL, Diana M. Different mechanisms for dopaminergic excitation induced by opiates and cannabinoids in the rat midbrain. *Prog Neuropsychopharmacol Biol Psychiatry*. (2000) 24:993–1006. doi: 10.1016/S0278-5846(00)00119-6

76. Braida D, Pozzi M, Cavallini R, Sala M. Conditioned place preference induced by the cannabinoid agonist CP 55,940: interaction with the opioid system. *Neuroscience*. (2001) 104:923–6. doi: 10.1016/S0306-4522(01)00210-X

77. Solinas M, Yasar S, Goldberg SR. Endocannabinoid system involvement in brain reward processes related to drug abuse. *Pharmacol Res*. (2007) 56:393–405. doi: 10.1016/j.phrs.2007.09.005

78. Carhart-Harris RL, Murphy K, Leech R, Erritzoe D, Wall MB, Ferguson B, et al. The effects of acutely administered 3,4-methylenedioxymethamphetamine on spontaneous brain function in healthy volunteers measured with arterial spin labeling and blood oxygen level-dependent resting state functional connectivity. *Biol Psychiatry*. (2015) 78:554–62. doi: 10.1016/j.biopsych.2013.12.015

79. Bloomfield MA, Morgan CJ, Egerton A, Kapur S, Curran HV, Howes OD. Dopaminergic function in cannabis users and its relationship to cannabis-induced psychotic symptoms. *Biol Psychiatry*. (2014) 75:470–8. doi: 10.1016/j.biopsych.2013.05.027

80. Leroy C, Karila L, Martinot JL, Lukasiewicz M, Duchesnay E, Comtat C, et al. Striatal and extrastriatal dopamine transporter in cannabis and tobacco addiction: a high-resolution PET study. *Addict Biol*. (2012) 17:981–90. doi: 10.1111/j.1369-1600.2011.00356.x

81. Van De Giessen E, Weinstein JJ, Cassidy CM, Haney M, Dong Z, Ghazzaoui R, et al. Deficits in striatal dopamine release in cannabis dependence. *Mol Psychiatry*. (2017) 22:68–75. doi: 10.1038/mp.2016.21

82. Marder E, Goaillard JM. Variability, compensation and homeostasis in neuron and network function. *Nat Rev Neurosci*. (2006) 7:563–74. doi: 10.1038/nrn1949

83. Hargus NJ, Thayer SA. Human immunodeficiency virus-1 Tat protein increases the number of inhibitory synapses between hippocampal neurons in culture. *J Neurosci*. (2013) 33:17908–20. doi: 10.1523/JNEUROSCI.1312-13.2013

84. Li ST, Matsushita M, Moriwaki A, Saheki Y, Lu YF, Tomizawa K, et al. HIV-1 Tat inhibits long-term potentiation and attenuates spatial learning [corrected]. *Ann Neurol*. (2004) 55:362–71. doi: 10.1002/ana.10844

85. Van Der Heijden WA, Van De Wijer L, Keramati F, Trypsteen W, Rutsaert S, Horst RT, et al. Chronic HIV infection induces transcriptional and functional reprogramming of innate immune cells. *JCI Insight*. (2021) 6:e145928. doi: 10.1172/jci.insight.145928

86. Failde-Garrido JM, Alvarez MR, Simon-Lopez MA. Neuropsychological impairment and gender differences in HIV-1 infection. *Psychiatry Clin Neurosci*. (2008) 62:494–502. doi: 10.1111/j.1440-1819.2008.01841.x

87. Xu C, Yadav-Samudrala BJ, Xu C, Nath B, Mistry T, Jiang W, et al. Inhibitory neurotransmission is sex-dependently affected by tat expression in transgenic mice and suppressed by the fatty acid amide hydrolase enzyme inhibitor PF3845 via cannabinoid type-1 receptor mechanisms. *Cells*. (2022) 11:857. doi: 10.3390/cells11050857

88. Putatunda R, Zhang Y, Li F, Fagan PR, Zhao H, Ramirez SH, et al. Sex-specific neurogenic deficits and neurocognitive disorders in middle-aged HIV-1 Tg26 transgenic mice. *Brain Behav Immun*. (2019) 80:488–99. doi: 10.1016/j.bbi.2019.04.029

89. Rubin LH, Sundermann EE, Dastgheyb R, Buchholz AS, Pasipanodya E, Heaton RK, et al. Sex differences in the patterns and predictors of cognitive function in HIV. *Front Neurol*. (2020) 11:551921. doi: 10.3389/fneur.2020.551921

90. Toma W, Paris JJ, Warncke UO, Nass SR, Caillaud M, Mckiver B, et al. Persistent sensory changes and sex differences in transgenic mice conditionally expressing HIV-1 Tat regulatory protein. *Exp Neurol*. (2022) 358:114226. doi: 10.1016/j.expneurol.2022.114226

91. Bagdas D, Paris JJ, Carper M, Wodarski R, Rice ASC, Knapp PE, et al. Conditional expression of HIV-1 Tat in the mouse alters the onset and progression of tonic, inflammatory, and neuropathic hypersensitivity in a sex-dependent manner. *Eur J Pain*. (2020) 24:1609–23. doi: 10.1002/ejp.1618

92. Maki PM, Rubin LH, Springer G, Seaberg EC, Sacktor N, Miller EN, et al. Differences in cognitive function between women and men with HIV. *J Acquir Immune Defic Syndr*. (2018) 79:101–7. doi: 10.1097/QAI.0000000000001764

93. Sundermann EE, Heaton RK, Pasipanodya E, Moore RC, Paolillo EW, Rubin LH, et al. Sex differences in HIV-associated cognitive impairment. *AIDS*. (2018) 32:2719–26. doi: 10.1097/QAD.0000000000002012

94. Alonso-Caraballo Y, Ferrario CR. Effects of the estrous cycle and ovarian hormones on cue-triggered motivation and intrinsic excitability of medium spiny neurons in the Nucleus Accumbens core of female rats. *Horm Behav*. (2019) 116:104583. doi: 10.1016/j.yhbeh.2019.104583

95. Benton NA, Russo KA, Brozek JM, Andrews RJ, Kim VJ, Kriegsfeld LJ, et al. Food restriction-induced changes in motivation differ with stages of the estrous cycle and are closely linked to RFamide-related peptide-3 but not kisspeptin in Syrian hamsters. *Physiol Behav*. (2018) 190:43–60. doi: 10.1016/j.physbeh.2017.06.009

96. Atchley DP, Weaver KL, Eckel LA. Taste responses to dilute sucrose solutions are modulated by stage of the estrous cycle and fenfluramine treatment in female rats. *Physiol Behav*. (2005) 86:265–71. doi: 10.1016/j.physbeh.2005.08.001

97. Jori A, Colturani F, Dolfini E, Rutczynski M. Modifications of the striatal dopamine metabolism during the estrus cycle in mice. *Neuroendocrinology*. (1976) 21:262–6. doi: 10.1159/000122531

98. Brabers NA, Nottet HS. Role of the pro-inflammatory cytokines TNF-alpha and IL-1beta in HIV-associated dementia. *Eur J Clin Invest*. (2006) 36:447–58. doi: 10.1111/j.1365-2362.2006.01657.x

99. Olmos G, Llado J. Tumor necrosis factor alpha: a link between neuroinflammation and excitotoxicity. *Mediators Inflammation*. (2014) 2014:861231. doi: 10.1155/2014/861231

100. Smith RL, De Boer R, Brul S, Budovskaya Y, Van Spek H. Premature and accelerated aging: HIV or HAART? *Front Genet*. (2012) 3:328. doi: 10.3389/fgene.2012.00328

101. Buckley S, Byrnes S, Cochrane C, Roche M, Estes JD, Selemidis S, et al. The role of oxidative stress in HIV-associated neurocognitive disorders. *Brain Behav Immun Health*. (2021) 13:100235. doi: 10.1016/j.bbih.2021.100235

102. Sanchez-Alavez M, Nguyen W, Mori S, Moroncini G, Viader A, Nomura DK, et al. Monoacylglycerol lipase regulates fever response. *PloS One*. (2015) 10:e0134437. doi: 10.1371/journal.pone.0134437

103. Wang B, Wu L, Chen J, Dong L, Chen C, Wen Z, et al. Metabolism pathways of arachidonic acids: mechanisms and potential therapeutic targets. *Signal Transduct Target Ther*. (2021) 6:94. doi: 10.1038/s41392-020-00443-w

104. Fitzgerald GA. Coxibs and cardiovascular disease. *N Engl J Med*. (2004) 351:1709–11. doi: 10.1056/NEJMp048288

105. Yu Y, Ricciotti E, Scalia R, Tang SY, Grant G, Yu Z, et al. Vascular COX-2 modulates blood pressure and thrombosis in mice. *Sci Transl Med*. (2012) 4:132ra154. doi: 10.1126/scitranslmed.3003787

106. Sharma V, Bhatia P, Alam O, Javed Naim M, Nawaz F, Ahmad Sheikh A, et al. Recent advancement in the discovery and development of COX-2 inhibitors: Insight into biological activities and SAR studies, (2008-2019). *Bioorg Chem*. (2019) 89:103007. doi: 10.1016/j.bioorg.2019.103007

107. Rouzer CA, Marnett LJ. Endocannabinoid oxygenation by cyclooxygenases, lipoxygenases, and cytochromes P450: cross-talk between the eicosanoid and endocannabinoid signaling pathways. *Chem Rev*. (2011) 111:5899–921. doi: 10.1021/cr2002799

108. Xie S, Qi X, Wu Q, Wei L, Zhang M, Xing Y, et al. Inhibition of 5-lipoxygenase is associated with downregulation of the leukotriene B4 receptor 1/Interleukin-12p35 pathway and ameliorates sepsis-induced myocardial injury. *Free Radic Biol Med*. (2021) 166:348–57. doi: 10.1016/j.freeradbiomed.2021.02.034

109. Nakashima F, Suzuki T, Gordon ON, Golding D, Okuno T, Gimenez-Bastida JA, et al. Biosynthetic crossover of 5-lipoxygenase and cyclooxygenase-2 yields 5-hydroxy-PGE(2) and 5-hydroxy-PGD(2). *JACS Au*. (2021) 1:1380–8. doi: 10.1021/jacsau.1c00177

110. Holloway CJ, Ntusi N, Suttie J, Mahmod M, Wainwright E, Clutton G, et al. Comprehensive cardiac magnetic resonance imaging and spectroscopy reveal a high burden of myocardial disease in HIV patients. *Circulation*. (2013) 128:814–22. doi: 10.1161/CIRCULATIONAHA.113.001719

111. So-Armah K, Benjamin LA, Bloomfield GS, Feinstein MJ, Hsue P, Njuguna B, et al. HIV and cardiovascular disease. *Lancet HIV*. (2020) 7:e279–93. doi: 10.1016/S2352-3018(20)30036-9

112. Bertin J, Barat C, Methot S, Tremblay MJ. Interactions between prostaglandins, leukotrienes and HIV-1: possible implications for the central nervous system. *Retrovirology*. (2012) 9:4. doi: 10.1186/1742-4690-9-4

113. Hostenbach S, Cambron M, D'haeseleer M, Kooijman R, De Keyser J. Astrocyte loss and astrogliosis in neuroinflammatory disorders. *Neurosci Lett*. (2014) 565:39–41. doi: 10.1016/j.neulet.2013.10.012

114. Chivero ET, Guo ML, Periyasamy P, Liao K, Callen SE, Buch S. HIV-1 tat primes and activates microglial NLRP3 inflammasome-mediated neuroinflammation. *J Neurosci*. (2017) 37:3599–609. doi: 10.1523/JNEUROSCI.3045-16.2017

115. Nath A, Haughey NJ, Jones M, Anderson C, Bell JE, Geiger JD. Synergistic neurotoxicity by human immunodeficiency virus proteins Tat and gp120: protection by memantine. *Ann Neurol*. (2000) 47:186–94. doi: 10.1002/1531-8249(200002)47:2186::AID-ANA8>3.3.CO;2-V

116. Santa-Cecilia FV, Leite CA, Del-Bel E, Raisman-Vozari R. The neuroprotective effect of doxycycline on neurodegenerative diseases. *Neurotox Res*. (2019) 35:981–6. doi: 10.1007/s12640-019-00015-z

117. Teeraananchai S, Kerr SJ, Amin J, Ruxrungtham K, Law MG. Life expectancy of HIV-positive people after starting combination antiretroviral therapy: a meta-analysis. *HIV Med*. (2017) 18:256–66. doi: 10.1111/hiv.12421

118. Stout SM, Cimino NM. Exogenous cannabinoids as substrates, inhibitors, and inducers of human drug metabolizing enzymes: a systematic review. *Drug Metab Rev*. (2014) 46:86–95. doi: 10.3109/03602532.2013.849268

119. Kosel BW, Aweeka FT, Benowitz NL, Shade SB, Hilton JF, Lizak PS, et al. The effects of cannabinoids on the pharmacokinetics of indinavir and nelfinavir. *AIDS*. (2002) 16:543–50. doi: 10.1097/00002030-200203080-00005

120. Abrams DI, Hilton JF, Leiser RJ, Shade SB, Elbeik TA, Aweeka FT, et al. Short-term effects of cannabinoids in patients with HIV-1 infection: a randomized, placebo-controlled clinical trial. *Ann Intern Med*. (2003) 139:258–66. doi: 10.7326/0003-4819-139-4-200308190-00008

frontiers | Frontiers in Immunology

TYPE Original Research
PUBLISHED 11 June 2024
DOI 10.3389/fimmu.2024.1381765

OPEN ACCESS

EDITED BY
Fawaz Alzaid,
Sorbonne Universités, France

REVIEWED BY
Rashid Karim,
Novartis Institutes for BioMedical Research, United States
Antonio Gennaro Nicotera,
University of Messina, Italy
Konda Mani Saravanan,
Bharath Institute of Higher Education and Research, India

*CORRESPONDENCE
Junhan Lin
linjunhanwymz@163.com
Ende Hu
18267839318@163.com

RECEIVED 04 February 2024
ACCEPTED 27 May 2024
PUBLISHED 11 June 2024

CITATION
Lin J, Liu C and Hu E (2024) Elucidating sleep disorders: a comprehensive bioinformatics analysis of functional gene sets and hub genes.
Front. Immunol. 15:1381765.
doi: 10.3389/fimmu.2024.1381765

Elucidating sleep disorders: a comprehensive bioinformatics analysis of functional gene sets and hub genes

Junhan Lin[1,2]*, Changyuan Liu[1,2] and Ende Hu[1,2]*

[1]Department of Anesthesiology and Perioperative Medicine, The Second Affiliated Hospital and Yuying Children's Hospital of Wenzhou Medical University, Key Laboratory of Pediatric Anesthesiology, Ministry of Education, Wenzhou Medical University, Wenzhou, China, [2]Laboratory of Anesthesiology of Zhejiang Province, Wenzhou Medical University, Wenzhou, China

Background: Sleep disorders (SD) are known to have a profound impact on human health and quality of life although their exact pathogenic mechanisms remain poorly understood.

Methods: The study first accessed SD datasets from the GEO and identified DEGs. These DEGs were then subjected to gene set enrichment analysis. Several advanced techniques, including the RF, SVM-RFE, PPI networks, and LASSO methodologies, were utilized to identify hub genes closely associated with SD. Additionally, the ssGSEA approach was employed to analyze immune cell infiltration and functional gene set scores in SD. DEGs were also scrutinized in relation to miRNA, and the DGIdb database was used to explore potential pharmacological treatments for SD. Furthermore, in an SD murine model, the expression levels of these hub genes were confirmed through RT-qPCR and Western Blot analyses.

Results: The findings of the study indicate that DEGs are significantly enriched in functions and pathways related to immune cell activity, stress response, and neural system regulation. The analysis of immunoinfiltration demonstrated a marked elevation in the levels of Activated CD4+ T cells and CD8+ T cells in the SD cohort, accompanied by a notable rise in Central memory CD4 T cells, Central memory CD8 T cells, and Natural killer T cells. Using machine learning algorithms, the study also identified hub genes closely associated with SD, including IPO9, RAP2A, DDX17, MBNL2, PIK3AP1, and ZNF385A. Based on these genes, an SD diagnostic model was constructed and its efficacy validated across multiple datasets. In the SD murine model, the mRNA and protein expressions of these 6 hub genes were found to be consistent with the results of the bioinformatics analysis.

Conclusion: In conclusion, this study identified 6 genes closely linked to SD, which may play pivotal roles in neural system development, the immune microenvironment, and inflammatory responses. Additionally, the key gene-

based SD diagnostic model constructed in this study, validated on multiple datasets showed a high degree of reliability and accuracy, predicting its wide potential for clinical applications. However, limited by the range of data sources and sample size, this may affect the generalizability of the results.

KEYWORDS

sleep disorders, functional gene sets, hub genes, diagnostic model, drugs

1 Introduction

Sleep is recognized as an essential physiological requirement for humans, crucial not only for standard physical growth and development but also for the stabilization and integration of memory (1). Sleep disorders (SD) represent a group of conditions characterized by difficulties in initiating sleep, maintaining sleep, or experiencing restorative sleep. The 2017 third edition of the "International Classification of Sleep Disorders" (ICSD-3) by the American Academy of Sleep Medicine classifies SD into seven categories: insomnia, sleep-related breathing disorders, central disorders of hypersomnolence, circadian rhythm sleep-wake disorders, parasomnias, sleep-related movement disorders, and miscellaneous SD (2). In light of the evolving economy and society, factors such as increasing work and life stress, along with lifestyle modifications, have made sleep disorders (SD) a progressively more significant concern. These disorders not only impact an individual's physical and mental well-being but also have a substantial influence on social and emotional functioning, affecting both adults and children (3). Research into SD is currently in its infancy, and its etiological factors are intricate, encompassing various causative elements such as physiological and psychological aspects, genetic inheritance, body constitution, environmental conditions, social and interpersonal dynamics, mental stimuli, somatic diseases, psychiatric disorders, and adverse drug reactions (4, 5). These factors may induce abnormalities in the brain's sleep centers and their functions or provoke neurobiochemical alterations, consequently disrupting the structure and process of sleep (6).

A significant proportion of adults persistently fail to meet the recommended sleep duration, despite the growing recognition of the importance of healthy sleep. This renders the enhancement of sleep quality a critical concern for global health policy. Research demonstrates that adults exhibit heightened susceptibility to the impacts of sleep quality and circadian rhythm disruptions, potentially aggravating chronic health conditions (7, 8).

Furthermore, the modern 24/7 lifestyle, coupled with the pervasive use of electronic devices and social media, has precipitated widespread sleep deprivation among children and adolescents, posing potential risks to their neurological development, mental well-being, and cardiovascular health (9). Empirical research also indicates that sleep deprivation is intricately linked with suboptimal cardiac metabolic health, cognitive deterioration, and a heightened risk of dementia in older adults, emerging as a significant modifiable risk factor in contemporary health (10, 11).

In this study, we conducted a comprehensive investigation of physiological functions, expression pathways, and gene expression associated with SD by analyzing datasets from the GEO database. This led to the identification of genes that hold significant diagnostic and therapeutic potential. Based on these findings, we formulated a diagnostic model predicated on hub genes and assessed the efficacy of these genes in discerning SD. The developed model offers substantial references for clinical diagnostics and therapeutics.

2 Methods

2.1 Data collection and normalization

We retrieved datasets related to SD and their corresponding control groups from the Gene Expression Omnibus (GEO) database (http://www.ncbi.nlm.nih.gov/geo) (12). Human RNA expression data from 17 individuals with SD and 25 healthy controls were obtained from the GSE208668 dataset, derived from the GPL10904 platform. For the validation of the subsequently identified hub genes, we utilized the GSE240851, GSE56931, and GSE98582 datasets, which were sourced from the GPL24676, GPL10379, and GPL6244 platforms, respectively. These datasets included varying numbers of SD patient and control samples. Additionally, the GSE165041 dataset, generated on the GPL18573 platform, comprised microRNA expression data from 10 SD patients and an equal number of healthy controls. All datasets were normalized using the "limma" package within the R software environment, version 4.1.2 (13).

2.2 Identification of differentially expressed genes

We utilized the limma package in R software to process the normalized datasets GSE240851 and GSE208668, aiming to identify DEGs. To ascertain statistical significance, DEGs were determined based on $|\log2\text{fold change}| \geq 0.58$ and a false discovery rate <0.05.

Subsequently, we employed the ggplot2 package to create volcano plots for the DEGs. Moreover, we selected the top 20 genes, ranked by |log2fold change|, to build heatmaps as part of our analysis.

2.3 Gene function enrichment analysis

The "c2.all.v2023.1.Hs.entrez" and "c5.all.v2023.1.Hs.entrez" datasets, which serve as reference gene sets, were downloaded from the GSEA official website originating from the MSigDB database (14). Gene set enrichment analysis (GSEA) was then performed using the "clusterProfiler" package in R software (15). Subsequently, the analysis results were visualized utilizing the "enrichplot" package in R software.

2.4 Immune infiltration analysis

We employed the ImmuCellAI and ssGSEA methodologies to estimate the abundance of 24 and 28 distinct types of immune cells, respectively, in the tissues of SD patients and a normal population, thereby enabling precise delineation of immune cell profile differences between the two groups (16, 17). Furthermore, we conducted Spearman correlation analysis to elucidate the interrelationships among the distributions of various immune cells.

2.5 ssGSEA

We downloaded the H: hallmark gene sets from the GSEA official website to probe the functional disparities between SD patients and the normal cohort. With these gene sets, we applied the ssGSEA algorithm to evaluate 50 gene sets, aiming to discern potential variances between the two groups. Subsequently, we utilized the Mantel algorithm to analyze the correlations among these gene sets (18). This approach allowed us to investigate the differences in gene expression profiles between the two cohorts and to identify potential molecular pathways associated with the disease.

2.6 Protein-protein interaction network construction

For protein interaction analysis, we utilized the STRING 4 online platform and specifically selected PPI pairs with a confidence score greater than 0.40. Subsequently, we employed the Cytoscape V3.9.0 software for visualizing the PPI network (19). Within the network, the significance of each node was determined by calculating their Degree values using the CytoHubba plugin. This analysis allowed us to identify the top 20 pivotal genes based on their ranking of importance (20).

2.7 Random forest gene selection

For gene selection, we utilized the Random Forest (RF) algorithm, a binary tree-based recursive partitioning method. The "randomForest" package in R was used, with parameters set to ntree=1000, mtry=3, and importance=true (21). Employing the Gini index as the primary assessment criterion, the Random Forest algorithm was used to rank the DEGs, and the top 20 genes with a significance value greater than 3 were earmarked for further analysis.

2.8 Support vector machine gene selection

We utilized the SVM-RFE (Recursive Feature Elimination) approach to optimize the predictive model by minimizing the number of feature vectors produced by the SVM. This approach, being an effective binary classification tool, operates by constructing a classification hyperplane to delineate decision boundaries. In order to enhance the algorithm's precision, we configured parameters to method=repeatedcv and repeats=10 in the R package "1071", and employed ten-fold cross-validation. This approach aimed at augmenting the algorithm's precision (22).

2.9 Model construction and evaluation

To develop the LASSO model (23), we integrated genes identified through CytoHubba, RF, and SVM algorithms. This method effectively enabled the identification of critical hub genes for diagnosing SD. We then employed the Logistic regression approach to investigate pivotal factors associated with SD, ultimately constructing a simplified model. Subsequently, we evaluated the classification performance of the model using the Receiver Operating Characteristic (ROC) curve and the corresponding Area Under the Curve (AUC).

2.10 Validation of the diagnostic model

In order to evaluate the robustness and general applicability of our developed diagnostic model, we computed the AUC of the ROC curve for the model using three distinct datasets: GSE240851, GSE56931, and GSE98582. This procedure aimed to ascertain the model's performance across diverse datasets. It was essential to assess its efficacy in different contexts and ensure its capability to perform consistently across varied data sources.

2.11 Exploration microRNAs targeting the genes

We utilized the Limma package in R to conduct a differential analysis of the expression matrix from GSE165041, aiming to identify miRNAs that were differentially expressed (DEmiRNAs). Our criteria for significance were miRNAs exhibiting a false discovery rate <0.05 and |log2fold change| >0.5. Moreover, we employed the miRNet database to investigate potential miRNAs associated with differentially expressed genes (DEGs), in order to gain further insight into their involvement in SD (24).

2.12 Drug and gene interaction scoring

We obtained data on drugs related to core genes from the Drug-Gene Interaction database (DGIdb) (25). We used the "ggplot2" package in R to create bar charts showing interaction scores, visually indicating the intensity of interactions between various drugs and core genes.

2.13 Establishment of animal models

The SD model, following the methodology outlined by Alkadhi and Alhaider (26), was established in 10-month-old male mice. The experimental mice were subjected to SD treatment for a duration of 8 weeks by being placed on a small fixed platform encircled by water, with access only to water and food. Meanwhile, for the control group, another set of mice was housed in a comfortable environment with a 12-hour light/dark cycle and unrestricted access to water and food. All mice received standard pellet feed, with the daily quantity of feed being maintained uniformly across all groups. This experimental design aimed to simulate the effects of SD on physiological functions, thus laying the groundwork for subsequent investigations into gene expression and drug treatment efficacy.

2.14 RT-qPCR

The cortex in SD mice was used for total RNA extraction, employing the TransZol Up Plus RNA Kit (TransGEN, Beijing, China) (27). The RNA concentration and quality were then assessed using the Nanodrop Spectrophotometer (Termo Scientifc, Waltham, MA, USA). Subsequently, reverse transcription was carried out using the TransScript® One-Step gDNA Removal and cDNA Synthesis SuperMix (AT311, TransGEN, Beijing, China). Amplification was monitored with the ChamQ Universal SYBR qPCR Master Mix (Novozymes Q711) and a QuantStudio™ 5 Real-Time PCR System (Thermo Fisher Scientific). The internal reference was β-actin, and the relative gene expression was determined using the 2-ΔΔCT formula. Detailed primer sequences can be found in Table 1.

TABLE 1 Primer sequences of mRNA for RT-qPCR.

Gene	Primer sequence, 5′–3′ Forward	Reverse
IPO9	CAGTGACAGCCTTGGT GAAA	TCTCCAGTAGGGCATG GACA
RAP2A	CAAACTGTACCACGCC CTCT	GTTGCTAGGTGGATTG GGCT
DDX17	TCTTCAGCCAACAATCCC AATC	GGCTCTATCGGTTTCAC TACG
MBNL2	CCCAAAAGTTGCCAGGT TGAA	CTGGGTTTTTAAGTGTGT CGGA
PIK3AP1	CTGGACTCTGCTTCTAA CCCC	TGACACCATTCCTCCGCATC
ZNF385A	CAGAACCAAGGGAAGG GGAC	GAAGGGCAG GATCTGCTTGA
β-Actin	GCAGGAGTACGATGAG TCCG	ACGCAGCTCAGTAACA GTCC

2.15 Immunoblotting for protein evaluation

Western blotting was performed for IPO9, RAP2A, DDX17, and GAPDH, as described previously (Table 2). Enhanced chemiluminescence reagents were used to detect protein expression, and quantitative analysis was conducted using Image J software (28).

2.16 Statistical analysis

The normality of the data was assessed using the Shapiro–Wilk test. The t-test was utilized to compare the data between two groups, while comparisons among multiple groups were conducted using one-way ANOVA, followed by either the LSD *post hoc* test or Tukey's *post hoc* test. The statistical analyses were conducted using R software version 4.2.1 and SPSS 25, with significance defined as $P < 0.05$. Furthermore, all experiments were independently repeated at least three times to ensure the validity of the results.

3 Results

3.1 Identification of DEGs

In the GSE208668 and GSE240851 datasets, a differential expression analysis was conducted on SD samples and normal control samples. The analysis identified 5964 DEGs in the GSE208668 dataset and 1375 DEGs in the GSE240851 dataset. Utilizing these DEGs, volcano plots (Figures 1A, B) were constructed, and the top 20 genes with the highest |log2fold change| values were selected for heatmap generation (Figures 1C, D). These results demonstrate the effectiveness of DEGs in distinguishing between the SD group and the normal control group.

3.2 Functional enrichment analysis of DEGs

The differential gene analysis of GSE208668, using MSigDB's C2 and C5 gene sets, unveiled substantial differential expression in gene clusters relevant to immune cell functions, stress responses, and nervous system activities. Specifically, within the C2 gene set, activation of the gene cluster associated with nervous system development was observed, while the gene cluster linked to the B lymphocyte network was suppressed. In the C5 gene set, gene clusters involved in stress response regulation exhibited a downregulated trend, indicating a potential imbalance in

TABLE 2 List of the primary antibodies.

Antibody	Catalogue number	Brand	Application	Dilution	Species	MW(kDa)
IPO9	abs134286	absin	WB	1:1000	Rabbit	116
RAP2A	abs105749	absin	WB	1:1000	Rabbit	21
DDX17	abs111924	absin	WB	1:1000	Rabbit	72
GAPDH	GB15002-100	Servicebio	WB	1:2000	Rabbit	36

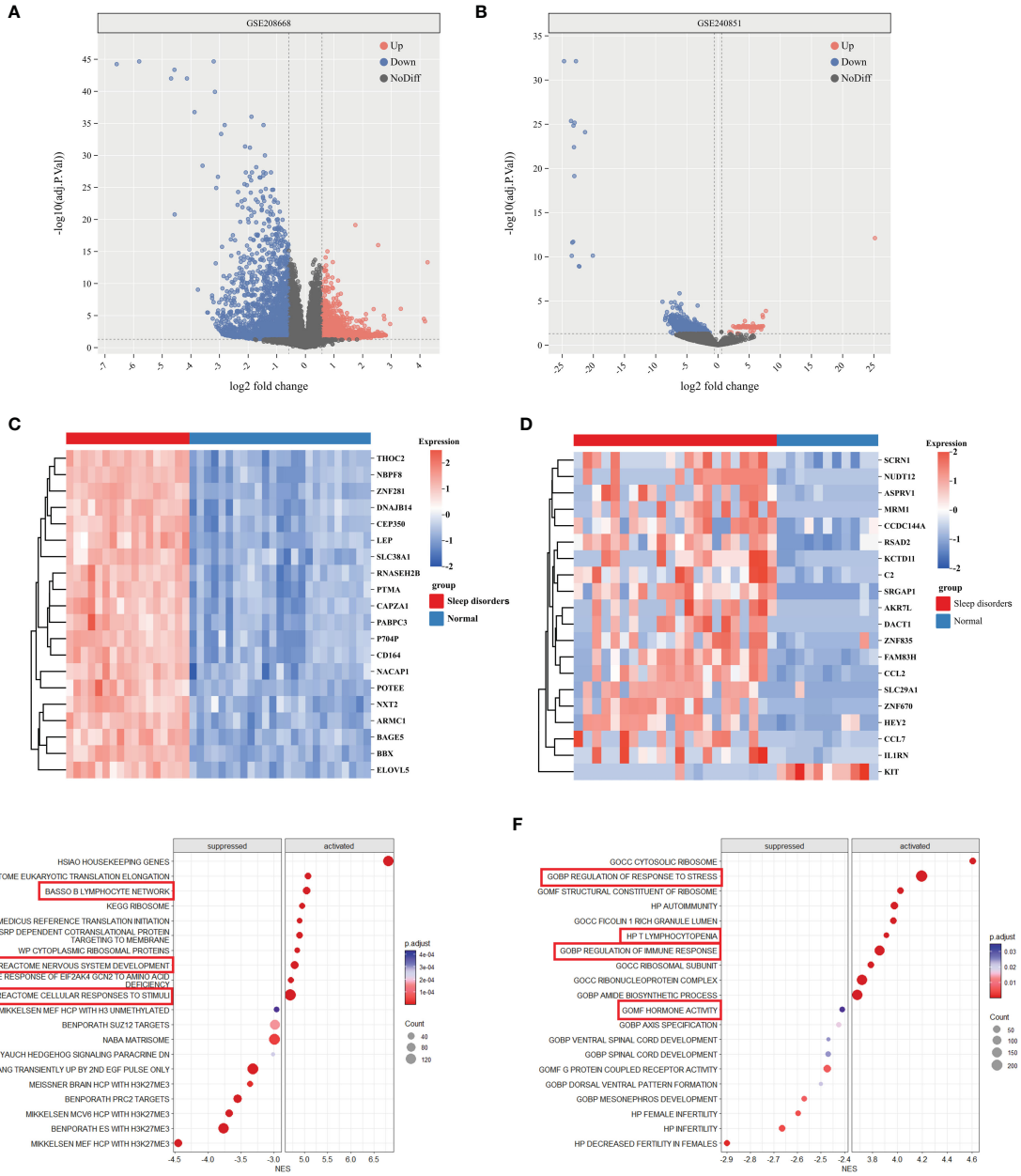

FIGURE 1
DEGs and enrichment analysis of SD. **(A, B)** Volcano plot of DEGs between Sleep disorders and Normal groups in GSE208668 and GSE240856. **(C, D)** Heatmap of top 20 DEGs in GSE208668 **(C)** and GSE240856 **(D)**. **(E, F)** The top 10 gene sets that areactivated or inhibited in the C2 **(E)** and C5 **(F)** gene sets of MSigDB.

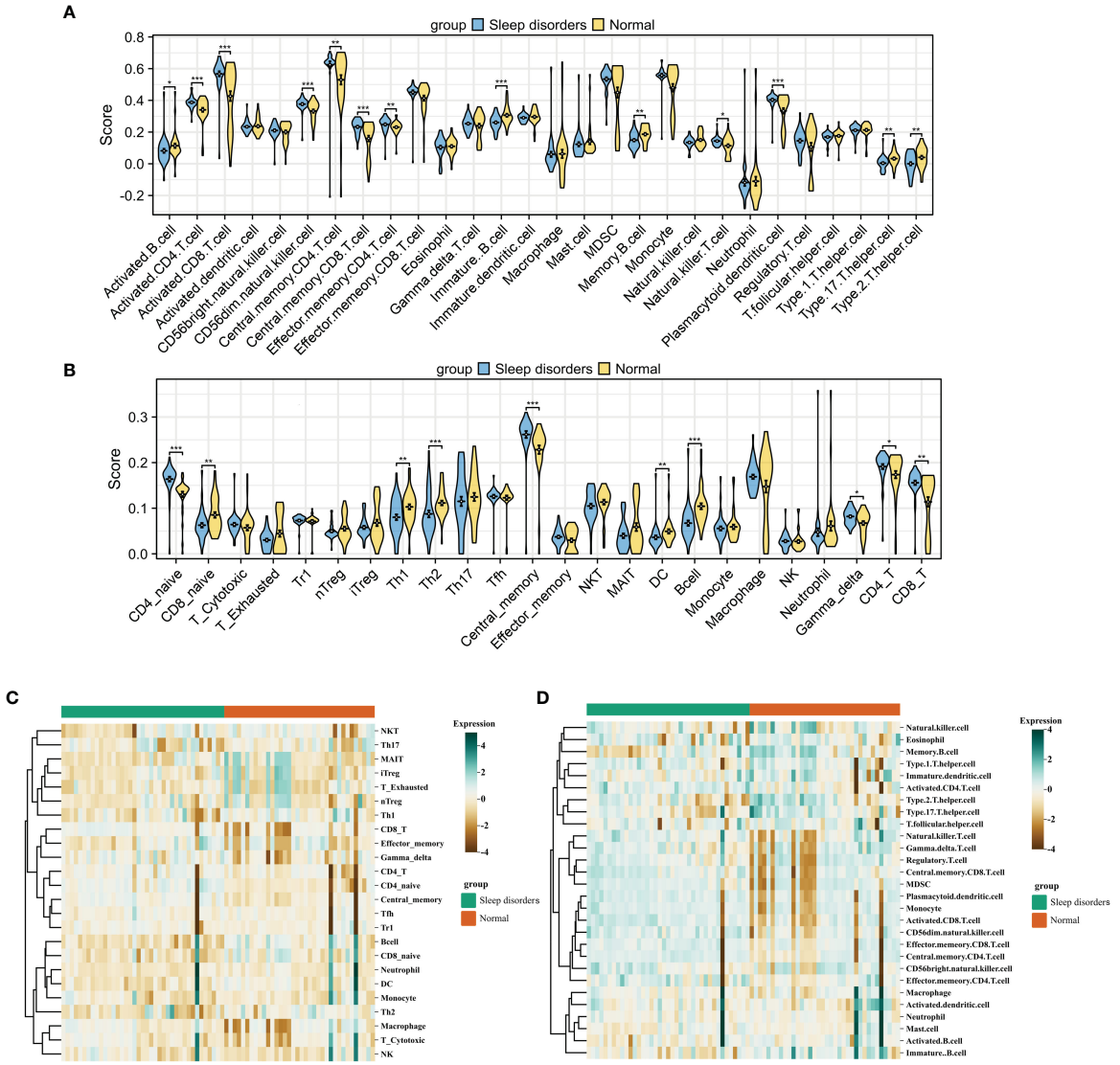

FIGURE 2
Immune Cell Infiltration **(A, B)** Violin plot comparing the results of two immune infiltration algorithms. ssGSEA **(A)** and ImmuCellAI **(B)**. **(C, D)** Heatmap of the proportions of two immune infiltration algorithms in the Sleep disorders and Normal groups. ImmuCellAI **(C)** and ssGSEA **(D)**. * $p < 0.05$, ** $p < 0.01$, *** $p < 0.001$.

environmental stress response regulation. Additionally, gene clusters associated with spinal cord development demonstrated differential expression. Moreover, immune-related gene clusters, including those implicated in autoimmunity and T-cell deficiency, exhibited alterations in expression levels (Figures 1E, F). Further comprehensive details can be found in Supplementary 1.

The results of the GSEA analysis demonstrated significant enrichment of terms in KEGG pathways closely associated with neurodegenerative diseases and metabolic pathways, such as Alzheimer's disease, leishmaniasis infection, lysosomal function, oxidative phosphorylation, Parkinson's disease, and viral myocarditis. Notably, major signaling factors involved in immune regulation, including IL-4, IL-8, and IL-12, were also found to be significantly enriched in various immune system pathways. Furthermore, signaling pathways related to neural signaling, including neurotrophic factor signaling, B cell receptor signaling, and tumor necrosis factor α signaling, demonstrated significant enrichment Supplementary 2.

3.3 Analysis of immune cell infiltration

After integrating the GSE208668 and GSE240851 datasets and mitigating batch effects, we observed significant discrepancies in the distribution of various immune cell types between patients with systemic lupus erythematosus (SD) and the normal control group. This was confirmed by employing two distinct immune infiltration scoring methods (Figures 2A–D). Notably, the infiltration scores for Activated CD4+ T cells and Activated CD8+ T cells were substantially higher in patients with SD compared to the normal group. Moreover, central memory CD4 T cells, central memory CD8 T cells, and natural killer T cells exhibited an increasing trend

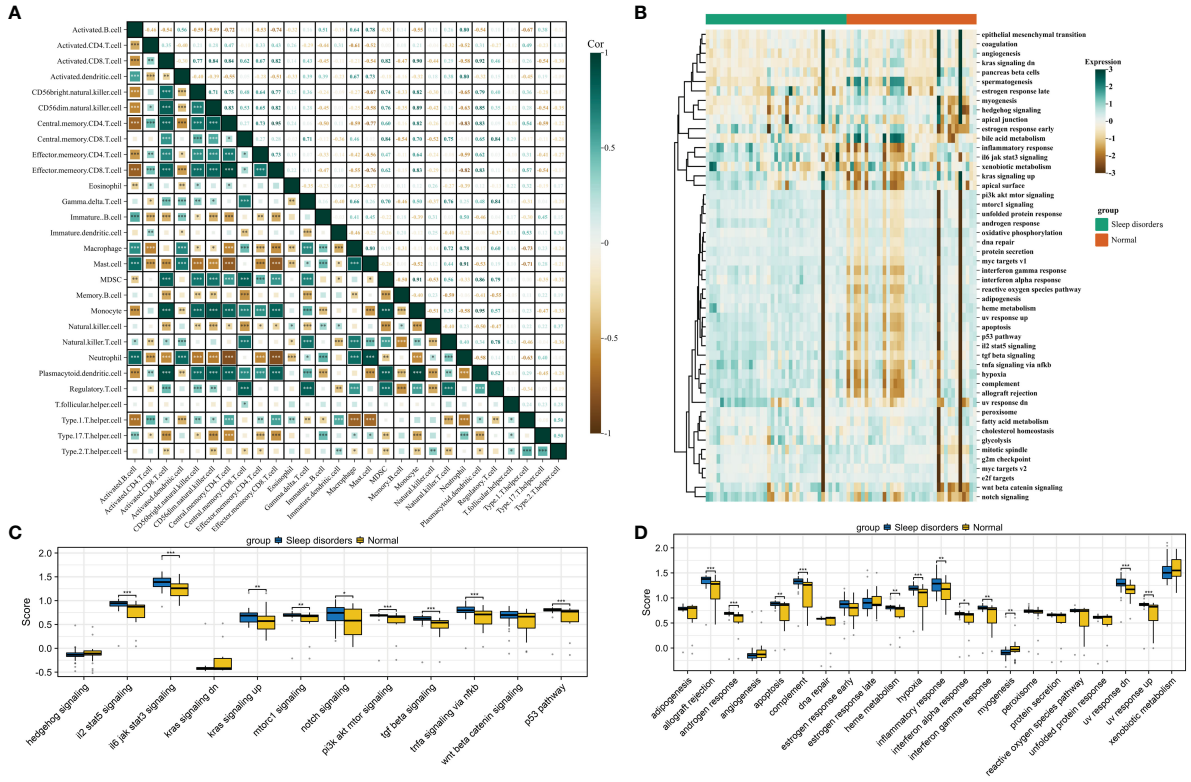

FIGURE 3
Gene set scoring. **(A)** Correlation graph for 28 types of immune cells. **(B)** Heatmap of scores for 50 gene sets. **(C)** Box plot comparing scores of 12 signaling pathways between Sleep disorders and Normal groups. **(D)** Box plot comparing scores of 22 physiological functions between Sleep disorders and Normal groups. * $p < 0.05$, ** $p < 0.01$, *** $p < 0.001$.

in SD patients. In contrast, the infiltration scores of Activated B cells, Immature B cells, Th17 cells, and Th2 cells demonstrated a declining trend in patients with SD relative to the normal group. Correlation analysis based on both algorithms indicated a level of concordance. Specifically, CD8+ T cells and memory T cells consistently showed a strong positive correlation, while neutrophils and regulatory T cells exhibited a negative or non-significant correlation (Figure 3A). For a detailed correlation analysis of the ImmuCellAI algorithm scores, please refer to Supplementary 3.

3.4 Gene set scoring based on ssGSEA

The heatmap in Figure 3B displays the scores for 50 gene sets, from which we chose 12 related to signaling pathways and 22 associated with physiological functions for further investigation. A comparative analysis of the gene set scores between the groups revealed that in the SD group, median scores for gene sets such as androgen response, apoptosis, complement, hypoxia, and inflammatory response were significantly higher, while the median score for the myogenesis gene set was notably lower compared to the normal group. Additionally, significant disparities were observed in signaling pathways such as il2 stat5 signaling, il6 jak stat3 signaling, the p53 pathway, and tgf beta signaling (Figures 3C, D).

We then focused on 12 gene sets with significant differences in physiological functions between the groups for further correlation analysis. These analyses revealed that, except for the inflammatory response gene set, other gene sets showed significant correlations with immune infiltration and signaling pathway scores. Moreover, the scores within these 12 biological function gene sets also exhibited a high degree of correlation (Supplementary 4). For detailed results on pathway scoring and physiological function scoring correlations, please refer to Supplementary 5.

3.5 Identification of key genes in PPI network

We first identified 138 co-expressed differential genes by intersecting the DEGs from the GSE208668 and GSE240851 datasets (Figure 4A). Subsequently, 52 genes were selected for network visualization in Cytoscape using the STRING database for PPI analysis with a medium confidence threshold of 0.4 (Figure 4B). To identify the top 20 key genes within the PPI network, the CytoHubba plugin in Cytoscape was employed (Figure 4C).

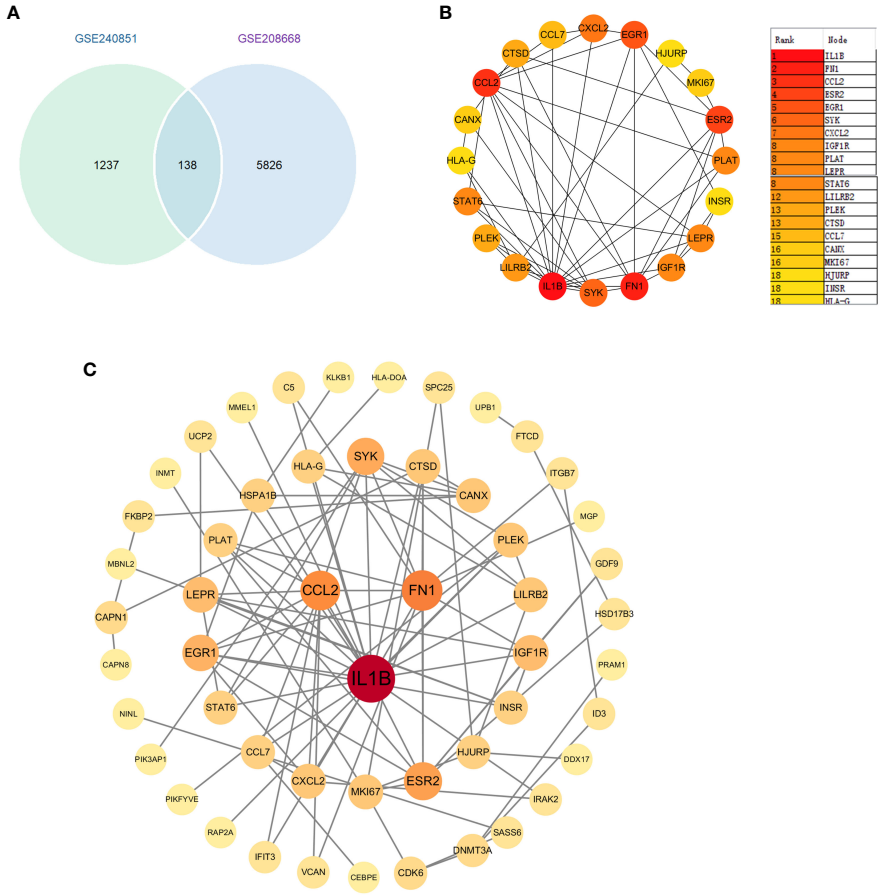

FIGURE 4
(A) Venn diagram of differential genes between datasets GSE20851 and GSE208668. **(B)** Identification of genes in the PPI network common to differential genes. **(C)**.Top 20 genes selected by the CytoHubba plugin.

3.6 Utilizing machine learning for enhanced feature gene selection

The assessment of hub genes started with the use of the GSE208668 dataset and the RF algorithm, which led to the identification of 138 co-expressed differential genes. The model's performance was then evaluated across a spectrum of tree quantities, showing a gradual decrease in the error rate as the number of trees increased, ultimately indicating enhanced stability and reliability (Figure 5A). Following this, the feature importance was assessed through the calculation of the percentage decrease in mean impurity (%IncMSE), which resulted in the identification of the top 20 genes that had the most significant contributions to the model's prediction (Figure 5B). Subsequently, the SVM algorithm was utilized to determine the hierarchical importance of the 138 genes (Figure 5C). The model's predictive efficacy was then measured using the Root Mean Square Error (RMSE) through cross-validation methodologies, as shown in Figure 5D. The results indicated that the model demonstrated its strongest predictive capability when N was set to 22, leading to the selection of these 22 genes for further analysis.

3.7 Development and verification of the diagnostic model

After identifying 40 key genes through the amalgamation of genes identified via CytoHubba, Random Forest, and SVM (Supplementary 6 for details), LASSO regression was utilized to select diagnostic genes. This process involved adjusting the regularization parameter λ and observing its effects on coefficient estimation (Figure 5E). The optimal λ value was determined through the ten-fold cross-validation method (Figure 5F). In the final analysis, diagnostic model construction involved the selection of IPO9, RAP2A, DDX17, MBNL2, PIK3AP1, and ZNF385A.

When compared to the normal group, these 6 hub genes demonstrated significant disparities (Figure 6A) and significant correlations with scores of biological function genes (Figure 6B). The interactions between hub genes and other functional scores are presented in Supplementary 7. A nomogram was constructed based on these 6 genes, with each gene correlating with a specific scoring criterion (Figure 6C). The calibration curve of the nomogram indicated commendable predictive performance of the model (Figure 6D). ROC curve analysis further demonstrated the

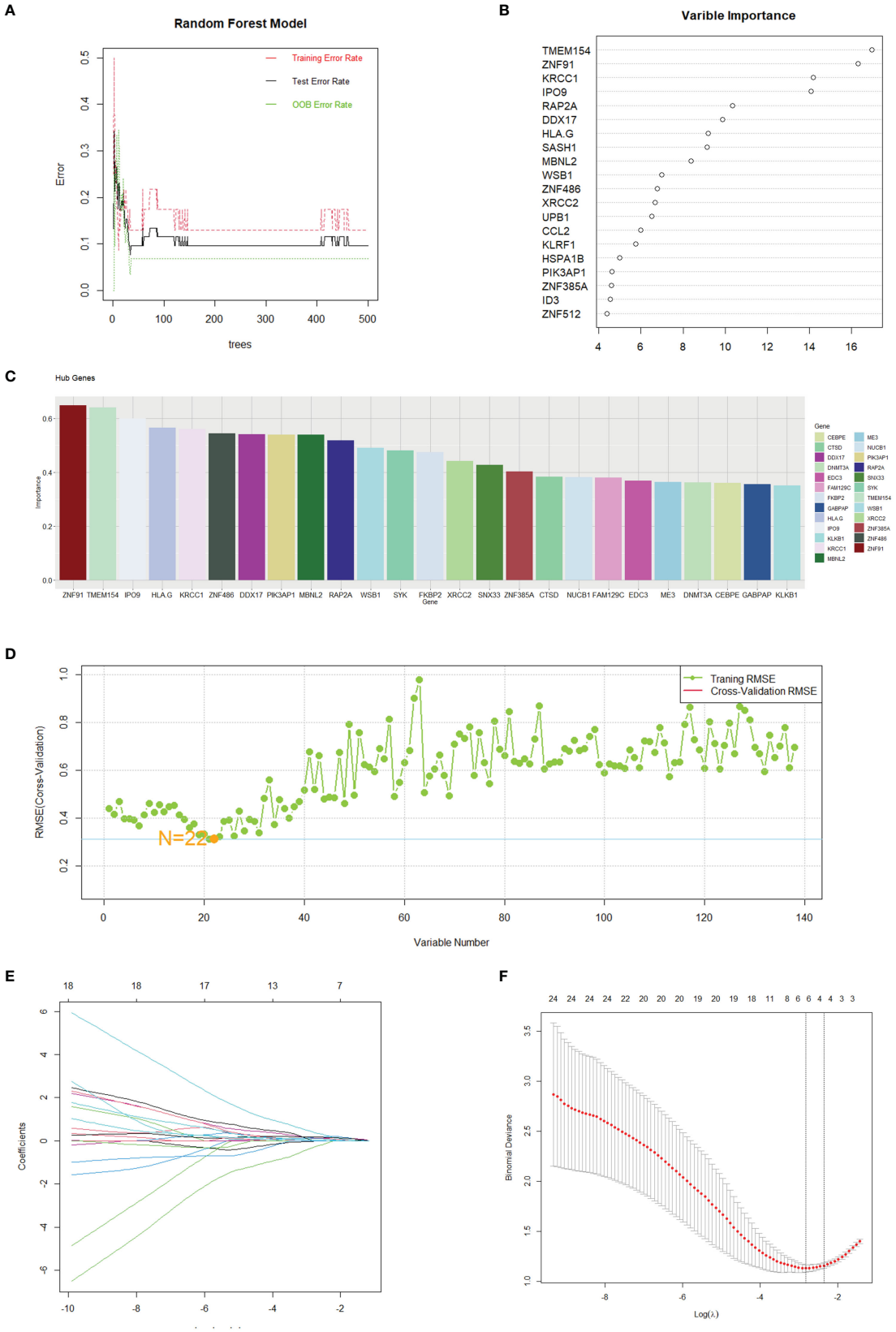

FIGURE 5
Gene selection through machine learning. **(A)** The correlation plot between the number of Random Forest trees and model error. **(B)** Top 20 genes selected by the RF method. **(C)** Top 25 genes identified by SVM, ranked by the percentage decrease in mean impurity. **(D)** Results obtained from the predictive model of the Root Mean Square Error through cross-validation. **(E, F)** Cvfit and lambda curves demonstrating the use of the LASSO regression, performed with the minimum criteria.

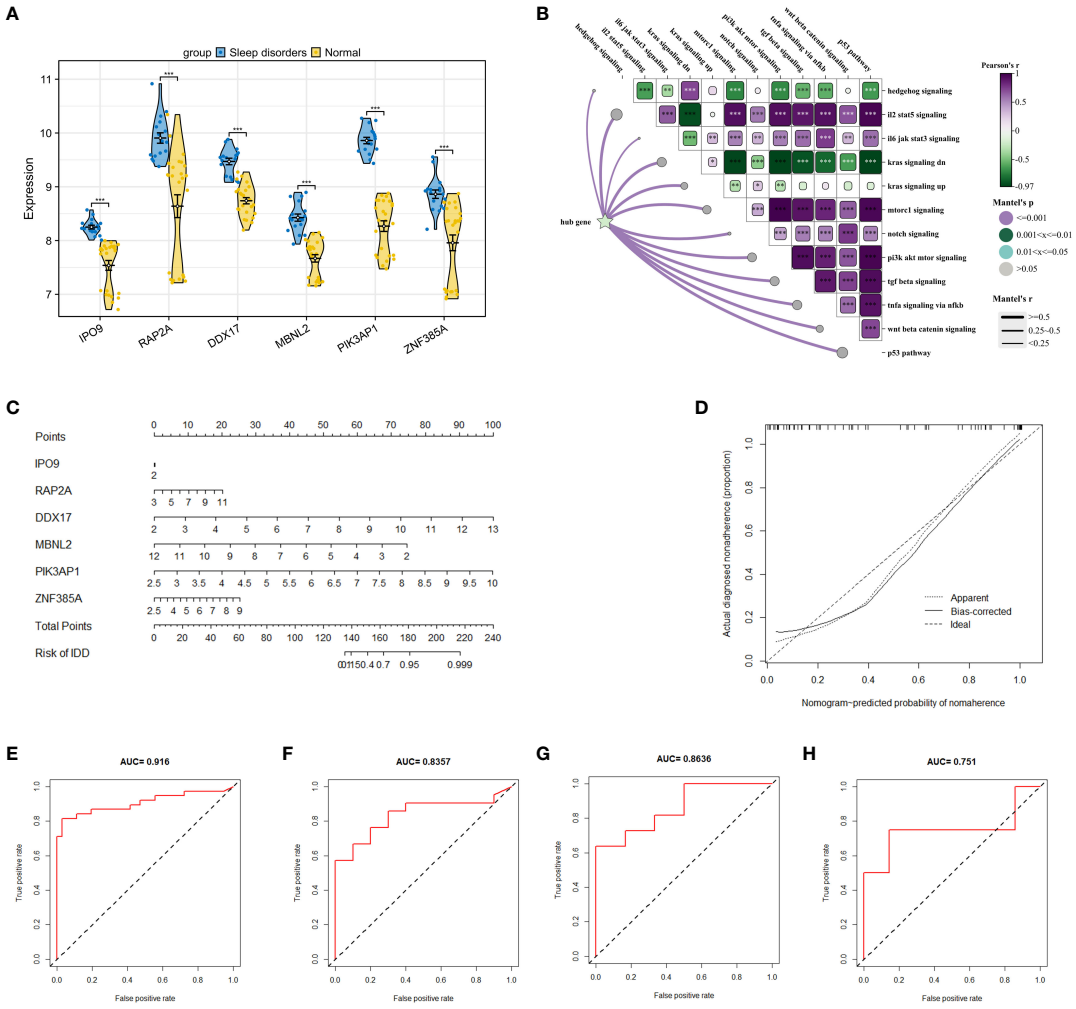

FIGURE 6
Construction of a research and diagnostic model based on hub genes. **(A)** Expression of 6 hub genes in dataset GSE208668. **(B)** Correlation between 6 key genes and crucial signaling pathways. **(C)** A nomogram model, incorporating 6 hub genes, was constructed to predict risk. **(D)** The calibration curve of the nomogram to test the predictive performance of the model. **(E)** ROC curves analysis of GSE208668 for the diagnostic model. **(F–H)** display ROC curve analyses of the diagnostic model applied to GSE240851, GSE98582, and GSE56931 datasets. * p < 0.05, ** p < 0.01, *** p < 0.001.

substantial diagnostic value of these genes with an overall AUC value of 0.916 (Figure 6E). To corroborate the accuracy of the model, three independent datasets were utilized in logistic regression analysis. The AUC values for GSE240851, GSE98582, and GSE56931 were 0.835, 0.863, and 0.751, respectively, demonstrating the stability and reliability of the model in diagnosing SD (Figures 6F–H).

3.8 Investigating miRNAs and prospective therapeutic agents

The analysis of the GSE165041 dataset revealed 9 upregulated DEmiRNAs that distinguished the SD group from the normal group, as evidenced in Figure 7A. Subsequently, an exploration of the association between these DEmiRNAs and the previously identified 138 DEGs was conducted using the miRnet database, resulting in the identification of 5 miRNAs with potential as therapeutic targets, as depicted in Figure 7B. Following this, a validation of the potential therapeutic efficacy of the 5 identified miRNAs and their corresponding key mRNAs was performed, as shown in Figure 7C. Subsequently, compounds with high interaction scores with the key genes were identified utilizing the DGIdb, as illustrated in Figure 7D. These findings indicate that the identified miRNAs and compounds might serve as potential therapeutic agents for the treatment of SD. Nevertheless, it is essential to note that further research is necessary to substantiate their efficacy and safety.

3.9 Analysis of predicted gene expression in brain tissue of SD mice

RT-qPCR was used to scrutinize the expression levels of 6 hub genes in the tissue. The mRNA expression levels of 6 genes in the SD group showed a significant elevation relative to the normal

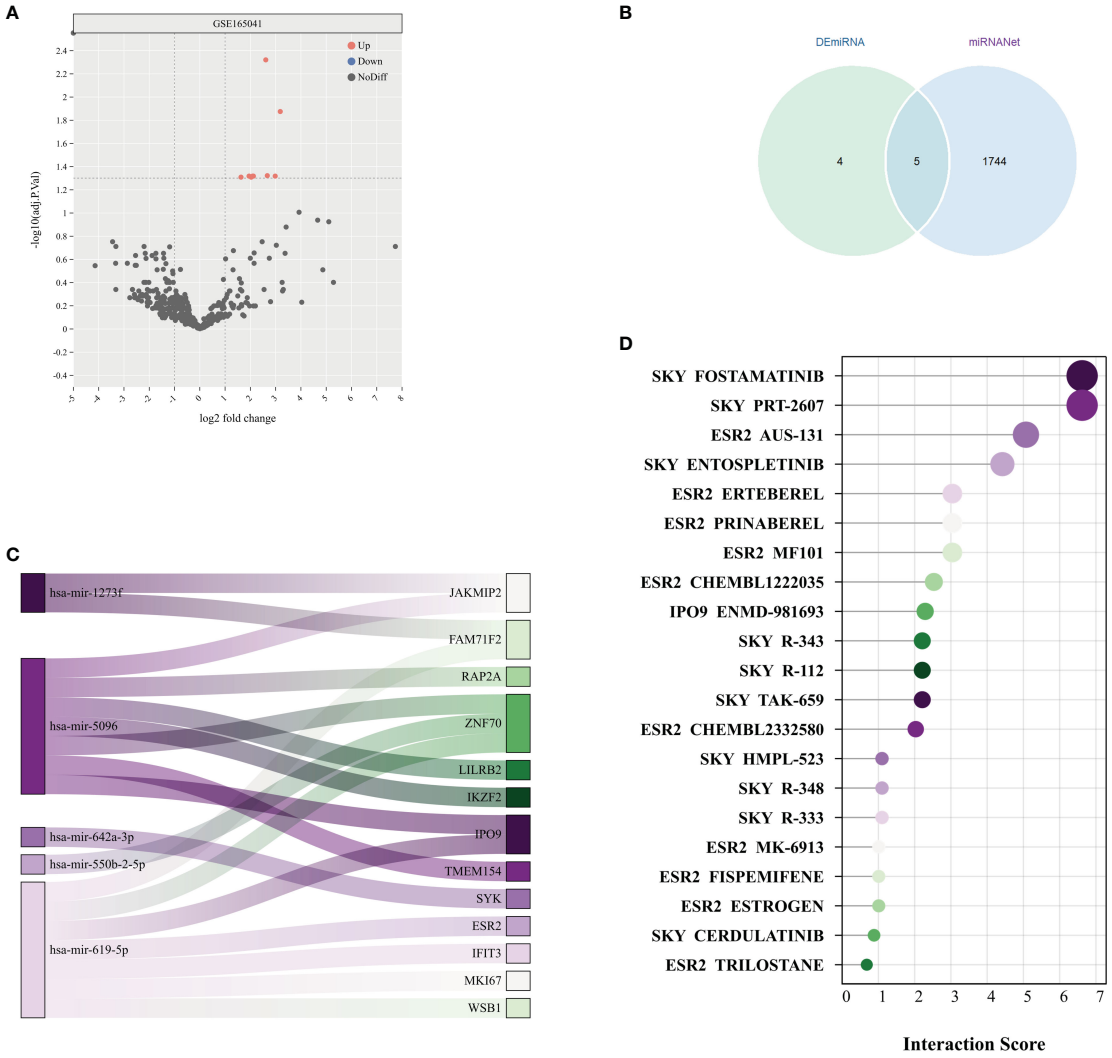

FIGURE 7
Potential therapeutic drug search based on miRNA. **(A)** Volcano plot of miRNA differential analysis results from the GSE165041 dataset. **(B)** Venn diagram of DEmiRNAs and miRNAs obtained from miRNANet. **(C)** The Sankey plot shows the relationships between 5 miRNAs and their target genes. **(D)** Interaction scores between genes and drugs were obtained from the DGIdb database.

group, as illustrated in Figure 8A. Moreover, Western blotting analysis revealed significant elevations in the protein levels of genes such as IPO9, RAP2A, and DDX17 within the cortical regions of mice suffering from SD, as depicted in Figures 8B, C. These findings align with previous bioinformatics analysis outcomes, providing further support for the correlation of expression levels among these 6 hub genes.

4 Discussion

Epidemiological research has revealed that SD are prevalent worldwide, with industrialized countries exhibiting a particularly high prevalence (29). The correlation between SD and a range of conditions, including cardiovascular diseases, diabetes, and mental disorders, has been extensively documented. This emphasizes the critical role of sleep quality in maintaining overall health. The integration of genomics, transcriptomics, and proteomics has significantly advanced the understanding of the molecular mechanisms underlying SD, leading to the discovery of numerous genes and molecular pathways associated with these disorders (30, 31). Particularly in terms of genetics, studies by Lee YY et al. have confirmed that genes play an important role in the development of SD (32). The etiology of SD involves a complex interplay of biological, psychological, and social factors, with principal neurobiological mechanisms comprising substances and regulators, genetic factors, lifestyle choices, and light exposure (33, 34).

This research used advanced bioinformatics approaches to analyze differentially expressed genes (DEGs) between patients with SD and a normal group, revealing significant differences in immune response, stress response, and nervous system development. Notably, the study uncovered a close correlation between inflammatory pathways (such as IL-2, IL-8, IL-12) and

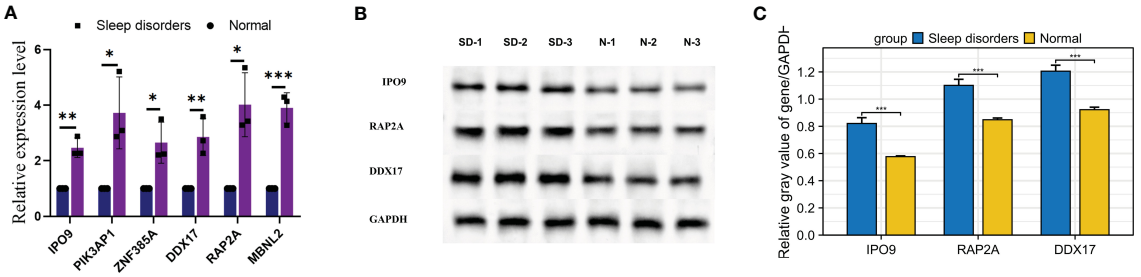

FIGURE 8
Expression of mRNA and proteins in mice with SD. **(A)** Relative mRNA expression of the 6 hub genes. **(B)** Western blot results for 3 relative proteins. **(C)** Relative protein expression. * $p < 0.05$, ** $p < 0.01$, *** $p < 0.001$.

pathways relevant to neurodegenerative diseases. The intimate association between sleep and the immune system suggests that SD may result in immune dysregulation (35). Murine models have shown that SD can influence the signaling of GM-CSF (Granulocyte-Macrophage Colony-Stimulating Factor) by regulating Th17 and activated CD4 T cells (36), which in turn interacts with myeloid cells, exacerbating the progression of autoimmune diseases. Simple sleep deprivation in rats has been found to increase Natural Killer (NK+) and T cells (CD8+) in the spleen and decrease B cells (37). Moreover, research indicates that patients with central hypersomnia exhibit significantly higher levels of activated CD4+ and CD8+ T cells in both peripheral blood and cerebrospinal fluid compared to healthy controls (38). These findings align with previous studies and reveal substantial alterations in activated CD4+ T cells, CD8+ T cells, central memory CD4 and CD8 T cells, natural killer T cells, activated B cells, immature B cells, Th17 cells, and Th2 cells in patients with SD. These results suggest that T cell-mediated autoimmune responses may contribute to the pathogenesis of SD, and the increase in memory T cells and other immune cells implies their intricate involvement in SD. All of these studies corroborate with the results of our analysis, suggesting the existence of complex physiological mechanisms of immune cells in SD. Furthermore, the alterations in B-cell and Th-cell infiltration scores identified in our research provide a new perspective for comprehensive investigation into the roles of these cells in the context of SD.

The implementation of gene set scoring methodologies has elucidated the expression patterns of distinct gene sets in various diseases, thereby aiding in the comprehension of the underlying biological processes and pathological mechanisms (39). A multitude of studies have demonstrated a close association between SD and diverse biological and pathological processes (40). For instance, research conducted by Séverine Lamon et al. found that total SD results in reduced testosterone levels and muscle protein synthesis in patients' plasma, while the mouse experiments by Yin Cao et al. observed excessive autophagy and apoptosis in hippocampal neuronal cells, concomitant with the activation of the PI3K/AKT signaling pathway (41, 42). Similarly, the study by Yongmei Li et al. indicates that SD leads to the upregulation of autophagy-related proteins, and Anna Brzecka et al. highlight that intermittent hypoxia resulting from SD may elevate the risk of certain cancers (43, 44). The research by Zhong Wang et al. demonstrates that SD may precipitate gut microbiota imbalance and cognitive function decline, with observations of the activation of the Toll-like receptor 4/nuclear factor-κB signaling pathway in mice with transplanted SD microbiota (45). In the context of signal pathway scoring, sleep deprivation has been found to activate the P53 pathway. This activation induces the expression of apoptotic proteins, such as Bax and Bcl-2, leading to the onset of tongue cancer (46). In a molecular mechanism study exploring the link between sleep and breast cancer, a positive correlation was identified between TGF-β and CRP levels and insomnia, while IL-6 showed a negative correlation with sleep-inducing medications (47). Such gene sets have substantiated the results of our bioinformatics research.

Our study findings uncovered a substantial correlation between the scores of 12 signaling pathways and various biological gene sets. Specifically, our results emphasized the significant association of the hedgehog and kras signaling pathways with various biological processes, suggesting their potential contribution to the onset of SD. Additionally, the il2, il6, notch, and PI3K/AKT/mTOR pathways also demonstrated relevance, signifying their potential as crucial areas for further investigation in SD studies. The above findings, which have been mentioned in other studies as having a potential link to SD (48).

Leveraging a comprehensive analysis of differential genes in the GEO dataset and various machine learning algorithms, our study identified 6 pivotal genes - IPO9, RAP2A, DDX17, MBNL2, PIK3AP1, and ZNF385A. These genes are instrumental in the identification of biomarkers and potential therapeutic targets for SD.

The IPO9 gene plays a key role in mediating the docking process of the importin/substrate complex with the nuclear pore complex, enabling the transport of the complex through the pore by binding to nucleoporin proteins using energy-dependent and Ran-dependent mechanisms (49). Research has indicated that the expression of IPO9 is regulated by m6A modification sites, which may be closely linked to the pathogenesis of obesity (50). RAP2A, a member of the RAS oncogene family, encodes a crucial protein that is essential for the activation of cAMP-dependent PKA and ERK signaling pathways. Additionally, it is involved in a signaling complex consisting of NEDD4, RAP2A, and TNIK, which regulates the growth and differentiation of neuronal dendrites (51). Furthermore, RAP2A is implicated in multiple signaling cascades, including cytoskeletal rearrangement, cell migration,

adhesion, and proliferation. It also exhibits abnormal expression in various tumors, such as breast, liver, and gastric cancers (52). The DDX17 gene encodes a DEAD box protein and is involved in multiple cellular processes that require alterations in RNA secondary structure (53). Research by Samaan et al. has demonstrated that DDX17 plays a significant role in estrogen and testosterone signaling pathways, influencing the use of alternative promoters in estrogen-responsive genes and affecting the transcription and splicing of many steroid hormone target genes (54). Changes in DDX17 expression may affect mRNA processing of hormones and neurotransmitters associated with sleep regulation, thereby modulating sleep cycle and quality. This finding not only explains the physiological role of DDX17, but may also guide future personalized treatment strategies for SD patients. MBNL2, a member of the muscleblind protein family, encodes a C3H type zinc finger protein that regulates the selective splicing of pre-mRNA (55). Knockout of the MBNL2 gene in mouse models has been associated with diabetes-related characteristics in the central nervous system, including abnormal rapid eye movement sleep tendencies and spatial memory deficits. Furthermore, these mice exhibited delayed recovery and prolonged sleep duration following general anesthesia when compared to wild-type mice (56). PIK3AP1 plays a crucial role in diverse inflammatory responses and the regulation of signal transduction. It connects B cell receptor signaling with the PI3K-Akt signaling pathway, facilitating signal transduction relevant to B cell development. It also links toll-like receptor signaling with PI3K activation, hence helping to prevent excessive production of inflammatory cytokines (57). ZNF385A, a zinc finger protein, modulates the activity of p53/TP53 through direct protein interactions, leading to cell cycle arrest. Emerging studies suggest that this gene may be associated with the decline in cognitive function in the elderly (58, 59). Finally, through the analysis of mRNA and its corresponding protein expression in a mouse model of SD, the involvement of these 6 genes in sleep disturbances was confirmed, revealing significant differences in their expression under diseased conditions.

In our study, using the miRNAnet platform, we identified 5 critical miRNAs targeting 13 genes implicated in SD. Among these findings, hsa-miR-5096, mediated by exosomes, stood out due to its potential to augment the heterogeneity of somatostatin receptors (60). Additionally, a strong correlation was observed between miR-642a-3p and the metabolic levels of adenosine and creatine in the metabolic analysis of varicose veins (61). Furthermore, our research integrated the DGIdb analysis, revealing the potential therapeutic value of drugs such as MF101, ENTOSPLETINIB, FISPEMIFENE, and FOSTAMATINIB. For instance, MF101 has the ability to selectively modulate estrogen receptor β, possibly aiding in the improvement of vasomotor symptoms and enhancing sleep quality in menopausal women (62). Similarly, FISPEMIFENE, a tissue-specific estrogen agonist/antagonist, is also considered beneficial for improving sleep quality, as evidenced in previous research (63).

Our study has yielded potential insights into the molecular mechanisms of SD; however, it is important to acknowledge its limitations. Firstly, our analysis relies on secondary data from existing databases, which raises potential concerns about data quality and representativeness. Furthermore, despite the identification of numerous genes and pathways associated with SD, there is a need for further investigation into the causal relationships and specific mechanisms of action among them. Lastly, our study primarily focuses on the genetic level and does not comprehensively account for the potential impacts of proteins, metabolites, and other non-coding RNAs. Future research efforts should concentrate on validating the biological and clinical significance of these findings, as well as further delineating the specific roles of non-genetic factors in the pathogenesis of SD.

Our research leverages cutting-edge bioinformatics tools to elucidate the genetic underpinnings of sleep disorders, representing a significant advantage in terms of technological application and data handling capacity. The multi-dataset validation process serves as a robust proof of concept, indicating that our findings have a high potential for generalizability across different populations. However, the study is not without its limitations. The dependence on publicly available genomic databases might limit our insights to the data quality and completeness of these resources. Furthermore, while our model shows promising results in computational validations, actual clinical utility will need to be established through prospective clinical trials involving diverse patient demographics to address the varying manifestations of sleep disorders.

Unlike previous studies on single genes and sleep disorders, this study combined bioinformatics to screen key genes and construct a diagnostic model for sleep disorders based on machine learning and big data modeling, which was finally validated on an animal model. Our investigation delves into the pathogenesis of SD from multifaceted perspectives, including genetics, physiology, and pharmacology. Through our analysis, we have discerned that specific gene expression patterns under diverse physiological and pathological conditions may either mitigate or exacerbate disease progression. This influence occurs through their impact on immune responses, epigenetic regulation, and numerous synergistic regulatory mechanisms. The interactions between these factors significantly contribute to our understanding of the complex nature of SD.

Data availability statement

The datasets presented in this study can be found in online repositories. The names of the repository/repositories and accession number(s) can be found in the article/Supplementary Material.

Ethics statement

Ethical approval was not required for the study involving humans in accordance with the local legislation and institutional requirements. Written informed consent to participate in this study was not required from the participants or the participants' legal guardians/next of kin in accordance with the national legislation

and the institutional requirements. The animal study was approved by laboratory animal ethics committee of Wenzhou Medical University. The study was conducted in accordance with the local legislation and institutional requirements.

Author contributions

JL: Data curation, Software, Validation, Visualization, Writing – original draft, Writing – review & editing, Conceptualization, Investigation, Methodology, Project administration, Supervision. CL: Data curation, Formal analysis, Software, Supervision, Validation, Writing – review & editing. EH: Conceptualization, Investigation, Project administration, Resources, Supervision, Visualization, Writing – original draft, Writing – review & editing.

Funding

The author(s) declare that no financial support was received for the research, authorship, and/or publication of this article.

Conflict of interest

The authors declare that the editorial was conducted in the absence of any commercial or financial relationships that could be construed as a potential conflict of interest.

Publisher's note

Supplementary material

The Supplementary Material for this article can be found online at: https://www.frontiersin.org/articles/10.3389/fimmu.2024.1381765/full#supplementary-material

References

1. Pavlova M K, Latreille V. Sleep disorders. *Am J Med*. (2019) 132:292–9. doi: 10.1016/j.amjmed.2018.09.021

2. Xie Z, Chen F, Li WA, Geng X, Li C, Meng X, et al. A review of sleep disorders and melatonin. *Neurol Res*. (2017) 39:559–65. doi: 10.1080/01616412.2017.1315864

3. Ramos AR, Wheaton AG, Johnson DA. Sleep deprivation, sleep disorders, and chronic disease. *Prev Chronic Dis*. (2023) 20:E77. doi: 10.5888/pcd20.230197

4. Sánchez-de-la-Torre M, Barbé F. Sleep disorders and cardiovascular disease. Trastornos del sueño y enfermedad cardiovascular. *Med Clin (Barc)*. (2022) 158:73–5. doi: 10.1016/j.medcli.2021.09.001

5. Deshpande SN, Simkin DR. Complementary and integrative approaches to sleep disorders in children. *Child Adolesc Psychiatr Clin N Am*. (2023) 32:243–72. doi: 10.1016/j.chc.2022.08.008

6. Chance Nicholson W, Pfeiffer K. Sleep disorders and mood, anxiety, and post-traumatic stress disorders: overview of clinical treatments in the context of sleep disturbances. *Nurs Clin North Am*. (2021) 56:229–47. doi: 10.1016/j.cnur.2021.02.003

7. Wang Q, Wang X, Yang C, Wang L. The role of sleep disorders in cardiovascular diseases: Culprit or accomplice? *Life Sci*. (2021) 283:119851. doi: 10.1016/j.lfs.2021.119851

8. Manolis TA, Manolis AA, Apostolopoulos EJ, Melita H, Manolis AS. Cardiovascular complications of sleep disorders: A better night's sleep for a healthier heart / from bench to bedside. *Curr Vasc Pharmacol*. (2021) 19:210–32. doi: 10.2174/1570161118666200325102411

9. Mainieri G, Montini A, Nicotera A, Di Rosa G, Provini F, Loddo G. The genetics of sleep disorders in children: A narrative review. *Brain Sci*. (2021) 11:1259. doi: 10.3390/brainsci11101259

10. Dijkstra F, de Volder I, Viaene M, Cras P, Crosiers D. Polysomnographic predictors of sleep, motor, and cognitive dysfunction progression in Parkinson's disease. *Curr Neurol Neurosci Rep*. (2022) 22:657–74. doi: 10.1007/s11910-022-01226-2

11. Sofer T, Kurniansyah N, Murray M, Ho YL, Abner E, Esko T, et al. Genome-wide association study of obstructive sleep apnoea in the Million Veteran Program uncovers genetic heterogeneity by sex. *EBioMedicine*. (2023) 90:104536. doi: 10.1016/j.ebiom.2023.104536

12. Barrett T, Wilhite SE, Ledoux P, Evangelista C, Kim IF, Tomashevsky M, et al. NCBI GEO: archive for functional genomics data sets–update. *Nucleic Acids Res*. (2013) 41:D991–5. doi: 10.1093/nar/gks1193

13. Ritchie ME, Phipson B, Wu D, Hu Y, Law CW, Shi W, et al. limma powers differential expression analyses for RNA-sequencing and microarray studies. *Nucleic Acids Res*. (2015) 43:e47. doi: 10.1093/nar/gkv007

14. Liberzon A, Birger C, Thorvaldsdóttir H, Ghandi M, Mesirov JP, Tamayo P. The Molecular Signatures Database (MSigDB) hallmark gene set collection. *Cell Syst*. (2015) 1:417–25. doi: 10.1016/j.cels.2015.12.004

15. Wu T, Hu E, Xu S, Chen M, Guo P, Dai Z, et al. clusterProfiler 4.0: A universal enrichment tool for interpreting omics data. *Innovation (Camb)*. (2021) 2:100141. doi: 10.1016/j.xinn.2021.100141

16. Miao YR, Zhang Q, Lei Q, Luo M, Xie GY, Wang H, et al. ImmuCellAI: A unique method for comprehensive T-cell subsets abundance prediction and its application in cancer immunotherapy. *Adv Sci (Weinh)*. (2020) 7:1902880. doi: 10.1002/advs.201902880

17. Newman AM, Liu CL, Green MR, Gentles AJ, Feng W, Xu Y, et al. Robust enumeration of cell subsets from tissue expression profiles. *Nat Method*. (2015) 12:453–7. doi: 10.1038/nmeth.3337

18. Quilodrán CS, Currat M, Montoya-Burgos JI. Benchmarking the Mantel test and derived methods for testing association between distance matrices. *Mol Ecol Resour*. (2023). doi: 10.1111/1755-0998.13898

19. Athanasios A, Charalampos V, Vasileios T, Ashraf GM. Protein-protein interaction (PPI) network: recent advances in drug discovery. *Curr Drug Metab*. (2017) 18:5–10. doi: 10.2174/1389200218011701190204832

20. Zeng Y, Cao S, Chen M. Integrated analysis and exploration of potential shared gene signatures between carotid atherosclerosis and periodontitis. *BMC Med Genomics*. (2022) 15:227. doi: 10.1186/s12920-022-01373-y

21. Outay F, Adnan M, Gazder U, Baqueri SFA, Awan HH. Random forest models for motorcycle accident prediction using naturalistic driving based big data. *Int J Inj Contr Saf Promot*. (2023) 30:282–93. doi: 10.1080/17457300.2022.2164310

22. Valkenborg D, Rousseau AJ, Geubbelmans M, Burzykowski T. Support vector machines. *Am J Orthod Dentofacial Orthop*. (2023) 164:754–7. doi: 10.1016/j.ajodo.2023.08.003

23. Wang Q, Qiao W, Zhang H, Liu B, Li J, Zang C, et al. Nomogram established on account of Lasso-Cox regression for predicting recurrence in patients with early-stage hepatocellular carcinoma. *Front Immunol*. (2022) 13:1019638. doi: 10.3389/fimmu.2022.1019638

24. Chang L, Zhou G, Soufan O, Xia J. miRNet 2.0: network-based visual analytics for miRNA functional analysis and systems biology. *Nucleic Acids Res*. (2020) 48:W244–51. doi: 10.1093/nar/gkaa467

25. Freshour SL, Kiwala S, Cotto KC, Coffman AC, McMichael JF, Song JJ, et al. Integration of the Drug-Gene Interaction Database (DGIdb 4.0) with open crowdsource efforts. *Nucleic Acids Res*. (2021) 49:D1144–51. doi: 10.1093/nar/gkaa1084

26. Alkadhi KA, Alhaider IA. Caffeine and REM sleep deprivation: Effect on basal levels of signaling molecules in area CA1. *Mol Cell Neurosci*. (2016) 71:125–31. doi: 10.1016/j.mcn.2015.12.015

27. Rocha DJ, Santos CS, Pacheco LG. Bacterial reference genes for gene expression studies by RT-qPCR: survey and analysis. *Antonie Van Leeuwenhoek*. (2015) 108:685–93. doi: 10.1007/s10482-015-0524-1

28. Sule R, Rivera G, Gomes AV. Western blotting (immunoblotting): history, theory, uses, protocol and problems. *Biotechniques*. (2023) 75:99–114. doi: 10.2144/btn-2022-0034

29. Yaremchuk K. Sleep disorders in the elderly. *Clin Geriatr Med*. (2018) 34:205–16. doi: 10.1016/j.cger.2018.01.008

30. Jiménez-Jiménez FJ, Alonso-Navarro H, García-Martín E, Agúndez JAG. Sleep disorders in patients with choreic syndromes. *Curr Neurol Neurosci Rep*. (2023) 23:361–79. doi: 10.1007/s11910-023-01274-2

31. Dey S, Sun E, Frishman WH, Aronow WS. Sleep disorders and coronary artery disease. *Cardiol Rev*. (2023) 31:219–24. doi: 10.1097/CRD.0000000000000478

32. Lee YY, Endale M, Wu G, Ruben MD, Francey LJ, Morris AR, et al. Integration of genome-scale data identifies candidate sleep regulators. *Sleep*. (2023) 46:zsac279. doi: 10.1093/sleep/zsac279

33. Ali R, Tariq S, Kareem O, Fayaz F, Aziz T, Meenu , et al. Nutraceuticals for sleep disorders. *Comb Chem High Throughput Screen*. (2021) 24:1583–92. doi: 10.2174/1386207324666210121111446

34. Pandi-Perumal SR, Saravanan KM, Paul S, Namasivayam GP, Chidambaram SB. Waking up the sleep field: an overview on the implications of genetics and bioinformatics of sleep. *Mol Biotechnol*. (2024) 66:919–31. doi: 10.1007/s12033-023-01009-1

35. Garbarino S, Lanteri P, Bragazzi NL, Magnavita N, Scoditti E. Role of sleep deprivation in immune-related disease risk and outcomes. *Commun Biol*. (2021) 4:1304. doi: 10.1038/s42003-021-02825-4

36. Liu X, Su Y, Huang Z, Lv J, Gu C, Li Z, et al. Sleep loss potentiates Th17-cell pathogenicity and promotes autoimmune uveitis. *Clin Transl Med*. (2023) 13:e1250. doi: 10.1002/ctm2.1250

37. Lippert J, Young P, Gross C, Meuth SG, Dräger B, Schirmacher A, et al. Specific T-cell activation in peripheral blood and cerebrospinal fluid in central disorders of hypersomnolence. *Sleep*. (2019) 42:10. doi: 10.1093/sleep/zsy223

38. Ibarra-Coronado EG, Velazquéz-Moctezuma J, Diaz D, Becerril-Villanueva LE, Pavón L, Morales-Montor J. Sleep deprivation induces changes in immunity in Trichinella spiralis-infected rats. *Int J Biol Sci*. (2015) 11:901–12. doi: 10.7150/ijbs.11907

39. Billings ME, Hale L, Johnson DA. Physical and social environment relationship with sleep health and disorders. *Chest*. (2020) 157:1304–12. doi: 10.1016/j.chest.2019.12.002

40. Chokroverty S. Overview of sleep & sleep disorders. *Indian J Med Res*. (2010) 131:126–40.

41. Lamon S, Morabito A, Arentson-Lantz E, Knowles O, Vincent GE, Condo D, et al. The effect of acute sleep deprivation on skeletal muscle protein synthesis and the hormonal environment. *Physiol Rep*. (2021) 9:e14660. doi: 10.14814/phy2.14660

42. Cao Y, Li Q, Liu L, Wu H, Huang F, Wang C, et al. Modafinil protects hippocampal neurons by suppressing excessive autophagy and apoptosis in mice with sleep deprivation. *Br J Pharmacol*. (2019) 176:1282–97. doi: 10.1111/bph.14626

43. Li Y, Zhang W, Liu M, Zhang Q, Lin Z, Jia M, et al. Imbalance of autophagy and apoptosis induced by oxidative stress may be involved in thyroid damage caused by sleep deprivation in rats. *Oxid Med Cell Longev*. (2021) 2021:5645090. doi: 10.1155/2021/5645090

44. Brzecka A, Sarul K, Dyła T, Avila-Rodriguez M, Cabezas-Perez R, Chubarev VN, et al. The association of sleep disorders, obesity and sleep-related hypoxia with cancer. *Curr Genomics*. (2020) 21:444–53. doi: 10.2174/1389202921999200403151720

45. Wang Z, Chen WH, Li SX, He ZM, Zhu WL, Ji YB, et al. Gut microbiota modulates the inflammatory response and cognitive impairment induced by sleep deprivation. *Mol Psychiatry*. (2021) 26:6277–92. doi: 10.1038/s41380-021-01113-1

46. Noguti J, Alvarenga TA, Marchi P, Oshima CT, Andersen ML, Ribeiro DA. The influence of sleep restriction on expression of apoptosis regulatory proteins p53, Bcl-2 and Bax following rat tongue carcinogenesis induced by 4-nitroquinoline 1-oxide. *J Oral Pathol Med*. (2015) 44:222–8. doi: 10.1111/jop.12225

47. Chang SL, Durocher F, Diorio C. Sleep quality traits correlate with inflammatory markers in the breast tissue of women. *Cytokine*. (2022) 160:156028. doi: 10.1016/j.cyto.2022.156028

48. Winkelmann J, Kimura M. Genetics of sleep disorders. *Handb Clin Neurol*. (2011) 99:681–93. doi: 10.1016/B978-0-444-52007-4.00002-3

49. Jäkel S, Mingot JM, Schwarzmaier P, Hartmann E, Görlich D. Importins fulfil a dual function as nuclear import receptors and cytoplasmic chaperones for exposed basic domains. *EMBO J*. (2002) 21:377–86. doi: 10.1093/emboj/21.3.377

50. Lin W, Xu H, Yuan Q, Zhang S. Integrative genomic analysis predicts regulatory role of N6-methyladenosine-associated SNPs for adiposity. *Front Cell Dev Biol*. (2020) 8:551. doi: 10.3389/fcell.2020.00551

51. Kumar N, Prasad P, Jash E, Saini M, Husain A, Goldman A, et al. Insights into exchange factor directly activated by cAMP (EPAC) as potential target for cancer treatment. *Mol Cell Biochem*. (2018) 447:77–92. doi: 10.1007/s11010-018-3294-z

52. Yang JR, Ling XL, Guan QL. RAP2A promotes apoptosis resistance of hepatocellular carcinoma cells via the mTOR pathway. *Clin Exp Med*. (2021) 21:545–54. doi: 10.1007/s10238-021-00723-x

53. Samaan S, Tranchevent LC, Dardenne E, Polay Espinoza M, Zonta E, Germann S, et al. The Ddx5 and Ddx17 RNA helicases are cornerstones in the complex regulatory array of steroid hormone-signaling pathways. *Nucleic Acids Res*. (2014) 42:2197–207. doi: 10.1093/nar/gkt1216

54. Dutertre M, Gratadou L, Dardenne E, Germann S, Samaan S, Lidereau R, et al. Estrogen regulation and physiopathologic significance of alternative promoters in breast cancer. *Cancer Res*. (2010) 70:3760–70. doi: 10.1158/0008-5472.CAN-09-3988

55. Charizanis K, Lee KY, Batra R, Goodwin M, Zhang C, Yuan Y, et al. Muscleblind-like 2-mediated alternative splicing in the developing brain and dysregulation in myotonic dystrophy. *Neuron*. (2012) 75:437–50. doi: 10.1016/j.neuron.2012.05.029

56. Edokpolor KS, Banerjee A, McEachin ZT, Gu J, Kosti A, Arboleda JD, et al. Altered behavioral responses show GABA sensitivity in muscleblind-like 2-deficient mice: implications for CNS symptoms in myotonic dystrophy. *eNeuro*. (2022) 9(5):0218–22. doi: 10.1523/ENEURO.0218-22.2022

57. Irizarry-Caro RA, McDaniel MM, Overcast GR, Jain VG, Troutman TD, Pasare C. TLR signaling adapter BCAP regulates inflammatory to reparatory macrophage transition by promoting histone lactylation. *Proc Natl Acad Sci U S A*. (2020) 117:30628–38. doi: 10.1073/pnas.2009778117

58. Sharma S, Dimasi D, Higginson K, Della NG. RZF, a zinc-finger protein in the photoreceptors of human retina. *Gene*. (2004) 342:219–29. doi: 10.1016/j.gene.2004.08.015

59. Yu L, Dawe RJ, Boyle PA, Gaiteri C, Yang J, Buchman AS, et al. Association between brain gene expression, DNA methylation, and alteration of ex vivo magnetic resonance imaging transverse relaxation in late-life cognitive decline. *JAMA Neurol*. (2017) 74:1473–80. doi: 10.1001/jamaneurol.2017.2807

60. Bocchini M, Tazzari M, Ravaioli S, Piccinini F, Foca F, Tebaldi M, et al. Circulating hsa-miR-5096 predicts 18F-FDG PET/CT positivity and modulates somatostatin receptor 2 expression: a novel miR-based assay for pancreatic neuroendocrine tumors. *Front Oncol*. (2023) 13:1136331. doi: 10.3389/fonc.2023.1136331

61. Anwar MA, Adesina-Georgiadis KN, Spagou K, Vorkas PA, Li JV, Shalhoub J, et al. A comprehensive characterisation of the metabolic profile of varicose veins; implications in elaborating plausible cellular pathways for disease pathogenesis. *Sci Rep*. (2017) 7:2989. doi: 10.1038/s41598-017-02529-y

62. Leitman DC, Christians U. MF101: a multi-component botanical selective estrogen receptor beta modulator for the treatment of menopausal vasomotor symptoms. *Expert Opin Investig Drugs*. (2012) 21:1031–42. doi: 10.1517/13543784.2012.685652

63. Shim S, Park KM, Chung YJ, Kim MR. Updates on therapeutic alternatives for genitourinary syndrome of menopause: hormonal and non-hormonal managements. *J Menopausal Med*. (2021) 27:1–7. doi: 10.6118/jmm.20034

frontiers | Frontiers in Neurology

TYPE Original Research
PUBLISHED 03 July 2024
DOI 10.3389/fneur.2024.1409038

OPEN ACCESS

EDITED BY
Fawaz Alzaid,
Sorbonne Universités, France

REVIEWED BY
Malgorzata Wojcik,
Jagiellonian University Medical College, Poland
Beata Labuz-Roszak,
Opole University, Poland

*CORRESPONDENCE
Edyta Matusik
✉ ematusik@sum.edu.pl

RECEIVED 29 March 2024
ACCEPTED 10 June 2024
PUBLISHED 03 July 2024

CITATION
Matusik E (2024) Usefulness of bioelectrical impedance analysis in multiple sclerosis patients—the interrelationship to the body mass index.
Front. Neurol. 15:1409038.
doi: 10.3389/fneur.2024.1409038

Usefulness of bioelectrical impedance analysis in multiple sclerosis patients—the interrelationship to the body mass index

Edyta Matusik*

Department of Rehabilitation, Faculty of Health Sciences in Katowice, Medical University of Silesia, Katowice, Poland

Background: Patients with multiple sclerosis (MS) have many potential factors (disease duration, spasticity, immobilization, or glucocorticoid use) that can deteriorate their nutritional status and impact both the progression and prognosis of the disease. Body mass index (BMI), the most widely used nutritional status assessment tool, has important limitations because it does not provide any data on body composition.

Aim: This study aimed to assess the interrelationship between nutritional status assessment by both body mass index (BMI) and body composition using bioelectrical impedance analysis (BIA) and the consistency of diagnosis for underweight/underfat, normal weight/healthy, overweight/overfat, and obesity/obese MS patients.

Methods: Anthropometric [BMI and waist-to-height ratio (WHtR)] and body composition (BIA) data were evaluated in 176 patients with MS. Patients were categorized into four nutritional status subgroups (underweight, normal weight, overweight, obese according to BMI, and underfat, healthy, overfat, and obese according to fat mass% by BIA). The median Expanded Disability Status Scale score was 4.5. Patients were then divided according to EDSS score as mild (EDSS 1.0–4.0) or moderate (EDSS 4.5–6.5) disability subgroups.

Results: Based on BIA assessment, there was a significantly higher prevalence of overfat than of overweight based on BMI [$n = 50$ (28.41%) vs. $n = 38$ (21.59%); $p < 0.05$]. However, the prevalence of obesity did not differ significantly regardless of the mode of diagnosis and was not significantly lower when assessed using BIA [$n = 26$ (14.77%) vs. $n = 30$ (17.05%), respectively]. The overall compatibility rates (CR) of diagnoses made using both BMI and BIA were 75.6, 77.0, and 70.1% for all patients with MS and the mild and moderate subgroups, respectively. The lowest CR was observed in the overweight group. Adiposity significantly underestimated BMI in all subgroups. In the moderate MS subgroup, BMI significantly overcategorized patients with MS as having a normal weight ($p < 0.05$). Stratification for abdominal obesity (WHtR > 0.5) showed that BMI significantly underestimated the prevalence of MS in overweight and obese vs. overfat and obese patients, as assessed using BIA (60.5 vs. 67%; $p < 0.05$). Clinical status (EDSS and ΔEDSS) was more closely related to the nutritional status categorized by FAT% assessed using BIA than using BMI cutoff points. However, the relationship was not statistically significant.

Conclusion: Using the BMI cutoff point for nutritional status assessment in patients with MS is associated with a significant underestimation of excess fat

mass. BIA-based FAT% based on BIA have a better relationship with abdominal obesity and disability status than with BMI in patients with MS. The highest rate of false-negative diagnoses was based on the BMI in patients with MS and moderate disability. Adiposity assessment using BIA appears to be a useful method for proper nutritional status assessment in the patients group.

KEYWORDS

multiple sclerosis, bioelectrical impedance analysis (BIA), body mass index (BMI), obesity, waist-to-height ratio (WHtR)

1 Introduction

Multiple sclerosis (MS) is caused by an autoimmune process that leads to diffuse demyelination of the central nervous system (CNS) (1). The symptomatology of MS consists of a variety of signs and symptoms, such as weakness and fatigue, spasticity, reduced mobility and ambulation, impaired coordination, sexual dysfunction, and depression. The most commonly proposed theory is that the etiology of MS is related to complex interactions between genetic predispositions and environmental factors. Some of these factors can be modified, which can influence not only the development of the disease but also the progression of disability and prognosis of the treatment outcomes. One of the recently underlined modifiable factors is impaired nutritional status (especially excessive overweight and obesity) (2–5). A study conducted by Hedström et al. in a large-scale Swedish population showed that subjects whose BMI exceeded 27 kg/m^2 at age 20 had a 2-fold increased risk of developing MS compared to normal-weight persons (4). Moreover, higher depression levels, lower functional capacity, and worse self-rated health status in overweight MS patients were shown by Cambil-Martin et al. (6) compared to the normal-weight MS control group. In a recently published review showing data available over the last 10 years (5), the authors found a significant relationship between obesity onset in pediatric patients and MS development. Body mass index (BMI), the most widely used nutritional status assessment tool, has important limitations because it does not provide any data on body composition. The limitation of using BMI in patients with MS was described by Pilutti et al. (7) and in a review by Dionyssiotis (8), who reported that BMI assessment may underestimate adiposity in patients with multiple sclerosis. However, it is important to distinguish between body weight and fat mass accumulation because of the confirmed relationship between the hormonal function of adipose tissue in obesity (pro-inflammatory adipokine production) and neuroimmunity in patients with MS (9, 10). The two most widely used methods for proper body composition analysis [fat mass (FM), fat-free mass (FFM), and muscle mass (MM)] must be performed: dual energy X-ray absorptiometry (DXA) and bioelectrical impedance analysis (BIA). However, body composition in individuals with MS has not been extensively studied. Moreover, patients with multiple sclerosis (MS) have many other potential factors (disease duration, spasticity, immobilization, or glucocorticoid use) that can deteriorate their anthropometrical status and body composition and may potentially impact both the progression and prognosis of the disease. Our recently published papers confirmed a significant correlation between anthropometric parameters [waist-to-height ratio (WHtR), fat mass, and fat-free mass] and disability level (EDSS) in patients with MS, but body mass index (BMI) was not related to EDSS (11, 12). Despite the increasing availability of bioelectrical impedance analysis (BIA), data showing the usefulness of this method in clinical settings are limited. Therefore, this study aimed to assess the interrelationship between nutritional status assessment using both body mass index (BMI) and bioelectrical impedance analysis (BIA) and the consistency of diagnosis for underweight, normal weight, overweight, and obesity in MS patients.

2 Materials and methods

2.1 Studied population

In total, 195 patients (132 females/63 males) that were consecutively admitted to the Multiple Sclerosis Management Center were recruited for the study. Subjects who had not experienced an exacerbation within the 30 past days and had no medical conditions, such as cardiac diseases, endocrine disorders, musculoskeletal system diseases, current glucocorticoid therapy, or respiratory diseases, were included. Patients who met the inclusion criteria were included in the final study group ($N = 176$, 128 females/48 males). All the patients had a definite diagnosis of relapsing–remitting or secondary progressive MS according to the McDonald criteria (13) and preservation of at least some ambulatory function [Expanded Disability Status Scale (EDSS) 1.0–6.5, median score 4.5; age 45.68 ± 12.01 years]. The initial EDSS score was obtained retrospectively from medical history at the time of MS diagnosis. The assessment of neurological status on the EDSS was performed by two experienced neurostatus-certified neurologists (EM and BK). Patients were then divided according to EDSS score as mild (EDSS 1.0–4.0) or moderate (EDSS 4.5–6.5) disability subgroup. The baseline clinical and anthropometrical characteristics of the study group is presented in Table 1.

2.2 Anthropometric measurements and body composition analysis

Anthropometric measurements were recorded on the day of the visit. Standing height was measured to the nearest 0.1 cm. Weight (in underwear) was measured using an electronic scale with readings accurate to 0.1 kg. Body mass index (BMI) was then calculated, using the standard formula (kilograms per meter squared) and classify using standard cut-off points: underweight, BMI < 18.5 kg/m^2; normal

TABLE 1 Baseline clinical characteristics and anthropometrical parameters.

	Stadied population $N = 176$ (F/M = 128/48)			
	Mean	Minimum	Maximum	SD
Age (years)	45.68	20	73	12.01
EDSS initial	2.2	1.0	4.5	0.7
EDSS	3.3	1.0	6.5	1.6
Height (cm)	167.2	152.1	196.1	8.7
Weight (kg)	69.5	40.6	114	16.0
BMI (kg/m^2)	24.87	16.10	40.30	4.94
Waist c. (cm)	90.4	61.0	126.0	13.5
WHtR	0.54	0.38	0.75	0.08
FM (kg)	20.7	2.6	52.7	9.2
FM (%)	28.8	6.2	48.1	8.4
FFM (kg)	48.9	34.8	75.6	10.1
FFM (%)	71.2	51.9	93.8	8.3

EDSS, Expanded disability status scale; BMI, Body mass index; WHtR, Waist-to-height-ratio; FM, Fat mass; and FFM, Fat-free mass.

weight, BMI = 18.5–24.9 kg/m^2; overweight, BMI = 25.0–29.9 kg/m^2; obese, BMI ≥ 30.0 kg/m^2. Waist circumference was also measured, and the waist-to-height ratio (WHtR) was calculated. Body composition parameters: fat mass (FM) and fat-free mass (FFM) were assessed [in kilograms (kg) or as percentages of body weight (%)] based on bioelectrical impedance using a leg-to-leg body composition analyzer (BC-420MA Tanita Europe BV, Hoofddorp, The Netherlands) (14). Based on FM%, the patients were classified as underfat, healthy, overfat, or obese. The cut-off points for age and sex are presented in Table 2. All anthropometric and body composition parameters were measured at the same time points as in the subsequent EDSS assessment.

2.3 Ethical considerations

This study was approved by the Ethics Committee of the Medical University of Silesia (approval no. KNW/0022/KB/179/17). All the participants provided informed consent. The patient rights were approved according to the Declaration of Helsinki.

2.4 Statistical analysis

Differences in the distribution of each nutritional status category based on BMI and BIA were assessed using the chi-square test. The interrelationship and compatibility rate between the diagnoses made using BMI and BIA in the entire group and disability status subgroups were assessed using frequency tables.

TABLE 2 Fat mass (FM) (%) ranges for adults.

Age (years)	Women			
	Underfat	Healthy	Overfat	Obese
20–39	≤ 21.0%	21.1–33.0%	33.1–39.5%	≥39.6%
40–59	≤ 23.0%	23.2–34.0%	34.3–40.0%	≥40.1%
60–79	≤ 24.0%	24.1–35.2%	35.3–41.5%	≥41.6%
Age (years)	Men			
	Underfat	Healthy	Overfat	Obese
20–39	≤ 7.0%	7.1–20.0%	20.1–25.0%	≥25.1%
40–59	≤ 10.5%	10.6–22.0%	22.1–28.2%	≥28.3%
60–79	≤ 12.2%	12.3–25.0%	25.1–30.0%	≥30.1%

(Based on https://tanita.eu/understanding-YO-measurements/body-fat-percentage).

Clinical status differences (expressed as EDSS and ΔEDSS) within different nutritional status categories for both BMI and BIA were assessed using one-way ANOVA. All statistical analyses were conducted using the Statistica™ 12 PL software and a p value less than 0.05 was considered significant.

3 Results

3.1 Prevalence of every nutritional status category based on BMI vs. BIA assessment in the entire group of MS patients

The distribution of nutritional status categories diagnosed by BMI cutoff points was as follows: underweight, $n = 11$ (6.25%); normal weight, $n = 97$ (55.11%); overweight, $n = 38$ (21.59%); and obese, $n = 30$ (17.05%). Bioimpedance (BIA) revealed a significantly lower prevalence of underfat and healthy individuals [$n = 10$ (5.69) and $n = 90$ (51.14%), respectively] in the study group. Based on BIA assessment, there was a significantly higher prevalence of overfat than of overweight based on BMI [$n = 50$ (28.41%) vs. $n = 38$ (21.59%); $p < 0.05$]. However, the prevalence of obesity did not differ significantly regardless of the mode of diagnosis and was not significantly lower when assessed using BIA [$n = 26$ (14.77%) vs. $n = 30$ (17.05%), respectively]. The distribution of each nutritional status category for both BMI and BIA assessments is shown in Figure 1.

3.2 Compatibility of the nutritional status diagnoses based on BMI vs. BIA assessment in the entire group of MS patients

The overall compatibility rate (CR) of diagnoses made using both BMI and BIA was 75.6% ($n = 133$) for the entire patient group. The lowest CR was observed in the overweight group. Only 71.1% ($n = 27$) of the MS patients diagnosed as overweight by BMI were also overweight by BIA, accounting for only 54% of all overweight MS patients. The best compatibility was found for the healthy category by BIA, in which the CR with a BMI normal weight diagnosis was 90%. Detailed diagnoses based on BMI, BIA interrelationship, and compatibility are presented in Tables 3, 4.

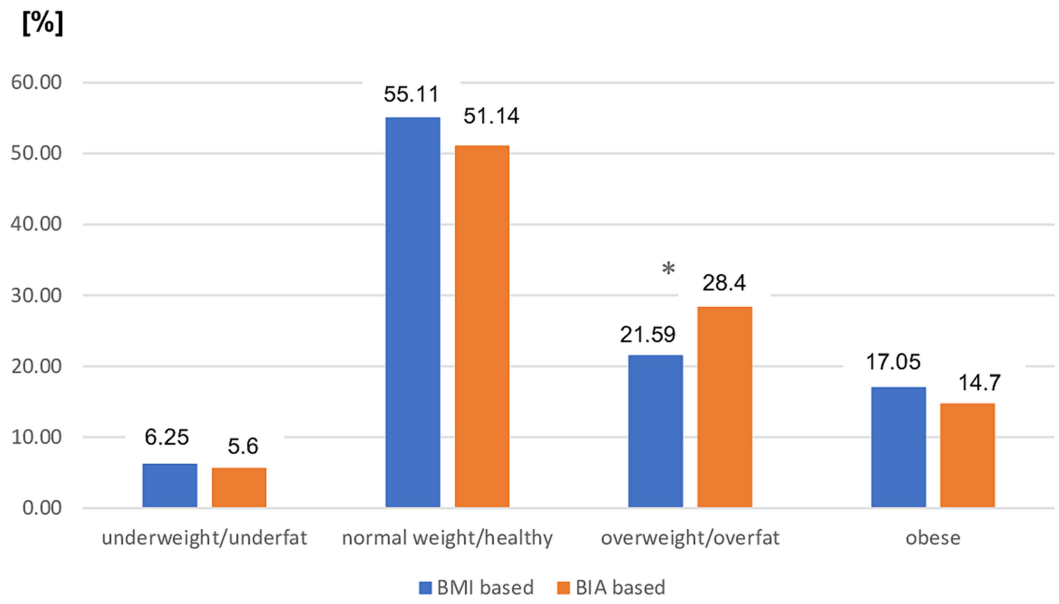

FIGURE 1
Prevalence of different nutritional status in the entire MS patients group based on BMI vs. BIA. BMI, Body mass index; BIA, Bioelectrical impedance analysis; *$p < 0.05$ (chi-square test).

TABLE 3 Interrelationship between different nutritional status diagnosis based on BMI vs. BIA in the entire study group.

Diagnosis by BMI (*n*)	Diagnosis by BIA (*n*)				*BMI all*
	underfat	healthy	overfat	obese	
Underweight	7	4	0	0	*11*
Normal	3	**81**	11	2	**97**
Overweight	0	5	**27**	6	**38**
Obesity	0	0	12	**18**	**30**
BIA all	**10**	**90**	**50**	**26**	**133/176 (75.6%)**

BMI, Body mass index; BIA, Bioelectrical impedance analysis. Bold numbers indicate the concordance of diagnoses between the described methods used to identify adequate nutritional status.

TABLE 4 Two-sided compatibility rate for all MS patients.

Nutritional status	All (*n* = 176)		*p*
	BMI vs. BIA	BIA vs. BMI	
Underweight/underfat	63.6% (7/11)	70.0% (7/10)	NS
Normal/healthy	83.5% (81/97)	90.0% (81/90)	NS
Overweight/overfat	**71.1% (27/38)**	**54.0% (27/50)**	**$p < 0.05$**
Obesity/obese	60% (18/30)	69.2% (18/26)	NS

BMI, Body mass index; BAI, Bioimpedance analysis. *p* values were determined using the chi-square test. Bold numbers refer to significant differences in the diagnosis of nutritional status between the methods used to assess it.

3.3 Prevalence of every nutritional status category based on BMI vs. BIA assessment in mild and moderate disability subgroups of MS patients

The distribution of nutritional status categories diagnosed by both BMI and BIA cutoff points in patients with MS with mild disability was similar to that in the entire study group. There was a significant difference between the prevalence of overweight (assessed using BMI) and the overfat category assessed using BIA ($p < 0.05$). The prevalence of other nutritional statuses did not differ significantly between the two modes of diagnosis in this subgroup of patients with MS (Figure 2).

However, the use of BMI cutoff points was related to a significant overestimation of normal weight status ($p < 0.01$) and underestimation of overweight status ($p < 0.01$) in patients with MS with moderate disability status assessed using EDSS (Figure 3).

3.4 Compatibility of nutritional status diagnoses based on BMI vs. BIA assessment in the mild and moderate disability subgroups of MS patients

The overall CR of diagnoses made using both BMI and BIA in patients with MS with mild disability was not significantly higher than that in the entire group (77.0 vs. 75.6%). The lowest CR was observed in the overweight/overfat group (Table 5). The lowest overall CR was observed in patients with moderately disabled

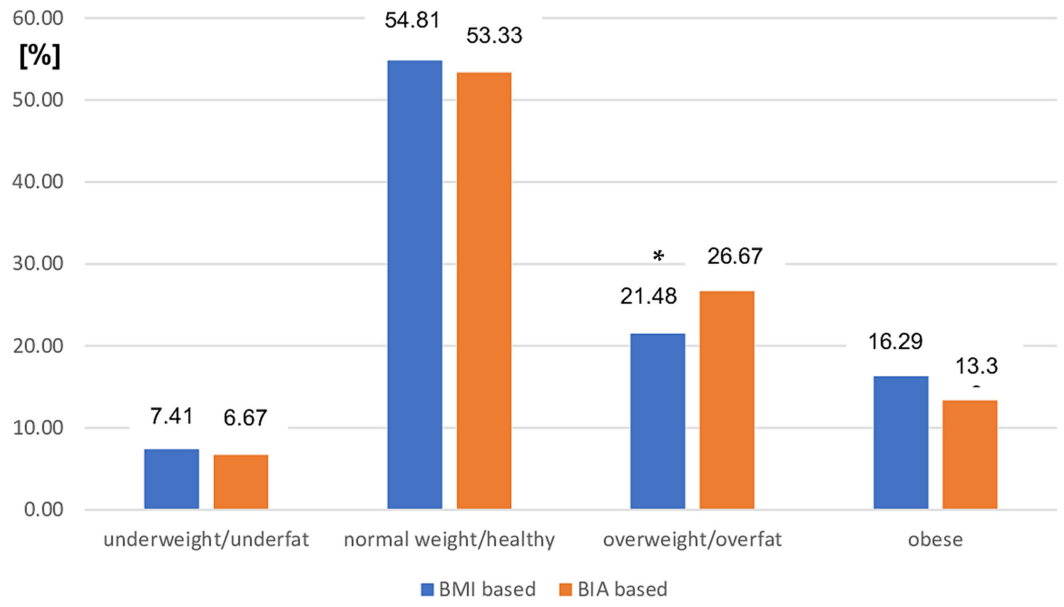

FIGURE 2
Prevalence of different nutritional status in mild MS patients subgroup based on BMI vs. BIA. BMI, Body mass index; BIA, Bioelectrical impedance analysis; *$p < 0.05$ (chi-square test).

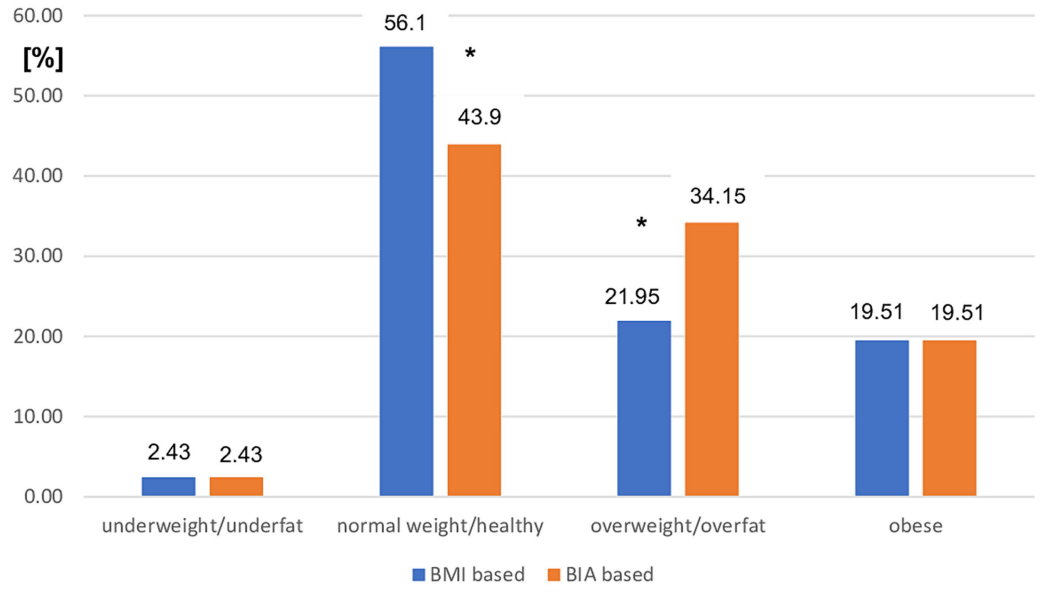

FIGURE 3
Prevalence of different nutritional status in moderate MS patients subgroup based on BMI vs. BIA. BMI, Body mass index; BIA, Bioelectrical impedance analysis; *$p < 0.01$ (chi-square test).

MS. Only 70.7% of patients in this group had the same diagnoses (Tables 5, 6). Analyzing the two-sided CR between both modes of nutritional status assessment, significant differences were found for overweight/overfat diagnosis in both moderate and mild MS subgroups ($p < 0.01$ vs. $p < 0.05$, respectively) and for the normal weight/healthy category only in moderately disabled MS patients ($p < 0.05$) (Table 7).

3.5 Nutritional status distribution measured by BMI vs. BIA after the stratification by abdominal obesity diagnosed as WHtR > 0.5

The study groups were stratified according to fat mass distribution. Abdominal obesity was diagnosed by calculating the waist-to-height ratio (WHtR). The cutoff point for the diagnosis

TABLE 5 Interrelationship between different nutritional status diagnoses based on BMI vs. BIA in the mild MS subgroup.

Diagnosis by BMI (n)	Diagnosis by BIA (n)				*BMI all*
	Underfat	Healthy	Overfat	Obese	
Underweight	6	4	0	0	*10*
Normal	3	**65**	5	1	**74**
Overweight	0	3	**21**	5	**29**
Obesity	0	0	10	**12**	**22**
BIA all	**9**	**72**	**36**	**18**	**104/135 (77.0%)**

BMI, Body mass index; BAI, Bioimpedance analysis. Bold numbers refer to significant differences in the diagnosis of nutritional status between the methods used to assess it.

TABLE 6 Interrelationship between different nutritional status diagnoses based on BMI vs. BIA in the moderate MS subgroup.

Diagnosis by BMI (n)	Diagnosis by BIA (n)				*BMI all*
	Underfat	Healthy	Overfat	Obese	
Underweight	**1**	0	0	0	**1**
Normal	0	**16**	6	1	**23**
Overweight	0	2	**6**	1	**9**
Obesity	0	0	2	**6**	**8**
BIA all	**1**	**18**	**14**	**8**	**29/41 (70.7%)**

BMI, Body mass index; BAI, Bioimpedance analysis. Bold numbers indicate the concordance of diagnoses between the described methods used to identify adequate nutritional status.

TABLE 7 Two-sided compatibility rate (CR) in moderate and mild MS subgroups.

Nutritional status	Moderate MS ($n = 41$)	*p*	Mild MS ($n = 135$)		*p*	
	BMI vs. BIA	BIA vs. BMI		BMI vs. BIA	BIA vs. BMI	
Underweight/underfat	100% (1/1)	100% (1/1)	NS	60.0% (6/10)	66.7% (6/9)	NS
Normal/healthy	**69.6% (16/23)**	**88.9% (16/18)**	**$p < 0.05$**	87.8% (65/74)	90.3% (65/72)	NS
Overweight/overfat	**66.7% (6/9)**	**42.9% (6/14)**	**$p < 0.01$**	**72.4% (21/29)**	**58.3% (21/36)**	**$p < 0.05$**
Obesity/obese	75% (6/8)	75% (6/8)	NS	54.5% (12/22)	66.7% (12/18)	NS

BMI, Body mass index; BAI, Bioimpedance analysis. *p* values were determined using the chi-square test. Bold numbers indicate the concordance of diagnoses between the described methods used to identify adequate nutritional status.

of abdominal obesity was WHtR > 0.5. While, in the group of patients with WHtR ≤ 0.5 there were no significant differences between BMI vs. BIA assessment ones in the subgroup of patients with abdominal obesity (WHtR <0.5) BMI significantly underestimated the prevalence of MS patients with overweight and obesity vs. overfat and obese (60.5% vs. 67%; $p < 0.05$) (Figure 4).

3.6 Nutritional status distribution measured by BMI vs. BIA after the stratification by abdominal obesity

To analyze the interrelationship between both methods and the disability level of patients with MS, the present clinical status (assessed by EDSS) and MS progression (assessed by EDSS) were assessed. The study group was first stratified for the different nutritional status category based on both BMI and BIA and then one-way ANOVA was performed for EDSS and ΔEDSS, respectively. Both EDSS and ΔEDSS were more related to the nutritional status categorized by FAT% assessed by BIA than using BMI cut-off points. However, this relationship was not statistically significant (Figure 5A for EDSS and Figure 5B for ΔEDSS).

4 Discussion

In our study, we assessed the consistency of the distribution of nutritional status categories based on BMI cutoff points and bioelectrical impedance analysis (BIA) by fat mass percentage (FM%). We observed that FM assessed by BIA revealed a significantly lower prevalence of underfat and healthy persons; however, there was a significantly higher prevalence of overfat patients with MS than overweight patients based on the BMI cutoff point. However, the prevalence of obesity did not differ significantly, regardless of the method of diagnosis, and was not significantly lower when assessed using BIA. The overall compatibility rate (CR) of the diagnoses made using both BMI and BIA was 75.6% in the entire patient group. After stratification for disability status (based on the EDSS), a similar CR was found for patients with MS in the mild disability group (77.0%).

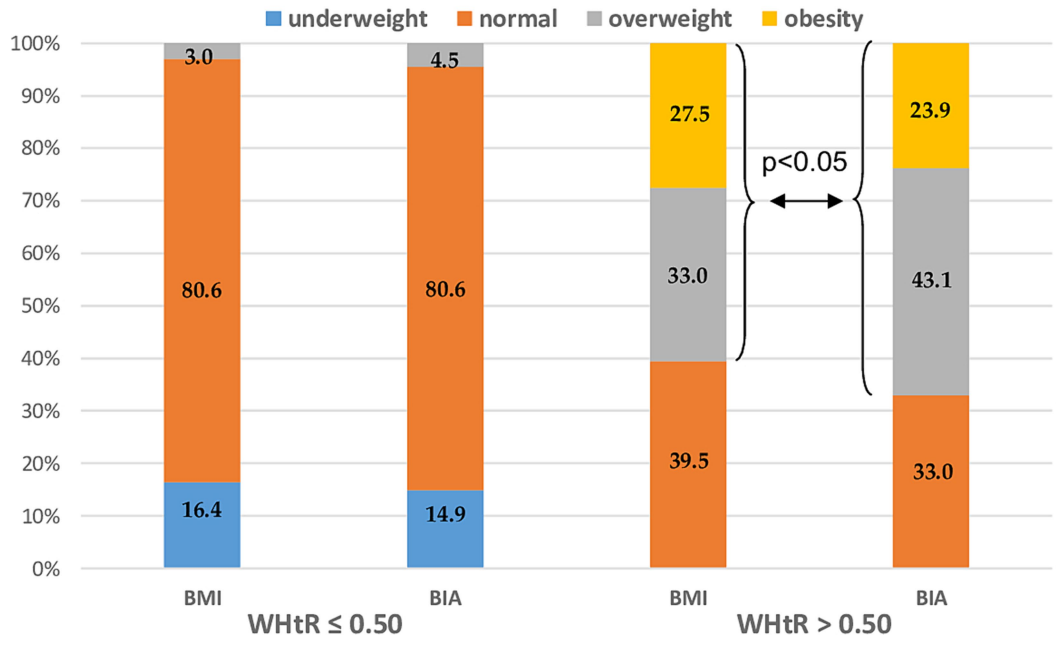

FIGURE 4
Nutritional status distribution measured by BMI vs. BIA after the stratification by abdominal obesity diagnosed as WHtR > 0.5. BMI, Body mass index; BIA, Bioelectrical impedance analysis; and WHtR, Waist-to-height ratio.

However, the CR was distinctly lower in patients in the moderate MS subgroup. The distribution of nutritional status categories diagnosed by both BMI and BIA cutoff points in patients with MS with mild disability was similar to that in the entire study group. Again, there was a significant difference between the prevalence of overweight (assessed by BMI) and the overfat category assessed by BIA. However, the use of BMI cut-off points was related to a significant overestimation of normal weight status and underestimation of overweight status in MS patients with moderate disability. Analyzing the two-sided CR between both methods of nutritional status assessment, significant differences were found for overweight/overfat diagnosis in both moderate and mild MS subgroups, and for the normal weight/healthy category only in moderately disabled MS patients.

Our findings confirm the data from the study by Hedström et al. (4), which showed that BMI assessment may cause an underestimation of adiposity in patients with MS compared with body composition measured by DXA. The same conclusions were drawn by Wingo et al. (15), who showed significantly higher fat mass and lower fat-free mass in men with MS than in healthy BMI-matched controls. The limitation of using BMI in patients with MS was also presented in a study showing a relationship between MS and longitudinal changes in BMI (16). The authors make three main observations. Baseline BMI in patients with MS was significantly higher than that in healthy controls; BMI was significantly higher in healthy controls with increasing age, and there were no longitudinal associations between BMI and EDSS. A recently published study postulated the use of a simple model to estimate the percentage of body fat in individuals with MS based only on BMI and sex using a special mathematical formula. However, it was cross-validated with DXA body composition in only 33 patients with MS (six males) and was not related to disability status (17). Dual-energy X-ray absorptiometry (DXA) is currently the gold standard for diagnosing osteoporosis and evaluating fat mass. However, a noninvasive body composition assessment technique based on bioelectrical impedance analysis (BIA) is currently available. Good correlation between BIA and DXA has been reported for estimating both fat mass and fat-free mass in different populations (18, 19). BIA is a relatively inexpensive, quick, simple, readily accessible, and non-invasive technique. Body composition analysis using BIA in patients with MS has been used in two studies that focused mainly on nutritional intake rather than on nutritional status (20, 21). The MS patient group was relatively small ($n = 20$ and $n = 37$, respectively) MS patients and the body fat percentage assessed by BIA was only shown as a mean result for the studied population; however, the authors did not show any detailed results related to body composition.

In analyzing fat tissue, it is important to remember that, from a metabolic point of view, body fat distribution has great importance and is closely related to the special risk for abdominal/visceral obesity, which cannot be properly assessed by BMI itself. The waist-to-height ratio (WHtR) is now widely studied to determine relatively simple parameters of fat tissue distribution in connection with visceral obesity and its comorbidities. A recent analysis showed that WHtR is the best parameter for the prognosis of visceral fat and its comorbidities (22). Our recently published study showed a significant correlation between this parameter and the disability status, disease duration, and glucocorticoid use in patients (12). Moreover, in a study performed by Cozart et al. (23), a higher waist-to-height ratio (WtHR) was associated with worse physical performance outcomes in patients with MS, as measured by the 6-min walk test (6 MWT) and the Timed 25 Foot Walk (T25FW). Another aspect of the potential influence of adiposity on MS progression is the generation of adipose tissue-related inflammation and oxidative stress. A recent study by Drehmer et al. (24) revealed a significant correlation between fat mass distribution

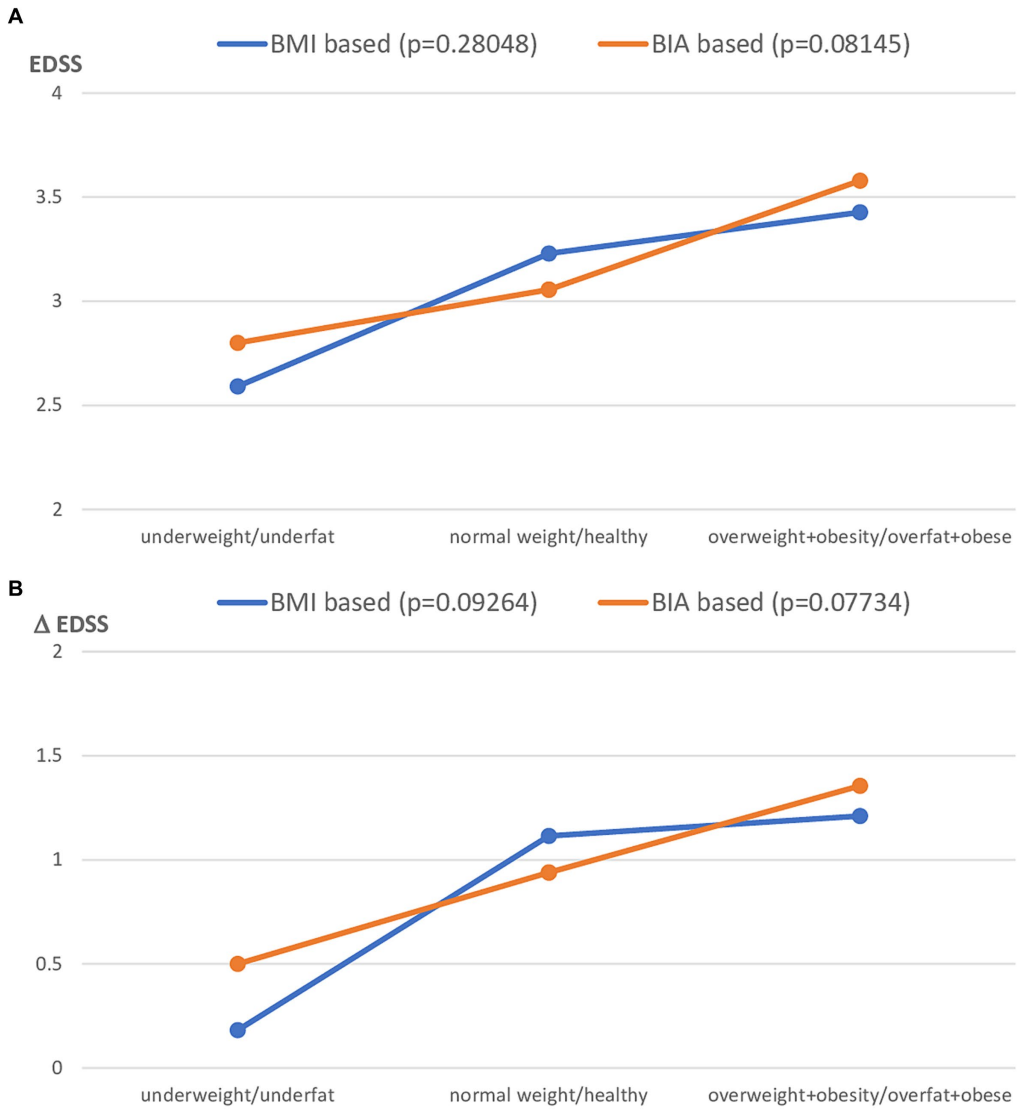

FIGURE 5
Clinical status of MS patients expressed as EDSS **(A)** and ΔEDSS **(B)**, after the stratification to the different nutritional status subgroups based on BMI vs. FAT% by BIA classification. BMI, Body mass index; BIA, Bioelectrical impedance analysis.

assessed by both waist circumference and WHtR and oxidative stress and inflammation markers in obese patients with MS. In the present study, the study group was stratified according to the diagnosis of abdominal obesity, which was assessed by calculating the calculation of waist-to-height ratio (WHtR). Leg-to-leg BIA methodology does not provide information on fat mass distribution. In the group of patients with a normal WHtR, there were no significant differences between BMI and BIA assessment in the subgroup of patients with abdominal obesity (WHtR < 0.5), and BMI significantly underestimated the prevalence of overweight and obesity vs. overweight and obese patients.

In the present study, we found that clinical status and disease progression assessed by EDSS were more closely related to nutritional status diagnosed by body composition (BIA) than to standard anthropometrical diagnosis based on BMI. However, the relationship was not statistically significant. These findings are similar to those reported by Pilutti et al. (25), who revealed that FM assessed using DXA was significantly higher in MS patients with moderate disability. Moreover, they did not find a significant difference in BMI between the mild and moderate disability groups. The lack of a significant correlation between BMI and disability status scores has recently been confirmed by several authors (12, 16, 25). Our recently published studies also showed a significant correlation between body composition parameters (FM% and FFM%) and disability status in patients (11, 12). However, conflicting results regarding the lack of significant correlations between the EDSS and BMI, Waist c., WHR, and FM% from BIA were noted in a group of 137 Brazilian patients (26).

Body composition parameter assessment seems to be important because in patients with MS, the risk of sarcopenia related to the level of disability is very high. A study conducted by Wens et al. (27) revealed a higher fat percentage and lower lean mass in muscle biopsies of patients with MS. Other data published by Ward et al. (28) and Wingo et al. (15) showed that higher FM% and lower FFM% were

associated with lower limb physical function, suggesting that body composition, specifically reducing adiposity and increasing lean mass, may be a potential target for MS interventions. It is also important to realize that lean mass is strongly related to the bone mineral density (BMD), either in whole body and lumbar spine projection (29).

This study has some limitations. First, the number of patients was relatively small, especially in the moderate MS subgroup. Second, data describing the initial nutritional status of patients with MS are lacking. These limitations indicate that future studies should focus on prospective longitudinal body composition assessments in larger cohorts of MS patients.

5 Conclusion

Using BMI cutoff points for assessing the nutritional status in patients with MS is associated with a significant underestimation of excess fat mass. BIA-based FAT% based on BIA have a better relationship with abdominal obesity and disability status than with BMI in patients with MS. The highest rate of false-negative diagnoses was based on the BMI in patients with MS and moderate disability. Adiposity assessment using BIA appears to be a useful method for proper nutritional status assessment in the patients group.

Data availability statement

The raw data supporting the conclusions of this article will be made available by the authors, without undue reservation.

Ethics statement

The studies involving humans were approved by Ethics Committee of the Medical University of Silesia (Approval No. KNW/0022/KB/179/17). The studies were conducted in accordance with the local legislation and institutional requirements. The participants provided their written informed consent to participate in this study.

Author contributions

EM: Writing – review & editing, Writing – original draft, Validation, Supervision, Resources, Project administration, Methodology, Investigation, Funding acquisition, Formal analysis, Data curation, Conceptualization.

Funding

The author declares that financial support was received for the research, authorship, and/or publication of this article. This study was supported by the Medical University of Silesia (grant no. BNW-1-118/N/3/Z, funded by the Ministry of Science).

Acknowledgments

The author would like to thank Barbara Kściuk for providing access to the patient database.

Conflict of interest

The author declares that the research was conducted in the absence of any commercial or financial relationships that could be construed as a potential conflict of interest.

Publisher's note

References

1. Lassmann H, Bruck W, Lucchinetti CF. The immunopathology of multiple sclerosis: an overview. *Brain Pathol.* (2007) 17:210–8. doi: 10.1111/j.1750-3639.2007.00064.x

2. Ascherio A, Munger KL. Environmental risk factors for multiple sclerosis, part II: noninfectious factors. *Ann Neurol.* (2007) 61:504–13. doi: 10.1002/ana.21141

3. Palavra F, Almeida L, Ambrosio AF, Reis F. Obesity and brain inflammation: a focus on multiple sclerosis. *Obes Rev*. (2016) 17:211–24. doi: 10.1111/obr.12363

4. Hedström AK, Olsson T, Alfredsson L. High body mass index before age 20 is associated with increased risk for multiple sclerosis in both men and women. *Mult Scler J.* (2012) 18:1334–6. doi: 10.1177/1352458512436596

5. Schreiner TG, Genes TM. Obesity and multiple sclerosis—a multifaceted association. *J Clin Med*. (2021) 10:2689. doi: 10.3390/jcm10122689

6. Cambil-Martín J, Galiano-Castillo N, Muñoz-Hellín E, Díaz-Rodríguez L, Laguarta-Val S, Fernández-de-las-Peñas C, et al. Influence of body mass index on psychological and functional outcomes in patients with multiple sclerosis: a cross-sectional study. *Nutr Neurosci*. (2016) 19:79–85. doi: 10.1179/1476830514Y.0000000156

7. Pilutti LA, Motl RW. Body mass index underestimates adiposity in persons with multiple sclerosis. *Arch Phys Med Rehabil*. (2016) 97:405–12. doi: 10.1016/j.apmr.2015.09.014

8. Dionyssiotis Y. Body composition in multiple sclerosis. *Hippokratia*. (2013) 17:7–11.

9. Guerrero-García JJ, Carrera-Quintanar L, López-Roa RI, Márquez-Aguirre AL, Rojas-Mayorquín AE, Ortuño-Sahagún D. Multiple sclerosis and obesity: possible roles of Adipokines. *Mediat Inflamm*. (2016) 2016:1–24. doi: 10.1155/2016/4036232

10. Correale J, Marrodan M. Multiple sclerosis and obesity: the role of adipokines. *Front Immunol.* (2022) 13:1038393. doi: 10.3389/fimmu.2022.1038393

11. Matusik E, Augustak A, Durmala J. Functional mobility and basic motor skills in patients with multiple sclerosis and its relation to the anthropometrical status and body composition parameters. *Medicina*. (2019) 55:773. doi: 10.3390/medicina55120773

12. Matusik E, Durmala J, Ksciuk B, Matusik P. Body composition in multiple sclerosis patients and its relationship to the disability level, disease duration and glucocorticoid therapy. *Nutrients*. (2022) 14:4249. doi: 10.3390/nu14204249

13. Polman CH, Reingold SC, Banwell B, Clanet M, Cohen JA, Filippi M, et al. Diagnostic criteria for multiple sclerosis: 2010 revisions to the McDonald criteria. *Ann Neurol*. (2011) 69:292–302. doi: 10.1002/ana.22366

14. Erdoğan E, Tutal E, Uyar ME, Bal Z, Demirci BG, Sayın B, et al. Reliability of bioelectrical impedance analysis in the evaluation of the nutritional status of hemodialysis patients—a comparison with Mini nutritional assessment. *Transplant Proc*. (2013) 45:3485–8. doi: 10.1016/j.transproceed.2013.08.096

15. Wingo BC, Young HJ, Motl RW. Body composition differences between adults with multiple sclerosis and BMI-matched controls without MS. *Disabil Health J*. (2018) 11:243–8. doi: 10.1016/j.dhjo.2017.10.003

16. Bove R, Musallam A, Xia Z, Baruch N, Messina S, Healy BC, et al. Longitudinal BMI trajectories in multiple sclerosis: sex differences in association with disease severity. *Mult Scler Relat Disord*. (2016) 8:136–40. doi: 10.1016/j.msard.2016.05.019

17. Bertapelli F, Silveira SL, Agiovlasitis S, Motl RW. Development and cross-validation of a simple model to estimate percent body fat in persons with multiple sclerosis. *Int J MS Care*. (2021) 23:193–8. doi: 10.7224/1537-2073.2020-034

18. Chen KT, Chen YY, Wang CW, Chuang CL, Chiang LM, Lai CL, et al. Comparison of standing posture bioelectrical impedance analysis with DXA for body composition in a large, healthy Chinese population. *PLoS One*. (2016) 11:e0160105. doi: 10.1371/journal.pone.0160105

19. Thomson R, Brinkworth GD, Buckley JD, Noakes M, Clifton PM. Good agreement between bioelectrical impedance and dual-energy X-ray absorptiometry for estimating changes in body composition during weight loss in overweight young women. *Clin Nutr*. (2007) 26:771–7. doi: 10.1016/j.clnu.2007.08.003

20. Bromley L, Horvath PJ, Bennett SE, Weinstock-Guttman B, Ray AD. Impact of nutritional intake on function in people with mild-to-moderate multiple sclerosis. *Int J MS Care*. (2019) 21:1–9. doi: 10.7224/1537-2073.2017-039

21. Saka M, Saka M, Koseler E, Metin S, Bilen S, Aslanyavrusu M, et al. Nutritional status and anthropometric measurements of patients with multiple sclerosis. *Saudi Med J*. (2012) 33:160–6.

22. Browning LM, Hsieh SD, Ashwell M. A systematic review of waist-to-height ratio as a screening tool for the prediction of cardiovascular disease and diabetes: 0–5 could be a suitable global boundary value. *Nutr Res Rev*. (2010) 23:247–69. doi: 10.1017/S0954422410000144

23. Cozart JS, Bruce AS, Shook RP, Befort C, Siengsukon C, Simon S, et al. Body metrics are associated with clinical, free-living, and self-report measures of mobility in a cohort of adults with obesity and multiple sclerosis. *Mult Scler Relat Disord*. (2023) 79:105010. doi: 10.1016/j.msard.2023.105010

24. Drehmer E, Platero JL, Carrera-Juliá S, Moreno ML, Tvarijonaviciute A, Navarro MA, et al. The relation between eating habits and abdominal fat, anthropometry, PON1 and IL-6 levels in patients with multiple sclerosis. *Nutrients*. (2020) 12:744. doi: 10.3390/nu12030744

25. Pilutti LA, Motl RW. Body composition and disability in people with multiple sclerosis: a dual energy x-ray absorptiometry study. *Mult Scler Relat Disord*. (2019) 29:41–7. doi: 10.1016/j.msard.2019.01.009

26. Da Costa Silva BY, De Carvalho Sampaio HA, Shivappa N, Hébert J, Da Silva AL, Ferreira Carioca AA, et al. Interactions between dietary inflammatory index, nutritional state and multiple sclerosis clinical condition. *Clin Nutr ESPEN*. (2018) 26:35–41. doi: 10.1016/j.clnesp.2018.04.018

27. Wens I, Dalgas U, Vandenabeele F, Krekels M, Grevendonk L, Eijnde BO. Multiple sclerosis affects skeletal muscle characteristics. *PLoS One*. (2014) 9:e108158. doi: 10.1371/journal.pone.0108158

28. Ward CL, Suh Y, Lane AD, Yan H, Ranadive SM, Fernhall B, et al. Body composition and physical function in women with multiple sclerosis. *J Rehabil Res Dev*. (2013) 50:1139–48. doi: 10.1682/JRRD.2012.08.0144

29. Mojtahedi MC, Snook EM, Motl RW, Evans EM. Bone health in ambulatory individuals with multiple sclerosis: impact of physical activity, glucocorticoid use, and body composition. *J Rehabil Res Dev*. (2008) 45:851–62. doi: 10.1682/JRRD.2007.10.0159

Frontiers in Neurology

Explores neurological illness to improve patient care

The third most-cited clinical neurology journal explores the diagnosis, causes, treatment, and public health aspects of neurological illnesses. Its ultimate aim is to inform improvements in patient care.

Discover the latest Research Topics

See more →

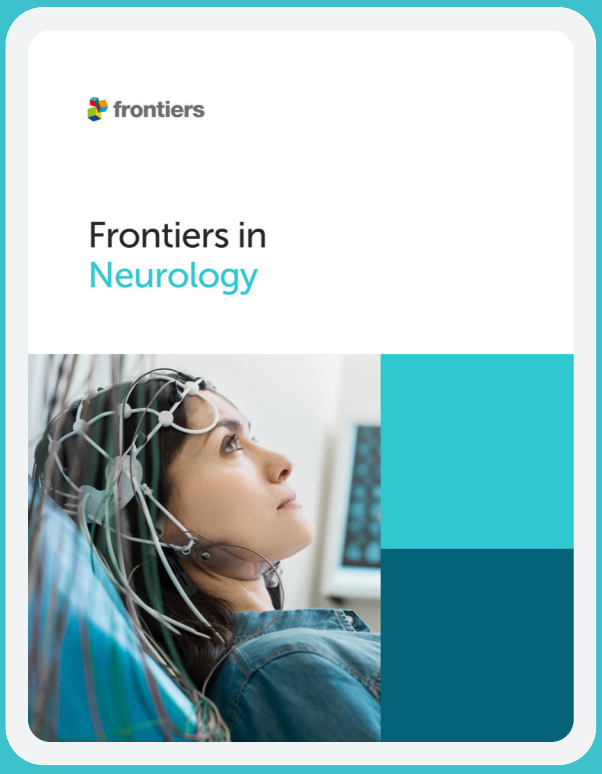

Frontiers

Avenue du Tribunal-Fédéral 34
1005 Lausanne, Switzerland
frontiersin.org

Contact us

+41 (0)21 510 17 00
frontiersin.org/about/contact